Author:
Hamilton, Hugh B

Title:
Magnesium and zirconium Lewis acids for cooperative Lewis pair chemistry

Magnesium and zirconium Lewis acids for cooperative Lewis pair chemistry

Hugh B. Hamilton

PhD Thesis

Supervised by
Prof. Duncan F. Wass

Co-supervised by
Prof. Michael S. Hill

A dissertation submitted to the University of Bristol in accordance with the requirements for award of the degree of Doctor of Philosophy in the School of Chemistry, Faculty of Science

July 2019

Word count: 40,938

Abstract

An exploration of Lewis pair chemistry is contained within this thesis, with a particular focus on frustrated Lewis pair (FLP) type reactivity using Zr or Mg based Lewis acids in combination with a phosphine, amine, or pyridine base. Chapter 1 provides a background to both Zr and Mg chemistry where it relates to this work. Chapter 2 details the development of intermolecular Zr/N FLPs, employing two separate zirconocene species in combination with a selection of pyridine and amine Lewis bases. These were themselves analysed, before being reacted with a series of small molecules (D_2, CO_2, THF, and PhCCD), resulting in varying reactivity that is controlled by the steric and electronic properties of the Lewis base. Chapter 3 builds on this work by examining the catalytic capability of the same Lewis pairs through the dehydrocoupling of $Me_2NH{\cdot}BH_3$, with activity shown to match or exceed that previously reported using phosphines in certain cases. Chapter 4 investigates intermolecular Lewis pair systems for small molecule activation (H_2, PhCCD, pentanone, benzaldehyde, and mesitaldehyde) using a novel Mg Lewis acid in combination with phosphines, pyridines, and amines, with limited success. However, more success was seen upon the use of the same Lewis pairs for the catalytic dehydrocoupling of $Me_2NH{\cdot}BH_3$, especially upon an increase in reaction temperature to 60 $^{\circ}$C—where activity of the Mg Lewis acid by itself approached that of Zr/P systems. Finally, Chapter 5 reports the synthesis of a novel intramolecular Mg/P Lewis pair, which was then tested for its small molecule activation (H_2, C_2H_4, CO_2, CD_2Cl_2, PhCCD, PhNCO, 3-pentanone, benzaldehyde, and mesitaldehyde) and catalytic capability (dehydrocoupling of $Me_2NH{\cdot}BH_3$). The reactivity displayed gives an improved understanding of the steric and electronic environments necessary to achieve desired results, aiding in the design of future compounds.

Acknowledgements

The last few years have been a genuine pleasure, and that is largely thanks to the people on this page, without whom the experience would have been far more difficult and much less enjoyable. Firstly, I would like to thank Duncan for giving me this opportunity, being a great supervisor, and for opening my mind to culinary delights I may never experience again. I would also like to thank Mike for very useful discussions, helping to keep my work on track.

Secondly, I would like to thank Rich for putting up with my constant questions and being unendingly helpful throughout my PhD. More importantly, however, I would like to thank him for some top-quality discussions about horror films and comics! Hope, some of my absolute best Bristol memories have been shared with you! You kept the office fun, and taught me the sanctity of vibes, and how they must be kept "good". Al, always remember to use your looks for good, not evil. I'll also be the first to sponsor your national Spoons tour (don't leave us all disappointed). Ash, may you continue your search for the fine line between annoying and funny. I'll miss the laughs, but I won't miss your music. Thanks to Katy for great chat (and top notch goss), to Owen for TEAM FLP, and the rest of the Wass group for making my time here so memorable.

A massive thanks to the Pringles and the Bedfords for all the wonderful times and endless trips to The Colston Arms (not to mention all the things I've "borrowed" from your labs over the years). Adam, we *will* win the FA cup one day, and I'm sorry for what I said about your head, it's lovely. Georgiaaaaaa, we will always let the groove get us to move, and it will always be alright (alright) alright. I'll be seeing you both in Switzerland soon, no doubt about it.

I would like to thank Paul Lawrence for a huge amount of help over the years with all aspects of NMR, Dr Paul Gates for help with Mass Spectrometry, and Dr Hazel Sparkes and Dr Natalie Pridmore for all the X-ray experiments.

Thank you to both my parents for being supportive and helping me get through the hard times. Lastly, thank you to Ari. It is quite hard to put into words quite how difficult this would have been without you. You have done so much to help me when I've needed it, you have raised me I've been down, and given me so many reasons to keep going when I didn't want to. You turned that tiny little flat into our own little paradise and made our time in Bristol special. I only hope I can support you as much as you have supported me.

Author's declaration

I declare that the work in this dissertation was carried out in accordance with the requirements of the University's *Regulations and Code of Practice for Research Degree Programmes* and that it has not been submitted for any other academic award. Except where indicated by specific reference in the text, the work is the candidate's own work. Work done in collaboration with, or with the assistance of, others, is indicated as such. Any views expressed in the dissertation are those of the author.

Hugh B. Hamilton

University of Bristol

Contents

List of Figures

List of Schemes

List of Tables

List of Abbreviations

FLP	Frustrated Lewis pair
HOMO	Highest occupied molecular orbital
LUMO	Lowest unoccupied molecular orbital
LB	Lewis base
TM	Transition metal
NMR	Nuclear magnetic resonance
DOSY	Diffusion ordered spectroscopy
DEPT	Distortionless enhancement by polarization transfer
HMBC	Heteronuclear multiple bond correlation
ppm	Parts per million
TOF	Turnover frequency
Ae	Alkaline earth
AN	Acceptor number
^{i}Pr	Isopropyl, -$CH(CH_3)_2$
Mes	Mesityl (2,4,6-trimethylphenyl)
DCM	Dichloromethane
9-BBN	9-Borabicyclo[3.3.1]nonane, $C_8H_{15}BH$
^{t}Bu	Tertiary butyl, -$C(CH_3)_3$
^{n}Bu	Normal butyl, -$CH_2CH_2CH_2CH_3$
HBpin	Pinacolborane, $(CH_3)_4C_2O_2BH$
Et	Ethyl, -CH_2CH_3
tol	Tolyl, -$C_6H_4(CH_3)$
Ad	Adamantyl, -$C_{10}H_{16}$
Ph	Phenyl, -C_6H_5
DIPP	Diisopropylphenyl, 2,6-$^{i}Pr_2$-C_6H_3N-
Cp*	Pentamethylcyclopentadienyl, $(C_5Me_5)^-$
THF	Tetrahydrofuran
Cy	Cyclohexyl, -C_6H_{11}
Cp	Cyclopentadienyl, $(C_5H_5)^-$
Me	Methyl, -CH_3
D	Diffusion coefficient
Py	Pyridine, NC_5H_5
TMEDA	Tetramethylethylenediamine

Chapter 1

Introduction

1.1 Lewis pairs

The formation of a new bond upon the combination of a two-electron donor with an electron-acceptor is a fundamental process in chemistry, and the existence of Lewis pairs can be found throughout the different realms of chemical research. The concept was first described by Gilbert Newton Lewis in 1923,[1] and has been of greater research focus since the advent of frustrated Lewis pairs (FLPs) in 2006.[2] The discovery that deliberate separation of the two Lewis pair moieties could produce useful and interesting chemistry was made by Stephan and co-workers. The separation of the Lewis acid and base can be achieved relatively straightforwardly, with the inclusion of significant steric bulk about each component precluding the formation of a formal bond (Figure 1.1).

In efforts to find new and interesting reactivity, elements from across the periodic table have been employed as both the Lewis acidic and Lewis basic moieties within FLPs. The work within this thesis focuses on the use of Zr and Mg based Lewis acids in combination with a phosphine, amine, or pyridine base, with the following sections of the introduction

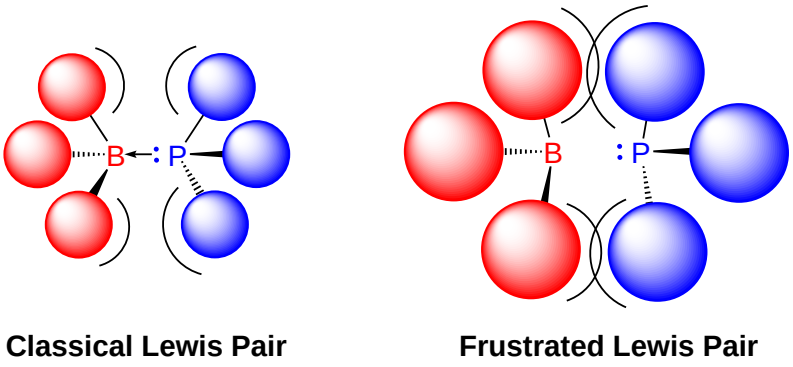

Figure 1.1: The difference in reactivity between a classical, and a frustrated Lewis pair.

exploring these two metals separately.

1.2 Zirconium in frustrated Lewis pairs

The vast majority of work using FLPs has involved main group acids and bases, with the pursuit of metal-free alternatives for common activation and transformation reactions one of the main aims.[3–5] However, transition metals (TMs) are capable of performing useful reaction processes such as oxidative addition and migratory insertion, which are highly important steps in a multitude of reactions but are of particular importance to catalysis. Transition metal compounds are generally found to be much more reactive than main group alternatives, and research into the use of TM components generally proceeds with the goal of combining the high reactivity of transition metals with the strong reactive potential of FLPs.[6]

The first intentional use of a zirconium species to perform a small molecule activation within an FLP framework was by Stephan and co-workers in 2011, when a zirconocene was used in conjunction with a phosphine for the activation of N_2O, after both titanocene and zirconocene cations were used to exchange $^{t}Bu_3P(N_2O)$ with a borane (Scheme 1.1).[7]

Work using zirconocenes developed rapidly since this initial publication, with both

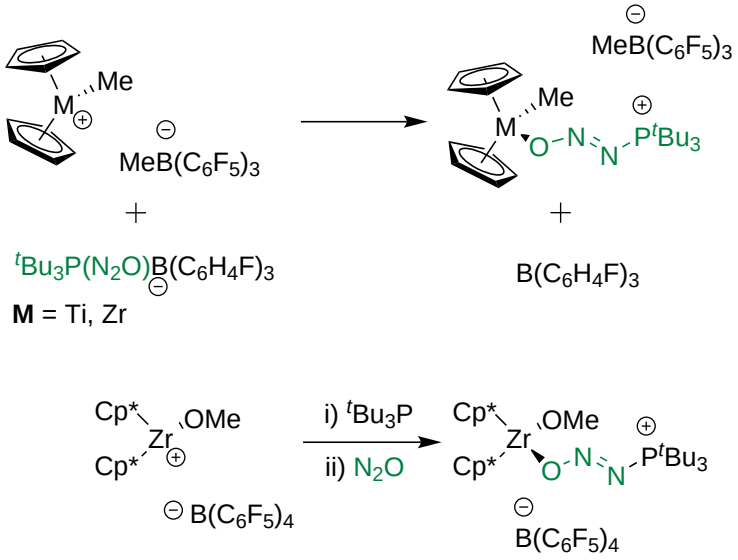

Scheme 1.1: Lewis acid exchange between metallocenes and $B(C_6H_4F)_3$ (top). Activation of N_2O using a zirconocene cation and P^tBu_3 (bottom).

inter- and *intra*-molecular FLPs shown to be effective. These two areas have been examined separately for the purposes of simplification, with the next section looking at intramolecular systems.

1.2.1 Intramolecular zirconium FLPs

With zirconocene cations already shown to assume the Lewis acidic role within an FLP, work within the Wass group sought to develop this by combining it with the Lewis basic moiety to form an intramolecular system. Complexes **1.1**–**1.5** were consequently made (Figure 1.2), containing a zirconocene (with either Cp or Cp* ligands) and a phosphinoaryloxide.[8] Interestingly, no Zr–P bond is seen for **1.2** or **1.5** in either the solid or solution states, with the Zr instead coordinating to PhCl solvent.

Differences in reactivity are found to exist even between these very similar complexes, with **1.1** unable to heterolytically cleave dihydrogen gas, whereas **1.2**, **1.3**, and **1.5** are able to perform the same reaction with ease—with conversions of >99% (Scheme 1.2).

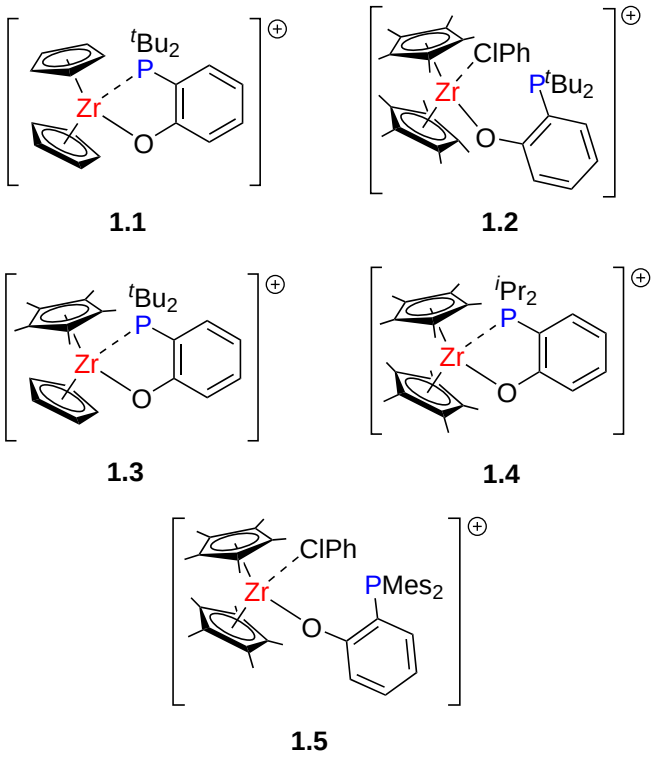

Figure 1.2: The intramolecular Zr/P FLP systems **1.1**–**1.5**. $[B(C_6F_5)_4]^-$ counterions omitted for clarity.

However, **1.4** only manages a conversion of ≈10%. At least one Cp* ligand is required for this reaction to proceed, and this is attributed to the extra electron density afforded by the Cp* ligands, which appears to stabilise the η^2-dihydrogen intermediate through backbonding.[9] In addition to this, the reaction with **1.2** is irreversible, whereas that with **1.3** is reversible, showing how subtle ligand alterations can have significant effects on reactivity. This is one of many examples shown in this chapter that demonstrate that steric influence is not always the most important factor in FLP chemistry. However, it is still a necessary characteristic of many of these compounds, as **1.4** demonstrates that a loss of some steric bulk can result in a fall in reactivity.

These complexes are also found to be effective for the activation of a variety of other small molecules. In particular, **1.2** is capable of performing all of the reactions shown

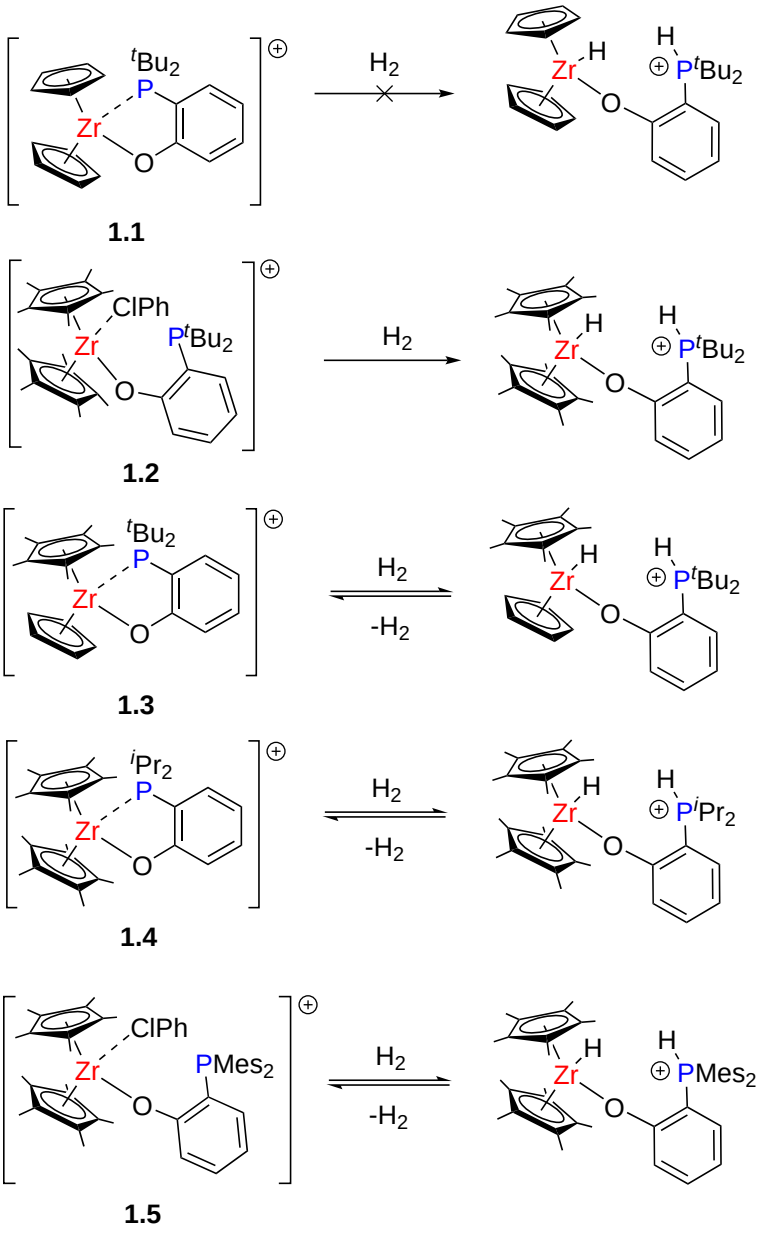

Scheme 1.2: The reaction of H_2 gas with **1.1**–**1.5**. $[B(C_6F_5)_4]^-$ counterions omitted for clarity.

in Scheme 1.3. Additionally, although **1.1** is able to activate of CO_2, phenylacetylene, alkyl halides, THF, and Et_2O, it demonstrates no reactivity with CO. Some of the more interesting reactivity demonstrated by **1.2** is the cleavage of C–O bonds in non-cyclic dialkyl ethers, S_N2 and E2 reactions with alkyl chlorides and fluorides, and the conversion of acetone to an enolate—all of which have not yet been reported for main group FLPs.

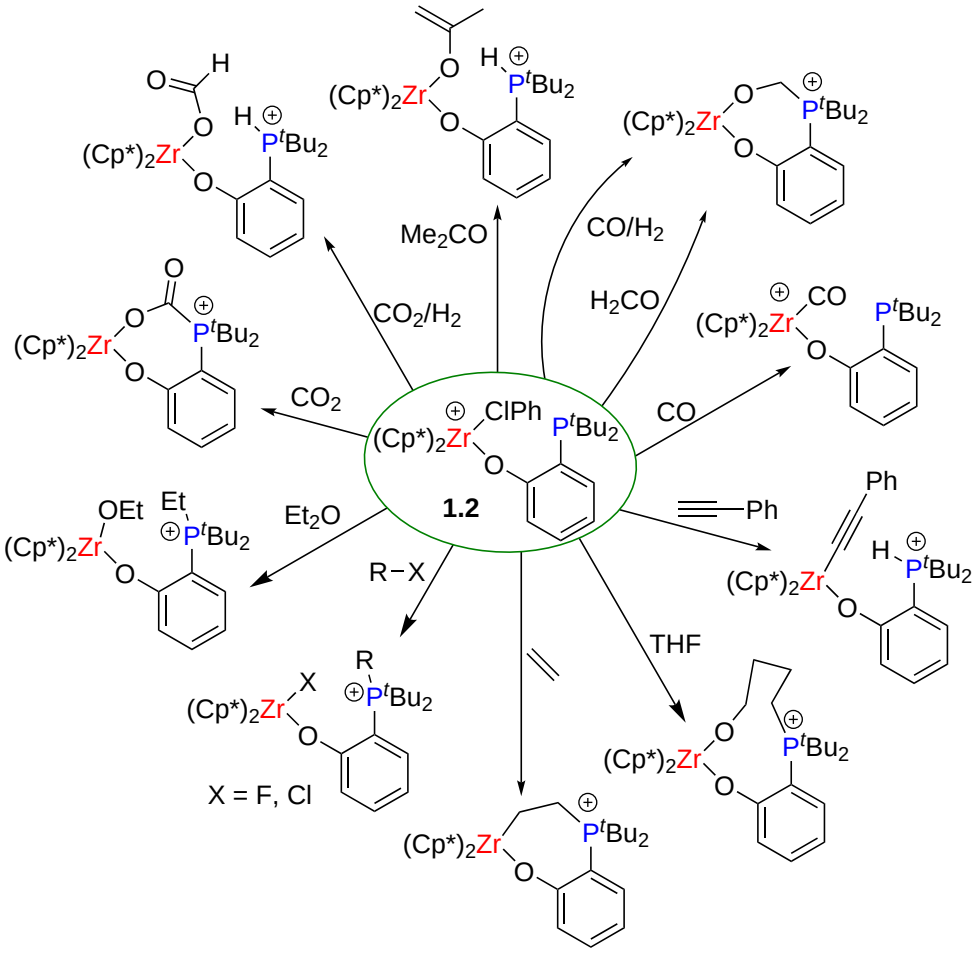

Scheme 1.3: Small molecule activation reactions of **1.2**. $[B(C_6F_5)_4]^-$ counterions omitted for clarity.

Other interesting results are the successful reduction reactions of both CO_2 and CO, resulting in the formation of bound formate, and formaldehyde respectively. These are promising results that demonstrate the potential of these systems to facilitate the conversion of CO_2 and CO to more valuable compounds such as formaldehyde, formic acid, or possibly methanol. However, despite these encouraging results the strong Zr–O bonds that are formed prevent further hydrogenation and subsequent release of the bound formate or formaldehyde. Not only does this hinder complete conversion of the substrate to a more useful compound, but also prevents the reaction developing from a stoichiometric regime

to a catalytic one.

1.1 and **1.2** are also used for the dehydrocoupling of a series of amine-boranes, with **1.1** proving to be especially reactive for the dehydrocoupling of $Me_2NH{\cdot}BH_3$—achieving 100% conversion within 10 min with a catalyst loading of 1 mol%. This results in an impressive turnover frequency (TOF) of around 500 h^{-1}. As a catalyst, **1.1** (5 mol%) also achieves complete conversion of $^{i}Pr_2NH{\cdot}BH_3$ to $^{i}Pr_2N{=}BH_2$ within 3 h, as well as the conversion of $H_3N{\cdot}BH_3$ into borazine and $[BH_2NH_2]_n$ polymer (Scheme 1.4). **1.2** is able to catalyse the same reactions, although it is much less reactive, requiring a 5 mol% catalyst loading and 8.5 h to achieve the full conversion of $Me_2NH{\cdot}BH_3$.[10]

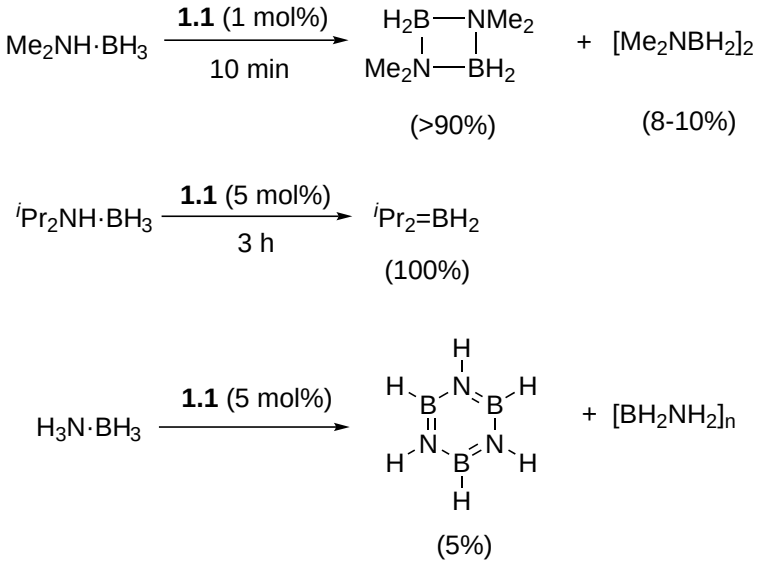

Scheme 1.4: Catalytic amine-borane dehydrocoupling reactions using **1.1**.

The Zr complexes **1.6**–**1.9** shown in Figure 1.3 have also been used for amine-borane dehydrocoupling reactions.[11] Compound **1.6** demonstrates the highest activity, reaching reaction completion within a minute with a TOF of >600 h^{-1} using a catalytic loading of 5 mol%. **1.7** and **1.8** are also highly effective, reaching reaction completion in 4 min and 9 min respectively (TOFs: 282 and 138 h^{-1} respectively). However, **1.9** demonstrates no

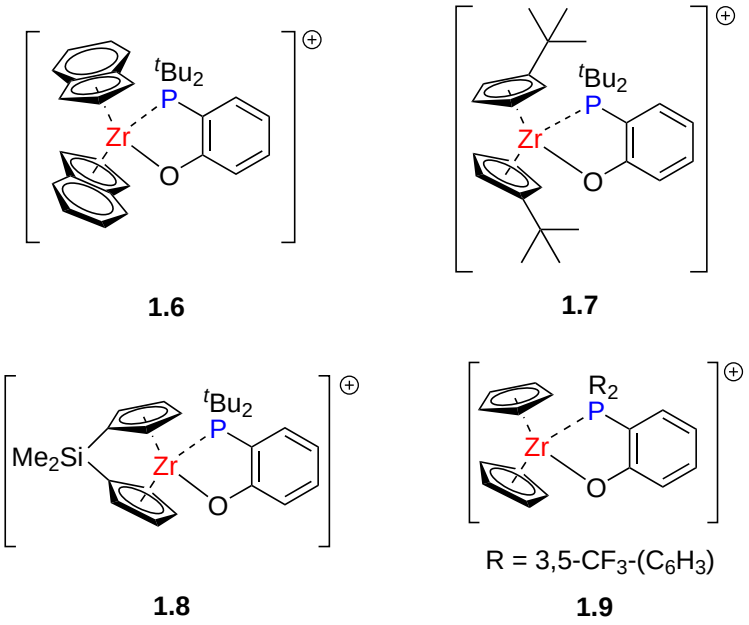

Figure 1.3: Intramolecular Zr/P FLPs used for catalytic amine-borane dehydrocoupling. $[B(C_6F_5)_4]^-$ counterions omitted for clarity.

activity in this reaction. Both steric and electronic factors affect the reactivity of each system, with the bulkier zirconocenes showing increased reaction rate, along with the more electron donating groups. **1.6** is both bulky and possesses electron rich indenyl groups, making it a very effective catalyst.

Zirconocenes with phosphinoaryloxide ligands are not the only intramolecular Zr/P FLPs to be developed, however, with compounds **1.10**–**1.16** (Figure 1.4) also shown to exhibit reactivity towards small molecule activation. Compounds **1.10**–**1.14** have been developed by Erker and co-workers,[12–19] with **1.15**–**1.16** reported by the Wass group.[20]

Compound **1.10**, which is formed by the 1,1-carbometallation of a trimethylsilyl-(diarylphosphino)acetylene, demonstrates typical FLP-type reactivity. The activation of CO_2, PhCHO, PhNO, SO_2, PhNSO, and H_2CO has been performed, along with the catalytic dimerisation of phenylacetylene. Despite this, the complex also possesses some more typical transition metal character, with the reaction of **1.10** with CO preceding an inser-

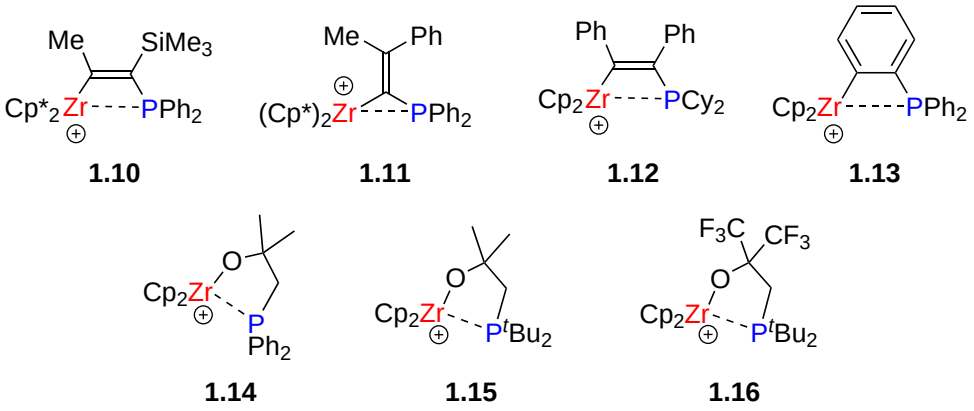

Figure 1.4: A series of Zr/P FLPs developed by Erker and co-workers (**1.10**–**1.14**), along with two FLPs developed by the Wass group (**1.15**–**1.16**). $[B(C_6F_5)_4]^-$ or $[MeB(C_6F_5)_3]^-$ counterions omitted for clarity.

tion mechanism that results in the formation of a (η^2-ketene)zirconocene product (Scheme 1.5).[12,13]

Compound **1.11**, just like **1.10**, is formed through an addition reaction upon the combination of $[Cp^*_2ZrMe][B(C_6F_5)_4]$ with a phosphinoalkyne. However, in this case the use of a slightly different alkyne results in a 1,2-addition, rather than a 1,1-addition, affording the geminal FLP species. **1.11** displays some typical FLP-type reactivity with the activation of CO_2, mesityl azide, an enone, an ynone, and *t*-butyl isocyanate, in addition to the insertion of O into the Zr–P bond upon reaction with N_2O—coinciding with release of N_2 (Scheme 1.6). However, reaction with H_2 (although initially involving FLP-type heterolytic cleavage) results in the loss of the phosphinoalkyl moiety through protonation of the α-C position.[14,15]

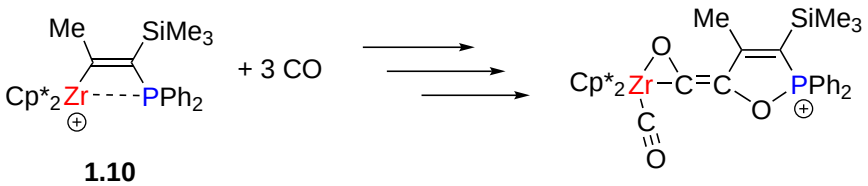

Scheme 1.5: The reaction of **1.10** with CO gas. $[B(C_6F_5)_4]^-$ counterions omitted for clarity.

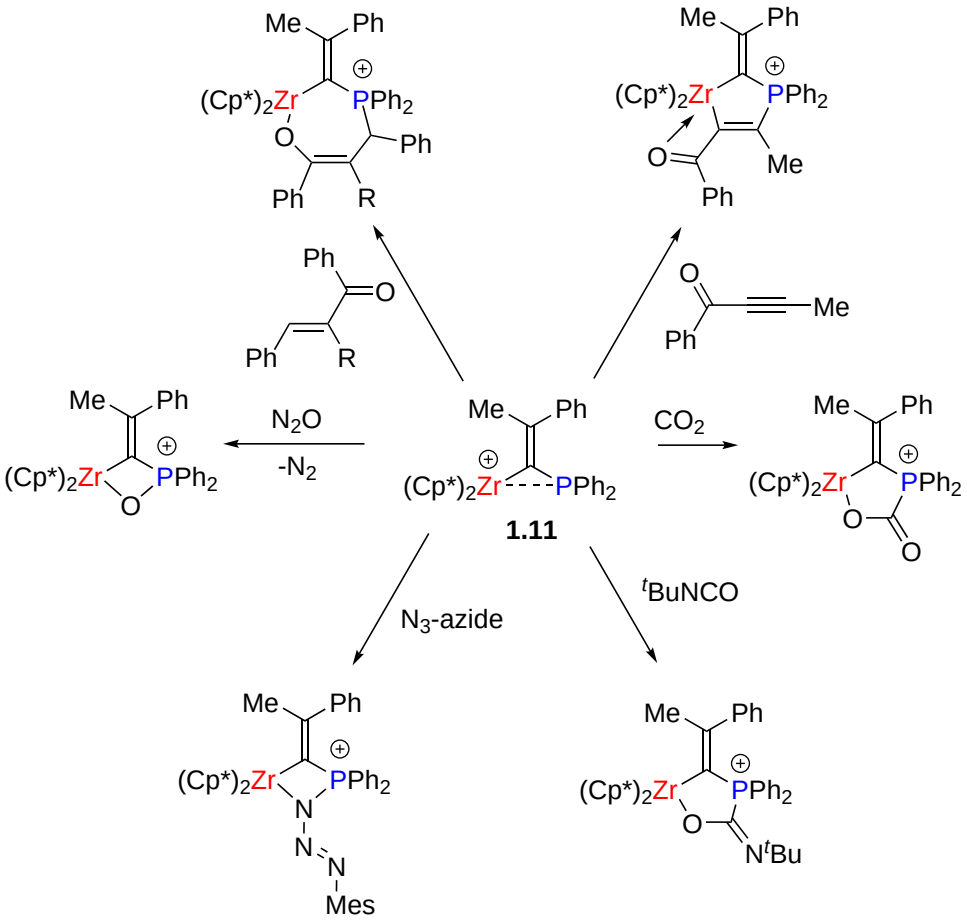

Scheme 1.6: FLP-type small molecule activation reactions of **1.11**. $[B(C_6F_5)_4]^-$ counterions omitted for clarity.

Compound **1.12** is very similar to **1.10** and **1.11**, but is formed via a slightly different synthesis—with the [2+2] cycloaddition of diphenylacetylene and a Zr=P bond. The compound is highly reminiscent of a Zr complex reported by Stephan and co-workers in 1996 (**1.17**, Figure 1.5),[21,22] which although not referred to in terms of FLP chemistry at the time (particularly as the phosphine is not behaving as a Lewis base), is shown to be capable of activating a series of small molecules (including phenylacetylene, styrene oxide, acetone, benzaldehyde, and benzonitrile) in a manner not too dissimilar from what is now considered FLP chemistry. Compound **1.12** itself is used for the activation of benzaldehyde, ferrocene carboxaldehyde, and chalcone, in addition to the reversible activation of

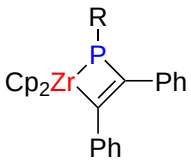

1.17

R = C_6H_2-2,4,6-^{t}Bu

Figure 1.5: The Zr complex reported by Stephan and co-workers in 1996.

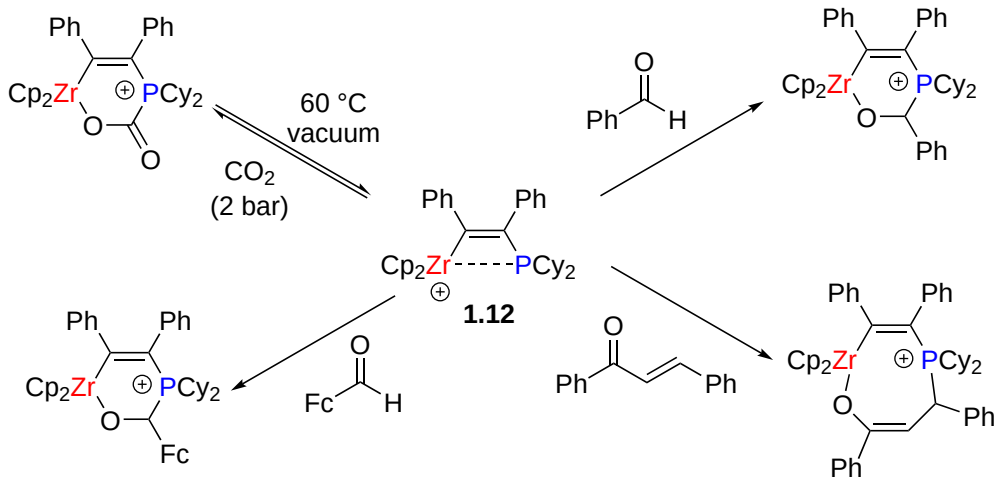

Scheme 1.7: Small molecule activation reactions of **1.12**. $[MeB(C_6F_5)_3]^-$ counterions omitted. Fc = ferrocenyl.

CO_2 (Scheme 1.7).[17]

Compound **1.13** contains a simple phenyl bridge between the Zr and phosphine centres, and is formed by the salt metathesis reaction of $Cp_2Zr(CH_3)Cl$ and a lithiated triphenylphosphine, followed by abstraction of the methyl group. This compound has been proven to be highly effective for the activation of carbonyl containing species—reactions with several ketones and aldehydes forming the expected FLP product—with attack at the carbonyl position favoured even when alkenes or alkynes are present within the substrate. The activation of phenylisocyanate, phenylthiocyanate, enones, and CO_2 also followed the expected route of FLP-type reactivity, however, **1.13** shows no affinity for the activation of THF. Reaction with H_2 also proceeds slightly differently, with initial FLP-type het-

erolytic cleavage preceding hydrogen-bridged dimer formation. Insertion between the Zr and phenyl ring results from reaction with dialkylcyanamides and CO, while reaction with ^{t}BuCl affords the product shown in Scheme 1.8, along with loss of isobutylene.[19]

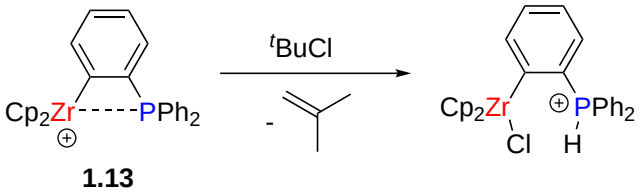

1.13

Scheme 1.8: Reaction of **1.13** with ^{t}BuCl. $[B(C_6F_5)_4]^-$ counterions omitted for clarity.

Compound **1.14** is much more similar to the phosphinoaryloxide complexes developed by the Wass group (and almost identical to compounds **1.15** and **1.16**). Unlike the complex without β-methyl groups, **1.14** does not form a dimer when in solution or solid state. Despite not being tested extensively in small molecule activation reactions, it is found to be capable of activating chalcone, benzaldehyde, nitrosobenzene, and a conjugated ynone, whilst the phosphine moiety is oxidised upon reaction with NO, releasing N_2O.[16]

Compounds **1.15** and **1.16** preceded **1.14**, and are formed through the reaction of Cp_2ZrMe_2 with the corresponding phosphine alkoxide, prior to methyl abstraction using $B(C_6F_5)_3$. They have been shown to be capable of heterolytically cleaving dihydrogen, however, the resultant products react with the $[MeB(C_6F_5)_3]^-$ anion, forming $[HB(C_6F_5)_3]^-$ and releasing methane. The importance of using a suitable counterion is highlighted here. Unfortunately, decomposition of **1.15** and **1.16** occurs when the more weakly coordinating $[B(C_6F_5)_4]^-$ counterion was used in place of $[MeB(C_6F_5)_3]^-$.[20]

1.2.2 Intermolecular zirconium FLPs

Intermolecular main group FLPs have been investigated far more extensively than their TM counterparts, however, the Wass group has been exploring both Zr and Ti intermolec-

ular FLPs over the last few years.[6,8,10,20,23–27] The aim when developing these systems has been to take the metal phosphinoaryloxide FLP complexes and simply remove the tether between the phosphine group and the metal complex (Scheme 1.9). Not only does this allow the exploration of how this affects reactivity, but it also simplifies the synthetic process due to the ability to more readily test the chemical effects (both electronic and steric) of a range of different phosphines in combination with a Zr cation.

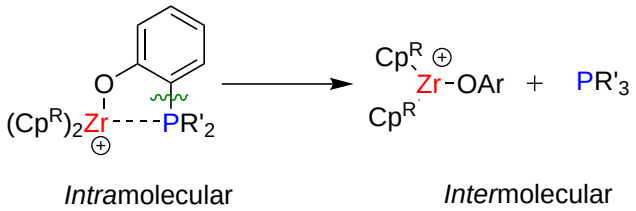

Scheme 1.9: Removing the tether converts the intramolecular FLP to an intermolecular FLP.

Scheme 1.10 shows the ability of the intermolecular Zr/P FLPs **1.18**–**1.23** to activate various small molecules.[25] For H_2 activation, Cp* ligands are required in place of Cp ligands (as with the intramolecular systems), with the more basic phosphines of PCy_3 and PEt_3 also required. Cp* ligands are not essential for the reactions with CO_2 as the same two phosphines react with both the Zr cations to give the FLP-activated product, with no reaction seen with the other Lewis bases. THF activation has been found to be slightly more successful, with PPh_3 also effectively fulfilling the role of the Lewis base in addition to PCy_3 and PEt_3. The mechanism by which these reactions occur is thought to proceed through initial binding of the THF substrate, before nucleophilic attack by the Lewis base causes ring-opening of THF.

One particularly important deduction from these investigations is that although it is necessary for the phosphine to have sufficient basicity for the FLP to be effective, steric bulk is not a key factor. In fact, the least sterically bulky phosphine, PEt_3, provides the

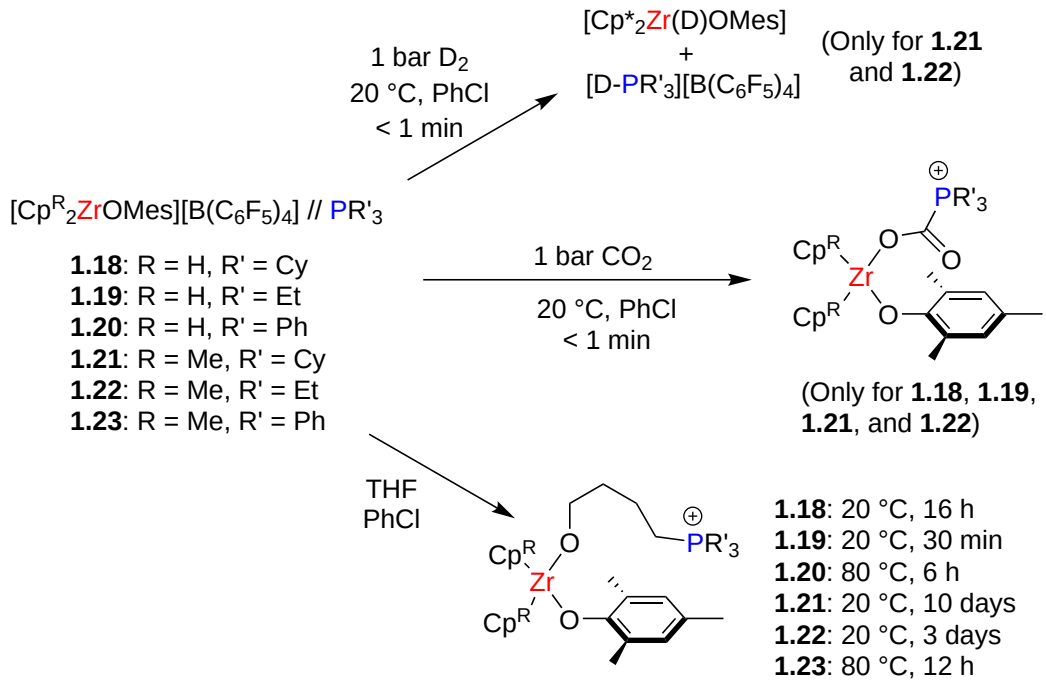

Scheme 1.10: Reactions of $[Cp^R{}_2ZrOMes]^+/PR'_3$ FLPs with D_2, CO_2, and THF. Some $[B(C_6F_5)_4]^-$ counterions omitted for clarity.

cleanest results. Diffusion ordered spectroscopy (DOSY) studies also demonstrate that the actual frustration between Lewis acid and Lewis base is limited in some cases, but as long as the Zr–P is dynamic and not persistent, FLP-type reactivity is still possible. Another point of note is the effect of phosphine bulk/basicity on reaction selectivity, as evidenced by the reaction of the Zr/P FLPs with phenylacetylene. As shown in Scheme 1.11, the larger PR_3 Lewis bases (where R = Mes or Cy) result in a deprotonation reaction, whereas the application of PPh_3 results in a 1,2-addition.[25]

These intermolecular FLPs have also been tested for their ability to catalytically dehydrocouple amine-boranes, and it has been found that the $[Cp^*{}_2ZrOMes]^+$ cation is ineffective when used with any of the phosphines P^tBu_3, PCy_3, PEt_3, PPh_3, $PMes_3$, or $P(C_6F_5)_3$ for the conversion of $Me_2NH{\cdot}BH_3$ to $[Me_2N–BH_2]_2$—with no reaction attaining conversion greater than 5%—and the reactions using PPh_3, $PMes_3$, and $P(C_6F_5)_3$ show-

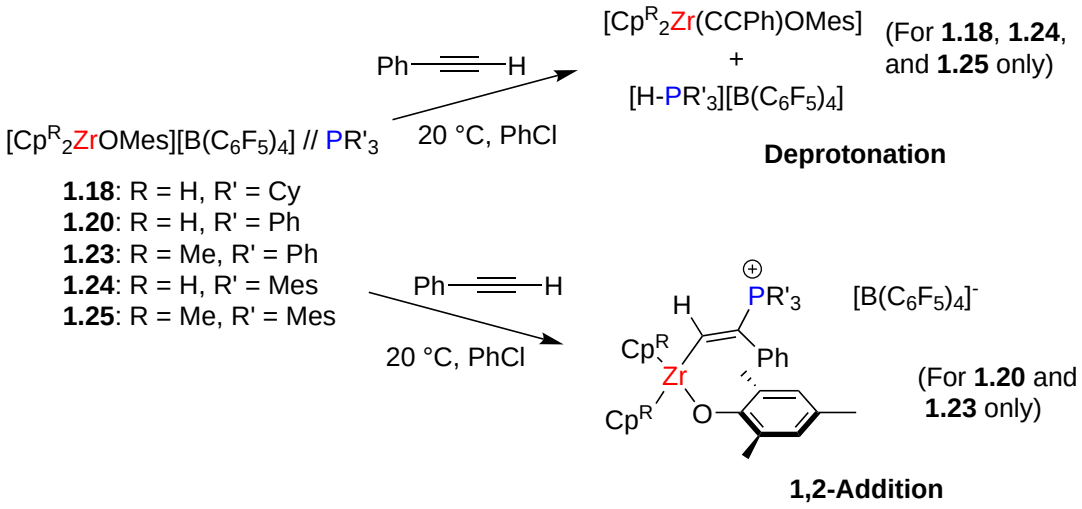

Scheme 1.11: Reaction of **1.18**, **1.20**, and **1.23**–**1.25** with phenylacetylene.

ing no reactivity whatsoever. However, changing from the Cp* cation to the Cp cation results in significant improvement, with a yield of 97% achieved in 7.5 h using the Cp cation in combination with P^tBu_3. In this case it appears that the Lewis base needs to be both of sufficient basicity, and to possess a certain level of steric bulk. The mechanism has been proposed to follow that shown in Scheme 1.12, with the Lewis base assisting deprotonation of the substrate in Cycle A, and the Zr cation also active in a second cycle, that involves coupling together of $Me_2NH{\cdot}BH_3$ with the deprotonated substrate, followed by an internal rearrangement of the formed Me_2NH–BH_2–Me_2N–BH_3 species to release $Me_2N{=}BH_2$. $Me_2N{=}BH_2$ then forms the cyclic product in an addition reaction with more $Me_2N{=}BH_2$.[11] The CpZr/P^tBu_3 FLP was also able to catalytically convert $^iPr_2NH{\cdot}BH_3$ to $^iPr_2N{=}BH_2$ with a conversion of 73% over 14 h.

Other work by the Wass group sees the catalytic hydrogenation of imines using the same Zr cations shown here, whereby the system effectively operates as an intermolecular FLP.[26] However, this will be discussed in more detail in Section 1.2.3.

Work by other groups has also explored intermolecular Zr FLP chemistry, the first

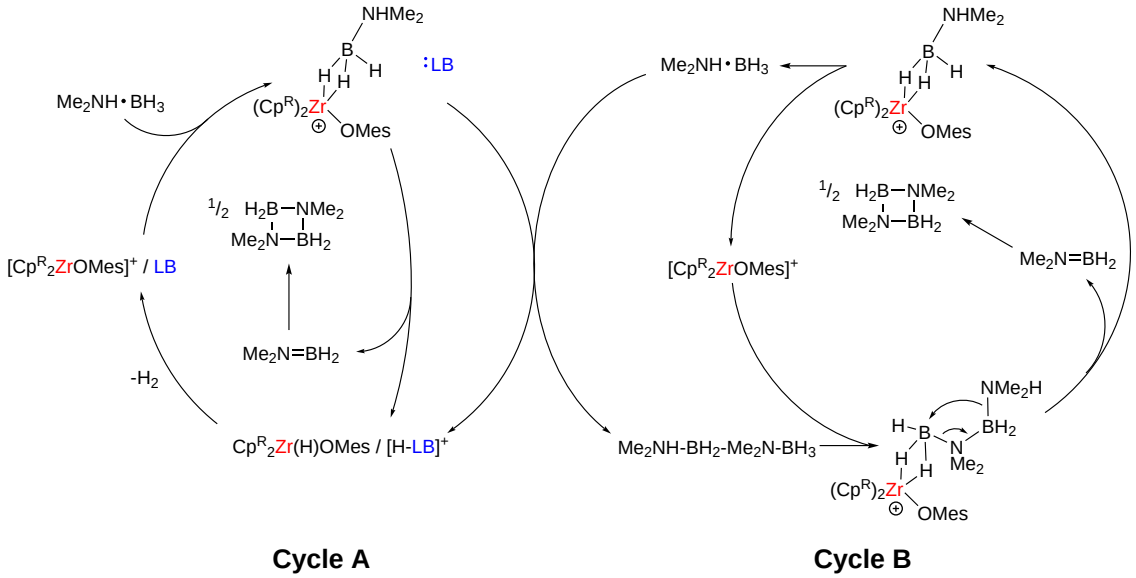

Scheme 1.12: Proposed reaction mechanism for the catalytic dehydrocoupling of $Me_2NH{\cdot}BH_3$ using a Zr(IV)/FLP. The $[B(C_6F_5)_4]^-$ counterion has been omitted for clarity.

of which was (as mentioned earlier) demonstrated by Stephan and co-workers with the activation of N_2O using **1.26**, as shown in Scheme 1.13.[7]

The Erker group has also carried out a significant amount of work with Zr FLPs, and they have combined an intramolecular P/B FLP with a Zr cation to include an element of competition within the FLP framework.[28] When the FLP **1.27** is combined with either Cp_2ZrMe_2 or $Cp^*_2ZrMe_2$, two different products are formed (**1.28** and **1.29**, Scheme 1.14). Reaction with Cp_2ZrMe_2 results in abstraction of a methyl group and formation of a Zr/P Lewis pair. Reaction with $Cp^*_2ZrMe_2$ also involves methyl abstraction, but the Zr cation interacts with the P/B molecule through hydrogen bonding with the abstracted

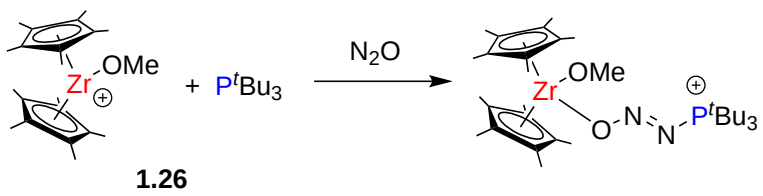

1.26

Scheme 1.13: Activation of N_2O with **1.26**. $[B(C_6F_5)_4]^-$ counterions omitted for clarity.

methyl group. The extra steric bulk of the Cp* ligands appears to be the cause of this difference. An advantage of these FLPs may be that the counterion is included within the system, which makes the overall compound/s neutral.

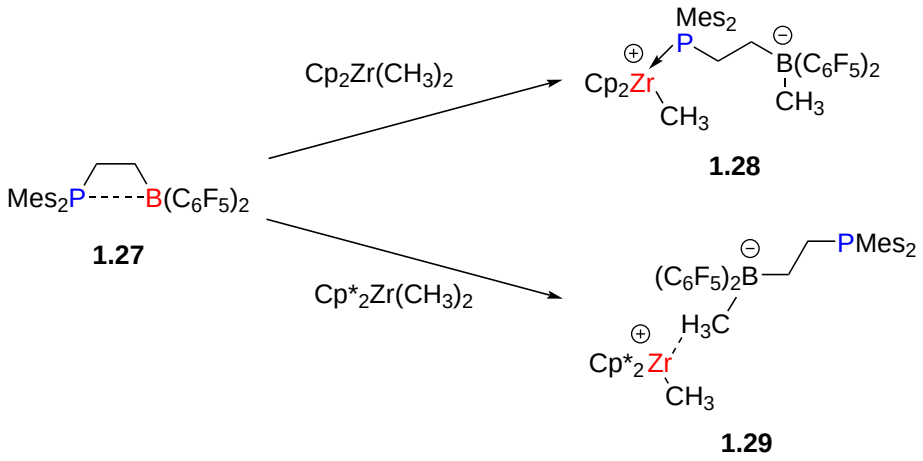

Scheme 1.14: Reaction of **1.27** with $Cp_2Zr(CH_3)_2$ and $Cp^*_2Zr(CH_3)_2$ to form **1.28** and **1.29**.

Although there is a significant interaction between both moieties in **1.28** and **1.29**—consolidated in their solid state crystal structures—the lack of a tether means that they still behave as intermolecular systems, all the more so when any interaction is dynamic (although this is not explicitly stated for **1.28** as it was for **1.18**–**1.25**). The presence of a methyl group (instead of the -OMes ligand in **1.18**–**1.25**) may also be one reason why a Zr–P bond is not seen for these compounds, whereas it is for **1.28**.

FLP **1.27** behaves as expected when reacting with benzaldehyde and CO_2, forming the typical FLP products **1.30** and **1.31** (Scheme 1.15).[29] **1.28** and **1.29** react in a very similar manner; the reaction of **1.28** with benzaldehyde gives the 1,2-addition product **1.32** (Scheme 1.16), and the reaction of both with CO_2 gives the congeners **1.33** and **1.34** (Scheme 1.17). **1.28** has also been used to activate *p*-tolyl isocyanate to give **1.35** (Scheme 1.18), with the phosphine bonding to the isocyanate carbon, and the Zr bonding

to the charge across the conjugated OCN system.

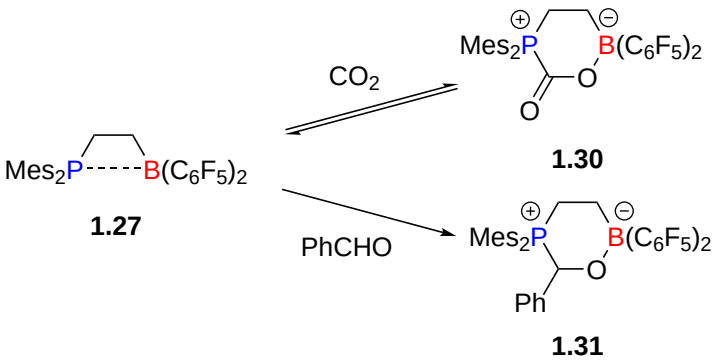

Scheme 1.15: Reactions of **1.27** with PhCHO and CO_2 to form **1.30** and **1.31**.

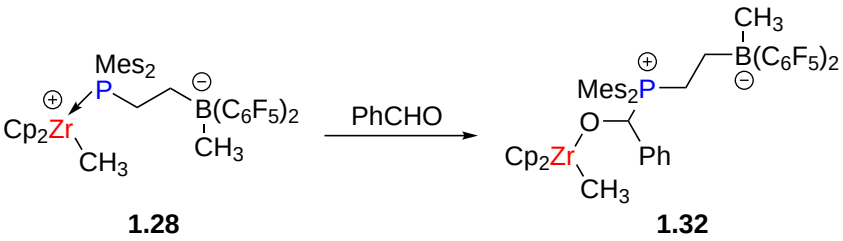

Scheme 1.16: Reaction of **1.28** with benzaldehyde to form **1.32**.

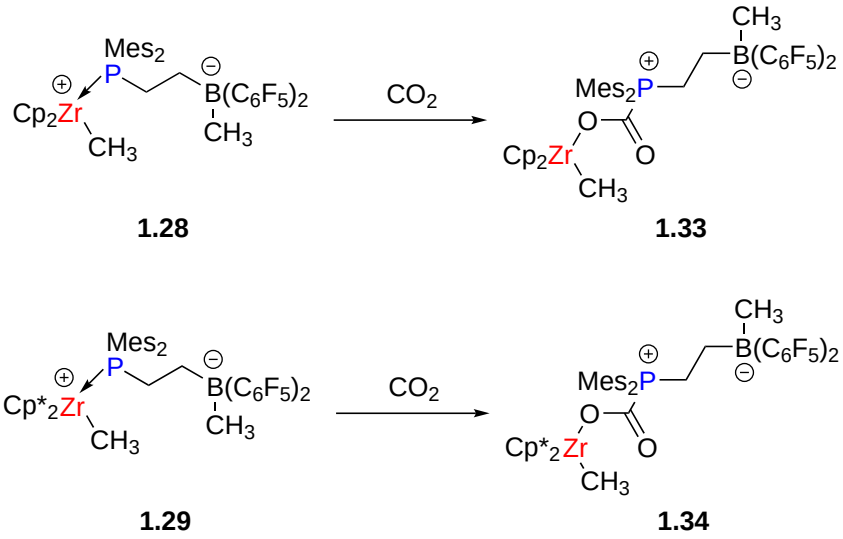

Scheme 1.17: Reactions of **1.28** and **1.29** with CO_2.

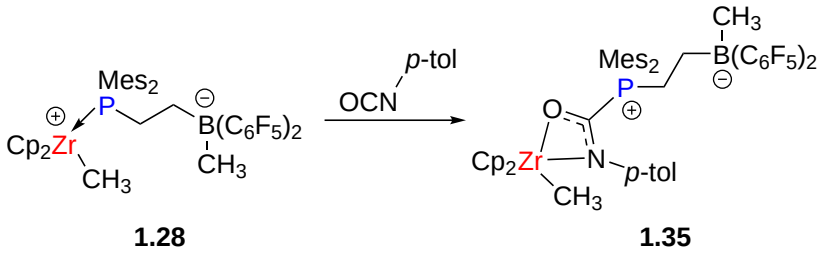

1.28 **1.35**

Scheme 1.18: The reaction of **1.28** with *p*-tolyl isocyanate.

A similar FLP to **1.28** is formed when **1.36** is reacted with $B(C_6F_5)_3$ to give **1.37** (Scheme 1.19).[30] This compound is capable of C–Cl bond cleavage in addition to isocyanate activation. One point of note is the slightly different bonding seen between **1.35** and **1.39**, with the latter showing a Zr–O bond, rather than the Zr interacting with a conjugated O–C–N moiety. The reaction with dichloromethane shows that other Zr/P FLPs are capable of activating R–Cl bonds, in addition to those mentioned earlier in this chapter.

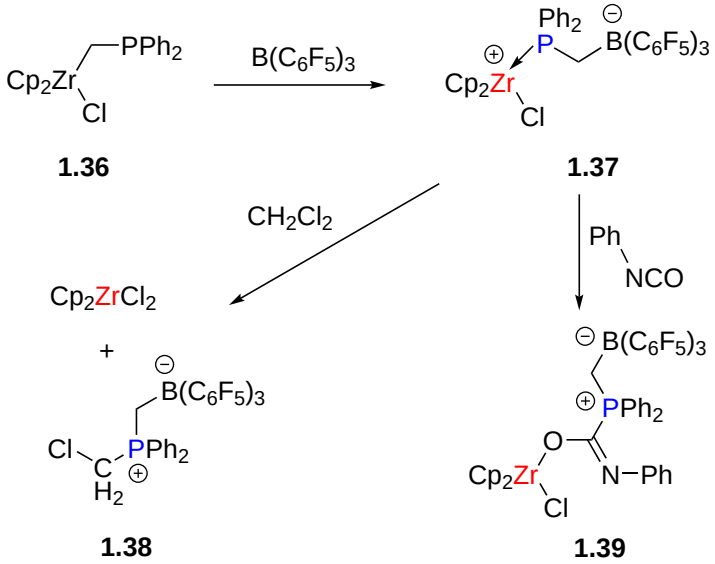

1.36 **1.37** **1.38** **1.39**

Scheme 1.19: Synthesis of **1.37** and subsequent reaction with CH_2Cl_2 and phenyl isocyanate.

Perhaps of greater interest is the reaction that occurs when **1.36**, $B(C_6F_5)_3$, and benzaldehyde are all combined in solution (Scheme 1.20). In this case, the active Lewis

pair is that between the phosphine and borane moieties, rather than with the Zr. Perhaps this is because **1.37** has not had time to form before reaction with benzaldehyde occurs. However, it could also be an example of two competing FLP environments, with the P/B FLP favoured over the Zr/P FLP.

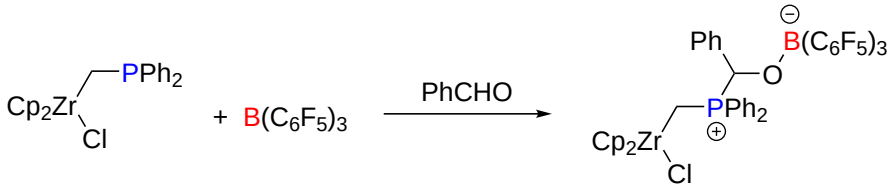

1.36 **1.40**

Scheme 1.20: Reaction of **1.36**, $B(C_6F_5)_3$, and PhCHO in solution.

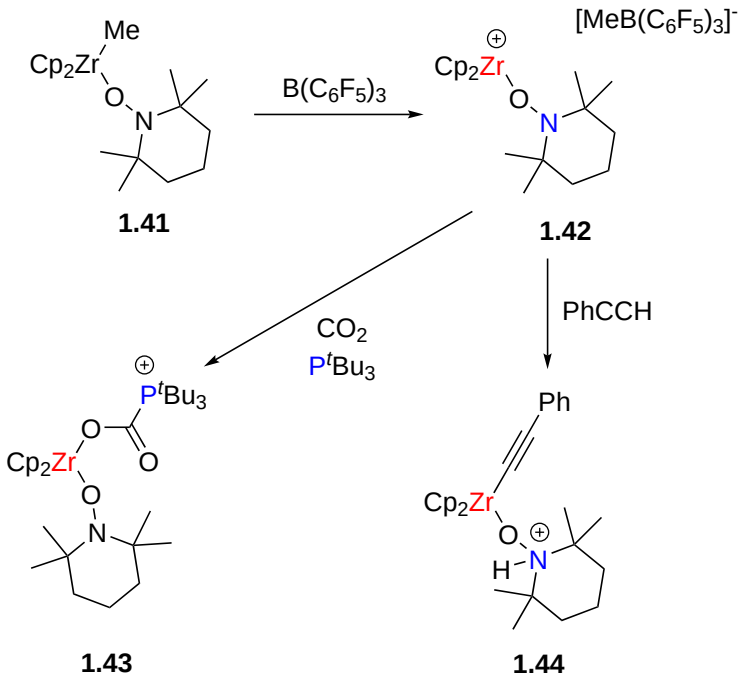

1.41 **1.42** **1.43** **1.44**

Scheme 1.21: Formation of **1.42** followed by reaction with P^tBu_3/CO_2 and phenylacetylene.

Another intermolecular Zr FLP reported by Erker and co-workers is shown in Scheme 1.21, with the Zr cation containing a TEMPO moiety. Upon formation of **1.42** through reaction of **1.41** with $B(C_6F_5)_3$ an intramolecular FLP is formed, with the TEMPO ni-

trogen atom acting as a Lewis base, as demonstrated when this compound is used for the activation of phenylacetylene to form **1.44**. However, when P^tBu_3 is added to **1.42**, an intermolecular FLP is formed, which is capable of activating CO_2 to form **1.43**. This is another example of competition, with reaction with the phosphine favoured over TEMPO.[50]

1.2.3 Zirconium-nitrogen frustrated Lewis pairs

The prevalence of Zr/N FLPs (either intra- or inter-molecular) in the literature is far lower than their Zr/P counterparts, although examples do exist. Nitrogen itself has been extensively used as the Lewis basic component in main group FLP chemistry, with an abundance of different FLPs showing their ability to perform a wide variety of reactions.[5,31–33] Pyridine and piperidine based compounds appear to be most commonly used,[34–42] however, the use of other species such as amines have also been reported.[43–45]

Although not always mentioned as such, the hydrogenation of imines using a Lewis acid catalyst often contains FLP chemistry, with heterolytic cleavage of dihydrogen occurring between the Lewis acid and Lewis basic imine. $B(C_6F_5)_3$ in particular has been used for the hydrogenation of a wide range of imines, in addition to other borane based Lewis acids.[46–48] The general mechanism for these reactions is shown in Scheme 1.22, where the FLP behaviour is evident in the initial step.[49]

Imine hydrogenation has also been performed using Zr based FLPs, with **1.6**–**1.9** all used for the hydrogenation of ^{t}BuN=CHPh, albeit with poor reactivity.[26] However, removal of the phosphine moiety results in a significant improvement in reactivity, with cations **1.45**–**1.49** (Figure 1.6) able to catalyse the reaction. **1.48** has been found to be the most effective, and is also used to activate a selection of different imines. The more sterically bulky catalysts appear to perform better, which perhaps makes it surprising

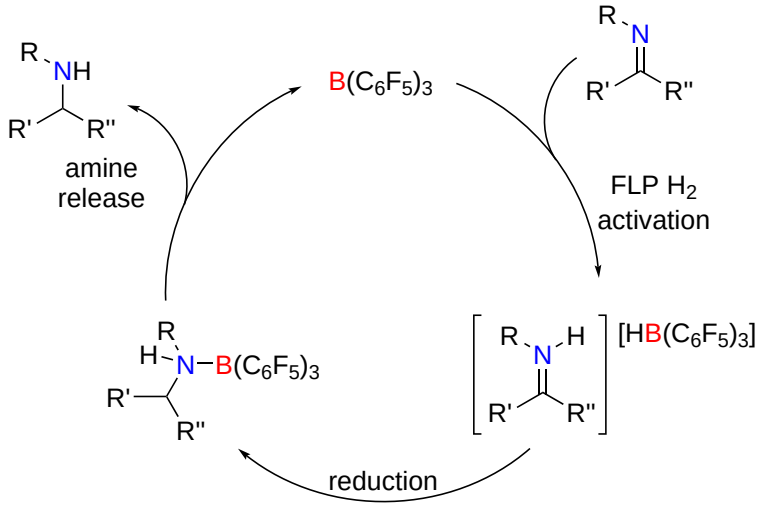

Scheme 1.22: Reported catalytic cycle for the hydrogenation of an imine with $B(C_6F_5)_3$.

that **1.49** displayed no catalytic activity, with the reaction stopping after the initial H_2 activation step. This may be because **1.49** is excessively bulky and does not allow for binding of the protonated imine species at the Zr centre in the second reaction step. It is also surprising that **1.45** displays catalytic reactivity, as work discussed previously in this chapter (and indeed, work within this thesis) shows **1.45** (in combination with an amine or pyridine) to be incapable of activating hydrogen due to the absence of a Cp* ligand. This may indicate a separate reaction mechanism for **1.45**, one which involves direct activation of the imine rather than initial activation of H_2.

As shown in the proposed catalytic cycle in Scheme 1.23,[26] the reaction mechanism appears to replicate that shown for $B(C_6F_5)_3$ (Scheme 1.22). Not only is this useful for demonstrating the efficacy of Zr cations as potential Lewis acid catalysts, but it also shows the potential of intermolecular Zr/N FLPs and is one of the instigators for the Zr/N work reported within this thesis.

Currently, there seems to be only two other reported examples of Zr/N FLPs, both by the Erker group. The first is compound **1.42** discussed in the previous section, and is used

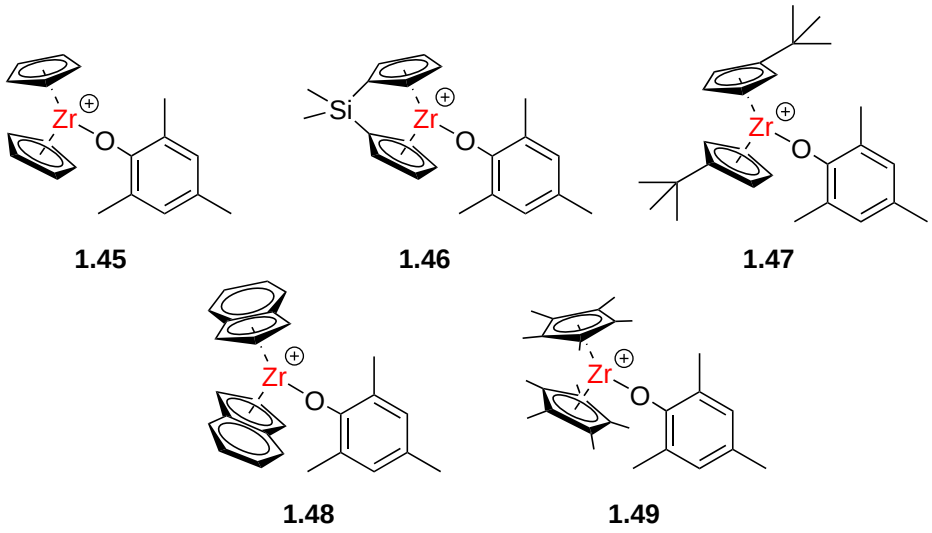

Figure 1.6: Zr cations used for imine hydrogenation. $[B(C_6F_5)_4]^-$ counterion omitted for clarity.

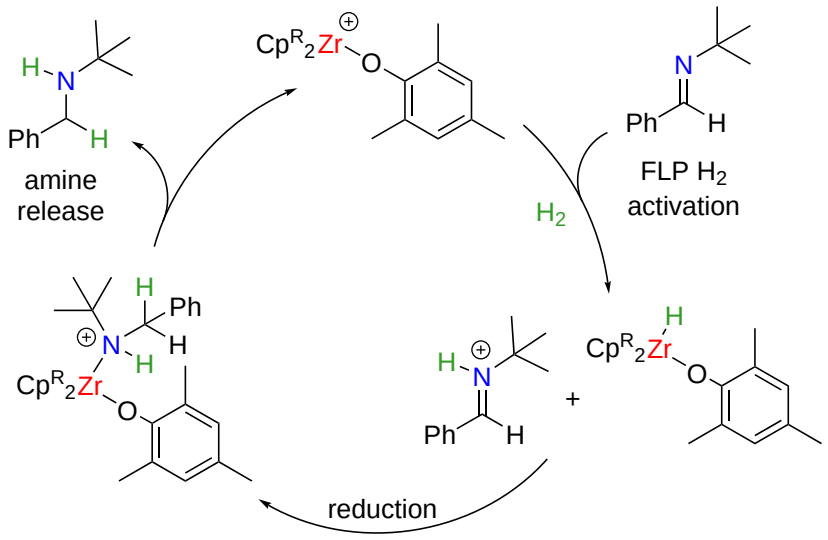

Scheme 1.23: The hydrogenation of ^{t}BuN=CHPh with Zr cations. $[B(C_6F_5)_4]^-$ counterion omitted for clarity.

for the activation of phenylacetylene.[50] The second is compound **1.50** shown in Scheme 1.24, which is a diisopropylamino analogue to **1.14** and **1.15**. Synthesised in a similar manner, through the reaction of $Cp^*_2ZrMe_2$ with the relevant aminoethanol compound followed by methyl abstraction with $[CPh_3][B(C_6F_5)_4]$, **1.50** has been demonstrated to be effective for a number of different reactions.[51] Typical FLP reactivity was seen upon

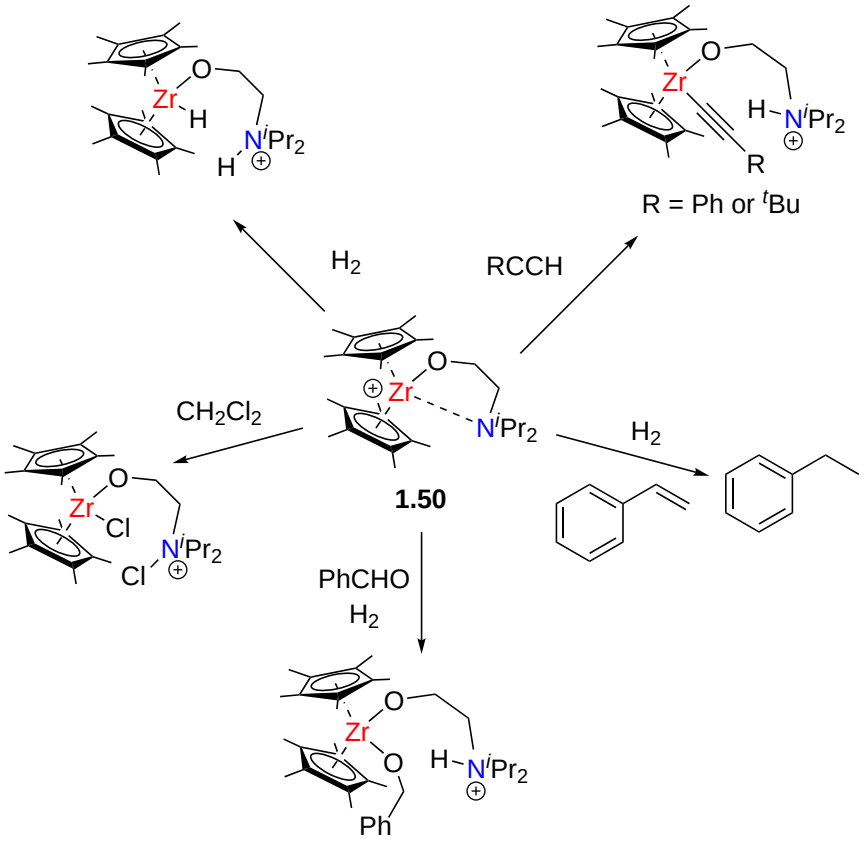

Scheme 1.24: Small molecule activation and hydrogenation reactions of **1.50**. $[B(C_6F_5)_4]^-$ counterions omitted for clarity.

reaction with H_2, CH_2Cl_2, phenylacetylene, and *tert*-butylacetylene. However, perhaps of greater interest is the two hydrogenation reactions that it successfully carries out. The first is the hydrogenation of benzaldehyde, with the protonated product remaining bound to the metal, which is typical for the previously discussed Zr FLP reactions with carbonyl containing substrates. The second is the hydrogenation of styrene, which results in clean release of the ethylbenzene product. This reaction is of particular interest as it shows the catalytic potential of **1.50**. Indeed, **1.50** has been used for the hydrogenation of a wide range of different alkenes and alkynes, with >99% conversion achieved for certain substrates with 4 mol% catalyst loading within 3 h. The mechanism is proposed to involve initial heterolytic cleavage of H_2 by **1.50**, followed by insertion of the substrate into the Zr–

H bond, before the N–H proton is transferred to the bound substrate and the hydrogenated product is then released.

It is clear from examining the literature that the lack of research into Zr/N FLPs paves the way for further work to be carried out in this area. The viability of Zr/N FLPs is displayed by the activity of **1.50**, and the potential for intermolecular Zr/N FLPs is shown by the hydrogenation of imines with **1.45**–**1.48**. The work in Chapters 2 and 3 seeks to take a step towards understanding the capabilities of intermolecular Zr/N systems and demonstrates that they are indeed able to perform small molecule activation, as well as catalytic, reactions.

1.3 Coordination chemistry of magnesium

For the majority of the 20th century, the chemistry of magnesium was dominated by the stoichiometric Grignard reaction, which was first reported in 1900 and still remains one of the most useful tools in chemical synthesis.[52] However, the perception of the utility of magnesium (and indeed, the rest of the alkaline earths) has significantly changed, with Mg complexes used for a wide variety of transformations, both stoichiometrically and catalytically.[53–56] The desire to explore group 2 chemistry has been driven by the need for cheaper alternatives to industrially important precious metal catalysts, and the relative abundance of the alkaline earths makes them a prime subject for study.

One of the reasons why transition metals (TMs) have often been favoured in place of their group 2 counterparts is that the relatively stable +2 oxidation state the alkaline earths (Ae) usually possess—but not always—does not allow for the variable oxidation states that have made TMs so useful. The bonding of the heavier group 2 elements also

tends to be of an ionic nature as the elements become more polarised moving down the group (Figure 1.7), however, the bonding of magnesium seems to be of a more covalent nature. This is one of the reasons why Mg complexes are less likely to undergo Schlenk-type equilibria, whereby ligand exchange between complexes can result in undesired species (Scheme 1.25), perhaps making them more practical choices for certain reactions. Efforts to combat this unwanted rearrangement often involve the use of large stabilising ligands that are strongly bound and prevent ligand exchange by surrounding the metal centre; examples include β-diketiminates,[57–59] borates,[60] and bisimidazolines.[61]

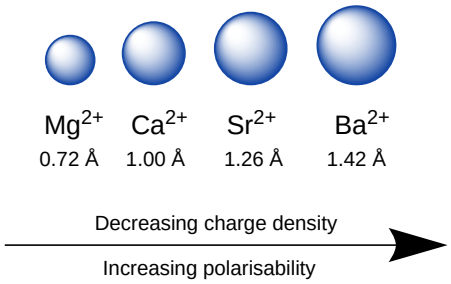

Figure 1.7: Change in radii of the alkaline earths.[56]

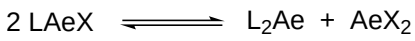

Scheme 1.25: A Schlenk-type equilibrium.

The Ae^{2+} state is often compared to trivalent lanthanide complexes (with the structure L_2LnX) which are also redox inactive, possessing a d^0 electronic configuration. The reactivity of the lanthanides is dominated by polarised insertion and σ-bond metathesis steps in the mechanistic cycle.[62,63] The chemistry of both Ae^{2+} and Ln^{3+} metal centre mediated catalysis incorporates the mechanistic steps shown in Scheme 1.26.[64] The polarity of the E–H substrate controls whether the σ-metathesis step results in the formation of a metal hydride or a L_2M–E fragment, which then continue in the catalytic cycle to complete a heterofunctionalisation reaction.[56,65]

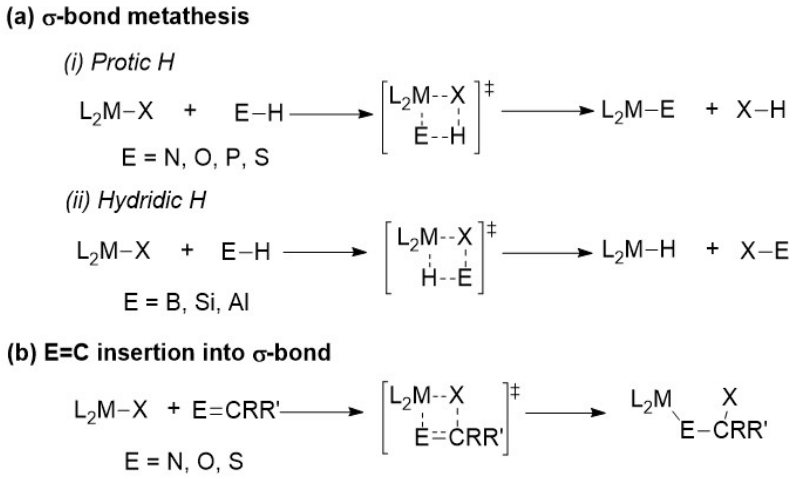

Scheme 1.26: The key steps in Ae^{2+} and Ln^{3+} mediated catalysis.[56]

Much work has been done with a plethora of different Mg complexes, however, in this introduction only the chemistry most relevant to this research has been examined,[65] therefore the rest of this section will look at Mg β-diketiminate species and instances of Mg Lewis acids used in coordination chemistry.

1.3.1 Magnesium β-diketiminate chemistry

The magnesium chemistry reported within this thesis utilises β-diketiminate ligands, which not only help to stabilise the complex and prevent Schlenk rearrangements, but also have a wealth of reported reactivity within the literature which demonstrates their efficacy for the research shown in Chapters 4 and 5. The first Mg β-diketiminate complexes were reported by Gibson *et al.* in 2000, with the structure of the complexes varying depending on the steric bulk of the MgR_2 precursors alkyl ligands, and whether a coordinating solvent was used (Scheme 1.27).[66] Since then, the use of β-diketiminate ligands for Mg coordination chemistry has steadily increased, with the number of applications of these compounds rising year-on-year. Although Mg(I) chemistry has been the focus of much research since a stable Mg(I) dimer was first reported by Jones and co-workers in 2007,[67] this topic is

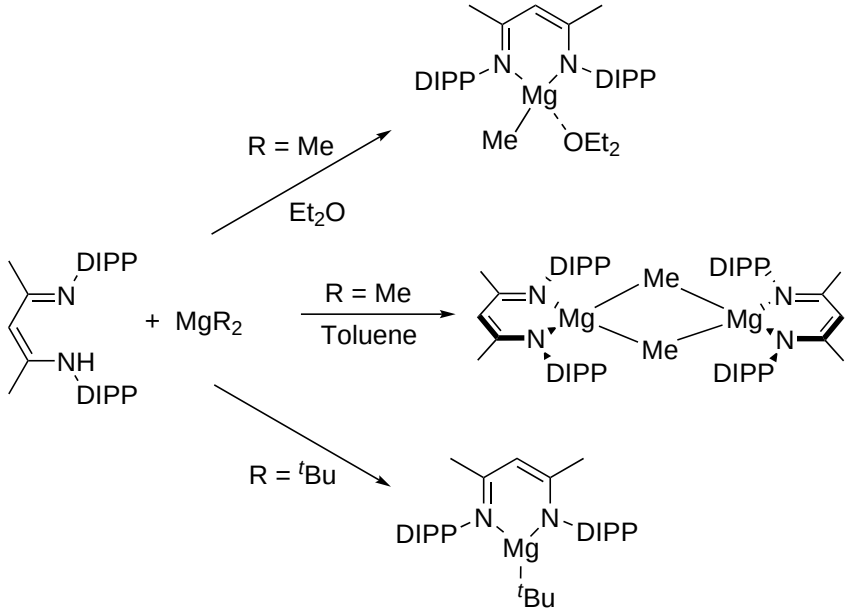

Scheme 1.27: Synthesis of β-diketiminates by Gibson *et al.* DIPP = diisopropylphenyl.

not discussed in much detail in this chapter in order to focus on chemistry that is more closely relevant to that conducted within this thesis.

1.3.1.1 Magnesium β-diketiminate hydrides

Many of the practical applications of Mg β-diketiminates involve hydride chemistry, particularly with regards to catalytic reactions, which often see Mg–H species playing a role in the catalytic cycle.[68] One of the initial driving forces behind research into Mg–H species was the search for new hydrogen storage materials, as other hydrogen-storage chemicals such as ammonia-borane have irreversible processes.[69] The Mg bridging hydride species **1.52** was first reported by Jones and co-workers in 2008,[70] through the reaction of **1.51** with $PhSiH_3$ (Scheme 1.28). A higher reaction temperature was required to form the slightly bulkier congener **1.54** from **1.53**.[71]

The Mg(I) β-diketiminate dimeric species **1.55**, which was also first reported by Jones and co-workers,[67] does not react with H_2 to form these compounds, supposedly as a result

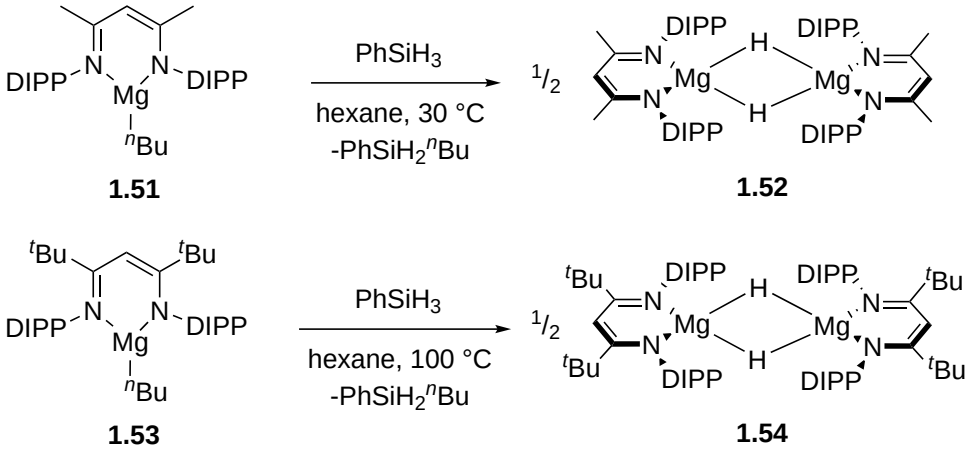

Scheme 1.28: Synthesis of the Mg hydride **1.52** and **1.54** through the reaction of **1.51** and **1.53** with $PhSiH_3$. DIPP = diisopropylphenyl.

of the kinetic barrier.[68,72] Instead, the bridging hydrides **1.54** and **1.57** are formed through reaction of the respective Mg(I) complexes with 1,3-cyclohexadiene,[73] which is found to be a more practical transfer reagent than Al(III) hydrides (Scheme 1.29).[74]

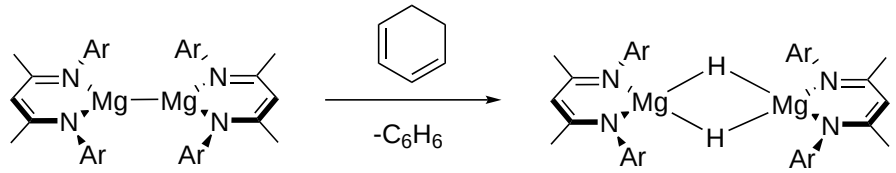

1.55: Ar = Ar = 2,6-$^{i}Pr_2$-C_6H_3
1.56: Ar = Ar = 2,6-Et_2-C_6H_3

1.54: Ar = 2,6-$^{i}Pr_2$-C_6H_3
1.57: Ar = 2,6-Et_2-C_6H_3

Scheme 1.29: Synthesis of the bridging hydride species **1.54** and **1.57** from the respective Mg(I) species.

Terminal Mg β-diketiminate hydride species have also been synthesised and isolated, with compound **1.59** formed from the reaction of **1.58** with $PhSiH_3$ (Scheme 1.30)—the more sterically bulky aryl groups prevent dimer formation.[75] Other terminal hydrides have been synthesised with less bulky aryl groups, however, a coordinating ligand is generally required to prevent dimerisation.[71]

Mg β-diketiminate hydrides have been used for the dearomatisation of pyridine and quinoline derivatives, with hydrogenation at the para position generally favoured, although

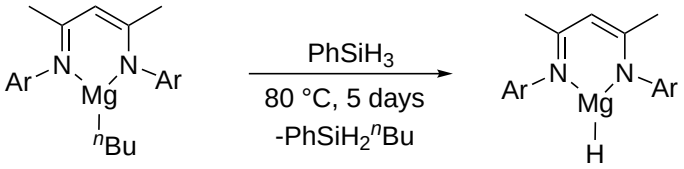

1.58 **1.59**

Ar = 2,6-$CHPh_2$-4-Me-C_6H_2

Scheme 1.30: Synthesis of a terminal Mg β-diketiminate hydride.

ortho substitution is also seen where this is not possible.[76,77]

1.3.1.2 Hydroboration

One of the reactions for which Mg β-diketiminates have found particular use is hydroboration,[78] with the catalytic coupling of a series of pyridines with pinacol-borane (HBpin) using **1.51** initially reported by Hill and co-workers in 2011.[79] However, the equivalent reaction with phenylsilane did not react catalytically, with the interaction between the pyridine and Mg centre preventing reaction with the silane. The hydroboration reactivity was extended to imines, nitriles, carbodiimides, isocyanates, isonitriles, aldehydes, and ketones–both aromatic and aliphatic—with the reactions proceeding under mild conditions and with low catalyst loading.[80–85] It is believed that the catalytic cycle involves formation of the Mg hydride species **1.54** (Scheme 1.31), which occurs upon reaction of HBpin with **1.51**.

The hydroboration of pyridines was also reported by Harder and co-workers,[86] making use of the multinuclear magnesium hydride species **1.60** and **1.61** (Figure 1.8). Differences were seen between the two species when used for the hydride reduction of pyridine, with **1.60** favouring reduction at the 2 position, and **1.61** favouring reduction at the 4 position. The extended bridge in **1.61** appears to shift reactivity, making it more similar to that

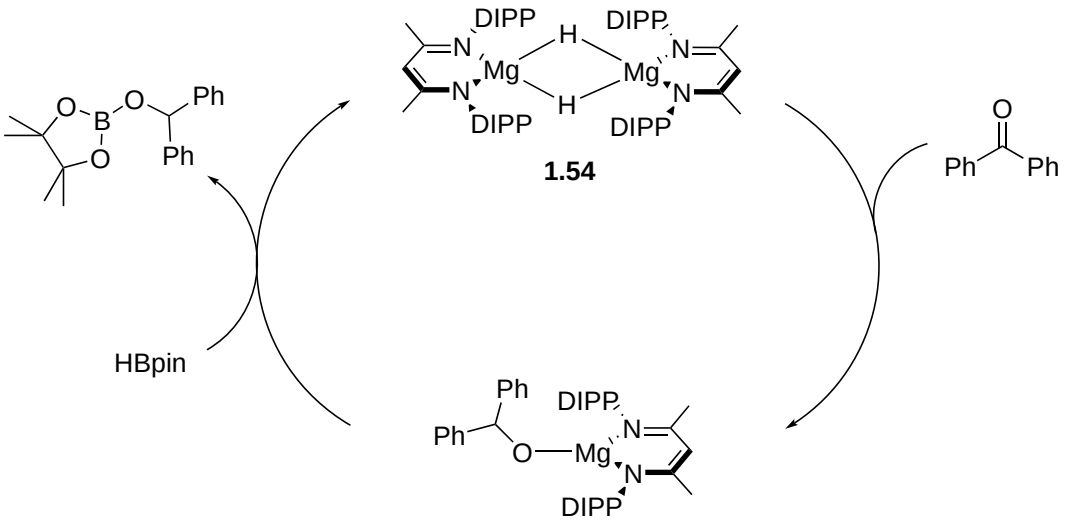

Scheme 1.31: Catalytic cycle for the hydroboration of benzophenone. **1.54** is generated in situ from **1.51**. DIPP = diisopropylphenyl.

of mononuclear hydride species. However, when used as a catalyst for the hydroboration of pyridine, **1.61** was found to be almost completely inactive, whereas **1.60** was found to not only be reactive, but also to be selective for certain substrates. 2-Picoline was reacted with HBpin to exclusively give the 1,4-product, and 4-picoline, quinoline, and isoquinoline all reacted to give the 1,2-products with 92%, 91%, and 100% selectivity respectively.

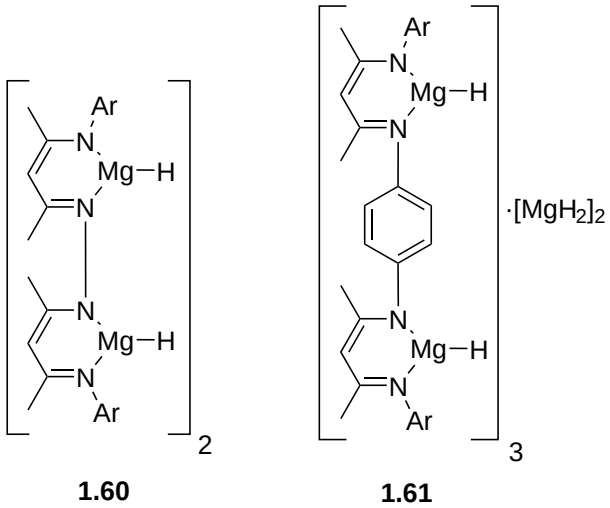

Figure 1.8: The multinuclear magnesium hydride species **1.60** and **1.61**. Ar = 2,6-^{i}Pr$_2$-C$_6$H$_3$.

1.3.1.3 Amine-borane dehydrocoupling

Amine-borane dehydrocoupling is an area of chemistry that has received an increased level of interest in recent years in the search for effective hydrogen storage materials, and magnesium chemistry has been applied in this endeavour. Initial reactions of Mg β-diketiminates with amine-boranes resulted in stoichiometric conversion to dehydrocoupled products, whereas the calcium analogues were able to perform the reactions catalytically—charge density and cationic radius are deemed to be key reasons for this difference.[87–89] This was thought to have been upgraded to a catalytic regime when cyclic boranes were used, with **1.51** appearing to attain full conversions for the reactions of HBpin and 9-BBN with a variety of amines within 1 h (Scheme 1.32).[90] However, these reactions were later shown to proceed in the absence of a catalyst.[91]

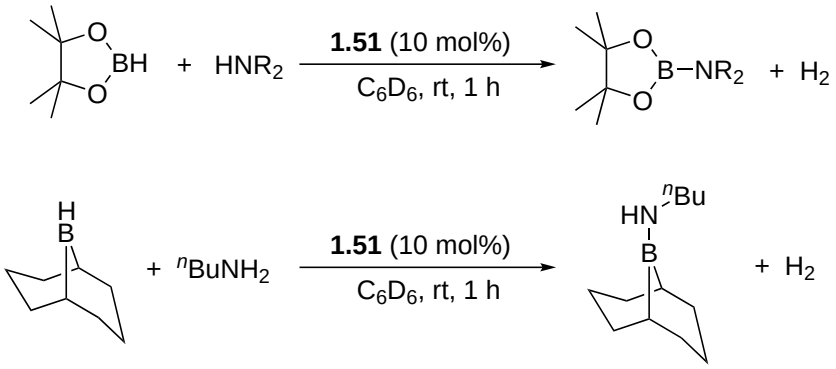

Scheme 1.32: Amine-borane dehydrocoupling of HBpin (top) and 9-BBN (bottom) using **1.51**.

1.3.1.4 Hydroamination

Hydroamination reactions using Ca β-diketiminate complex was reported by Hill and co-workers in 2005,[92] with Ca and Sr amides also found to be effective for the reaction in 2008.[93] The Mg β-diketiminate **1.62** was then used for the intramolecular hydroamination

of a series of aminoalkenes.[94] The reaction involves the σ-bond metathesis chemistry that is typical of group 2 elements, with the insertion of the alkene into the Mg–N bond as the rate-determining step (Scheme 1.33). Despite **1.62** attaining high yields for a number of different aminoalkenes, a similar calcium catalyst was still found to be more effective, with the larger atomic radii of Ca allowing for greater substrate binding capability.[95]

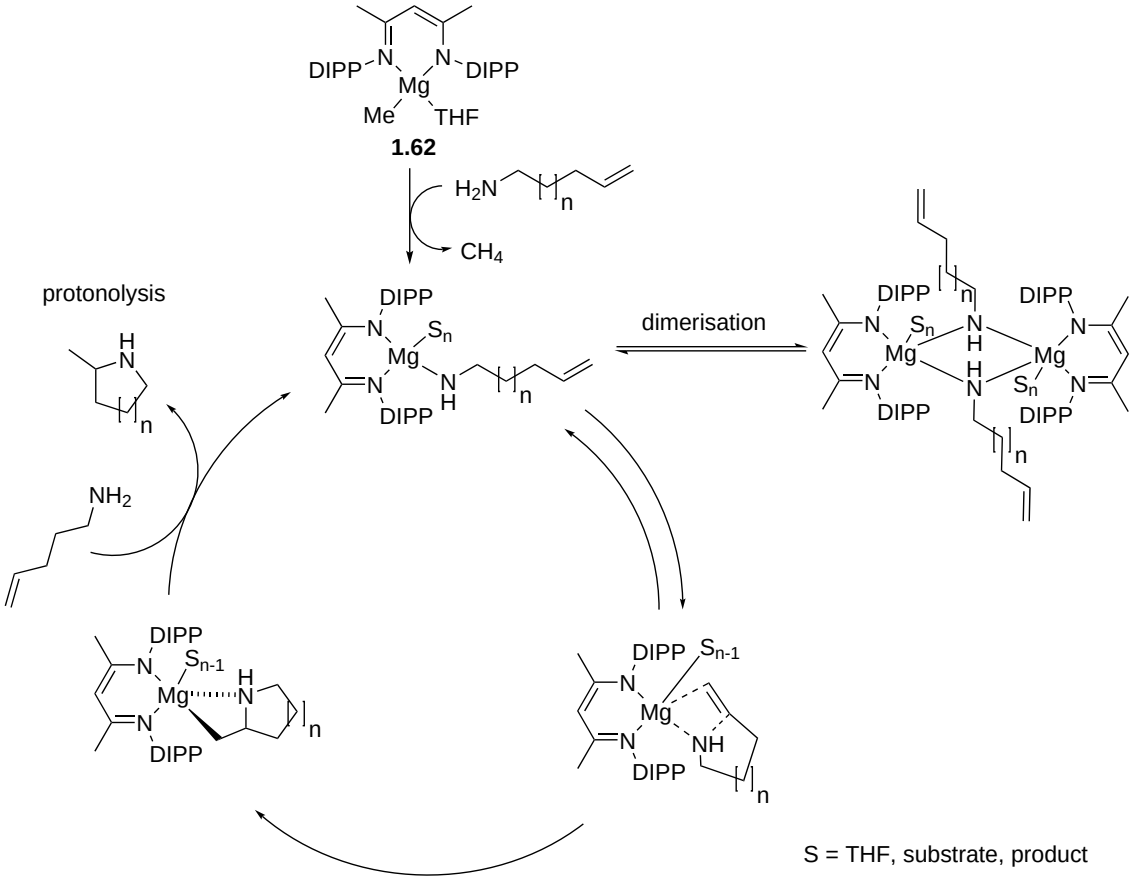

Scheme 1.33: Proposed mechanism for the intramolecular hydroamination of aminoalkenes using **1.62**. DIPP = diisopropylphenyl.

1.3.1.5 Small molecule activation and transformation

Being able to convert small molecules into more valuable products is a constant goal of chemists, and Mg β-diketiminates have been used with this aim in mind. The Hevia group has recently used compounds **1.63** and **1.64** (Figure 1.9) for the activation of both

C–H and C–F bonds in fluoroarenes.[96–98] Initially, **1.63** was used for the metallation of fluoroarenes before it was used in a Negishi cross-coupling with iodobenzene. However, when **1.64** is reacted with 2-(2,4-difluorophenyl)pyridine it results in the stoichiometric substitution of a fluoride with the ^{n}Bu group on **1.64**, with a bridging Mg fluoride species forming concurrently. It has been worked out that the use of different ligands in place of -^{n}Bu could allow for the coupling of a variety of different compounds, which is demonstrated with the coupling of 2-(2,4-difluorophenyl)pyridine with benzofuran. In this reaction, **1.63** is used for the activation of both a C–H and a C–F bond (Scheme 1.34).

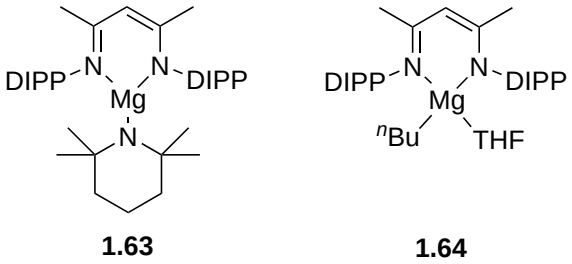

1.63 **1.64**

Figure 1.9: Compounds used for fluoroarene activation and cross-coupling. DIPP = diisopropylphenyl.

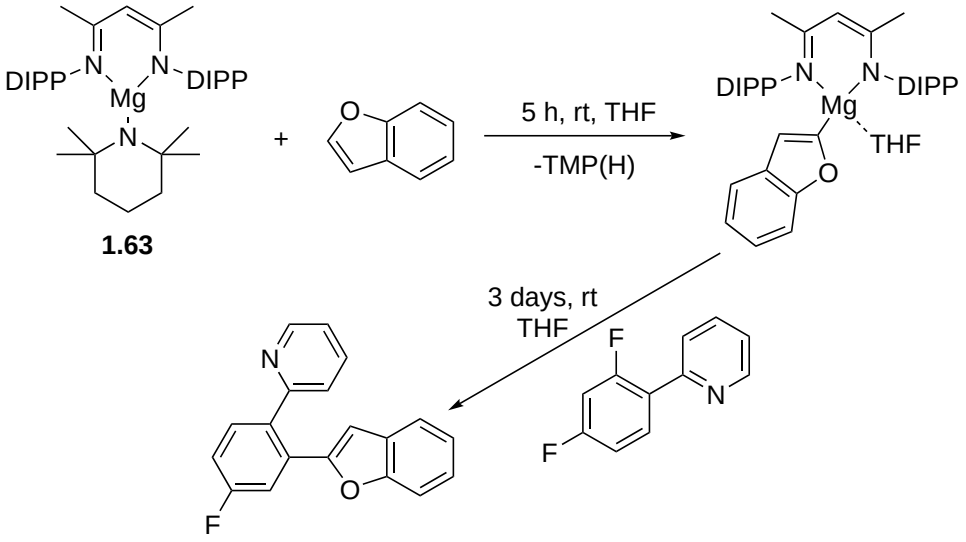

Scheme 1.34: Cross-coupling of benzofuran with 2-(2,4-difluorophenyl)pyridine using **1.63**. DIPP = diisopropylphenyl.

In addition to the further cross-coupling of non-directional fluoroarenes and both cyclic and non-cyclic amines, a further difference in reactivity between **1.63** and **1.64** has also been demonstrated. **1.63** was shown to favour C–H activation in the first instance, whereas **1.64** favours C–F activation (Scheme 1.35).[98]

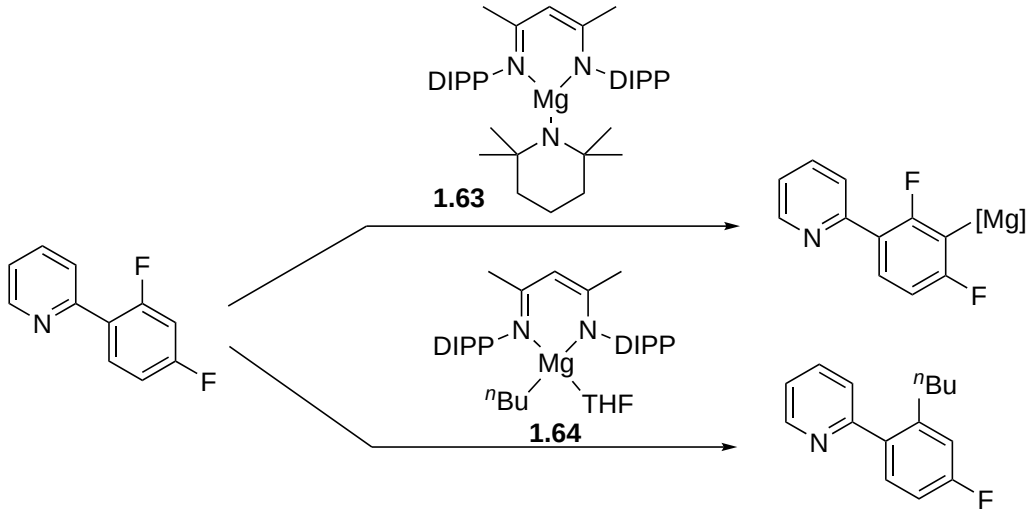

Scheme 1.35: Differences in reactivity between **1.63** and **1.64**.

Mg β-diketiminates have also been used for CO reduction. The Mg hydride **1.52** is shown to reduce CO upon reaction at room temperature (Scheme 1.36) and, when combined with $PhSiH_3$, this results in the catalytic formation of methylphenylsilane.[99,100]

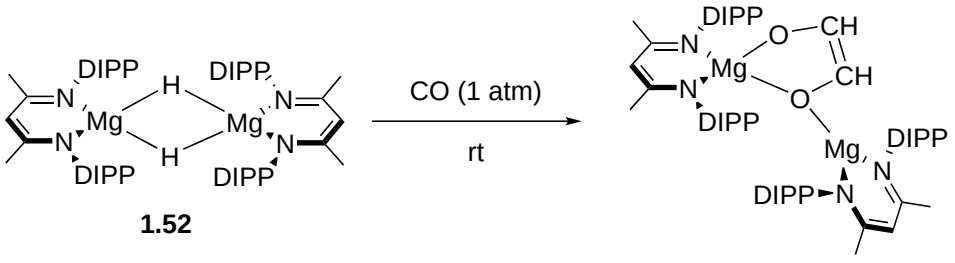

Scheme 1.36: The reduction of CO using **1.52**. DIPP = diisopropylphenyl.

More recently, the Ma group has used **1.51** for the activation of a series of chalcogen compounds,[101] and reaction with octasulfur results in the formation of a dimeric bridging species where sulfur atoms have inserted in the Mg–^{n}Bu bond (Scheme 1.37). The reaction

proceeds slightly differently when **1.51** is reacted with cyclooctaselenium in the presence of THF, with a mononuclear complex forming which contains two Se atoms both bonded to the Mg centre, having inserted into the Mg–^{n}Bu bond. The reaction could perhaps result in dimerisation in the absence of THF.

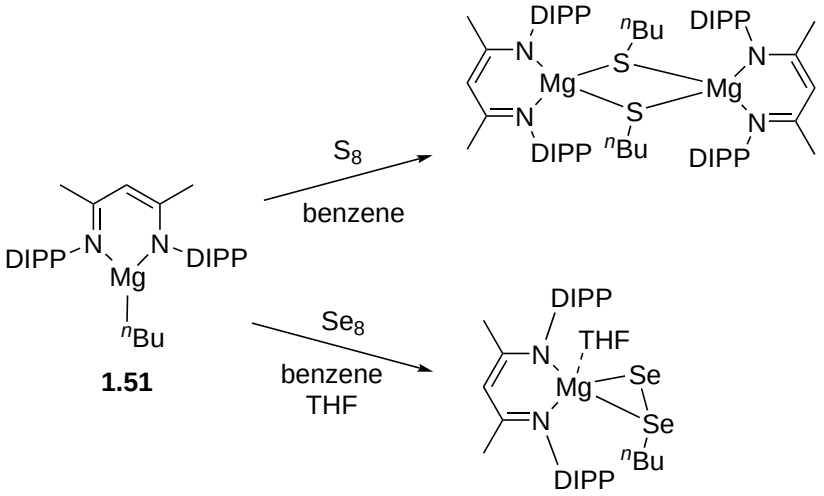

Scheme 1.37: Reaction of **1.51** with octasulfur and cyclooctaselenium. DIPP = diisopropylphenyl.

1.51 has also been reacted with diphenyl disulfide and diphenyl diselenide to give the magnesium phenyl chalcogenolate products (Scheme 1.38), occurring alongside the release of a PhE^{n}Bu side-product (E = S or Se).[101]

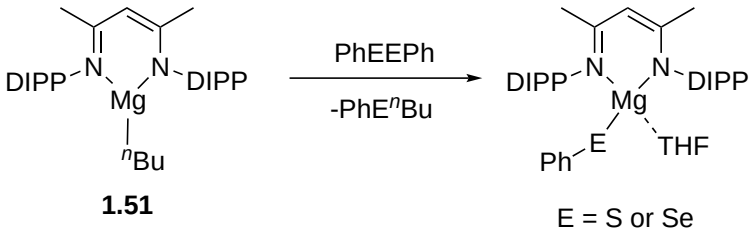

Scheme 1.38: The reaction of **1.51** with diphenyl disulphide and diphenyl diselenide. DIPP = diisopropylphenyl.

Reactions with the unsaturated compounds benzonitrile and phenylisothiocyanate have also been performed (Scheme 1.39).[101] The reaction of **1.51** with benzonitrile (2 eq.) in

the presence of dimethoxyethane (DME) results in the insertion of the substrate in the Mg–^{n}Bu bond, in addition to 1,3-hydrogen migration from a ^{n}Bu carbon to the nitrogen, resulting in the formation of a magnesium-1-azaallyl complex. Reaction of **1.51** with two equivalents of phenylisothiocyanate proceeds differently. One PhNCS molecule bonds to the Mg centre through the conjugated SCN moiety, whereas a second molecule acts as a bridge between the Mg centre and the central carbon of the β-diketiminate ligand. This is a binding mode that has been seen with other metal β-diketiminates,[102] and indeed, occurs with other Mg β-diketiminates as well (*vide infra*).[103]

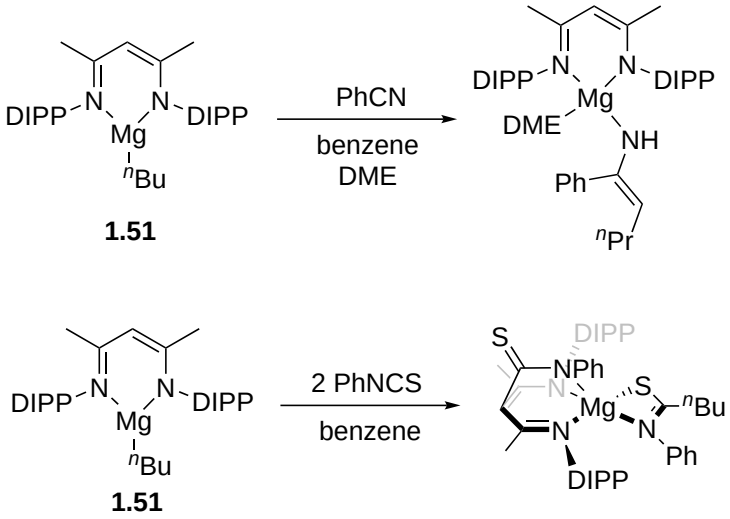

Scheme 1.39: Reaction of **1.51** with benzonitrile and phenylisothiocyanate. DIPP = diisopropylphenyl, DME = dimethoxyethane.

The activation of organoisocyanates has been performed using Mg dihydropyride complexes, with the product varying depending on the steric bulk of the substrate.[104] Upon reaction of **1.65** with ^{i}PrNCO or EtNCO, there is insertion of the isocyanate between the Mg and dihydropyride moiety (Scheme 1.40). In effect, the Mg centre and nitrogen compound are behaving as a Lewis pair, the binding mode of the product akin to that seen with some of the zirconium FLPs shown in the previous section. However, upon the

reaction of **1.65** with ^{t}BuNCO and AdNCO (Ad = adamantyl), C–H activation and C–C coupling at the 3 position is seen on the dihydropyride, with the proton migrating to the nitrogen of the isocyanate resulting in the formation of an amide.

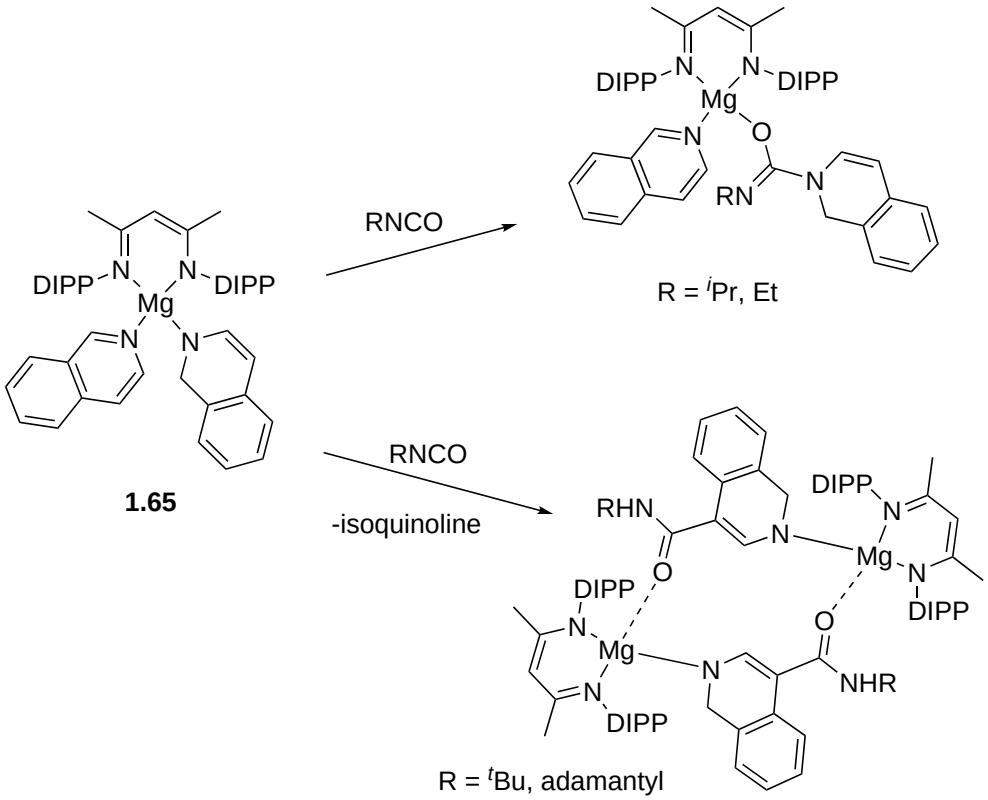

Scheme 1.40: The reactions of **1.65** with isocyanates of varying steric bulk. DIPP = diisopropylphenyl.

Oxygen activation has also been achieved with β-diketiminates, with the Lewiński group reacting the Mg complex **1.66** with dry air, both in the presence and absence of THF (Scheme 1.41).[105] In the absence of THF (using a toluene or dichloromethane solvent) a dimeric complex is formed, whereby the bridging moieties are formed from the insertion of O atoms into the Mg–$CH_2{}^{t}$Bu bonds. The inclusion of THF prevents dimer formation, and instead two atoms of O are inserted within the Mg–$CH_2{}^{t}$Bu bond, forming an alkylperoxide complex. The use of a phenyl group in place of the tert-butyl group resulted in slightly different reactivity (Scheme 1.42). Upon reaction of **1.67** with dry air

at -20 °C, the formation of a dimeric alkylperoxide was seen, which then converted to the alkoxide congener upon warming to room temperature.[106]

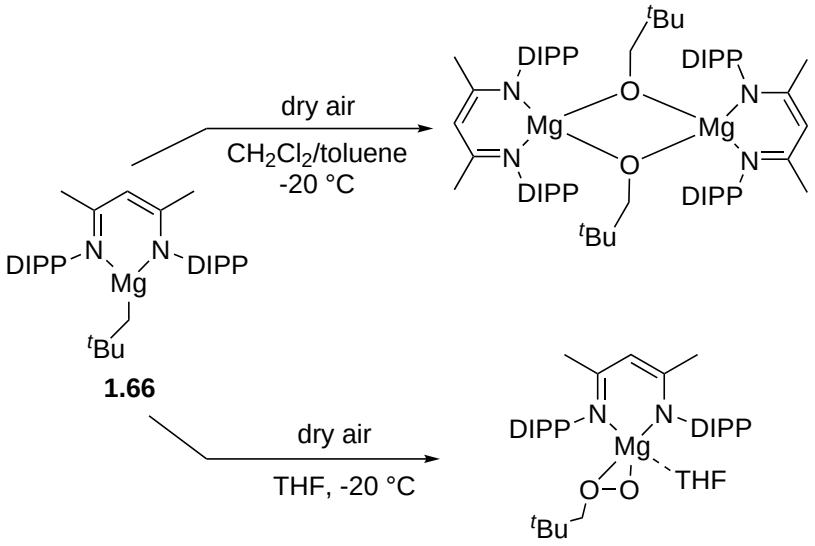

Scheme 1.41: Reactions of **1.66** with dry air. DIPP = diisopropylphenyl.

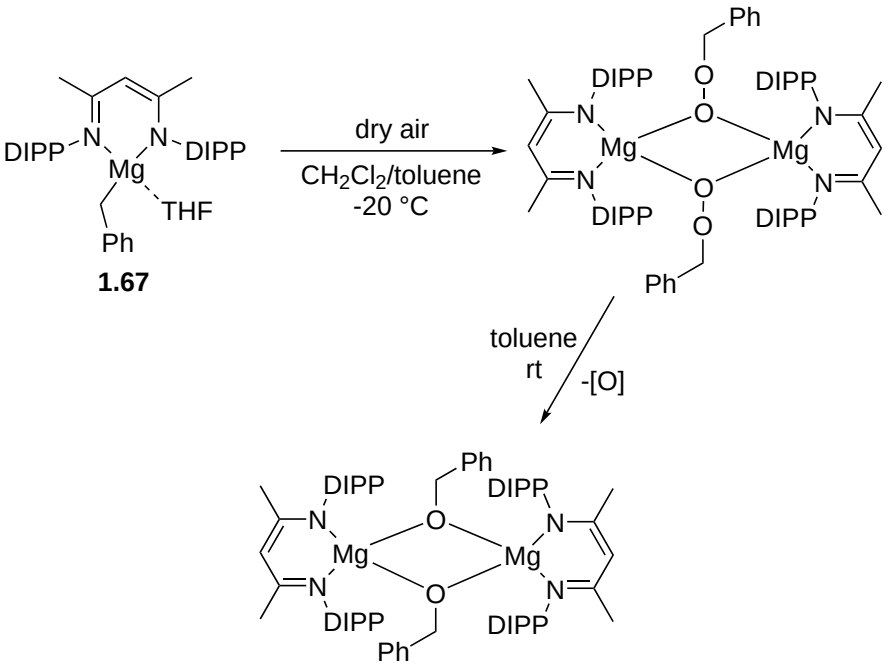

Scheme 1.42: Reaction of **1.67** with dry air. DIPP = diisopropylphenyl.

1.3.2 Magnesium Lewis acids

The work within this thesis is concerned with the use of Mg Lewis acids within the framework of cooperative or frustrated Lewis pair chemistry, however, this is not the first chemistry of this kind; a number of examples of Mg Lewis acids are present within the literature. Indeed, this topic has become much more popular, with an increase in articles focusing on this chemistry in both 2018 and 2019. Much of this work has focused on the synthesis of cationic Mg complexes to fill this role, where β-diketiminates are often chosen as the stabilising ligand.

Compound **1.69** shown in Scheme 1.43 was synthesised by Hill and co-workers in 2014,[103] and is formed of a Mg cation paired with an anionic borate partner. It is synthesised through the reaction of a previously published amidoborane complex with $B(C_6F_5)_3$,[88] resulting in the release of $[Me_2N–BH_2]_2$ and the ion pair. It has been shown to be capable of activating 2 equivalents of CO_2, forming the dimer shown in Scheme 1.44. This not only contains bridging formate, but also a CO_2 molecule bound between the Mg and γ-carbon on the β-diketiminate ligand, which in turn is bonded to $B(C_6F_5)_3$. **1.69** has also been used for the catalytic coupling of HBpin and CO_2 to form Bpin–O–Bpin and H_3COBpin.

Using a similar method that has been used for the formation of zirconocene cations (Section 1.2.1), the Mg complex **1.70** has been reacted with $[CPh_3][B(C_6F_5)_4]$ to form the Mg complex **1.71** (Scheme 1.45).[107] Only a very low yield of 12% is obtained, however, with the formation of clathrates proving an issue. The yield significantly improves upon the inclusion of benzene within the reaction solution, increasing the yield to 94%, with the benzene appearing to stabilise the product (**1.72**) through a stronger interaction than that seen with PhCl. In fact, the benzene proves irremovable from the complex even under

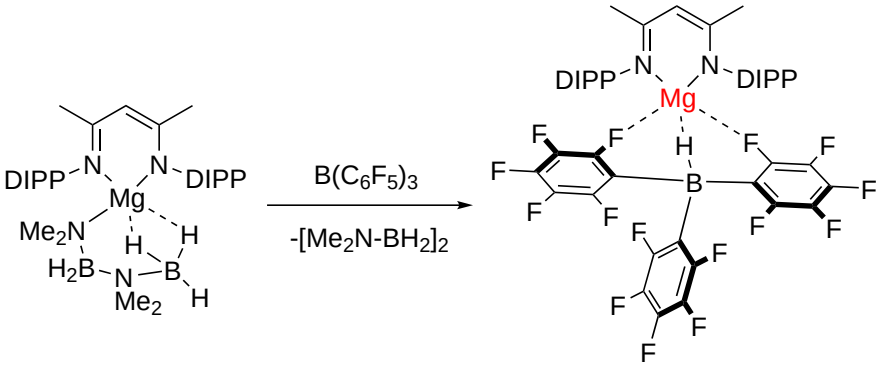

Scheme 1.43: Synthesis of **1.69** through the reaction of **1.68** with $B(C_6F_5)_3$. DIPP = diisopropylphenyl.

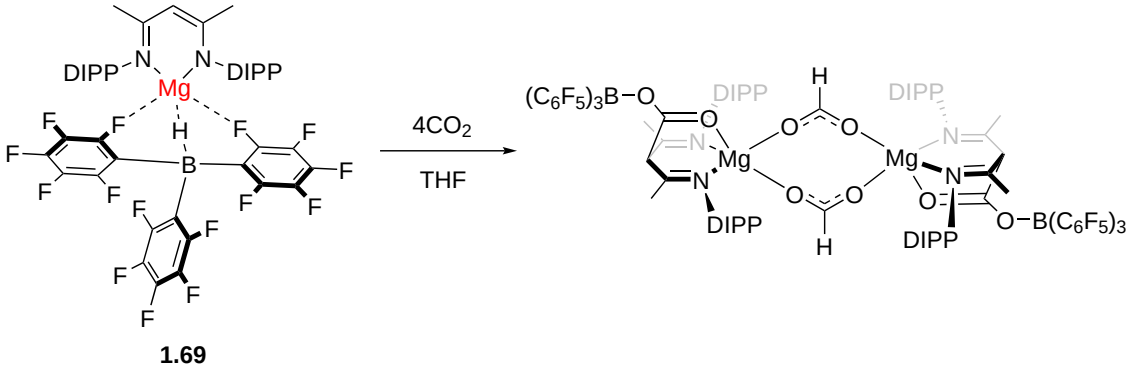

Scheme 1.44: Reaction of **1.69** with CO_2 in THF. DIPP = diisopropylphenyl.

high vacuum up to 60 °C. Reaction with an alkyne results in coordination to the Mg centre (**1.73**), with the Mg–alkyne bond calculated to be stronger than that with benzene.

The Gutmann-Beckett acceptor number (AN) has also been calculated for **1.71**, with a value of 70.3 obtained. This is lower than $B(C_6F_5)_3$ (AN = 77.1),[108] but could indicate that this species is better suited to product release, which can sometimes be an issue when using strong Lewis acids for catalysis. Interestingly, the analogous species with *tert*-butyl groups instead of methyl groups along the carbon backbone, have an AN value 76.0. This difference is attributed to the effect of the interactions with the anion in **1.71** which is not present in the bulkier compound. The *tert*-butyl groups push the DIPP groups closer to

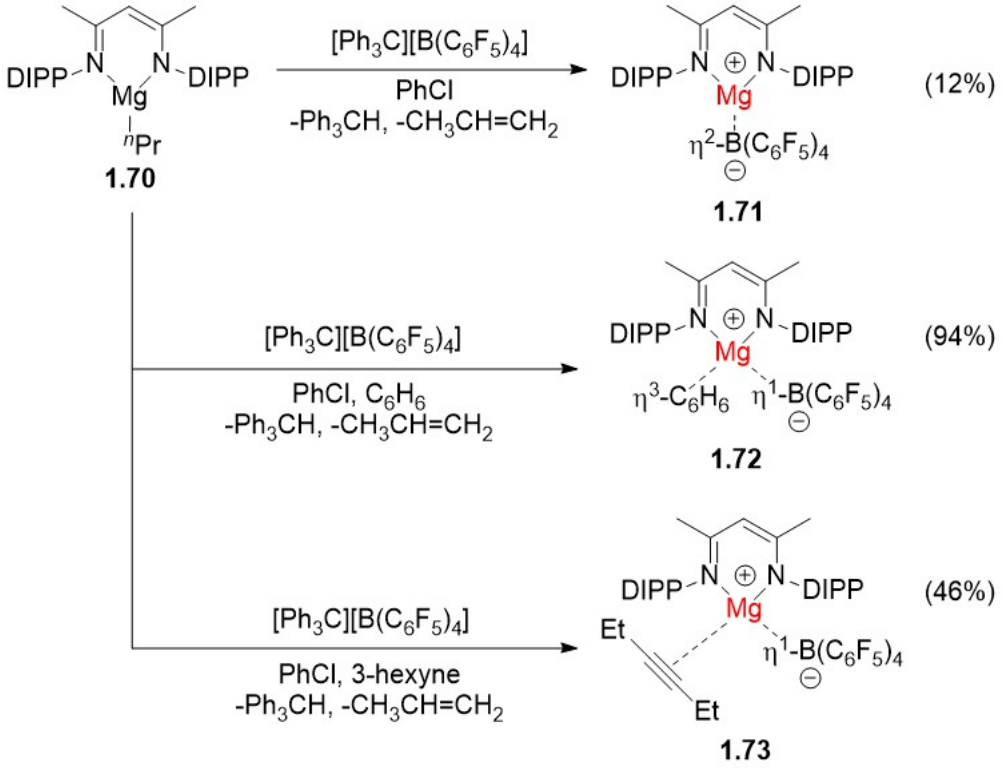

Scheme 1.45: Different synthetic routes to cationic Mg β-diketimates. DIPP = diisopropylphenyl.

the metal centre, reducing the available space for coordination of other molecules.[109]

Several other arene-coordinated Mg cations have also been synthesised; compounds **1.74** and **1.75** both reacted with triphenylphosphine for the formation of terminally coordinated phosphine adducts (Scheme 1.46). Although there is a formal Mg–P bond, clear comparisons can be made with cooperative or frustrated Lewis pairs, and it is not too difficult to imagine how an increase in lability of the Mg–P bond (through electronic or steric means) could result in the potential for interesting future reactivity.[110]

Other cationic species have been synthesised that do not employ a β-diketiminate ligand system, with the Sadow group[111] and Okuda and co-workers[112] reporting Mg cations with tris(oxazolinyl)borato and NNNN-macrocyclic ligand systems respectively.

The potential for Mg Lewis acids to operative within a cooperative or frustrated Lewis

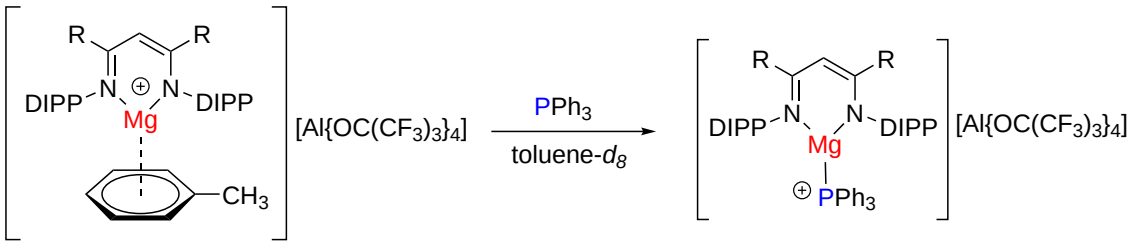

1.74: R = Me
1.75: R = ^{t}Bu

1.76: R = Me
1.77: R = ^{t}Bu

Scheme 1.46: The formation of terminally coordinated magnesium phosphine adducts.

pair system has already been discussed here with compounds **1.65**, **1.76**, and **1.77**. However, this has perhaps been more overtly displayed by the reaction shown in Scheme 1.47. Here we see both a monomeric magnesium complex and a magnesium dimer, with intramolecular phosphine moieties displaying coordination to the magnesium centres. Upon addition of THF, there is initial adduct formation, which develops into an FLP-type ring-opening reaction upon heating. The important factor here is the high lability of the Mg–P bond, which readily allows for THF insertion, whilst the HOMO-LUMO gap of the Lewis pair is of necessary size to allow for the ring-opening to take place.[113]

This concept was carried forward with the FLP-type activation of 1-butene oxide using the neutral Mg Lewis acids **1.81** and **1.82** in conjunction with PPh_3 to give **1.83** and **1.84** (Scheme 1.48).[114] Although coordination took place with other substrates (including carbodiimides, acetone, and an imine), no interaction with the Lewis base was seen. This is attributed to the lower Lewis acidity of **1.81** (AN = 58.9) and **1.82** (AN = 58.3), which is not deemed able to activate the substrates sufficiently for the nucleophilic attack of PPh_3—itself possessing low basicity. However, this does demonstrate that FLP-type reactivity of these complexes is possible, even if the right substrates and Lewis bases are required for reactivity to occur.

Much of the magnesium chemistry discussed within this chapter has been reported

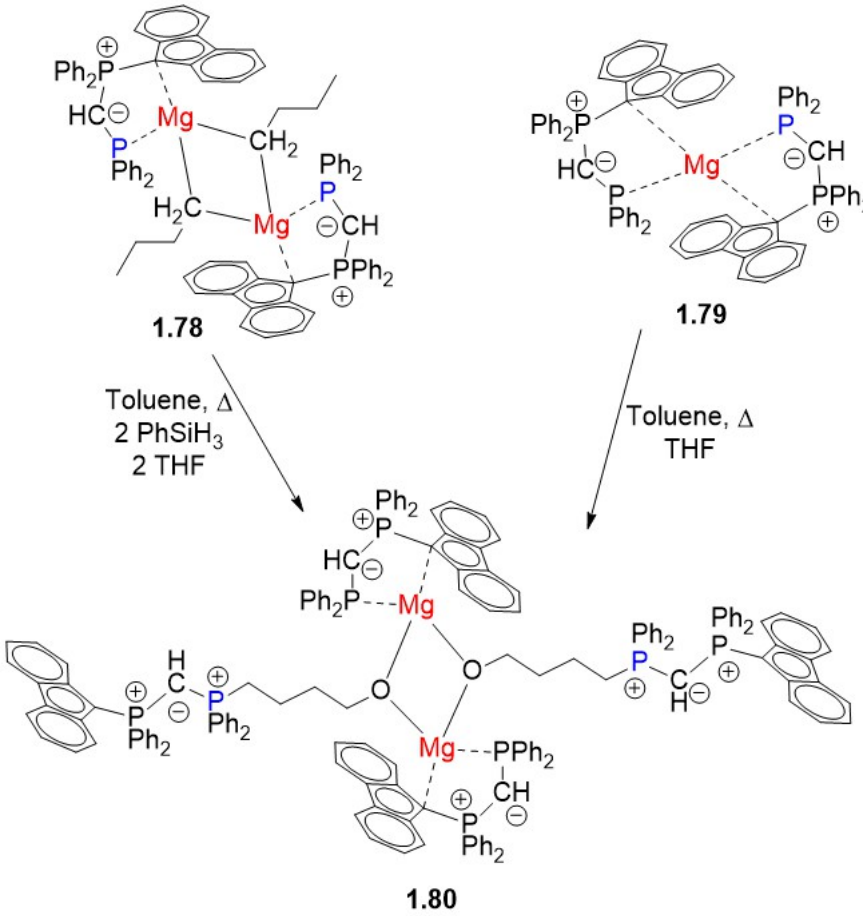

Scheme 1.47: The ring-opening of THF using compounds **1.78** and **1.79**.

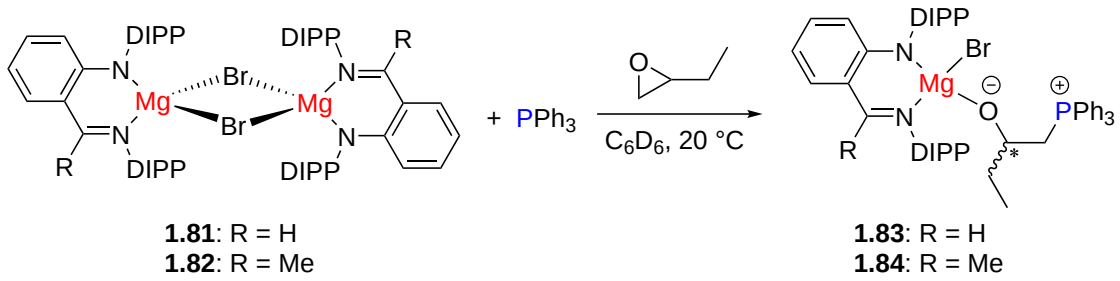

Scheme 1.48: FLP type ring-opening of an epoxide by **1.81** and **1.82** with PPh_3. DIPP = diisopropylphenyl.

within the last couple of years, and indeed some has been published since the experimental work for this thesis was ceased. However, the potential for the use of Mg Lewis acids in Lewis pair chemistry and beyond has been demonstrated, with this area of research still very much in its infancy with regards to how much it can still be explored. The work

reported in Chapters 4 and 5 of this thesis details a contribution towards this endeavour.

1.4 Aims & Objectives

Overall, the investigations conducted within this thesis have been carried out with the aim of improving the understanding of both Zr and Mg within FLP-type frameworks. With Zr FLPs, the aim is to vary the Lewis basic moiety in intermolecular systems in order to gauge the degree to which this alters reactivity. The majority of work with Zr FLPs has employed phosphines, and so nitrogen-based Lewis bases have been used here in order to not only try a different Lewis base, but to try and ascertain whether hard-soft acid-base chemistry has any effect on reactivity. The target is to therefore synthesise and analyse a new group of intermolecular Zr/N FLPs, before testing their aptitude for small molecule activation and catalysis.

Work with magnesium seeks to explore both the inter- and intra-molecular FLP environments, with Mg FLP-type systems far less explored than their Zr counterparts. Therefore, the target is to synthesise novel Mg Lewis acids for use with both phosphines and nitrogen-base Lewis bases, in addition to novel intramolecular Mg/P FLPs, using similar phosphine moieties as previously employed in Zr/P systems. These novel compounds can then be used for small molecule activation and catalysis, allowing a better understanding of the chemical environments necessary to allow for the desired reactivity to occur.

Chapter 2

Zirconium-nitrogen intermolecular frustrated Lewis pairs for small molecule activation

2.1 Introduction

The term "frustrated Lewis pair" (FLP) has now firmly found residence within the chemistry lexicon, and the associated compounds have been widely applied in a whole host of different reactions, with small molecule activation the predominant focus of much of the research undertaken so far.[4] The shift from using purely main group moieties to the application of transition metals has further broadened the FLP paradigm,[6,24,115–117] and has allowed for an increase in reaction diversity which now includes the activation of carbon-halogen bonds as well as catalytic amine-borane dehydrocoupling.[8,10]

Much of the work employing transition metals has revolved around the use of Zr(IV) cations incorporated into intramolecular Zr/P FLP systems,[12,13,15–18,30,51] and while a few examples have existed within the literature for some time,[7,28] it is only more recently that their intermolecular counterparts have been more thoroughly explored (Scheme 2.1).[11,25,26]

One of the initial principles guiding this research is the desire for less challenging syntheses from more readily available chemicals, and by separating the Lewis acid and base they can be synthesised and altered separately, or simply used directly from the bottle where appropriate.

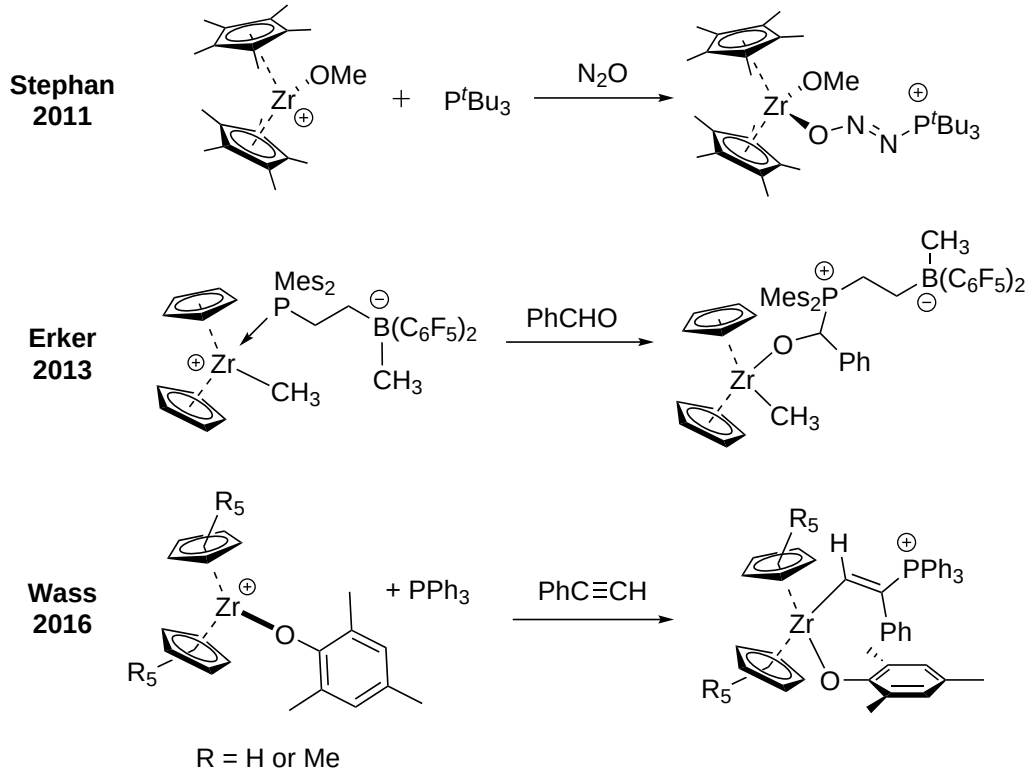

Scheme 2.1: Examples of intermolecular Zr/P FLPs used for small molecule activation.

Work within this chapter seeks to further advance the use of Zr(IV) cations within intermolecular systems by combining them with nitrogen Lewis bases. Although an intramolecular system has previously been developed,[51] and an intermolecular system is present in the catalytic hydrogenation of imines using Zr(IV) cations,[26] this research shows the first examples of intentional small molecule activation with a series of Zr/N intermolecular FLPs.

2.2 Aims & Objectives

The ability of Zr(IV) cationic centres to act as the Lewis acidic component of an FLP-type system has now been demonstrated by a number of different research groups. The differences in reactivity in comparison to main group systems has been one of the driving forces behind this research and has led to the development of more readily synthesised compounds that are able to perform the same transformations as their more complex progenitors.

Despite this, the vast majority of work exploring FLP chemistry with zirconium has employed phosphine-derived Lewis basic moieties, and so therein lies the opportunity to produce a clearer picture of how alteration of the Lewis base affects reactivity. In particular, the question of whether the hard-soft mismatch of the hard zirconocene Lewis acid with a soft phosphine plays a role in previous FLP systems seems important. The hard-hard combination of zirconocene with nitrogen-derived bases (e.g. amines) might be hypothesised to give a less frustrated system. With this overall aim in mind, objectives for this chapter are:

- Synthesise the new Zr/N Lewis pair systems
- Use analytical techniques to probe the Lewis acid/base interactions and try and gauge the degree of any steric or electronic effects
- Use these Lewis pairs for the activation of a series of small molecules

It should be noted that all X-ray crystallography experiments were performed by Dr Natalie Pridmore and Dr Hazel Sparkes (University of Bristol). Preliminary experiments were carried out by Ashley King as part of his final year undergraduate project (University of Bristol). Work within this chapter is also reported in a first author publication.[118]

2.3 Results & Discussion

2.3.1 Analysis of Intermolecular Zr/N FLPs

In order to allow comparison of this work to previous work with Zr/P intermolecular FLPs the same Zr(IV) cations have been employed, and were synthesised using the same literature method (Scheme 2.2).[25] For **2.1**, This involves protonolysis of dimethylzirconocene (Cp_2ZrMe_2) with 2,4,6-trimethylphenol (MesOH), followed by methyl abstraction with trityl tetrakis(pentafluorophenyl)borate ($[CPh_3][B(C_6F_5)_4]$) to give the cationic species (yield = 92%). For the synthesis of **2.2**, these steps are reversed, with the methyl abstraction step preceding the protonolysis step (yield = 81%).

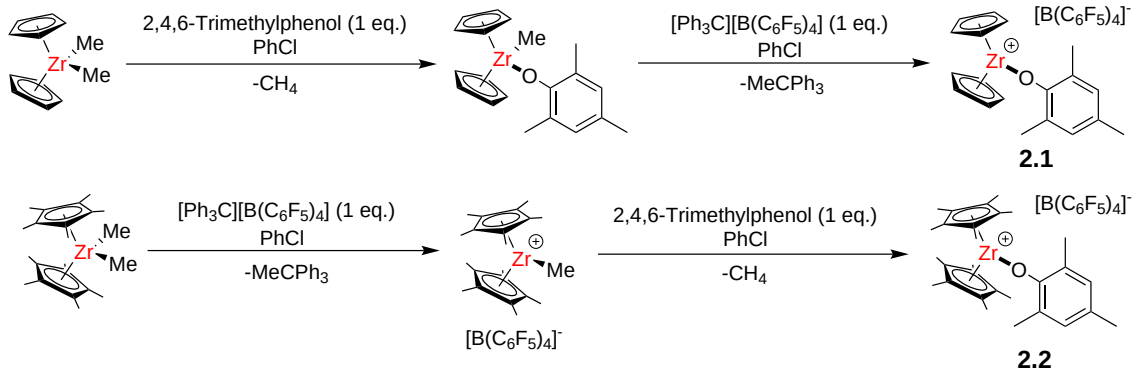

Scheme 2.2: Synthesis of Zr(IV) cations **2.1** and **2.2**.

The decision to use nitrogen Lewis bases in this work is a result of their frequent use within main group FLP chemistry, whilst very limited research on the reactivity with Zr(IV) cations has been done (see Chapter 1). The particular Lewis bases (Figure 2.1) were chosen due to their varying steric bulk and differing basicities, with NEt_3 (**a**, pK_a = 10.8) and $^{i}Pr_2NEt$ (**b**, pK_a = 11.4) being more basic than pyridine (**c**, pK_a = 5.3) and its derivatives 2-methylpyridine (**d**, pK_a = 5.9) and 2,6-dimethylpyridine (**e**, pK_a = 6.8).[119–122]

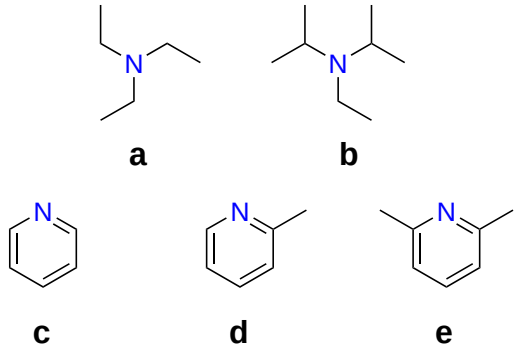

Figure 2.1: Nitrogen Lewis bases used in this research.

In Figure 2.2, we can see that the chosen Lewis bases **a**–**e** have basicities on a par with some of the phosphines previously used in this chemistry, with **b** having the same pK_a value as P^{t}Bu$_3$, **a** being more basic than PCy$_3$, and **c**–**e** possessing pK_a values between PPh$_3$ and PEt$_3$. It is difficult to compare the steric bulk of the pyridine derivatives as they cannot be compared via cone angles; however, **e** clearly is the most sterically bulky of the three, and further steric comparisons can be derived from the reactivity shown in this research.

The interaction between **a**–**e** and the cations **2.1** and **2.2** was initially probed via ^{1}H-

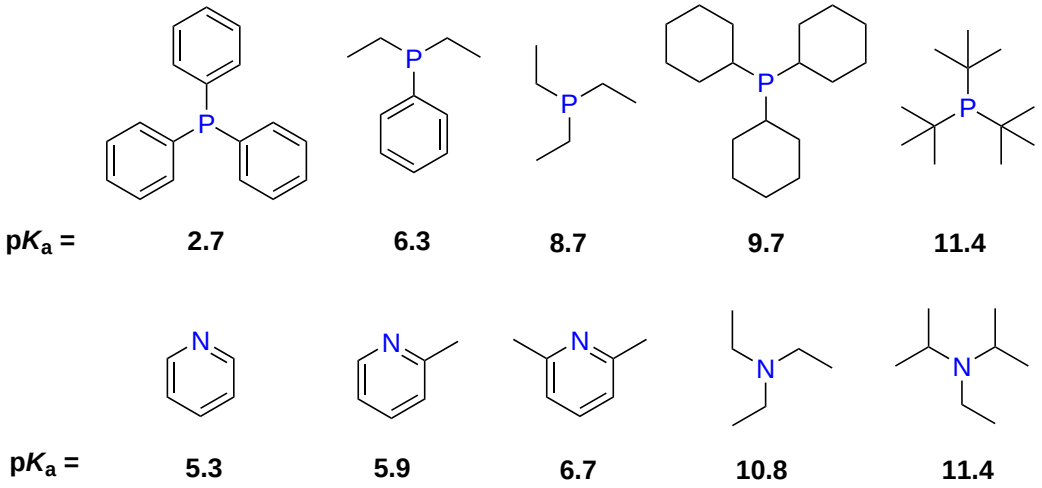

Figure 2.2: The pK_a values of the Lewis bases **a-e**, in addition to a selection of phosphines.[119–121,123,124]

^{15}N heteronuclear multiple bond correlation (^{15}N-HMBC) NMR spectroscopy (Table 2.1), which—much like ^{1}H-^{13}C-HMBC—gives multiple bond correlations between two different nuclei. The low abundance of ^{15}N makes this experiment especially useful as it is far more sensitive, requiring much shorter experiment times and smaller sample sizes than ^{15}N NMR. Indeed, when ^{15}N NMR spectroscopy was attempted, far greater quantities of compound were required than were experimentally practical, with experiments of reaction-scale samples ultimately unsuccessful. For the reactions of **2.1** with **a**–**e**, a lightening of the yellow solution was seen in all cases upon addition of the Lewis base. The reaction of **2.2** with **a**, **b**, and **e** resulted in a colour change to deep red, from dark orange, whereas the addition of **c** and **d** gave green and lighter orange solutions respectively.

Table 2.1: ^{15}N-HMBC NMR chemical shifts of the Lewis bases **a**–**e** and the Lewis pairs **2.1a**–**e** and **2.2a**–**e**.

Lewis base	^{15}N-HMBC NMR, δ/ppm	Zr/N	^{15}N-HMBC NMR, δ/ppm	Zr/N	^{15}N-HMBC NMR, δ/ppm
NEt_3 (**a**)	47.6	**2.1a**	163.5	**2.2a**	54.2
$^{i}Pr_2NEt$ (**b**)	57.5	**2.1b**	185.5	**2.2b**	–
C_5H_5N (**c**)	318.9	**2.1c**	–	**2.2c**	260.5
$C_5H_4(CH_3)N$ (**d**)	317.7	**2.1d**	302.1	**2.2d**	261.1
$C_5H_3(CH_3)_2N$ (**e**)	317.2	**2.1e**	249.8	**2.2e**	286.0

Unfortunately, no ^{15}N NMR signal data was obtained for **2.1c** and **2.2b**. In the case of **2.1c** this is due to a very weak signal in the ^{15}N-HMBC spectrum; this remained undetectable despite significant increases in quantity of compound and refining of the NMR experiment. For **2.2b**, degradation of the product appears to be a significant issue, as we see the formation of $[H–N(^{i}Pr)_2Et][B(C_6F_5)_4]$ crystals after several hours. The timeframe of the NMR experiment is between 6 and 12 h, so a large quantity of the product can be lost from solution before useful data can be collected. The same issue was seen previously when $P^{t}Bu_3$ was reacted with both **2.1** and **2.2**,[25] with $[H–P^{t}Bu_3][B(C_6F_5)_4]$ among the

products seen in those reactions, and indeed—as shown in Figure 2.2—P^{t}Bu$_3$ possesses the same pK_a value as **b**. However, unlike P^{t}Bu$_3$, **b** does not appear to produce the same borate salt product upon reaction with **2.1**.

Examining the **2.1** reactions first, we see a change from the free Lewis base chemical shift in all cases. For **2.1a** and **2.1b** this involves a downfield shift of over 100 ppm to δ 163.5 and 185.5 ppm respectively (from δ 47.6 and 57.5 ppm), demonstrating a clear interaction between the Lewis acid and base. An upfield shift is seen for **2.1d** and **2.1e**, which suggests a disruption of the aromaticity of the pyridinyl rings as a result of electron withdrawal by the Zr centre. Surprisingly, there is a greater upfield shift for **2.1e** than **2.1d** which implies that there is stronger bonding with the Zr centre despite greater steric bulk. It is difficult to explain why this may be the case, and any explanation will be speculative without isolation of the products; however, such a large chemical shift is unlikely to be the result of π–π interactions between **e** and the Cp ligands of **2.1**, if those interactions are present. The extra methyl group on **e** may alter the angle at which the Zr–N bond is formed relative to **2.1d**, perhaps resulting in improved overlap of the bonding orbitals, although a difference of 50 ppm in chemical shift between the two species hints at a different explanation.

The ^{15}N-HMBC NMR chemical shifts for **2.2a**–**e** follow a far more logical pattern. The NMR spectrum of **2.2a** reveals a peak at 54.2 ppm, which is very similar to the chemical shift for **a** at 47.6 ppm, suggesting minimal interaction between **2.2** and **a**, perhaps with no bonding between the N and Zr centres. The greater steric bulk of the Cp* ligands appears to prevent the same degree of bonding that is seen for **2.1a**. An upfield shift is seen for **2.2c**–**e**, giving a good indication of Zr–N bond interactions destabilising the aromaticity of the pyridinyl rings. The similarity in chemical shift between **2.2c** and **2.2d**

may indicate a similar Zr–N bond strength, which is further backed up by the similar Zr–N bond lengths of the two species (*vide infra*). The chemical shift of **2.2e** is further downfield, demonstrating that the greater steric bulk of **e** has resulted in a reduced level of bonding between the Zr and N centres.

To further gauge the degree of interaction between the cations and Lewis bases, DOSY (Diffusion-Ordered SpectroscopY) NMR studies were carried out. DOSY NMR is a technique that allows for the calculation of the diffusion coefficients (D) of species in solution. By determining the D values of the Lewis acids and bases when separated, and then when combined, it is possible to examine the level of interaction between the two moieties. In the event that two species are completely bound in solution, then they will be shown to possess the same D value. However, even if the combined species are shown not to be completely bound, interactions between them can still be revealed if there is a convergence in D from the separated to bound species. An example of this is shown in Figure 2.3, where we can see the DOSY spectra of **2.1** and **c** measured separately, as well as the spectrum of **2.1c**. This shows the greater difference in D when the species are separated to when they are combined, revealing that even though pyridine is not completely bound to **2.1**, a significant degree of interaction still exists between the pair.

The results of the DOSY study can be seen in Table 2.2. Examining the Lewis pairs containing **2.1**, we see significant changes in the diffusion coefficients (D) of the free Lewis bases in comparison to when they are combined in solution with **2.1**. For example, the D value of free **c** was 11.8×10^{-10} m^2 s^{-1}, and that of free **2.1** was 6.0×10^{-10} m^2 s^{-1}, but when combined in solution, these values become 5.7 and 3.3×10^{-10} m^2 s^{-1} respectively. This shows that although there is a significant bonding interaction between the Zr(IV) cation and pyridine, the two compounds are not irreversibly bound—otherwise they would

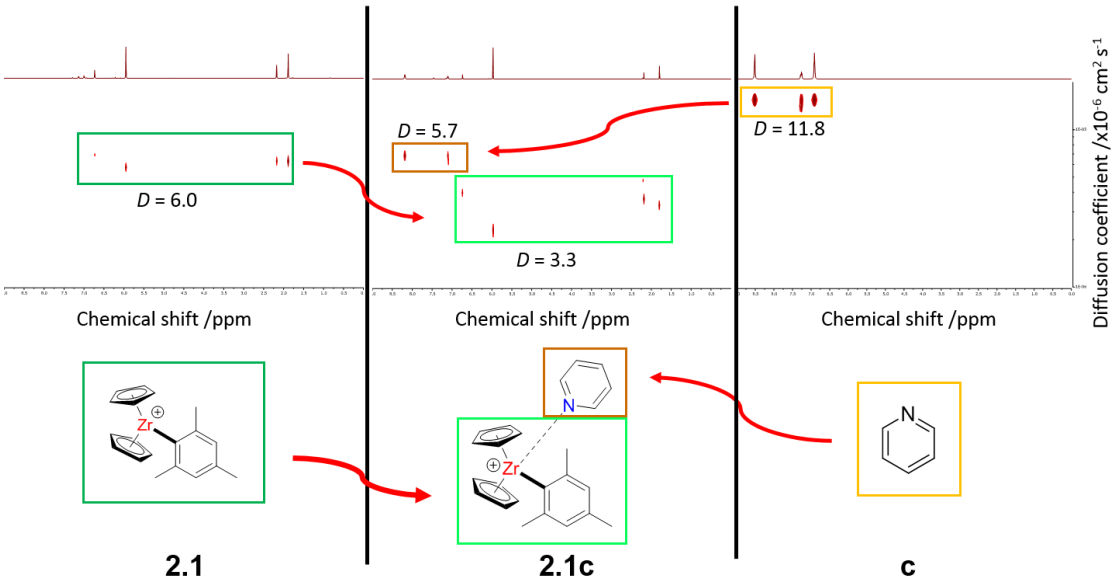

Figure 2.3: DOSY spectra for **2.1** (left), **c** (right), and the combined species **2.1c** (centre), with their diffusion coefficients. $[B(C_6F_5)_4]^-$ counterions omitted for clarity.

Table 2.2: The diffusion coefficients (D) of the free and combined Lewis pair species, with all results obtained using PhBr-d_5 and a concentration of 0.06 mol dm^{-3}. All values have units of $\times 10^{-6}$ cm^2 s^{-1}.

Lewis base	D of free base	D of free **2.1**[25]	D of free **2.2**[25]	D of base with **2.1**	D of **2.1** with base	D of base with **2.2**	D of **2.2** with base
NEt_3 (**a**)	9.2	6.0	8.6	8.2	3.3	8.7	4.4
$^i Pr_2NEt$ (**b**)	8.6	6.0	8.6	9.0	3.3	9.0	3.6
C_5H_5N (**c**)	11.8	6.0	8.6	5.7	3.3	4.0	3.3
$C_5H_4(CH_3)N$ (**d**)	11.0	6.0	8.6	5.2	2.5	5.2	2.3
$C_5H_3(CH_3)_2N$ (**e**)	9.7	6.0	8.6	6.8	2.3	6.8	2.1

have the exact same diffusion coefficient.

The same results can be seen for the **2.1d** and **2.1e** Lewis pairs; however, in both the cases the degree of change of D for **d** and **e** is less than for **c**, suggesting that, unsurprisingly, the increase in steric bulk around the Lewis base is reducing the level of interaction with **2.1**. Indeed, if we examine the "difference" between the D values of

the Lewis base and **2.1** together in solution, we see that **2.1c** has a difference of 2.4×10^{-10} m^2 s^{-1}, **2.1d** a difference of 2.7×10^{-10} m^2 s^{-1}, and **2.1e** a difference of 4.5×10^{-10} m^2 s^{-1}, showing an increase in the difference of the D values in line with an increase in steric bulk. The DOSY results for **2.1a** and **2.1b** Lewis pairs also suggest that, although there is an interaction between the Lewis acids and bases, the species remain unbound for a significant portion of time. It is also clear that both **a** and **b** have a less persistent interaction with **2.1** than **c**–**e**, with the results showing a much smaller shift in D values for **a** and **b**. Additionally, the bulkier *N*,*N*-diisopropylethylamine displays a reduced interaction when compared to triethylamine.

An almost identical trend is seen for **2.2**, with the most closely bound species being **2.2c**, and the least closely bound being **2.2b**. The differences in D values for both **2.1a**–**e** and **2.2a**–**e** are very similar apart from with **c**, which appears to be more noticeably bound to **2.2** than **2.1**. The Zr centre of **2.2** would be expected to be less electronegative than that of **2.1** due to the electron donating methyl groups on the Cp* ligands, which makes this result surprising as pyridine would be expected to bind more closely to **2.1**. One possible explanation for this might be to do with the Cp^R–Zr–Cp^R bond angles, which will be slightly larger for **2.2** than **2.1** due to the steric repulsion on the Cp* ligands. This results in a slight lowering in energy of the LUMO,[125] perhaps increasing the strength of the Zr–N bond. Less significant changes are seen with the other Lewis bases due to the greater steric bulk counteracting this effect. These interactions (for both **2.1** and **2.2**) may not only be a result of Zr–N bonding, but also due to weaker secondary interactions with ancillary ligands—particularly with the bulkier Lewis bases.

Isolation of all species **2.1a**–**e** and **2.2a**–**e** was attempted. Compounds **2.2c** and **2.2d** were the only species for which single crystals suitable for X-ray diffraction were obtained,

the structures for which are shown in Figure 2.4. **2.2c** possesses a shorter Zr–N bond (2.326(3) Å) than **2.2d** (2.386(4) Å), which is most likely a result of the slight steric bulk afforded by the methyl group on **d**. The stronger Zr–N bond in **2.2c** results in greater bending of the Zr1–O1–Mes bond angle (158.8(18)°) to that in **2.2d** (167.5(2)°). In unreacted **2.2**, this angle is almost completely linear (176.7(2)°), showing that both **c** and **d** reduce the multiple bond character between the Zr and O atoms.[25] In **2.2c** the pyridine ligand is slightly rotated in relation to the Zr1–N1 bond (Zr1–N1–C23 angle = 172.9(15)°), with this effect slightly enhanced in **2.2d** (Zr1–N1–C32 angle = 167.9(2)°). There is also a slight difference in the Cp*–Zr–Cp* bond angles between the two complexes, with angles of 135.5(7)° and 132.7(9)° respectively for **2.2c** and **2.2d**. Although this could well be a result of steric effects, it may also be due to the greater electron donation from the –OMes ligand in **2.2d**—as shown by the more linear Zr1–O1–Mes angle. This may indicate a greater contribution to the e^{*}_{1g} orbital which results in further bending of the Cp* ligands.[125] However, care must be taken when drawing these conclusions as alkoxides can be unreliable indicators of multiple-bonding character, and the possibility of a steric rationale remains.[25,126]

Interestingly, although the mass spectrometric data for **2.2c** shows a peak for the full complex (574.2645 *m/z*), only the Zr cation and separate Lewis base is seen in the **2.2d** spectrum. This suggests that in solution, **2.2d** possesses a far more labile Zr–N bond than **2.2c**. This may also be the reason why **2.2c** appears green in solution, whereas **2.2d** appears orange.

In the reaction between **2.2** and **d**, a second set of red crystals suitable for X-ray diffraction were also obtained (**2.3**, Figure 2.5). This is a cationic species with two zirconocene moieties lying roughly perpendicular to one another and bridged by an oxygen

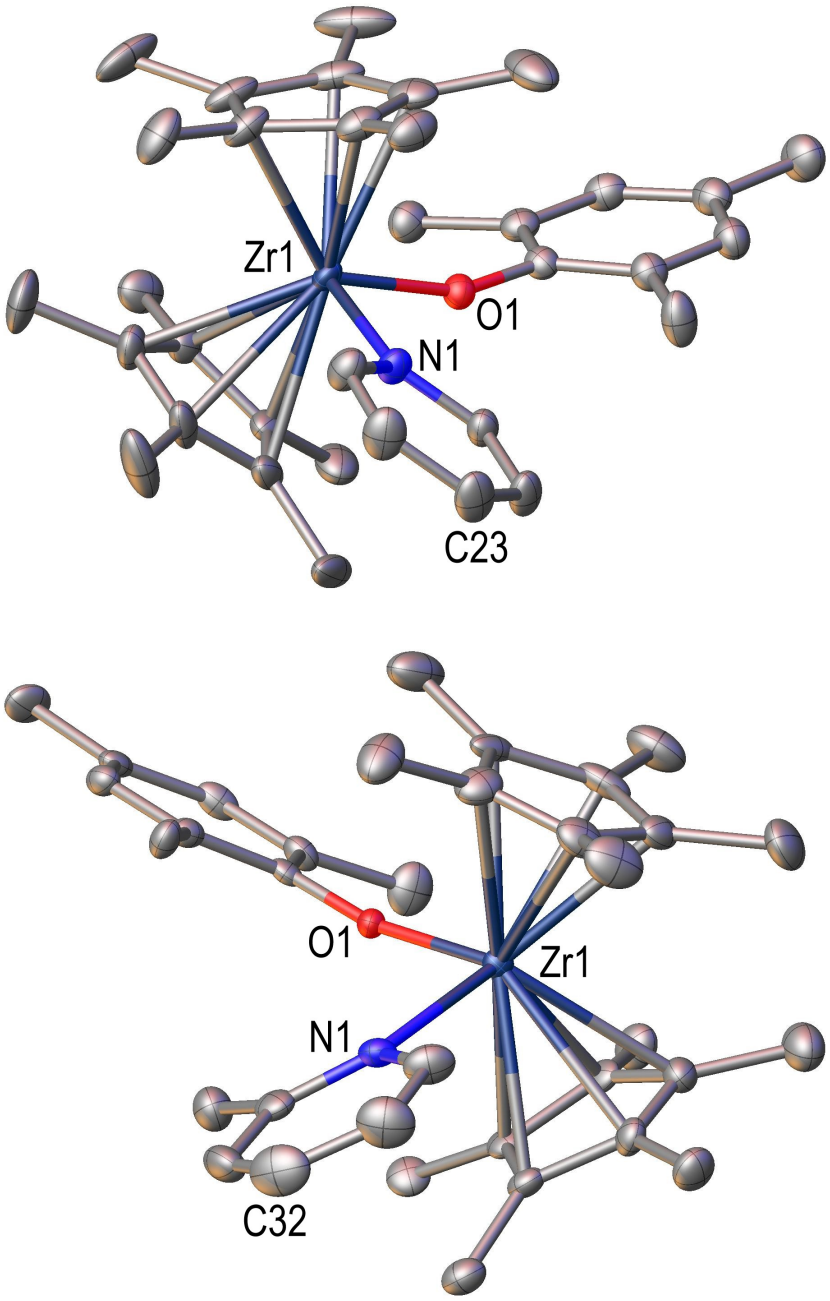

Figure 2.4: Molecular structures of **2.2c** (top) and **2.2d** (bottom), as determined by single crystal X-ray diffraction. Thermal ellipsoids are drawn at the 50% probability level. Hydrogen atoms, the $[B(C_6F_5)_4]^-$ counterion, and PhCl solvent of crystallization are omitted for clarity. Selected bond lengths (Å) and angles (deg): **2.2c**: Zr1–O1 1.982(2), Zr1–N1 2.326(3), O1–Mes 1.376(4), Zr1–O1–Mes 158.8(18), Cp*–Zr–Cp* 135.5(7). **2.2d**: Zr1–O1 1.975(3), Zr1–N1 2.386(4), O1–Mes 1.369(5), Zr1–O1–Mes 167.5(2), Cp*–Zr–Cp* 132.7(9).

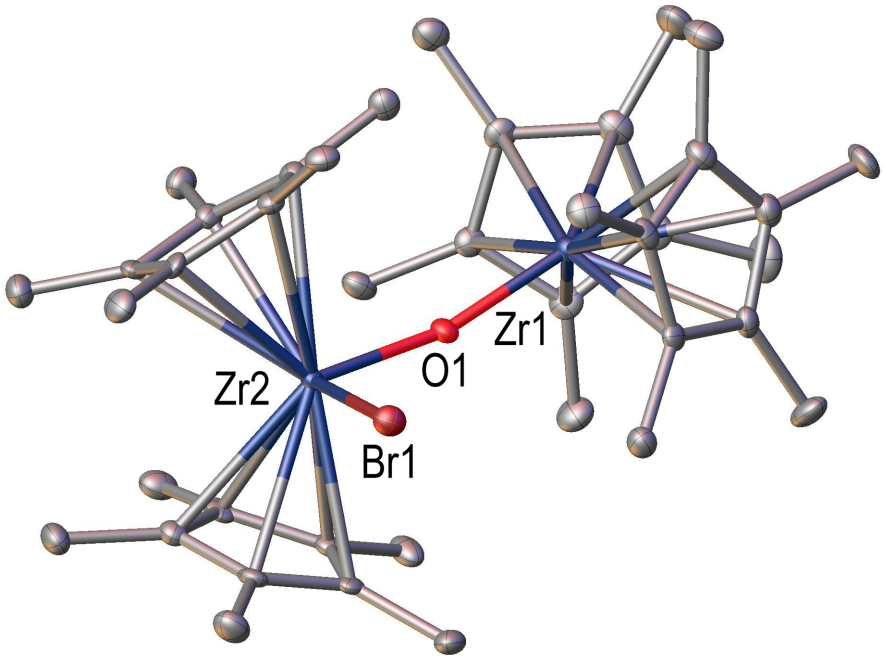

Figure 2.5: Molecular structure of **2.3** as determined by single crystal X-ray diffraction. Thermal ellipsoids are drawn at the 50% probability level. Hydrogen atoms and the $[B(C_6F_5)_4]^-$ counterion are omitted for clarity. Selected bond lengths (Å) and angles (deg): Zr1–O1 1.962(2), Zr2–O1 2.062(2), Zr2–Br1 2.628(5), Zr1–O1–Zr2 164.2(14), Cp*–Zr1–Cp* 129.8(6), Cp*–Zr2–Cp* 133.4(6).

atom; it is assumed to have been formed as a result of water entering the reaction (possibly in PhBr-d_5 solvent). One of the Zr centres is also bonded to a Br atom, which would have been abstracted from the solvent. The exact mechanism by which this compound forms is not known, but it is speculated that the formation of Zr hydroxide—through reaction with water—triggers loss of the aryloxide ligands (as alcohols) and formation of the bridged product, possibly assisted by the presence of the 2-methylpyridine base. Cationic zirconocene complexes have previously been shown to abstract halides from the solvent, resulting in the formation of bridging species.[127] Other work with similar zirconocene complexes has also shown degradation resulting in the formation of oxygen-bridged zirconocenes, with the O atom derived from a *t*-butoxide ligand.[128] However, as the formation of **2.3** is not seen in the absence of water, it is assumed that a similar process is not taking

place here, and the oxygen is not from the –OMes ligand in **2.2**—although further study would be required to confirm this.

The O atom in this complex lies slightly closer to Zr1 (Zr1–O1 = 1.962(2)$^\circ$) than Zr2 (Zr2–O1 = 2.062(2)$^\circ$), showing that the cationic Zr centre is more electron withdrawing than the centre bonded to Br. The Cp*–Zr–Cp* bond angles also differ, with that for Zr2 (133.4(6)$^\circ$) slightly less bent than that for Zr1 (129.8(6)$^\circ$). This perhaps suggests that the Br atom is contributing to a bonding orbital, rather than the non-bonding e^*_{1g} orbital (*vide supra*). The length of the Zr2–Br1 bond (2.6282(5) Å) is comparable to other zirconocene bromide complexes.[129]

2.3.2 Reactivity of the Zr/N Lewis pairs with hydrogen (D_2)

The first small molecule reaction for which the Zr/N FLPs were tested was for the activation of hydrogen (D_2), with the deuterium analogue of H_2 used to allow for more practical reaction monitoring by ^{2}H NMR spectroscopy. Dihydrogen cleavage is a characteristic reaction in FLP chemistry and is therefore a logical starting point for analysis of any activity towards small molecule activation. For **2.1a**–**e**, no reaction was observed upon addition of D_2 gas (1 bar) to a PhCl solution of the Lewis pair (Scheme 2.3). This is in line with previous work where at least one Cp* ligand was necessary for the reaction to proceed,[8] and adds credence to the hypothesis that transient binding of H_2 to the Zr centre is required for subsequent activation to occur. This means that simply changing the Lewis base from a phosphine to a nitrogen compound does not seem to have any effect. The Cp* ligand is believed to increase the electron density at the Zr centre, facilitating backbonding with η^2-dihydrogen intermediates.

D_2 gas (1 bar) was also added to PhCl solutions of **2.2a**–**e** and successful reactions

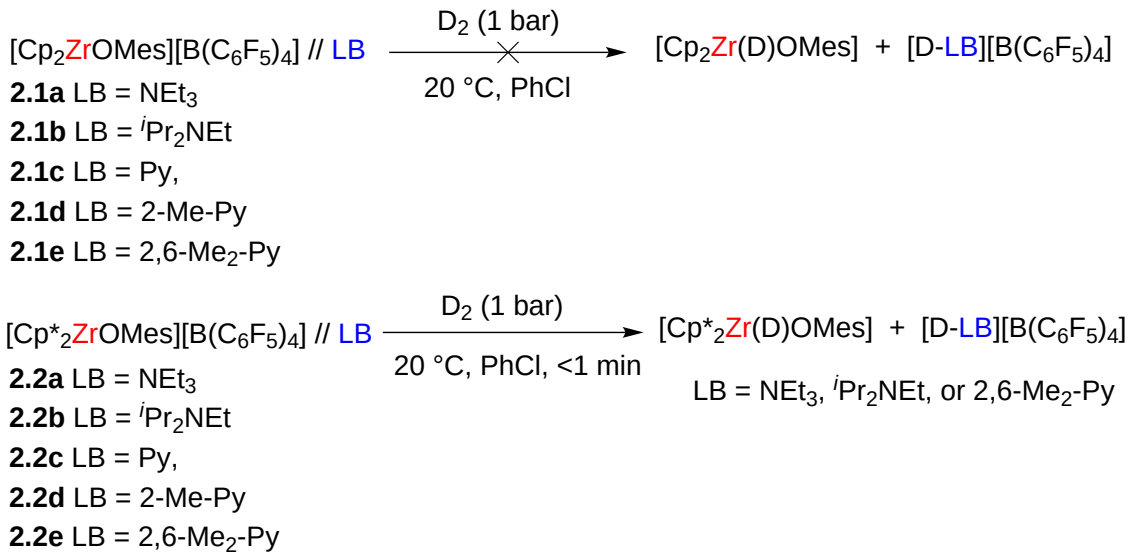

Scheme 2.3: Reactivity of Systems **2.1a–e** and **2.2a–e** with D_2 (1 bar).

occurred with **2.2a**, **2.2b**, and **2.2e**, while no reaction was seen for **2.2c** and **2.2d**. The reaction solution of **2.2a** instantly turned yellow upon addition of D_2 gas, with the reaction of **2.2b** taking around 5 min to change colour to yellow. **2.2e** rapidly changed colour to a lighter red after addition of the gas. In each of these three cases the Zr–D singlet was visible in the ^{2}H NMR (δ = 6.06 ppm, Figure 2.6), which was also previously seen for the reactions with phosphines.[25]

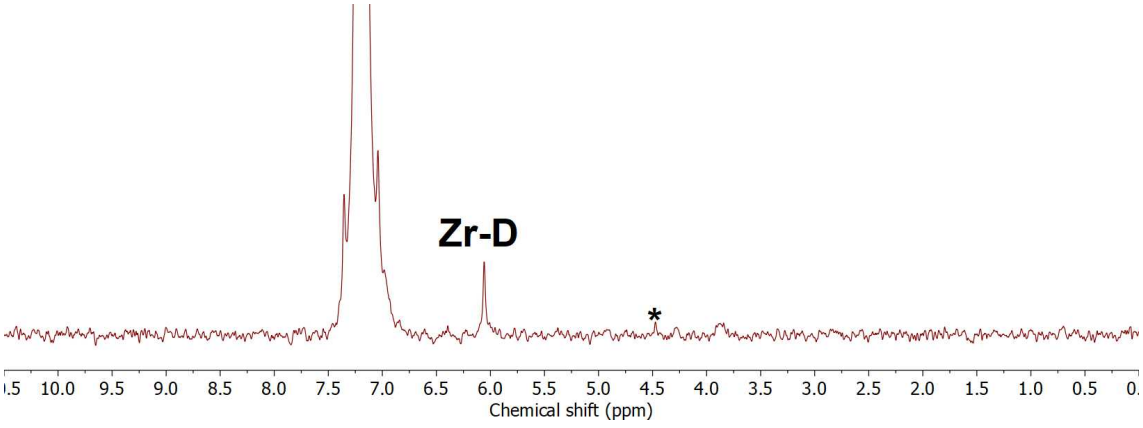

Figure 2.6: ^{2}H NMR spectrum of the reaction between **2.2a** and 1 bar D_2 (78 MHz, 25 °C, PhCl): δ = 6.06 ppm (s, Zr–D). * = D_2 gas. Large peak at 7.20 ppm is from several drops of C_6D_6 added to act as a reference.

Only the zirconium deuteride complexes were seen in the NMR spectra for **2.2a** and **2.2b**, which is a result of the $[D–NEt_3][B(C_6F_5)_4]$ and $[D–^{i}Pr_2NEt][B(C_6F_5)_4]$ salts being insoluble in the PhCl solution, with colourless crystals forming in both reaction vessels fairly soon after reaction completion. Both the Zr–D species, and the $[D–NC_5H_3(CH_3)_3][B(C_6F_5)_4]$ salt (δ = 12.42 ppm) are visible in the ^{2}H NMR spectrum of **2.2e**.

The unsuccessful reactions of **2.2c** and **2.2d** is likely due to a couple of reasons. Firstly, the lower basicity of **c** and **d** reduces the ability of the Lewis pairs to heterolytically cleave dihydrogen, and secondly the greater affinity that **c** and **d** have for the Zr centre means that binding of the dihydrogen to the metal is inhibited.

The exact mechanism by which this reaction proceeds could be via one of two processes with the first involving initial binding of the D_2 molecule to the metal centre followed by deprotonation by the Lewis base, and the second comprising of concerted heterolytic splitting of D_2 by a Lewis pair encounter complex (Scheme 2.4)—the latter being the generally accepted mechanism for H_2 activation using main group systems.[130,131] Previous

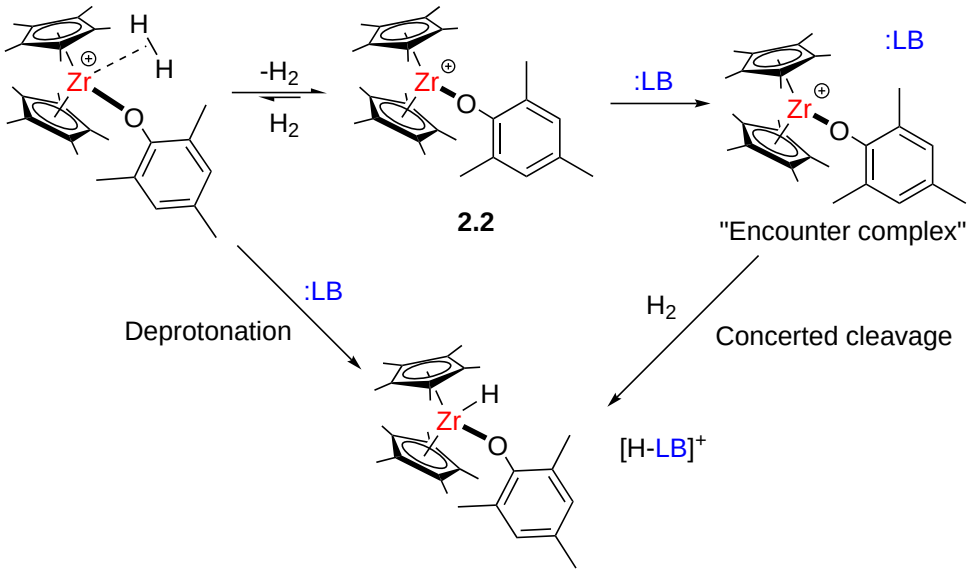

Scheme 2.4: The two possible mechanisms for the heterolytic cleavage of dihydrogen by **2.2a**, **2.2b**, and **2.2e**. The $[B(C_6F_5)_4]^-$ counterions have been omitted for clarity.

studies have been unable to observe the presence of a Zr–D_2 complex that would exist through the first mechanism,[25] with there also appearing to be no known examples of transition metal d^0 M–H_2 complexes in the literature.[132] The DOSY studies shown above clearly indicate a degree of preorganisation between the Lewis pairs, suggesting that the second mechanism is the more likely of the two. However, it may simply be the case that more sensitive experiments are required to detect the presence of a Zr–D_2 complex.

2.3.3 Reactivity of the Zr/N Lewis pairs with carbon dioxide (CO_2)

Another typical FLP reaction is the activation of carbon dioxide (CO_2), and so this was the next target for testing the Zr/N FLPs. All of the Lewis pairs **2.1a–e** and **2.2a–e** were reacted with CO_2 by charging PhBr-d_5 solutions of the species with 1 bar CO_2 (Scheme 2.5). **2.1a** and **2.1b** reacted almost instantly, with both turning much paler yellow. ^{15}N-HMBC NMR spectra showed new peaks at δ 446.0 and 446.5 ppm respectively, which were assigned to the CO_2 activated product as they correspond to a cationic N centre. In addition, the expected carbonyl peaks in the ^{13}C NMR spectra (δ 165.3 and 168.2 ppm respectively) were observed, which are in the same region as the corresponding product using phosphines.[25] No reaction was seen for **2.1c**; however, both **2.1d** and **2.1e** reacted more slowly (<20 min), with the signals at δ 450.1 and 464.0 ppm respectively in the ^{15}N-HMBC NMR spectra (^{13}C NMR Zr–CO_2–NR_2 peaks: **2.1d** δ 161.6 ppm; **2.1e** δ 160.9 ppm).

Upon addition of CO_2, **2.2a** instantly changed colour to yellow, with the new resonance in the ^{15}N-HMBC NMR spectrum ($\delta = 343.3$ ppm) assigned to the CO_2 activation product, with the ^{13}C NMR signal for the carbonyl also assigned (δ 162.7 ppm). In the case of **2.2b** a signal in the ^{15}N-HMBC NMR spectrum was not obtained (for the reasons

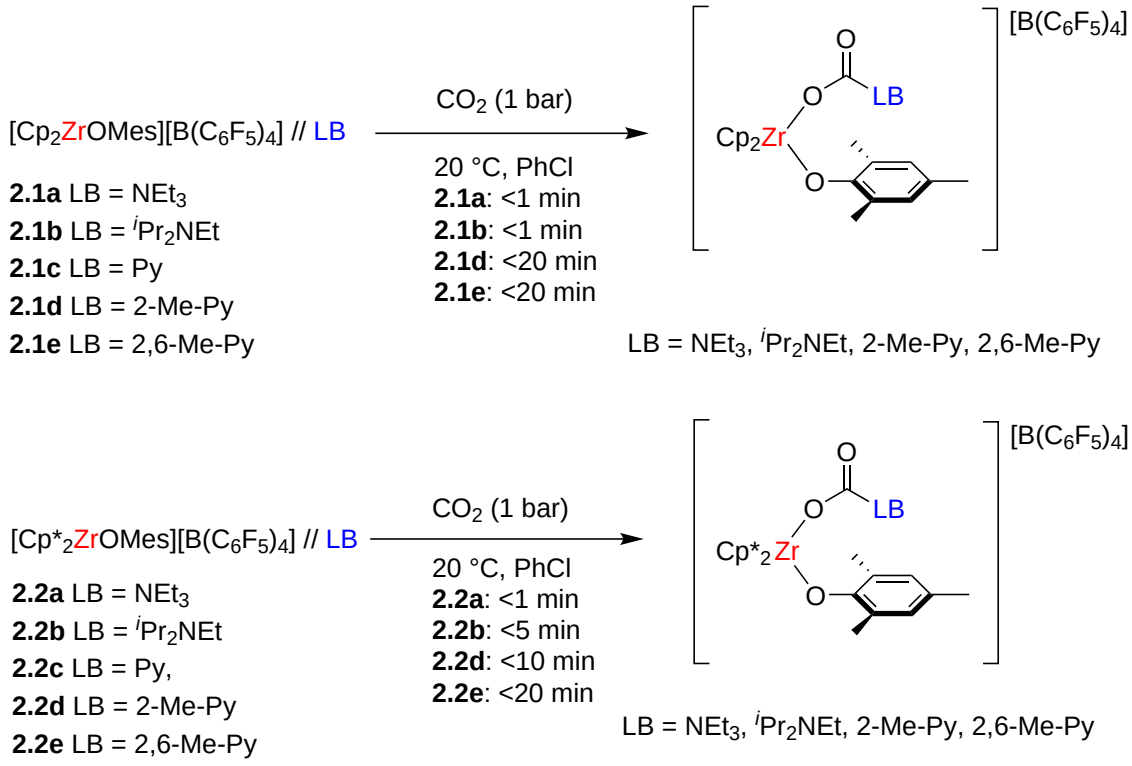

Scheme 2.5: Reaction of **2.1a–e** and **2.2a–e** with CO_2 gas (1 bar).

outlined previously), although the same colour change is seen for this reaction, in addition to the presence of ^{13}C NMR peak in the correct region for the activated CO_2 (δ 161.4 ppm). Reactions were also seen for both **2.2d** and **2.2e**, with the CO_2 activation products assigned in the ^{15}N-HMBC NMR (**2.2d**: δ = 438.1 ppm, **2.2e**: δ = 466.1 ppm), however, these samples required 10 and 20 min respectively for the reaction to occur. Compound **2.2c** was found to be inactive for CO_2 activation. Isolation of any products was not possible and was made particularly difficult due to the instability of these products outside of a CO_2 atmosphere.

It is worth noting that **2.1d** and **2.2d** were both able to activate CO_2 but were unable to activate D_2. This may be a result of a lower basicity requirement for this reaction, or may be due to the Zr centre having a greater affinity for the O atoms in CO_2 which, once bound, is a more favourable target for nucleophilic attack by **d**.

There is more than one possible mechanism for this reaction, including; insertion of CO_2 into the Zr–N bond, initial binding of CO_2 by Zr followed by nucleophilic attack from the Lewis base, or the formation of a Zr/LB encounter complex and concerted formation of the activation product. Initial formation of an encounter complex seems to be the most likely route of these three (Scheme 2.6). This is supported by the quicker reactions of **2.1a**, **2.1b**, **2.2a**, and **2.2b** which, according to the DOSY studies, have a less persistent Zr–N bond when compared to **2.1c**–**e** and **2.2c**–**e**. The reactions of **d** and **e** are also likely to be hampered by their lower basicity. However, initial coordination of CO_2 prior to attack from the Lewis base is still a possibility, with coordination of CO_2 to a zirconocene having been described previously,[133,134] although weak binding of CO_2 could make this route less likely.

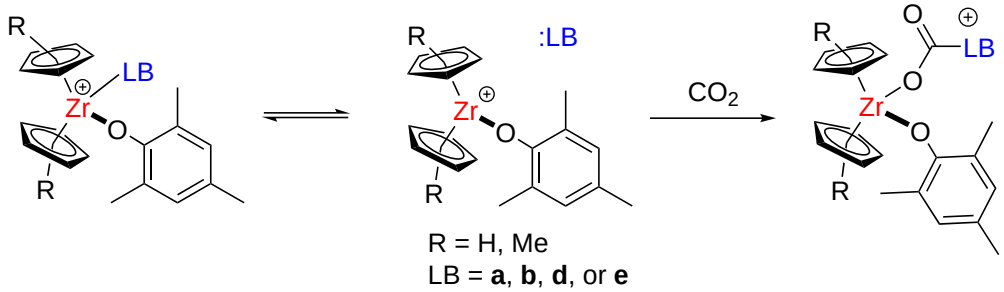

Scheme 2.6: Proposed mechanism for the activation of CO_2 by the Zr/N FLPs. $[B(C_6F_5)_4]^-$ counterions omitted for clarity.

2.3.4 Reactivity of the Zr/N Lewis pairs with tetrahydrofuran (THF)

The ring-opening of tetrahydrofuran (THF) is another reaction for which FLPs have been shown to be effective,[135] and was the next reaction for which the Lewis pairs **2.1a**–**e** and **2.2a**–**e** were tested (Scheme 2.7). When THF was added to PhBr-d_5 solutions of **2.1a**–**e**, the formation of a THF adduct was seen in all cases (with the exception of **2.1c**) within a short period of time—as evidenced by a change of colour to yellow (already yellow

solutions darkened in colour)—and confirmed by NMR. The THF adduct formed almost instantly with **2.1a** but required up to 10 min to form with **2.1b**, **2.1d**, and **2.1e**. This then preceded conversion to the ring-opened product, which was significantly quicker for **2.1a**, which was the only Lewis pair to achieve significant conversion at room temperature while also producing the highest yield at 82% after 24 h. **2.1b**, **2.1d**, and **2.1e** all proved to be much less reactive and required 3 days of heating at 80 °C in order to reach reaction completion. **2.1b** achieved the lowest conversion of these three reactions (≈20% by NMR), with too little product present for isolation. **2.1d** and **2.1e** achieved higher yields of 45% and 65% respectively, once again demonstrating an increase in line with higher steric bulk and Lewis basicity. **2.1c** initially remained stable to reaction with THF, however, after several days of heating at 80 °C the pyridine adduct was substituted by the THF although no further reaction was seen. THF is likely favoured over pyridine due to being more electron rich, and is therefore the preferred substrate for adduct formation with the electrophilic Zr centre.

THF was also added to **2.2a**–**e** with almost instantaneous formation of the THF adduct (yellow solution) seen with **2.2a**. However, **2.2b**, **2.2d**, and **2.2e** changed colour to yellow more slowly, at around 10 min. The reaction of **2.2b** did not result in the formation of any product due to the degradation of the FLP as outlined previously (*vide supra*). **2.2c** was heated at 80 °C for 10 days before the pyridine moiety was displaced by THF, with no further reaction seen. The other reactions all required heating at 80 °C to produce the ring-opened product, with 5 days required in each case for the reactions to reach completion. Surprisingly, **2.2d** was the most reactive of these three samples, achieving the highest yield (≈40% by ^{1}H NMR). The yield was calculated by comparing the intensity of the THF peak at δ 3.56 ppm with the intensity of the α-CH_2 and δ-CH_2 signals of

the product (δ 4.13-4.02 ppm). **2.2a** and **2.2e** had very low yields of ≈17% and ≈7% respectively (by ^{1}H NMR), which may be a result of the higher steric bulk being more inhibitory for this reaction when Cp* ligands are present instead of Cp.

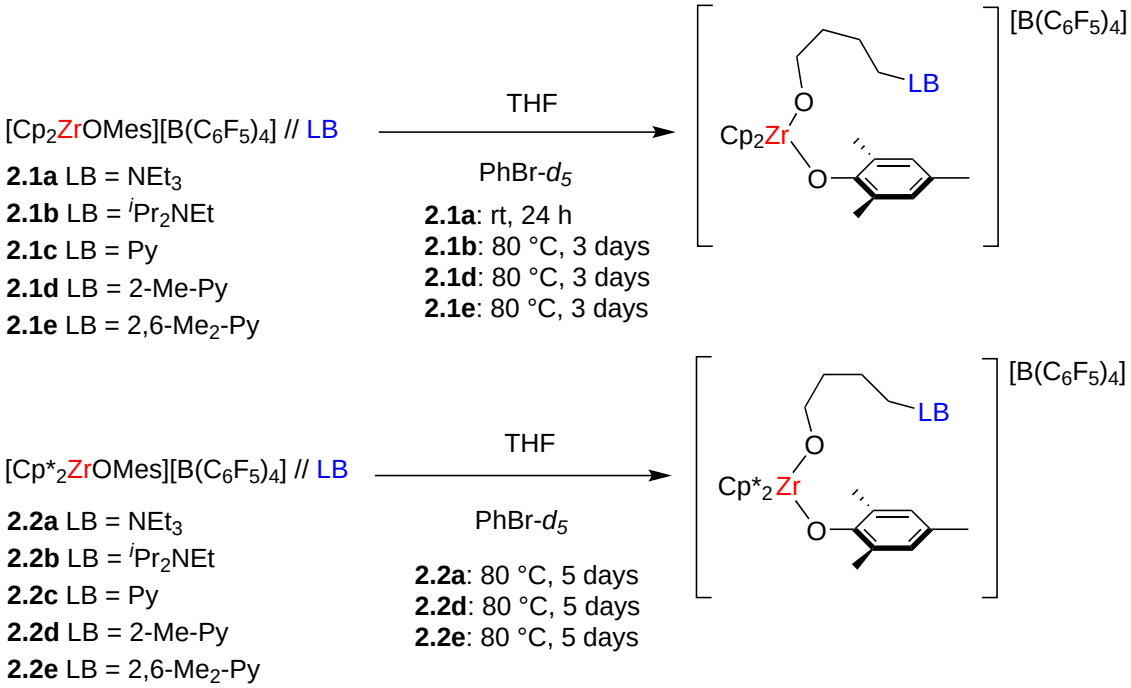

Scheme 2.7: Reactions of **2.1a–e** and **2.2a–e** with tetrahydrofuran (THF).

Despite the apparent speed of the reaction of **2.1a** when compared to the other THF reactions, all of the above reactions are sluggish in comparison to those previously achieved with phosphine, with PEt_3 in particular achieving stoichiometric conversion within 30 min at 20 °C in combination with **2.1**. Faster reactions at lower temperatures were also completed using PCy_3 and PPh_3, although these Lewis bases also reacted more slowly with **2.2** than **2.1**.[25] The fact that PPh_3 only possesses a pK_a value of 2.7, but is still a more effective Lewis base than the nitrogen compounds employed (which all have higher pK_a values) shows that basicity is not the most important factor in determining reactivity towards this transformation. However, it is difficult to directly compare the phosphines with these nitrogen compounds as even PEt_3 and NEt_3 possess different pK_a values. PEt_3

and NEt_3 *can* be directly compared in terms of steric bulk however, with PEt_3 possessing a smaller Tolman cone angle, which perhaps helps to highlight that the accessibility of the Lewis base centre is very much a determining factor in reactivity.[136]

2.3.5 Reactivity of the Zr/N Lewis pairs with phenylacetylene-*d* (PhCCD)

The last small molecule activation reaction for which the Zr/N intermolecular FLPs were tested is the activation of phenylacetylene-*d* (PhCCD). The partially deuterated version of phenylacetylene aids product determination by allowing us to distinguish ammonium salts formed through the reaction, and those formed through decomposition of the FLP (see Section 2.3.1). Phenylacetylene differs from the previous small molecules due to the fact that there are two known products for the reaction of terminal alkynes with FLPs, rather than the single products observed for D_2, CO_2, and THF in this chapter. The first possible product is formed as a result of 1,2-addition across the alkynyl bond, whereas the second results from deprotonation of the terminal hydrogen. The 1,2-addition products were initially seen with main group systems,[137–139] however, these were also obtained when either **2.1** or **2.2** was used in conjunction with PPh_3 (Scheme 2.8), and it appears that the lower basicity of this phosphine is what avoids the deprotonation route.[25] The deprotonation products are more common amongst zirconium systems, and were obtained through the use of **2.1**/PCy_3, **2.1**/$PMes_3$, and **2.2**/$PMes_3$, in addition to a series of Zr(IV) intramolecular systems.[8] In these cases we see formation of a Zr acetylide complex as well as a phosphonium salt. Selection between the two possible products appears to be controlled by a mixture of electronic and steric factors.

In the work carried out here, an excess of phenylacetylene-*d* was added to PhBr-d_5 solutions of **2.1a**–**e**. For **2.1a** (Scheme 2.9), this was followed by an instantaneous change

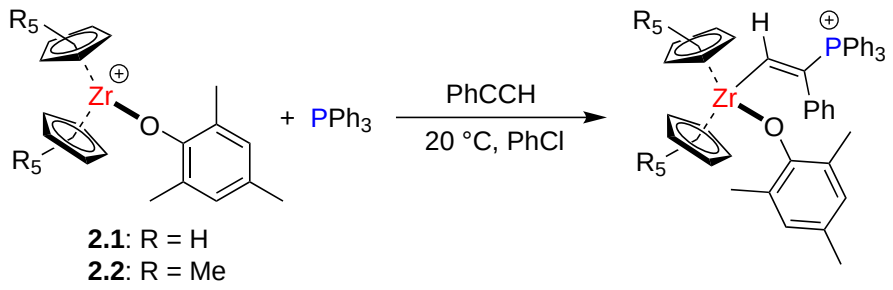

Scheme 2.8: 1,2-Addition of phenylacetylene to **2.1**/PPh_3 and **2.2**/PPh_3.[25]

in colour to a lighter yellow before rapid formation of [D–NEt_3][$B(C_6F_5)_4$] crystals within several minutes—alongside the Zr acetylide complex, for which the same ^{1}H NMR signals were seen in each successful reaction of **2.1** (selected peaks: δ 7.53 (o-ArH(-C_6H_5)), 7.18 (p-ArH(-C_6H_5)), 6.09 (Cp) ppm). Similar reactivity was seen for both **2.1b** and **2.1e**, although these reactions required timeframes of 5 and 30 min respectively. Neither **2.1c** nor **2.1d** demonstrated any reactivity, apparently as a result of the lower basicity of the Lewis bases in addition to their lower level of frustration within the FLPs.

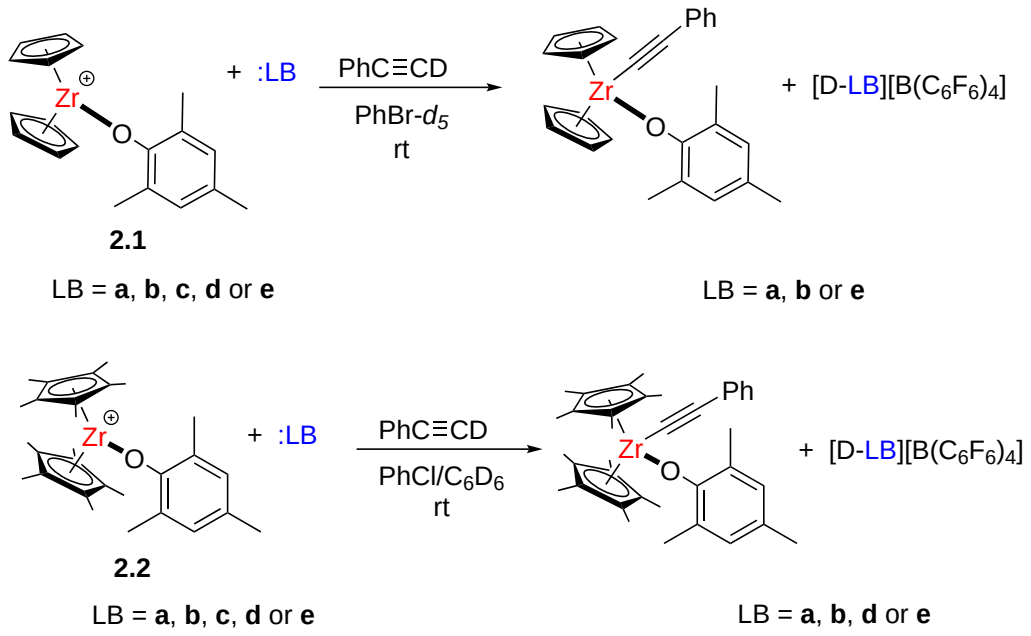

Scheme 2.9: Reactions of **2.1a–e** with phenylacetylene-d.

Excess phenylacetylene-*d* was also added to PhCl solutions of **2.2a**–**e** (Scheme 2.10), with **2.2a** once again proving to be the most reactive, demonstrating an instantaneous colour change (red to yellow) upon addition of the reagent, followed by rapid formation of the ammonium salt precipitate and Zr acetylide complex (Zr acetylide selected ^{1}H NMR peaks: δ 7.56 (*o*-Ar*H*(-C_6H_5)), 1.88 (Cp*) ppm). Successful reactions were also seen for **2.2b**, **2.2d**, and **2.2e** with these reactions taking several minutes to complete. It is perhaps surprising that **2.2b** is shown to be effective for this reaction, as the previously established degradation of the FLP has acted as a hindrance to other small molecule activations. The reaction is perhaps aided in this case by rapid reactivity, and subsequent precipitation of the ammonium salt product which—by removal from the reaction environment—is prevented from further interaction with the Zr species. It should be said, however, that although the [D–N(^{i}Pr)$_2$Et][B(C_6F_5)$_4$] salt was shown to present through mass spectrometry, [H–N(^{i}Pr)$_2$Et][B(C_6F_5)$_4$] was also revealed to be in the sample. This may indicate that the same degradation is still occurring, but may also simply be a result of H/D exchange with the sample solvent.

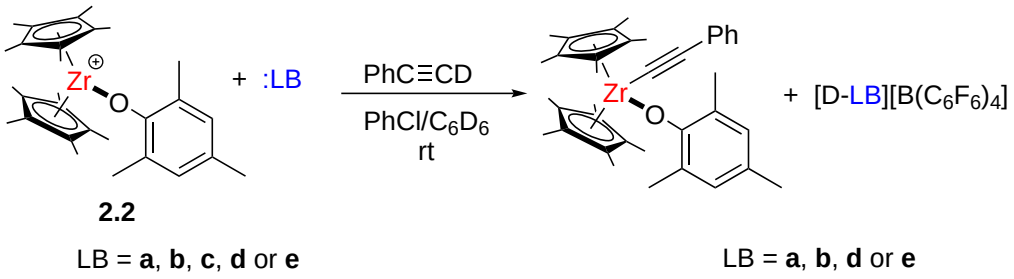

Scheme 2.10: Reactions of **2.2a**–**e** with phenylacetylene-*d*.

2.4 Conclusion

In this chapter, the first explicit intermolecular Zr/N frustrated Lewis pairs have been synthesised, allowing comparisons of how differing steric and electronic parameters change reactivity towards the activation of small molecules, and in particular how this reactivity compares to intermolecular Zr/P FLPs. DOSY NMR studies reveal the different degrees of interaction between the Lewis acids and bases, showing that some secondary interactions between the two moieties exist even when no formal bond is present. In addition to this the dynamic nature of any direct bonds between the Lewis acid and base is also elucidated, explaining why the Lewis pair **2.2d** is still able to perform small molecule activations despite a Zr–N bond being present in the solid state. Perhaps unsurprisingly, pyridine proved to be an ineffective Lewis base for these reactions and was unable to perform any small molecule activation reaction, with the Zr–N bond appearing to be far too stable and inert in solution.

The Lewis pairs were able to perform the same small molecule activation reactions that were previously performed using phosphines. The same issue of requiring at least one Cp* ligand in order to heterolytically cleave dihydrogen was seen, with this achieved by **2.2a**, **2.2b**, and **2.2e** but not by any of **2.1a**–**e**. A Lewis base of sufficient basicity and steric bulk is also necessary, although for the activation of CO_2 these factors are less significant. This is shown by less basic and sterically bulky 2-methylpyridine being able to execute this reaction, with **2.1** also effective as the Lewis acidic component. The deprotonation of phenylacetylene-*d* was performed by all Lewis pairs except **2.1c**, **2.1d**, and **2.2c**, with all Lewis bases appearing to be too basic to afford the 1,2-addition product.

The ring-opening of THF is one reaction for which clear disparities between the use

of nitrogen or phosphorus Lewis bases are demonstrated. While the transformation was performed by **2.1a**, **2.1b**, **2.1d**, **2.1e**, **2.2a**, **2.2d**, and **2.2e**, the reaction times were far inferior and point to an advantage of using phosphines. However, it is difficult to pinpoint precisely where this advantage lies, as the basicities and alkyl/aromatic groups are not directly comparable with the Lewis bases used here. It is significant to note that the least basic of all these species (PPh_3, $pK_a = 2.7$) was still able to perform the ring-opening of THF more rapidly than the nitrogen compounds, suggesting that basicity is not the most important factor in determining reactivity.

The use of alternative Lewis bases to phosphines has allowed greater elucidation of the electronic and steric requirements of intermolecular Zr FLP chemistry, and demonstrates the relative insignificance of the hardness or softness of the Lewis base in comparison to its steric bulk and basicity. The work here paves the way for the examination of the catalytic capabilities of these species, which will be discussed in the next chapter.

Chapter 3

Zirconium-nitrogen intermolecular frustrated Lewis pairs for the catalytic dehydrocoupling of dimethylamine-borane

3.1 Introduction

Amine-borane dehydrocoupling is a catalytic reaction that has received much research attention, both in search of a hydrogen storage material and through the exploration of new inorganic compounds (e.g. inorganic polymers).[140–147] Frustrated Lewis pairs (FLPs) have been used in order to achieve these transformations, with the majority of this work involving main group systems.[148] Work within the Wass group has broadened the scope of FLPs that are able to perform this reaction, with a series of intramolecular Zr/P systems producing very positive results (Scheme 3.1 and Figure 3.1).[10]

This work was then developed through the application of intermolecular Zr/P FLPs; these proved to be less active catalysts but the separation of Lewis acidic and basic functions provided mechanistic insight.[11] This chapter builds upon these results, replacing the

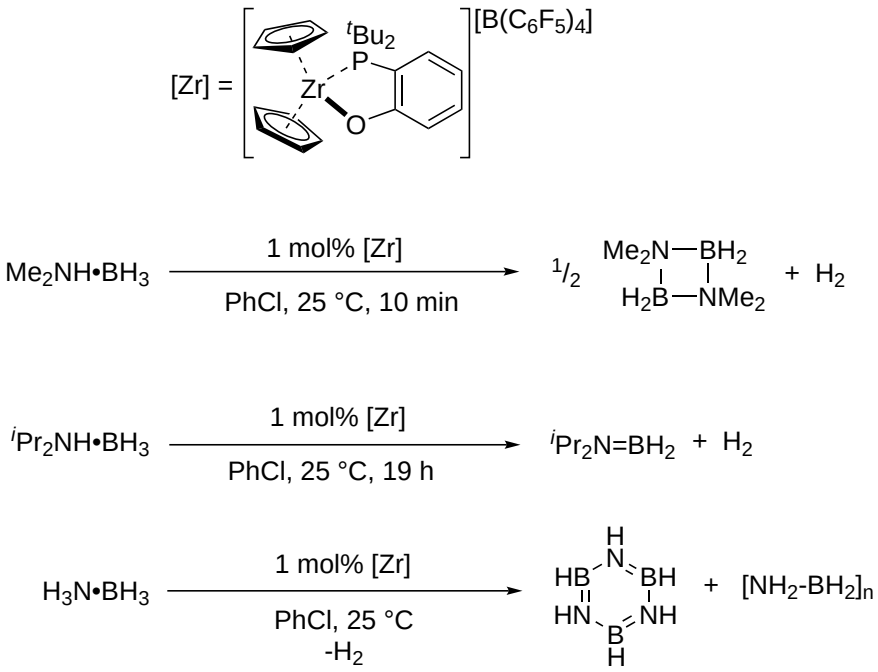

Scheme 3.1: Catalytic dehydrocoupling of amine-boranes using an intramolecular Zr/P FLP.

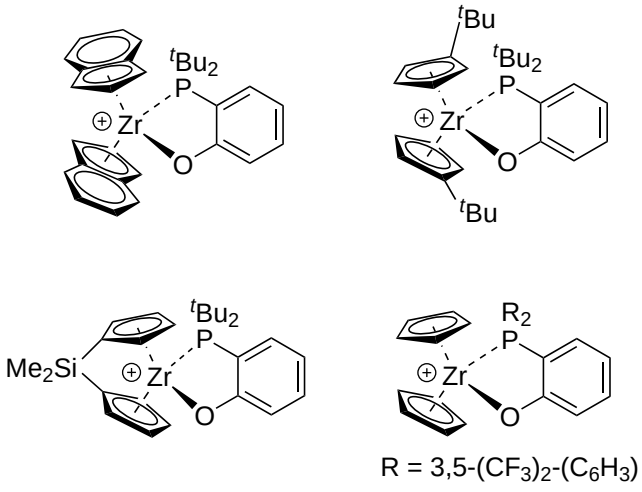

Figure 3.1: Intramolecular Zr/P FLPs used for catalytic amine-borane dehydrocoupling. Counterions omitted for clarity.

phosphine moieties with nitrogen Lewis bases, allowing for more direct comparisons than are possible with the small molecule activation reactions of the previous chapter.

3.2 Aims & Objectives

In the previous chapter, Zr/N Lewis pairs were shown to be effective for small molecule activation. Here, this work is extended by testing the catalytic capability of the same Lewis pairs. Specifically, their ability to perform the dehydrocoupling of $Me_2NH{\cdot}BH_3$ a reaction for which intermolecular Zr FLPs have previously been shown to be capable of performing when phosphines are used. By assessing the reactivity of these catalysts, it is hoped that greater insight into any electronic or steric differences between the Lewis bases affect reactivity, if at all, allowing for better understanding of the reactivity of the Zr/N Lewis pairs in general. In this chapter, the following was sought to be achieved:

- Test the Zr/N Lewis pairs for the dehydrocoupling of $Me_2NH{\cdot}BH_3$
- Alter reaction conditions to see if reactivity can be improved
- Compare the reactivity of individual catalysts to define structure-property relationships

Work within this chapter was also reported in a first author publication.[118]

3.3 Results & Discussion

Dimethylamine-borane ($Me_2NH{\cdot}BH_3$) is often used as a model substrate and indicator for the capability of any particular system to catalyse these dehydrocoupling reactions.[149,150] It has also been widely studied—making product/intermediate elucidation easier—and has been tested with the Zr/P FLPs previously developed by the Wass group,[10,11] allowing for useful comparisons. The catalysts used here are compounds **2.1a–e** and **2.2a–e** from the previous chapter (Figure 3.2), which include the cations developed by the Wass group.

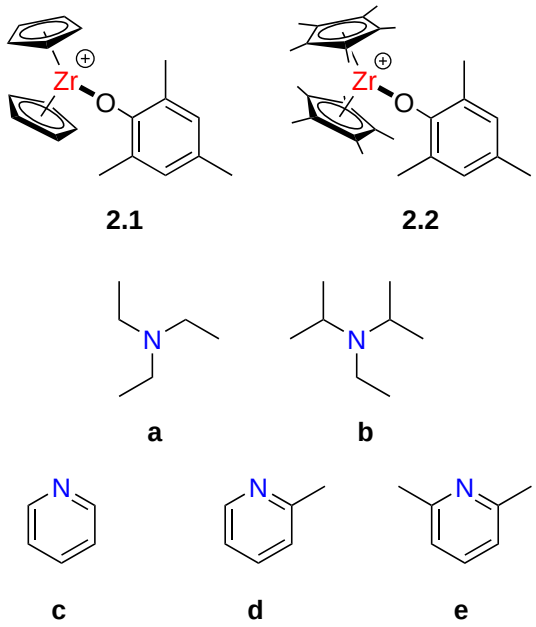

Figure 3.2: The Lewis acids and bases used in this chapter. $[B(C_6F_5)_4]^-$ counterions omitted for clarity.

The previously proposed catalytic cycle comprises two modes by which the product ($[Me_2N–BH_2]_2$) is produced (Scheme 3.2).[11] The first (Cycle A) involves initial binding of $Me_2NH{\cdot}BH_3$ to the Zr centre, followed by deprotonation of both the BH_3 and $HNMe_2$ moieties by the Zr centre and the Lewis base. The $Me_2N{=}BH_2$ that is formed subsequently dimerises to form the product. In Cycle B, $Me_2NH{\cdot}BH_3$ reacts with the bound reactant and the Lewis base, resulting in the formation of the linear diborazane $Me_2NH–BH_2–Me_2N–BH_3$, which may remain bound to the Zr centre or be released into solution before recoordination. Formation of the side-product $Me_2N(B_2H_5)$ can occur here through the loss of a terminal Me_2NH group. The bound $Me_2NH–BH_2–Me_2N–BH_3$ then undergoes an internal redistribution, resulting in the release of $Me_2N{=}BH_2$ which then dimerises.

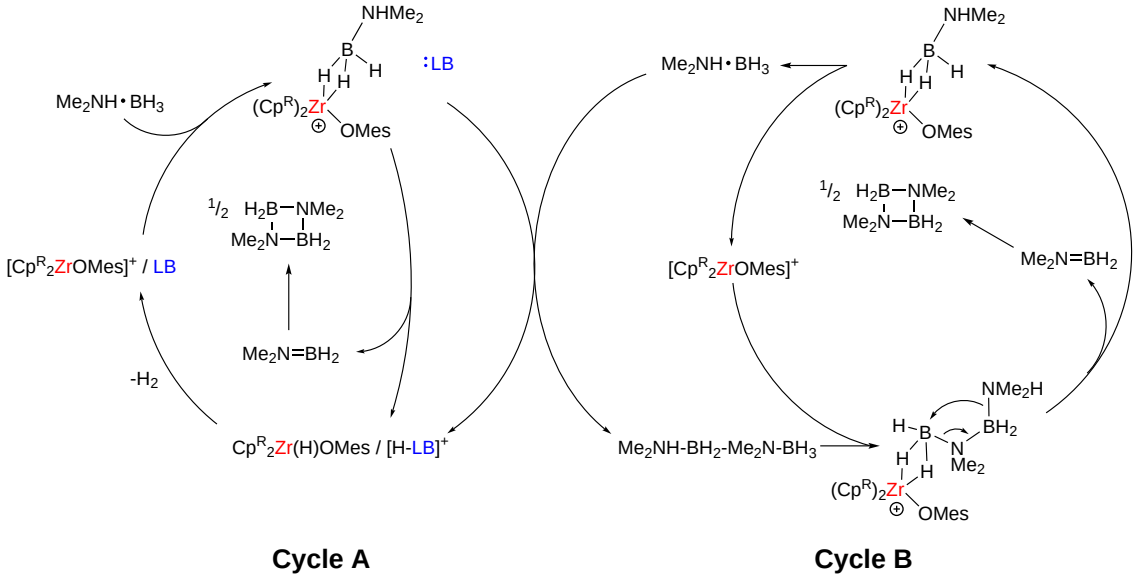

Scheme 3.2: Proposed reaction mechanism for the catalytic dehydrocoupling of $Me_2NH{\cdot}BH_3$ using a Zr(IV)/FLP. The $[B(C_6F_5)_4]^-$ counterion has been omitted for clarity.

3.3.1 Dehydrocoupling of $Me_2NH{\cdot}BH_3$ using 2.1

Initially, catalysts **2.1a**–**e** were tested for the $Me_2NH{\cdot}BH_3$ dehydrocoupling reaction with the substrate added to PhBr-d_5 solutions of each catalyst; the reactions were monitored by $^{11}B\{^1H\}$ NMR spectroscopy. The reactions were run at a temperature of 25 °C using a catalyst loading of 10 mol%, matching the conditions of the intermolecular Zr/P reactions for the benefit of comparing results. The yield and conversion data is derived by integrating the signals in the $^{11}B\{^1H\}$ NMR spectra, where the signal for $[B(C_6F_5)_4]^-$ is used as an internal reference. In general, the reactions show the same side-products and intermediates that are present in the reactions with phosphines (Figure 3.3),[11] implying the reactions follow the same proposed catalytic cycle.

Table 3.1 shows the results of the reactions of **2.1a**–**e**, and it is immediately clear that both **2.1a** and **2.1e** are the superior catalysts with full conversions and yields of 97% (9.5 h) and 96% (10.5 h). **2.1b** and **2.1d** share similar reactivity with poor yields of 7% and

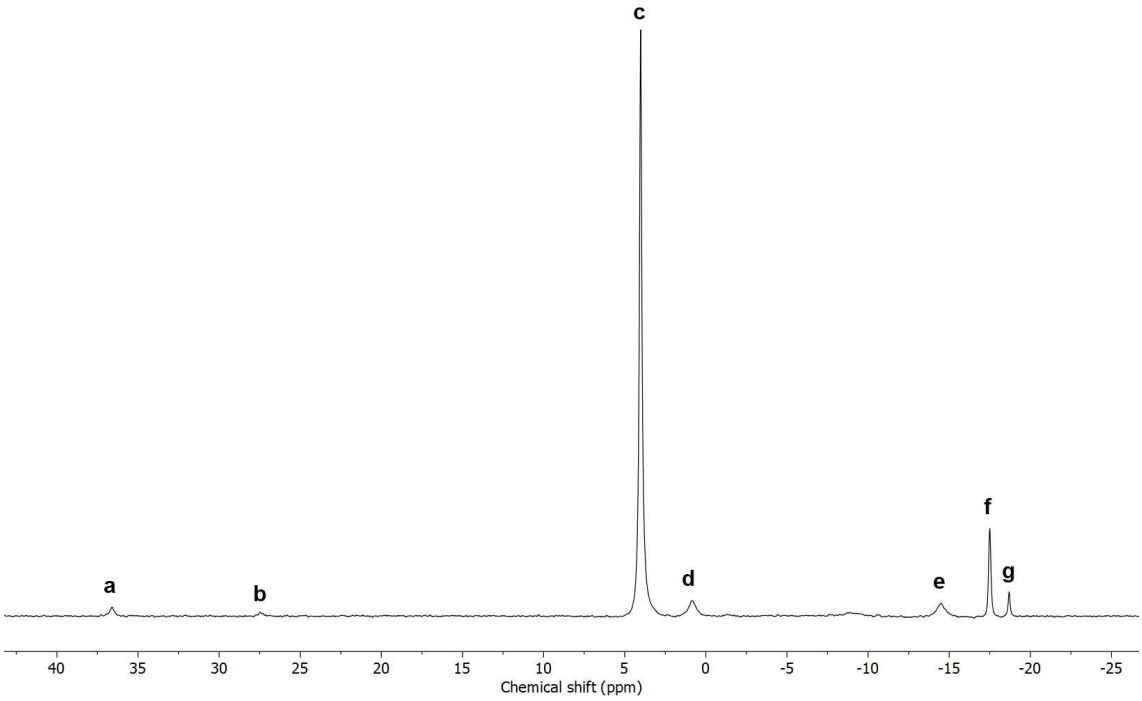

Figure 3.3: $^{11}B\{^{1}H\}$ NMR spectrum (160 MHz, 25 °C, PhBr-d_5, 7.5 h) for the reaction between $Me_2NH{\cdot}BH_3$ and 10 mol% **2.1b**. **a** = $Me_2N{=}BH_2$ (36.6 ppm), **b** = $HB(NMe_2)_2$ (27.5 ppm), **c** = $[Me_2N{-}BH_2]_2$ (4.0 ppm), **d** = $Me_2NH{-}BH_2{-}Me_2N{-}BH_3$ (0.8 ppm), **e** = $Me_2NH{\cdot}BH_3$ and $Me_2NH{-}BH_2{-}Me_2N{-}BH_3$ (-14.5 ppm), **f** = $[B(C_6F_5)_4]^-$ (-17.5 ppm), **g** = $Me_2N(B_2H_5)$ (-18.7 ppm).

9% after 14 h, while **2.1c** did not react at all (a comparison with the previously reported phosphine systems is discussed later).

Table 3.1: Catalytic dehydrocoupling of $Me_2NH{\cdot}BH_3$ using **2.1a**–**e**.

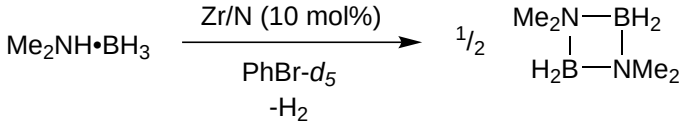

Catalyst	Temperature (°C)	Time (h)	Yield (%)	Conversion (%)
2.1a	25	9.5	97	100
2.1b	25	14	7	26
2.1c	25	14	0	0
2.1d	25	14	9	30
2.1e	25	7.5	79	92
2.1e	25	10.5	96	100
2.1e	25	14	98	100

If we examine the reaction profiles for **2.1a** and **2.1e** some differences become evident (Figures 3.4 and 3.5). Firstly, we can see that although both reactions reach completion after similar times, the reaction with **2.1e** is quicker at the beginning before the rate of consumption reduces towards the end. In the case of **2.1a**, the rate of consumption is slower at the beginning, and increases over time. This is paralleled by the quantity of the intermediate $Me_2NH–BH_2–Me_2N–BH_3$ present throughout each reaction, with the amount of this compound reaching its peak at around 340 min for **2.1a**, and 220 min for **2.1e**. In both cases, there is a constant but very low level of $Me_2N{=}BH_2$, which shows that it is converted to the product very rapidly. The side-products $Me_2N(B_2H_5)$ and $HB(NMe_2)_2$ also appear in both reactions, with slightly more $Me_2N(B_2H_5)$ present in the reaction of **2.1e**. Interestingly, the amount of $HB(NMe_2)_2$ in the reaction of **2.1a** increases after reaction completion, suggesting it is formed from the product, and is assisted by the presence of **a** rather than **e**. The similarity between NEt_3 and the Me_2NH moiety of the amine boranes may be a reason for this, or it may simply be a result of the higher basicity of **a**. Unfortunately, no further intermediate species could be seen or isolated to allow further elucidation of the processes involved.

The change in concentration of $Me_2NH{\cdot}BH_3$ for the reactions of **2.1a** and **2.1e** produces convex and concave curves respectively in their reaction profiles. Although indicating different rates for these reactions, the change in rate with respect to time for each reaction is more clearly revealed in Figures 3.6 and 3.7. Precise reaction rates cannot be derived from these graphs, as NMR derived data is not sufficient to provide accurate values, however, the shape of the graph can still provide useful information about the reaction in question. In the case of **2.1a**, there is a slow increase in rate at the beginning, which rapidly increases after roughly 5 h, before coming to an abrupt halt at around 8.5

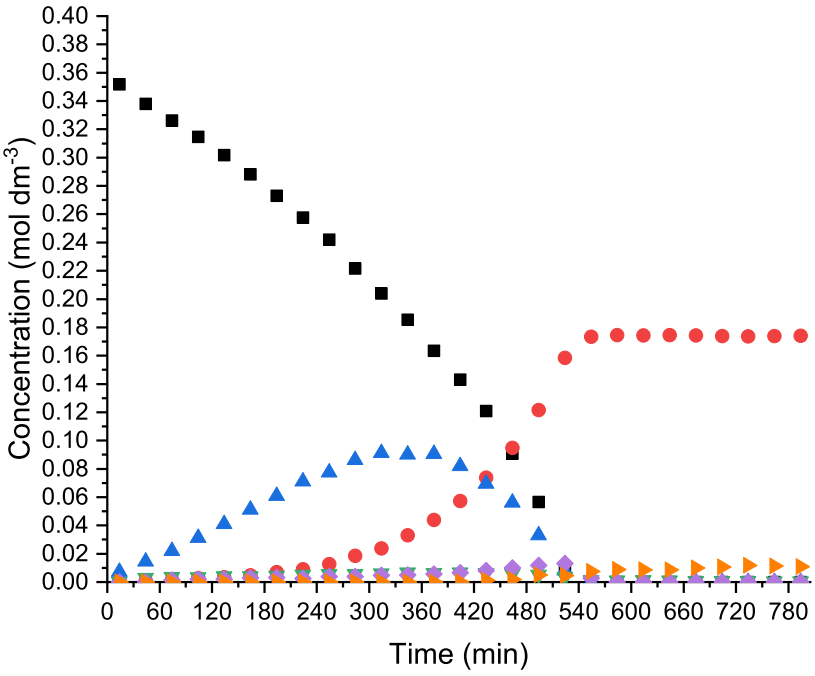

Figure 3.4: Reaction of **2.1a** with $Me_2NH{\cdot}BH_3$ (25 °C, PhBr-d_5, 14 h): (■) $Me_2NH{\cdot}BH_3$; (●) $[Me_2N–BH_2]_2$; (▲) $Me_2NH–BH_2–Me_2N–BH_3$; (◆) $Me_2N{=}BH_2$; (▼) $Me_2N(B_2H_5)$; (▶) $HB(NMe_2)_2$.

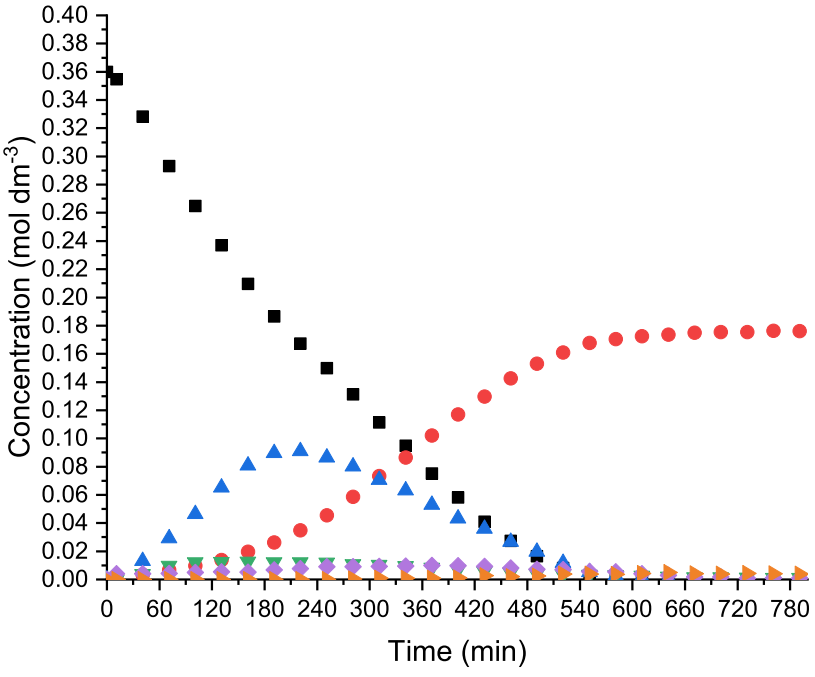

Figure 3.5: Reaction of **2.1e** with $Me_2NH{\cdot}BH_3$ (25 °C, PhBr-d_5, 14 h): (■) $Me_2NH{\cdot}BH_3$; (●) $[Me_2N–BH_2]_2$; (▲) $Me_2NH–BH_2–Me_2N–BH_3$; (◆) $Me_2N{=}BH_2$; (▼) $Me_2N(B_2H_5)$; (▶) $HB(NMe_2)_2$.

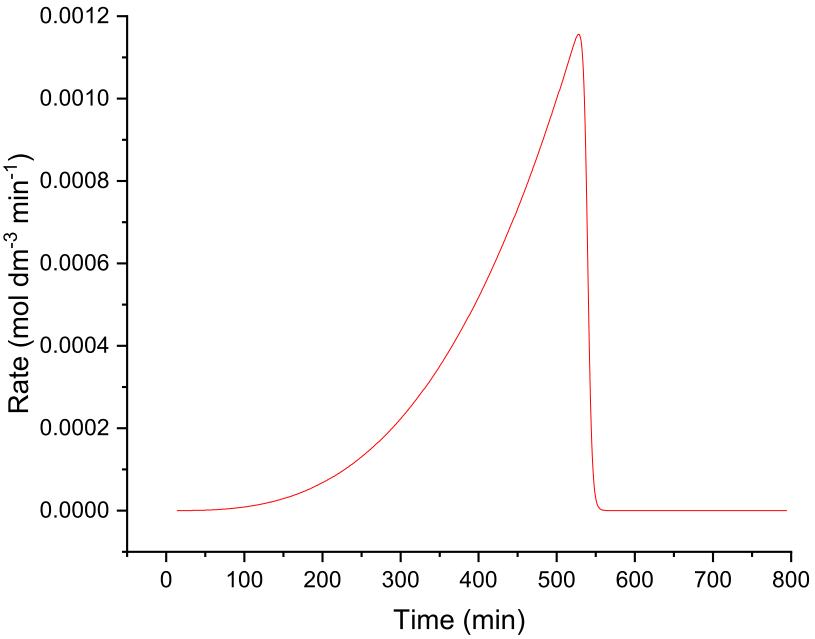

Figure 3.6: Graph showing the change in rate of reaction over time for the dehydrocoupling of $Me_2NH{\cdot}BH_3$ using **2.1a** (25 °C, PhBr-d_5). Rate derived from the change in concentration of $[Me_2N–BH_2]_2$ over time.

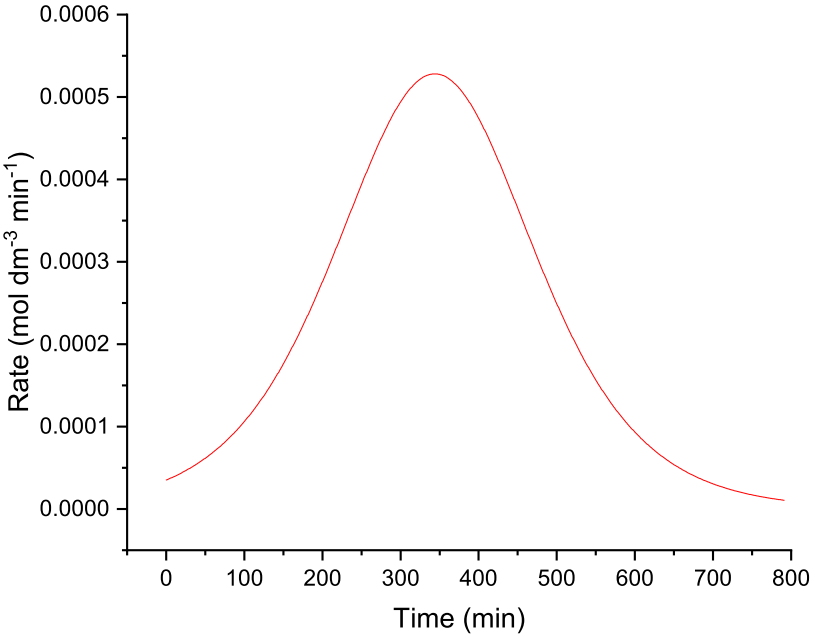

Figure 3.7: Graph showing the change in rate of reaction over time for the dehydrocoupling of $Me_2NH{\cdot}BH_3$ using **2.1e** (25 °C, PhBr-d_5). Rate derived from the change in concentration of $[Me_2N–BH_2]_2$ over time.

h after all reactant is consumed. The reaction proceeds quite differently for **2.1e** as there is initially a higher rate of reaction which steadily increases before reaching its peak at 6 h, before steadily declining.

The reaction rate for **2.1a** appears to continue to increase until no more reactant remains—suggesting the rate could increase further if more $Me_2NH{\cdot}BH_3$ were present—perhaps meaning that a lower catalyst loading could still be effective. The slow start to the reaction could be a result of several factors. One possibility is that the $[H–NEt_3]^+$ cation is relatively stable, and therefore does not release dihydrogen (in combination with the [Zr–H] species) as easily as in **2.1e** for example—with this issue becoming less significant as more $Me_2NH–BH_2–Me_2N–BH_3$ becomes available, and Cycle B becomes more prominent. More $Me_2NH–BH_2–Me_2N–BH_3$ would also mean that more [Zr–($Me_2NH–BH_2–Me_2N–BH_3$)] is present, with less [Zr–($Me_2NH{\cdot}BH_3$)] available for deprotonation with **a**.

The change in rate for the reaction of **2.1e** both indicates that the $[H–\mathbf{e}]^+$ cation is more susceptible to H_2 release than $[H–NEt_3]^+$, and that the reaction is greatly affected by reactant concentration, as the rate significantly decreases at around the 5 h mark, which is also the point at which the concentrations of reactant and product become roughly equal.

The increase in reaction rate of **2.1a** upon increase in concentration of $Me_2NH–BH_2–Me_2N–BH_3$ could perhaps also indicate that the Lewis base plays a role in Cycle B, aiding the rearrangement of the bound compound. However, it may simply be a result of $Me_2NH–BH_2–Me_2N–BH_3$ being in large enough quantity to have a significant effect on product formation.

The reaction profiles for **2.1b** and **2.1d** are shown in Figures 3.8 and 3.9 respectively, with the similar reactivity of both very apparent. In both graphs, far more $Me_2NH–BH_2–Me_2N–BH_3$ is present in comparison to $[Me_2N–BH_2]_2$, demonstrating that the product

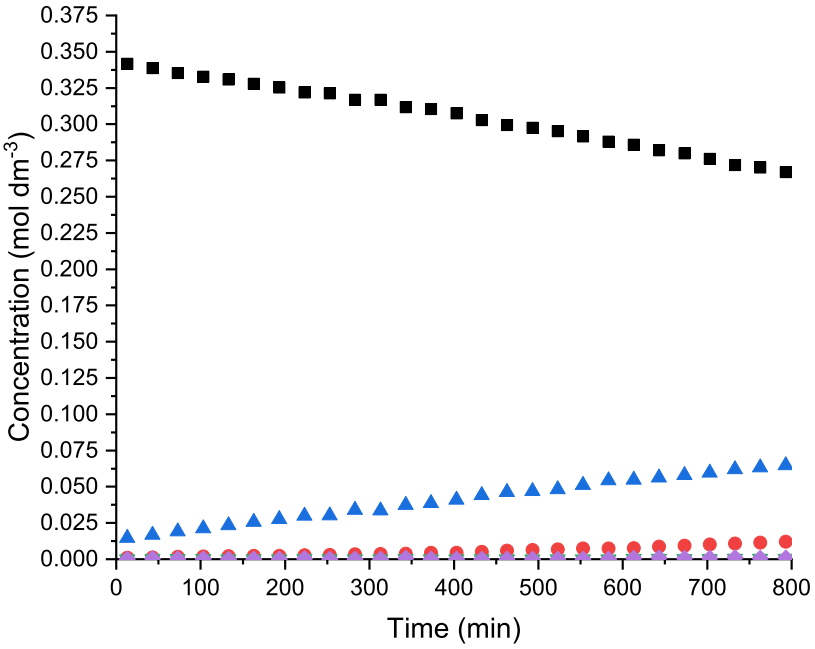

Figure 3.8: Reaction of **2.1b** with $Me_2NH{\cdot}BH_3$ (25 °C, PhBr-d_5, 14 h): (■) $Me_2NH{\cdot}BH_3$; (●) $[Me_2N–BH_2]_2$; (▲) $Me_2NH–BH_2–Me_2N–BH_3$; (◆) $Me_2N{=}BH_2$; (▼) $Me_2N(B_2H_5)$.

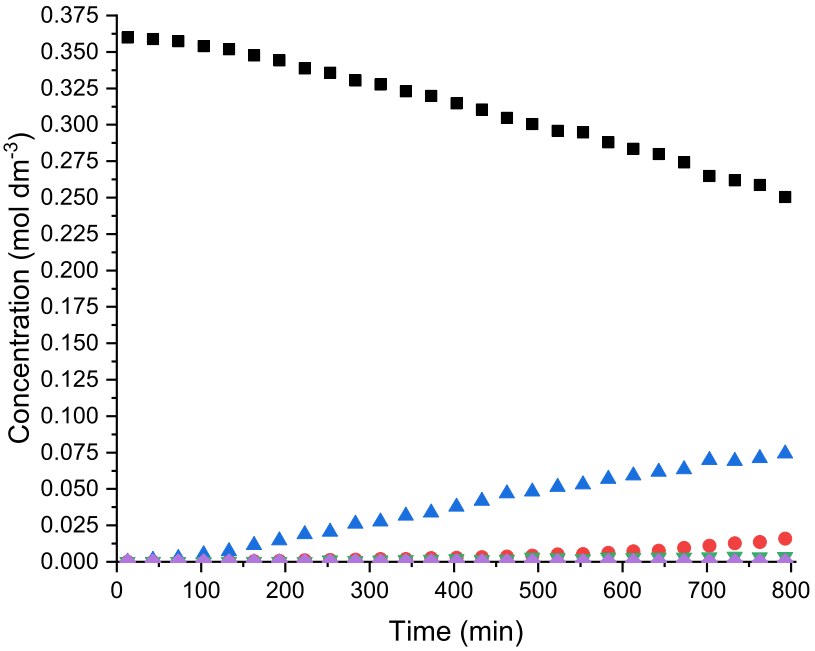

Figure 3.9: Reaction of **2.1d** with $Me_2NH{\cdot}BH_3$ (25 °C, PhBr-d_5, 14 h): (■) $Me_2NH{\cdot}BH_3$; (●) $[Me_2N–BH_2]_2$; (▲) $Me_2NH–BH_2–Me_2N–BH_3$; (◆) $Me_2N{=}BH_2$; (▼) $Me_2N(B_2H_5)$.

formation in Cycle B is relatively slow. By comparison with the reactions of **2.1a** and **2.1e**, there is a similar concentration of product present when the same quantity of Me_2NH–

BH_2–Me_2N–BH_3 is available in solution, suggesting that there is in fact no assistance by the Lewis base—agreeing with the initially proposed reaction mechanism. Another point to note in the reactions of **2.1b** and **2.1d** is that no $HB(NMe_2)_2$ is present in either solution. This may simply be a result of the slower reactions, and this intermediate could perhaps appear after a much longer timeframe, however, it could point towards a Lewis base assisted mechanism for its formation—where **a** and **e** are more effective in this regard.

2.1a and **2.1e** show similar activty to **2.1**/P^{t}Bu$_3$—which achieved 97% conversion in 7.5 h—whilst also proving to be superior to when PCy_3, PEt_3, PPh_3, $PMes_3$, and $P(C_6F_5)_3$ were used as the Lewis base (none reaching greater than 5% conversion after 14 h).[11] Once again this shows that a balance between electronic and steric effects is necessary for good reactivity to be attained. PCy_3 is more basic than **e**, and has high steric bulk, and yet is unable to match the reactivity of **e**. By contrast, the steric bulk of NEt_3 is less than PCy_3, similar to PEt_3, yet is a far more effective Lewis base in this reaction.

3.3.2 Dehydrocoupling of $Me_2NH{\cdot}BH_3$ using 2.2

Catalysts **2.2a**–**e** were also tested for their ability to catalyse the dehydrocoupling of $Me_2NH{\cdot}BH_3$. The same conditions were applied, using a 10 mol% loading of catalyst in PhBr-d_5 solutions at 25 °C, with the reactions monitored by $^{11}B\{^1H\}$ NMR spectroscopy over a 14 h period. The same products are seen for these reactions. The $^{11}B\{^1H\}$ NMR spectrum for the reaction of **2.2b** after 7 h is shown in Figure 3.10 and is very similar to that of **2.1b**, with the only difference being the lack of any $HB(NMe_2)_2$. In fact, **2.2c** is the only catalyst that produces visible quantities of this side-product.

The results for these reactions are shown in Table 3.2, and it is very clear that **2.2e** is the most effective catalyst from this group, with full conversion achieved after 6.5 h (yield

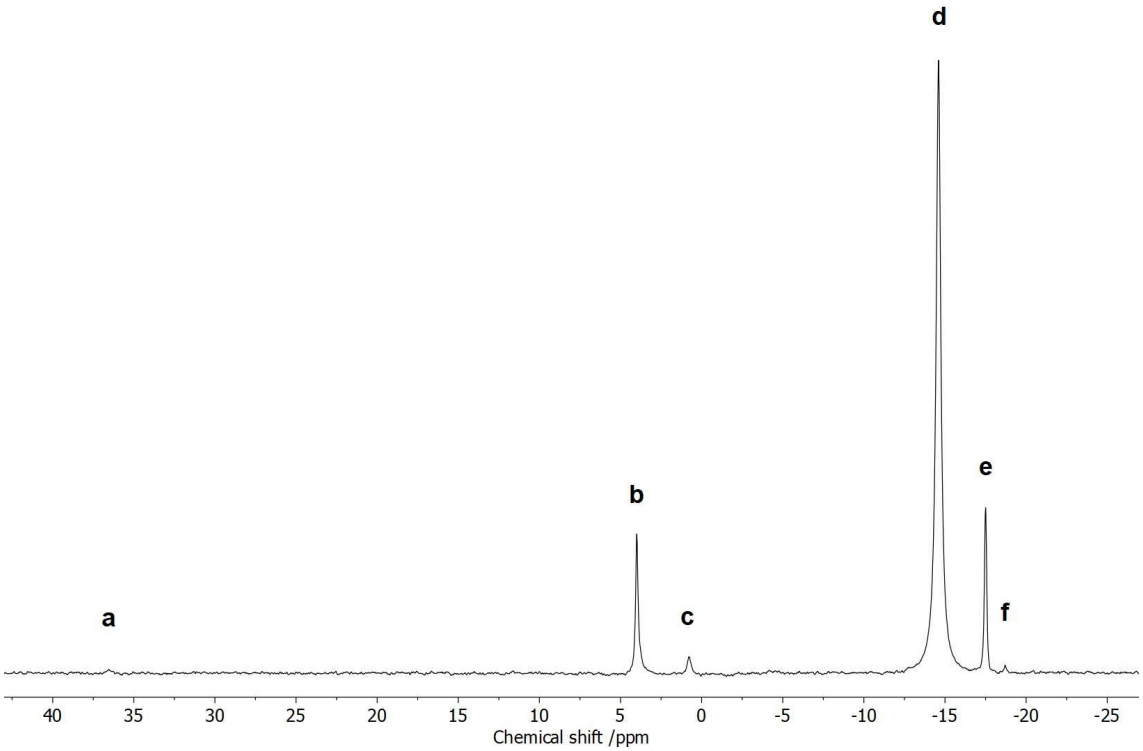

Figure 3.10: $^{11}B\{^{1}H\}$ NMR spectrum (160 MHz, 25 °C, PhBr-d_5, 7 h) for the reaction between $Me_2NH{\cdot}BH_3$ and 10 mol% **2.2b**. **a** = $Me_2N{=}BH_2$ (36.5 ppm), **b** = $[Me_2N{-}BH_2]_2$ (4.0 ppm), **c** = $Me_2NH{-}BH_2{-}Me_2N{-}BH_3$ (0.8 ppm), **d** = $Me_2NH{\cdot}BH_3$ and $Me_2NH{-}BH_2{-}Me_2N{-}BH_3$ (-14.6 ppm), **e** = $[B(C_6F_5)_4]^-$ (-17.5 ppm), **f** = $Me_2N(B_2H_5)$ (-18.7 ppm).

= 97%) and a yield that is over 99% after 7.5 h. This reactivity surpasses **2.1a** and **2.2e** which required 9.5 h and 10.5 h respectively to attain comparable results.

Table 3.2: Catalytic dehydrocoupling of $Me_2NH{\cdot}BH_3$ using **2.2a–e**.

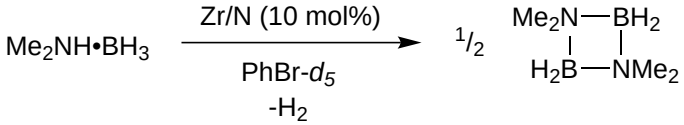

Catalyst	Temperature (°C)	Time (h)	Yield (%)	Conversion (%)
2.2a	25	14	9	10
2.2b	25	14	13	15
2.2c	25	14	47	47
2.2d	25	14	36	42
2.2e	25	6.5	97	100
2.2e	25	7.5	>99	100

The reaction profile for **2.2e** is shown in Figure 3.11, and (apart from the shorter reaction time) it is immediately clear that there is a far lower concentration of Me_2NH–BH_2–Me_2N–BH_3 compared to the reactions of **2.1a** and **2.1e**. This could be linked to Cycle A, the turnover of which would be much higher if the deprotonation of bound $Me_2NH{\cdot}BH_3$ and subsequent release of dihydrogen is quicker in this reaction. There would therefore be less time for the formation of Me_2NH–BH_2–Me_2N–BH_3 through the reaction of bound and unbound $Me_2NH{\cdot}BH_3$, as any bound $Me_2NH{\cdot}BH_3$ is rapidly being converted to $Me_2N{=}BH_2$ before this can take place. Another possibility is that because the $[Cp^*_2ZrOMes]^+$ cation is more sterically hindered, it inhibits the formation of Me_2NH–BH_2–Me_2N–BH_3.

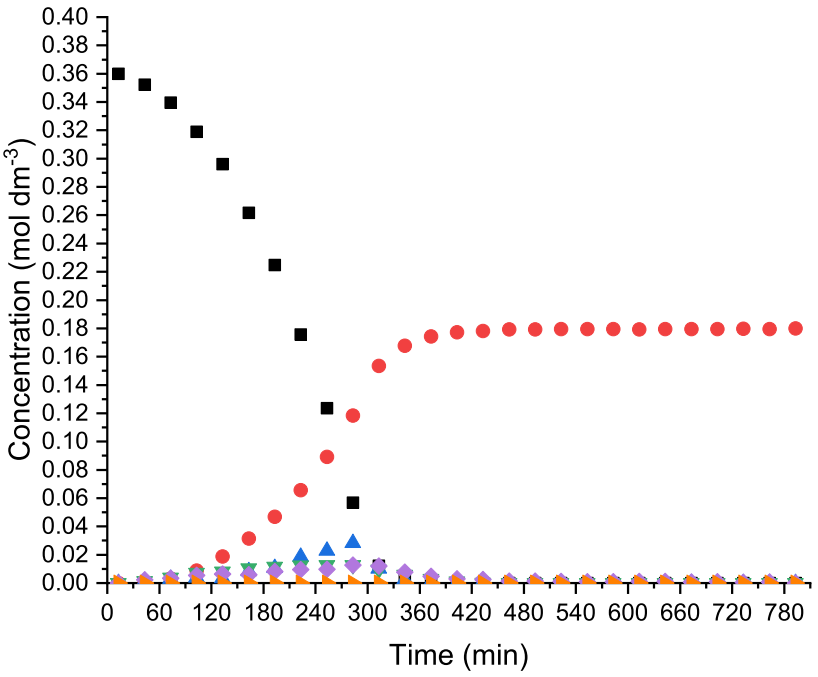

Figure 3.11: Reaction of **2.2e** with $Me_2NH{\cdot}BH_3$ (25 °C, PhBr-d_5, 14 h): (■) $Me_2NH{\cdot}BH_3$; (●) $[Me_2N{-}BH_2]_2$; (▲) Me_2NH–BH_2–Me_2N–BH_3; (◆) $Me_2N{=}BH_2$; (▼) $Me_2N(B_2H_5)$; (▶) $HB(NMe_2)_2$.

The lack of Me_2NH–BH_2–Me_2N–BH_3 in this reaction—in combination with the greater reactivity of **2.2e**—poses an interesting question: does a greater quantity of Me_2NH–BH_2–

Me_2N–BH_3 present in solution result in a slower reaction? In other words, is Cycle B significantly slower than Cycle A, meaning that the more Zr cation taking part in Cycle B, the slower the reaction? Although it cannot be confirmed whether the lower concentration of Me_2NH–BH_2–Me_2N–BH_3 observed in the reaction of **2.2e** contributes to a quicker reaction without further experimentation, it is certainly a possibility. Consequently, higher concentrations of Me_2NH–BH_2–Me_2N–BH_3 would result in less free Zr cation available to perform the transformations in Cycle A. This could perhaps even explain why **2.1e** does not react faster than **2.1a** despite having an apparently higher initial rate of reaction. If we examine the rate of reaction of **2.2e** (Figure 3.12), we can see that it reaches a peak after 4.8 h, which is nearly an hour earlier than **2.1e**.

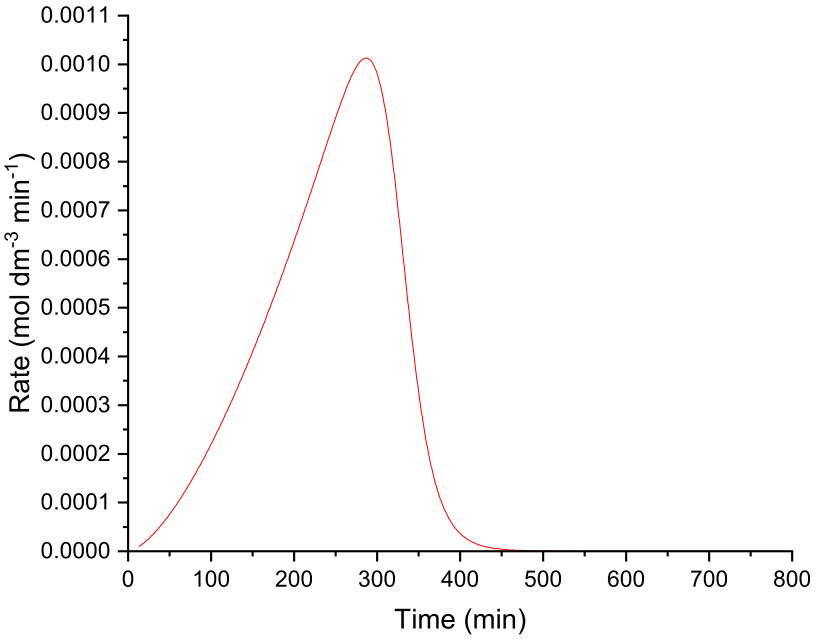

Figure 3.12: Graph showing the change in rate of reaction over time for the dehydrocoupling of $Me_2NH{\cdot}BH_3$ using **2.2e** (25 °C, PhBr-d_5). Rate derived from the change in concentration of $[Me_2N$–$BH_2]_2$ over time.

Surprisingly, the second most reactive catalyst of the series **2.2a**–**e** is **2.2c**, which achieves a yield of 47% and a conversion of 47%. If we examine the reaction profile

shown in Figure 3.13 we can see that the only side-product produced is a trace amount of $HB(NMe_2)_2$, with no visible quantity of the intermediate $Me_2NH–BH_2–Me_2N–BH_3$ throughout the reaction. We also see an induction period of around 3.3 h before any reactivity is observed, which is likely a result of the close interaction between the Lewis acid and base making initial binding of $Me_2NH{\cdot}BH_3$ more difficult. However, the fact that this reaction achieves a higher yield and conversion than **2.1b–d**, **2.2a**, **2.2b**, and **2.2d** perhaps provides strong evidence for the hypothesis that $Me_2NH–BH_2–Me_2N–BH_3$ inhibits overall product formation. In addition to this, the fact that almost no side-products are seen whatsoever perhaps indicates that the Lewis base *does* play a role in their formation. **2.2c** could be a more effective catalyst as it inhibits, or does not facilitate, the formation of side-products or the $Me_2NH–BH_2–Me_2N–BH_3$ intermediate.

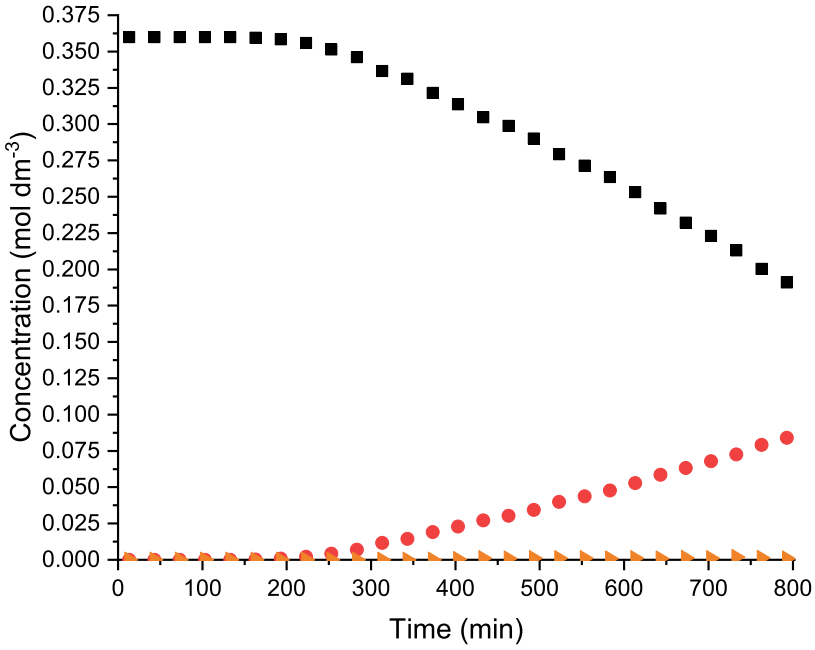

Figure 3.13: Reaction of **2.2c** with $Me_2NH{\cdot}BH_3$ (25 °C, PhBr-d_5, 14 h): (■) $Me_2NH{\cdot}BH_3$; (●) $[Me_2N–BH_2]_2$; (▶) $HB(NMe_2)_2$.

The reaction profile for **2.2d** is shown in Figure 3.14, and we can immediately see that the slightly bulkier 2-methylpyridine Lewis base allows for the $Me_2NH–BH_2–Me_2N–BH_3$

intermediate to be produced. Considering that this reaction does not possess a significant induction period (unlike **2.2c**), we would perhaps expect to achieve a higher conversion and yield than **2.2c**. However, the fact that this does not occur provides further evidence of the inhibitory nature of Me_2NH–BH_2–Me_2N–BH_3.

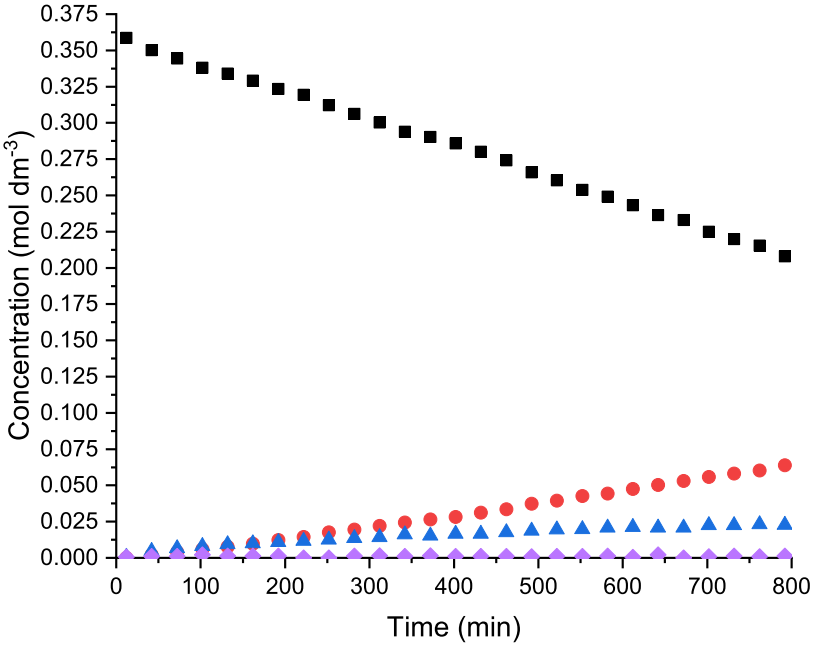

Figure 3.14: Reaction of **2.2d** with $Me_2NH{\cdot}BH_3$ (25 °C, PhBr-d_5, 14 h): (■) $Me_2NH{\cdot}BH_3$; (●) $[Me_2N–BH_2]_2$; (▲) $Me_2NH–BH_2–Me_2N–BH_3$; (◆) $Me_2N{=}BH_2$.

The reaction profiles of **2.2a** and **2.2b** can be seen in Figures 3.15 and 3.16 respectively, with both showing very limited reactivity. The reason for this is likely due the degradation of the catalyst—as outlined in the previous chapter—with apparent deprotonation of the Zr cation by the Lewis base. The $[H–LB][B(C_6F_5)_4]$ salts then precipitate out of solution when in significant enough quantities. However, steric constraints may also be a factor, with the bulkier Cp* ligands perhaps making **a** and **b** far less suitable as the Lewis basic moiety.

Interestingly, none of the previously tested phosphine Lewis bases (PPh_3, PEt_3, PCy_3, $PMes_3$, P^tBu_3, and $P(C_6F_5)_3$) were able to attain a yield greater than 5% in combina-

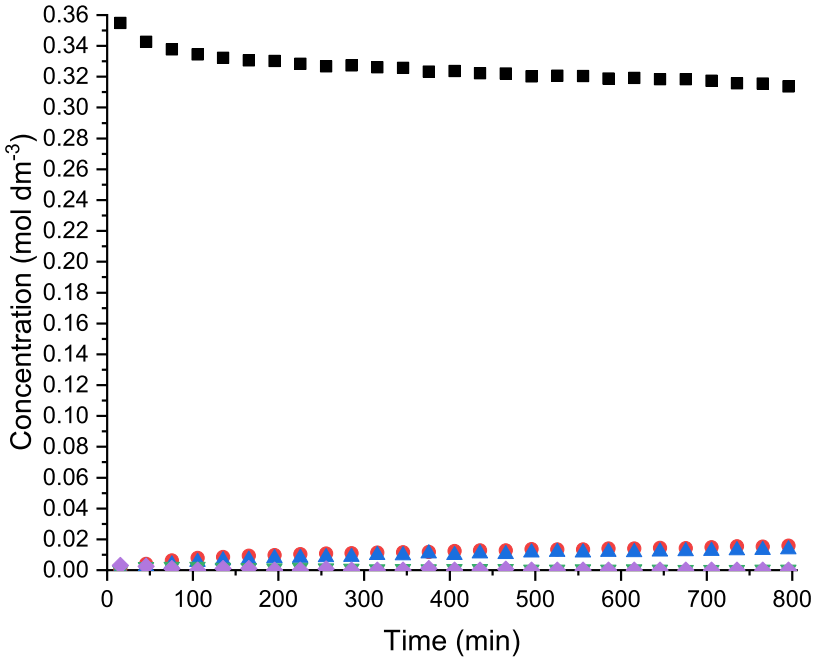

Figure 3.15: Reaction of **2.2a** with $Me_2NH{\cdot}BH_3$ (25 °C, PhBr-d_5, 14 h): (■) $Me_2NH{\cdot}BH_3$; (●) $[Me_2N–BH_2]_2$; (▲) $Me_2NH–BH_2–Me_2N–BH_3$; (◆) $Me_2N{=}BH_2$; (▼) $Me_2N(B_2H_5)$.

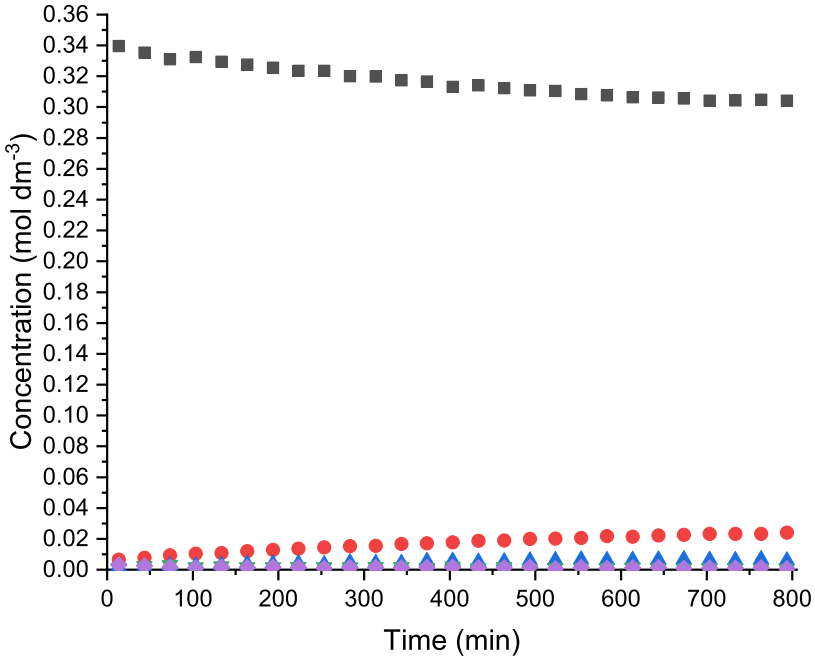

Figure 3.16: Reaction of **2.2b** with $Me_2NH{\cdot}BH_3$ (25 °C, PhBr-d_5, 14 h): (■) $Me_2NH{\cdot}BH_3$; (●) $[Me_2N–BH_2]_2$; (▲) $Me_2NH–BH_2–Me_2N–BH_3$; (◆) $Me_2N{=}BH_2$; (▼) $Me_2N(B_2H_5)$.

tion with **2.2**,[11] meaning that **e** is far superior when used for this reaction. This may predominantly be a result of steric effects, as 2,6-dimethylpyridine is the smallest of these compounds in addition to being relatively flat in comparison (yet still sterically bulkier and more basic than **c** and **d**).

3.3.3 Dehydrocoupling of $Me_2NH{\cdot}BH_3$ at 60 °C

The reactions of the most successful catalysts (**2.1a**, **2.1e**, and **2.2e**) were repeated at the higher temperature of 60 °C, with the results shown in Table 3.3 along with the relevant results at a lower temperature. As expected, a significant rate enhancement was observed for all the reactions at 60 °C, with all reactions reaching completion in 30 min or less.

Table 3.3: Catalytic dehydrocoupling of $Me_2NH{\cdot}BH_3$ using **2.1a**, **2.1e**, and **2.1e**.

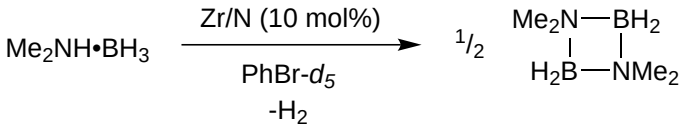

Catalyst	Temperature (°C)	Time (h)	Yield (%)	Conversion (%)
2.1a	25	9.5	97	100
2.1a	60	0.45	93	100
2.1e	25	10.5	96	100
2.1e	60	0.5	90	100
2.2e	25	6.5	97	100
2.2e	25	7.5	>99	100
2.2e	60	0.5	98	100

Firstly, looking at the reaction of **2.1a**, we can see that there is a small drop in yield compared to the reaction at 25 °C—93% compared 97%. By examining the reaction profile (Figure 3.17) we can see that this is the result of an increase in the concentration of $HB(NMe_2)_2$ towards the end of the reaction. After the reaction has reached completion, the amount of $HB(NMe_2)_2$ continues to rise—along with a slow decrease in the concen-

tration of $[Me_2N–BH_2]_2$—showing that it forms as a result of degradation of the product which is exacerbated by the higher temperature. The same degradation is seen in the 25 °C reaction but with less than half of the quantity of $HB(NMe_2)_2$ formed at 60 °C. Other differences between the higher and lower temperature reactions include the different maximum concentrations of $Me_2NH–BH_2–Me_2N–BH_3$ (0.091 mol dm^{-3} at 25 °C; 0.051 mol dm^{-3} at 60 °C) and $Me_2N{=}BH_2$ (0.013 mol dm^{-3} at 25 °C; 0.020 mol dm^{-3} at 60 °C).

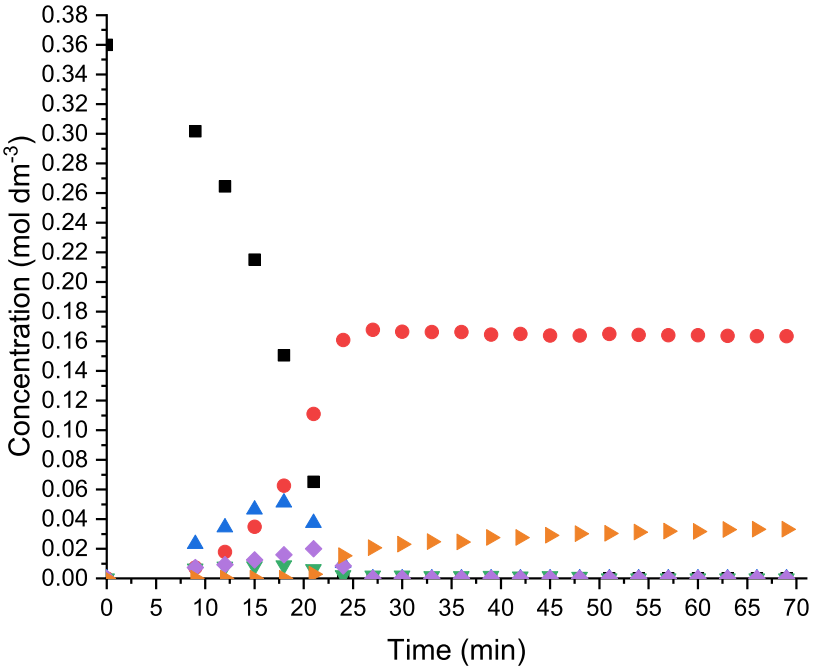

Figure 3.17: Reaction of **2.1a** with $Me_2NH{\cdot}BH_3$ (60 °C, PhBr-d_5, 1 h): (■) $Me_2NH{\cdot}BH_3$; (●) $[Me_2N–BH_2]_2$; (▲) $Me_2NH–BH_2–Me_2N–BH_3$; (◆) $Me_2N{=}BH_2$; (▼) $Me_2N(B_2H_5)$; (▶) $HB(NMe_2)_2$.

A similar reaction profile can be seen for **2.1e** (Figure 3.18), with a lower overall yield at 60 °C (90% compared to 96%) as a result of formation of $HB(NMe_2)_2$. There is also a lower maximum concentration of $Me_2NH–BH_2–Me_2N–BH_3$ at the higher temperature (0.091 mol dm^{-3} at 25 °C; 0.043 mol dm^{-3} at 60 °C), while there is a higher maximum concentration of $Me_2N{=}BH_2$ (0.010 mol dm^{-3} at 25 °C; 0.023 mol dm^{-3}). These two points

are likely correlated, as the slower conversion of $Me_2NH–BH_2–Me_2N–BH_3$ to $Me_2N=BH_2$ has already been shown, so in the reactions where there is more $Me_2NH–BH_2–Me_2N–BH_3$, there is less $Me_2N=BH_2$. However, another explanation could be that Cycle A is faster at the higher temperature, resulting in greater formation of $Me_2N=BH_2$, which dimerises slower than the rate of production.

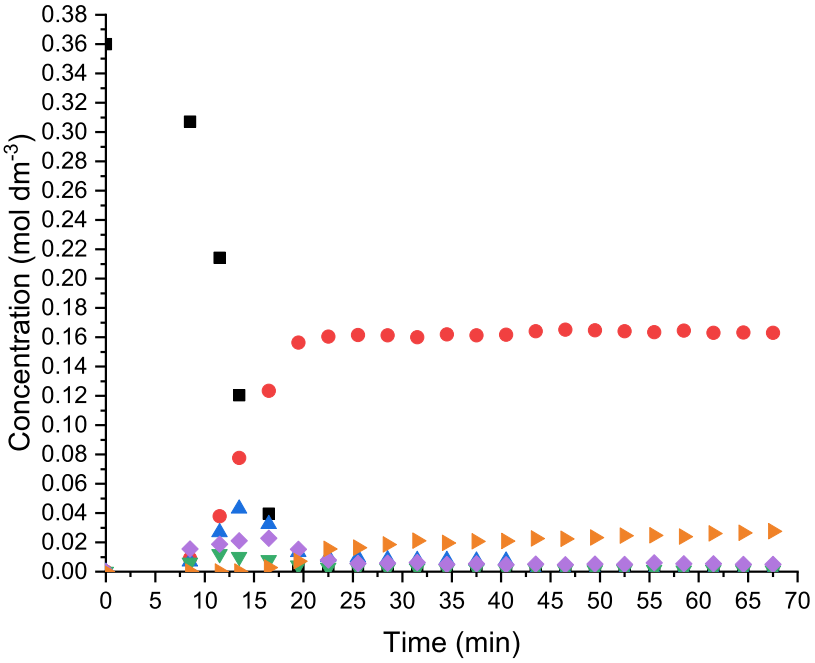

Figure 3.18: Reaction of **2.1e** with $Me_2NH{\cdot}BH_3$ (60 °C, PhBr-d_5, 1 h): (■) $Me_2NH{\cdot}BH_3$; (●) $[Me_2N–BH_2]_2$; (▲) $Me_2NH–BH_2–Me_2N–BH_3$; (◆) $Me_2N=BH_2$; (▼) $Me_2N(B_2H_5)$; (▶) $HB(NMe_2)_2$.

The final 60 °C reaction was for **2.2e**, and unlike **2.1a** and **2.1e** there was not a significant loss of yield (98% as opposed to >99% for the reaction at 25 °C). As shown in the reaction profile (Figure 3.19) we can see that significantly less $HB(NMe_2)_2$ is produced using **2.2e** than the other catalysts, which perhaps alludes to a role played by the Zr cation in its formation. However, more $Me_2N(B_2H_5)$ is formed, showing that a different side-product is favoured, although this does not continue after reaction completion.

The rate graphs for each of these three reactions are very similar (Figure 3.20), with

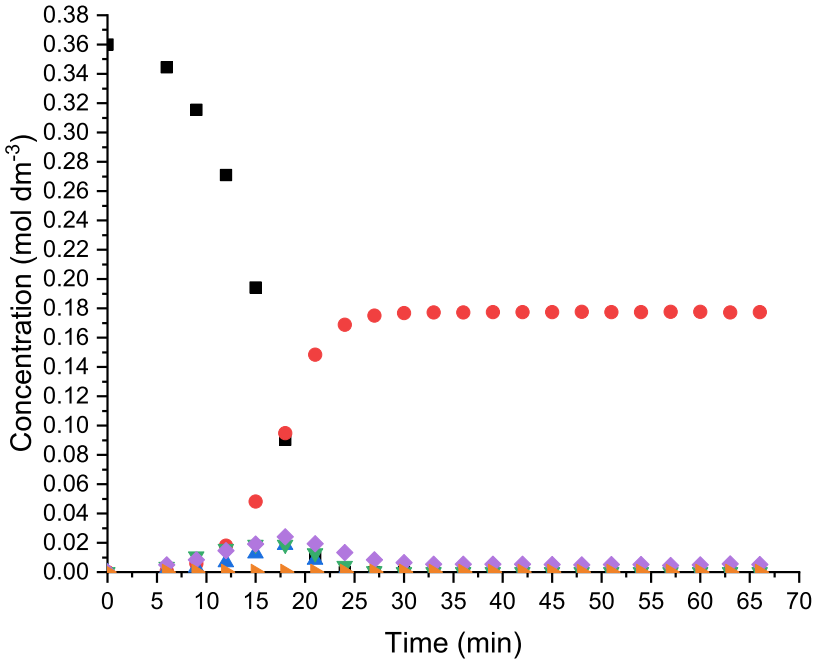

Figure 3.19: Reaction of **2.2e** with $Me_2NH{\cdot}BH_3$ (60 °C, PhBr-d_5, 1 h): (■) $Me_2NH{\cdot}BH_3$; (●) $[Me_2N–BH_2]_2$; (▲) $Me_2NH–BH_2–Me_2N–BH_3$; (◆) $Me_2N{=}BH_2$; (▼) $Me_2N(B_2H_5)$; (▶) $HB(NMe_2)_2$.

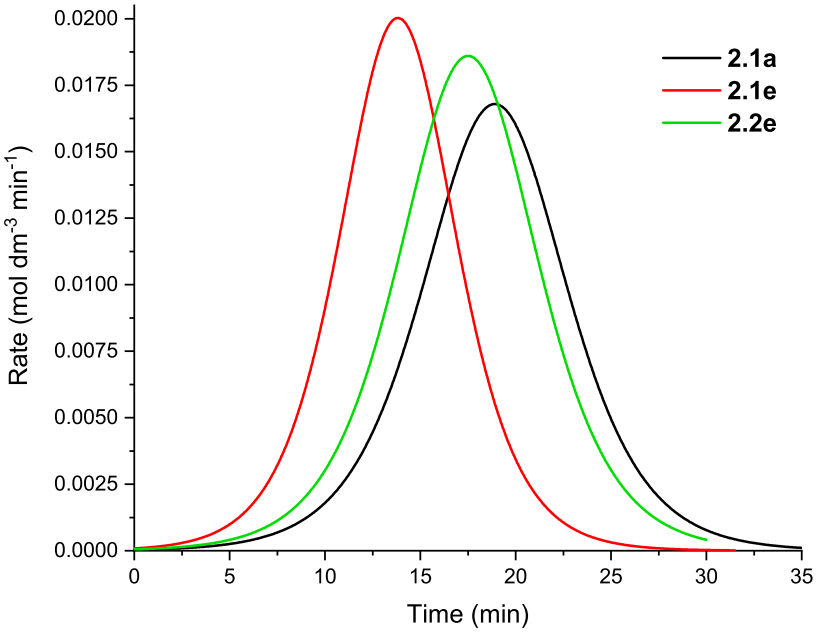

Figure 3.20: Graph showing the change in rate of reaction over time for the dehydrocoupling of $Me_2NH{\cdot}BH_3$ using **2.1a**, **2.1e**, and **2.2e** (60 °C, PhBr-d_5). Rate derived from the change in concentration of $[Me_2N–BH_2]_2$ over time.

2.1e reaching maximum rate the quickest, after only 14 min—**2.1a** and **2.2e** reach maximum rate at 19 and 18 min respectively.

3.4 Conclusion

In this chapter, $Me_2NH{\cdot}BH_3$ has been successfully dehydrocoupled to $[Me_2N–BH_2]_2$ using a series of Zr/N Lewis pair catalysts. The most effective catalysts were found to be **2.1a**, **2.1e**, and **2.2e**, with each achieving full conversion of the reactant with yields of 97%, 96%, and >99% respectively. The more dynamic Zr–N bond present within **2.1a**, **2.1e**, and **2.2e** appears to be a significant reason for their greater reactivity compared to the other Lewis pairs. The total reaction times for these three reactions were then vastly reduced by raising the reaction temperature from 25 °C to 60 °C, which resulted in slightly lower yields for **2.1a** and **2.1e** due to the formation of $HB(NMe_2)_2$ as a side-product.

Surprisingly, the next best catalyst was demonstrated to be **2.2c**, which has been attributed to the absence of any $Me_2NH–BH_2–Me_2N–BH_3$ intermediate, leading to the conclusion that this compound acts as an inhibitor of the reaction both by occupying the Zr cation and preventing it from taking part in the quicker Cycle A (see the reaction mechanism, Scheme 3.2), and by reducing the potential concentration of $Me_2N{=}BH_2$.

The reactivity of catalysts **2.1a**, **2.1e**, and **2.2e** was also shown to be comparable to **2.1**/P^tBu_3, and superior to all other previously tested phosphines. Additionally, **2.2** was found to work effectively in combination with **e**, when no tested phosphine was shown to do so.

Overall, Zr/N Lewis pairs have demonstrated their catalytic capabilities which, in combination with their effectiveness at small molecule activation (see Chapter 2), shows

that they can be used as alternatives to phosphines in intermolecular Zr FLP chemistry. Further insight has also been given into the subtle steric and electronic effects which play such a major role in this area of chemistry, highlighting the importance of selecting the right Lewis base with the right Lewis acid for any given reaction.

Chapter 4

Magnesium Lewis acids in intermolecular Lewis pair chemistry

4.1 Introduction

For the majority of the 20th century the coordination chemistry of magnesium was dominated by Grignard compounds,[52] with few other prominent applications of the element within this field. This changed towards the end of the last century, and there now exists a wealth of chemistry that shows magnesium, and the other alkaline earth metals, to be valuable elements capable of performing tasks previously seen as more suited to other areas of the periodic table.

Magnesium complexes employing β-diketiminates as ligands have received wide attention in particular, with these compounds used for a number of different reactions including hydroaminations,[94] fluoroarene functionalisation,[97] hydroborations,[79,80,82,84,86] and amine-borane dehydrocoupling (Scheme 4.1),[87,88,151?] in addition to these ligands being used to stabilise Mg(I) dimers.[56,67]

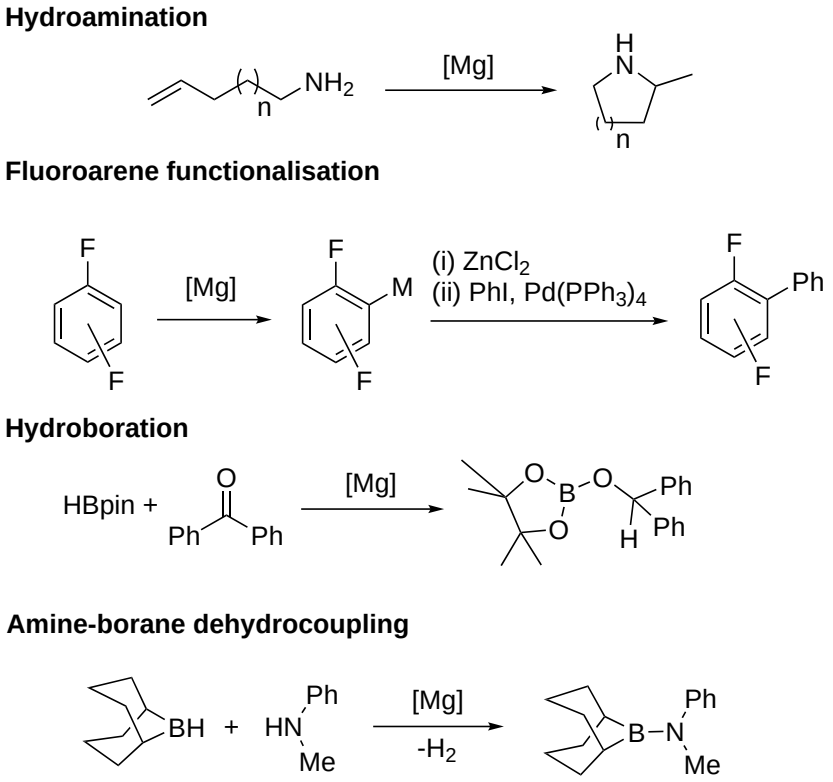

Scheme 4.1: Examples of transformations and functionalisations performed by Mg β-diketiminate complexes.

The work in this chapter seeks to further build upon the application of Mg β-diketiminate species by employing them in conjunction with Lewis bases, and to see whether the subsequent systems are capable of performing small molecule activations in a cooperative Lewis pair manner similar to that seen in Chapter 2. The catalytic capability of these Lewis pairs can also be investigated by testing their ability to perform the dehydrocoupling of amine-boranes.

4.2 Aims & Objectives

Frustrated Lewis pair (FLP) chemistry is an area of research that has vastly expanded over the past decade, with elements from across the periodic table employed as both the Lewis

acidic and Lewis basic components of the system. The study of group 2 elements and their uses as effective catalysts and reagents for chemical transformations has also become far more prominent. However, the exploration of group 2 elements within an FLP structure is rather more limited, so therein lies the possibility to explore to what degree group 2 complexes are capable of fulfilling the role of the Lewis acid in an FLP-type system. The following goals were set when carrying out this research:

- Synthesise novel Mg Lewis acids and analyse their interaction with a series of Lewis bases
- Use these Lewis pairs in order to carry out small molecule activations and transformations
- Explore the catalytic capability of these systems through amine-borane dehydrocoupling reactions

It should be noted that all X-ray crystallography experiments were performed by Dr Natalie Pridmore and Dr Hazel Sparkes (University of Bristol).

4.3 Results & Discussion

4.3.1 Synthesis of magnesium Lewis acids

In order to produce the desired Mg Lewis acids, a suitable magnesium precursor is first required. β-Diketiminates were chosen as the main ligand set for these compounds due to their high modifiability and already wide application in Mg chemistry (see Chapter 1). Initial experiments sought to synthesise the β-diketiminate **4.1** (Figure 4.1), which possesses sterically bulky diisopropylphenyl groups to help the stabilisation of future com-

pounds. Schlenk-type equilibria—whereby a complex of the form LAeX converts to L_2Ae and AeX_2 (Scheme 4.2)—can be an issue with group 2 complexes; however, β-diketiminate ligands have been demonstrated as highly effective in preventing this from happening by affording high steric bulk about the metal centre.[57–59] Although methyl groups are more commonly employed along the molecular backbone, these have been replaced by *tert*-butyl groups in order to avoid previously observed, unwanted deprotonation at this position.[102]

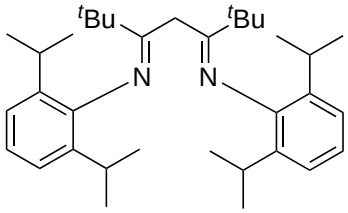

4.1

Figure 4.1: The desired β-diketiminate **4.1**.

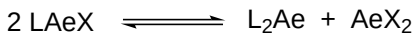

Scheme 4.2: A Schlenk-type equilibrium. Ae = alkaline earth.

The standard synthesis for β-diketiminate compounds involves a condensation reaction through the addition of the desired amine to a diketone in an acidic environment. However, when *tert*-butyl groups are required this synthetic route is not possible, with no product obtainable even after a week of reaction (Scheme 4.3).

Instead, a 4-step literature procedure was required to synthesise **4.1** (Scheme 4.4),[152]

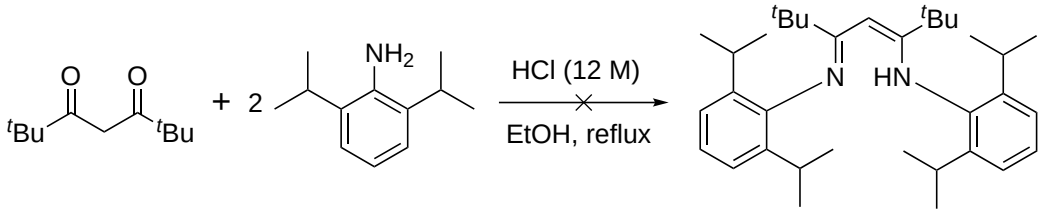

Scheme 4.3: Attempted formation of the desired β-diketiminate via the reaction of diisopropylaniline with 2,2,6,6-tetramethyl-3,5-heptanedione.

which involves initial nucleophilic substitution of pivaloyl chloride with 2,6-diisopropylaniline (yield = 42%) followed by conversion to a chloroimine (71%),[153] a portion of which is methylated (98%). The methylimine is then lithiated and reacted with the chloroimine to form **4.1** via salt metathesis (79%), giving a yield of 23% for the entire synthesis.

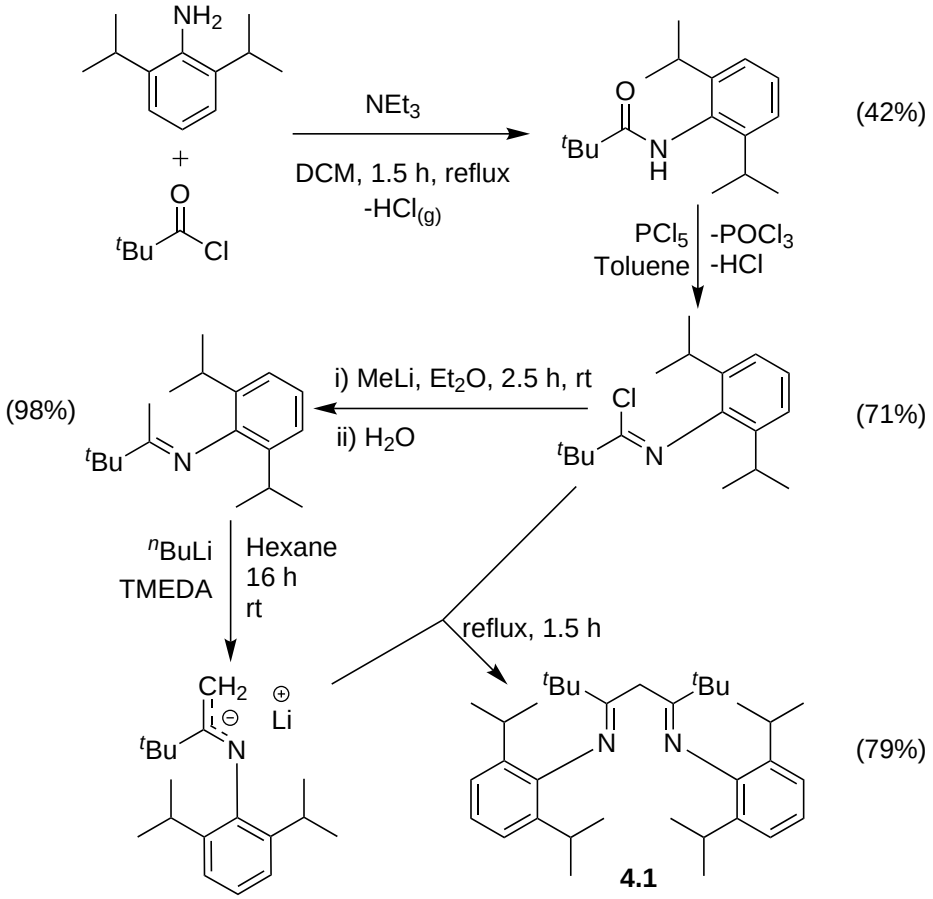

Scheme 4.4: Synthetic route to **4.1**. Yields for each step are shown in brackets.

The next step was to then synthesise the Mg precursor. Two methods were applied to try and achieve this (Scheme 4.5), the first of which involved the reaction of the imine-enamine with Mg^nBu_2 (Route A), with the second instead involving the use of the diimine (Route B). Both reactions involve the elimation of butane, however, in Route A an N–H proton is used for the elimination, whereas in Route B a proton is removed from the -CH_2 position. The disadvantage of Route B is that it requires the use of THF as the solvent,

which results in the formation of a THF adduct (discussed later). The presence of a THF ligand is undesirable as it could result in unwanted reactions during future small molecule activations, as well as potentially acting as the Lewis base in any Lewis pair chemistry.

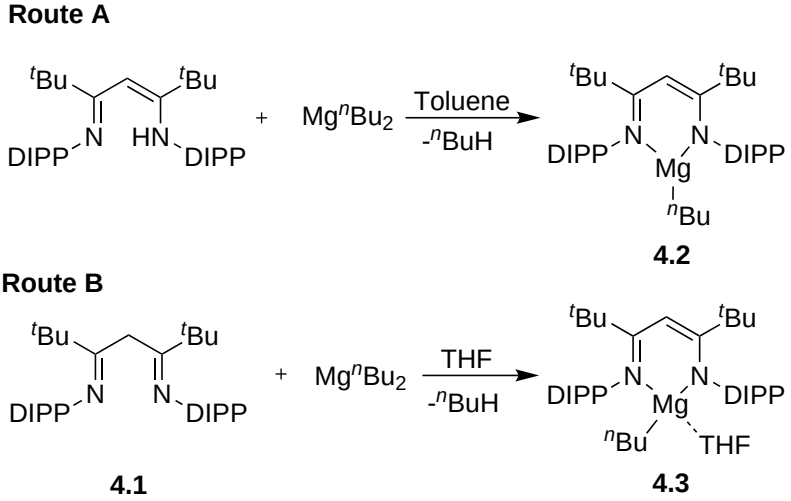

Scheme 4.5: Possible routes to the Mg precursor. DIPP = diisopropylphenyl.

Route A does not require a THF solvent; however, in addition to involving the conversion of the diimine to the imine-enamine (Scheme 4.6), the product is far less readily isolated. On the other hand, despite containing an undesirable THF adduct, **4.3** is far more readily isolated via crystallisation and so Route B was preferred. **4.3** reacted very poorly with 2,4,6-trimethylphenol even when heated to 80 °C. Therefore, removal of the THF adduct was attempted, with **4.3** was heated to 115 °C under high vacuum for 16 h, yielding **4.2** as a pure yellow solid (Scheme 4.7).

The synthesis of other Mg β-diketiminates was also attempted, with the ligands **4.4** and **4.5** (Figure 4.2) made using the same procedure as **4.1** with the corresponding amine. Unfortunately, the resultant magnesium complexes were not isolated, with the diisopropylphenyl apparently allowing for easier crystallisation, perhaps by reducing any rotation of the aryl rings.

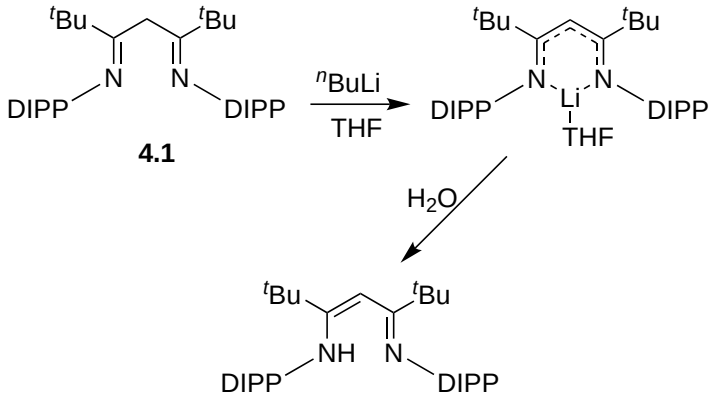

Scheme 4.6: Conversion of **4.1** to its imine-enamine tautomer. DIPP = diisopropylphenyl.

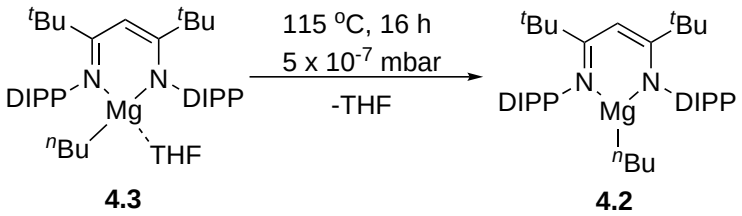

Scheme 4.7: Removal of the THF adduct from **4.3** to give **4.2**. DIPP = diisopropylphenyl.

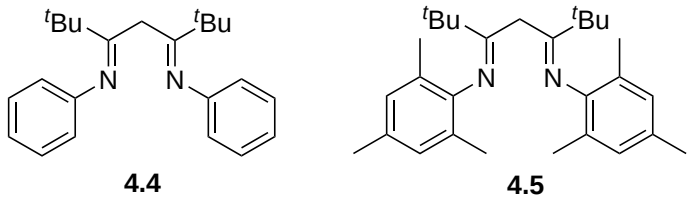

Figure 4.2: Synthesised β-diketiminates.

In order to try and increase the electrophilicity at the Mg centre, alternative ligands to the -^{n}Bu group were sought. Initially, 2,4,6-trimethylphenoxide was chosen as an appropriate ancillary ligand as it is both electron-withdrawing and known to help stabilise reactive centres (as seen with the compounds **2.1** and **2.2** see Chapters 2 and 3). The synthesis of this compound (**4.6**, Scheme 4.8) was found to be very straightforward and achieved by the stirring together of **4.2** with 2,4,6-trimethylphenol in pentane at room

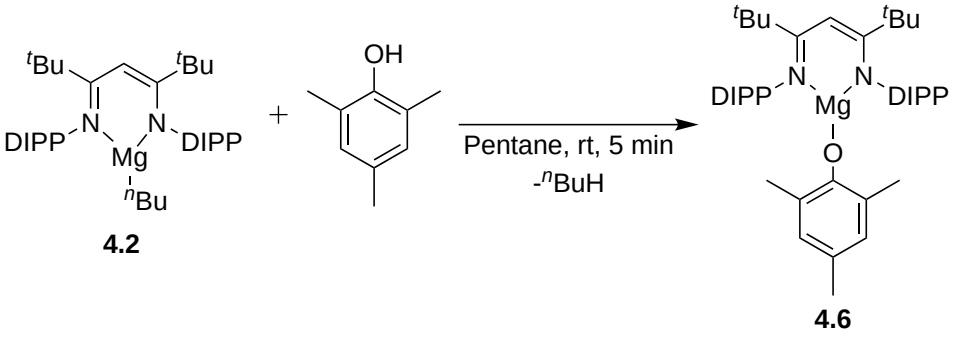

Scheme 4.8: Synthesis of **4.6**.

temperature.

The X-ray crystal structure of **4.6** is shown in Figure 4.3, and we can see that the Mg–O–C bond angle is nearly linear at 176.45(11)° which could indicate a contribution from a lone pair on the O atom in the Mg–O bond. It is also clear that unlike some other three-coordinate Mg β-diketiminate species there is no dimerisation of the complex in the solid state,[71] which is both a result of the extra steric bulk provided by the -OMes group and the tendency of the -^{t}Bu groups on the ligand to push the aryl rings closer to the magnesium centre, thereby increasing steric bulk.[154] Additionally, the bond lengths between the Mg centre and the two N atoms are almost identical (2.0013(15) Å and 2.0065(14) Å), indicating conjugation around the heterocycle.

The syntheses of alternative Mg β-diketiminate phenoxide species were attempted, with substituted phenols chosen that could change the electron-withdrawing properties of the ancillary ligand and perhaps result in different reactivity of the resultant Lewis acid. Unfortunately, each of these reactions proved to be unsuccessful. The reactions shown in Scheme 4.9 were carried out, with no desired product obtained or identified in each case. For the reactions with 3,5-bis(trifluoromethyl)phenol and 2,3,4,5,6-pentafluorophenol, heating to reflux overnight resulted in no improvement. Insoluble solids were obtained for each

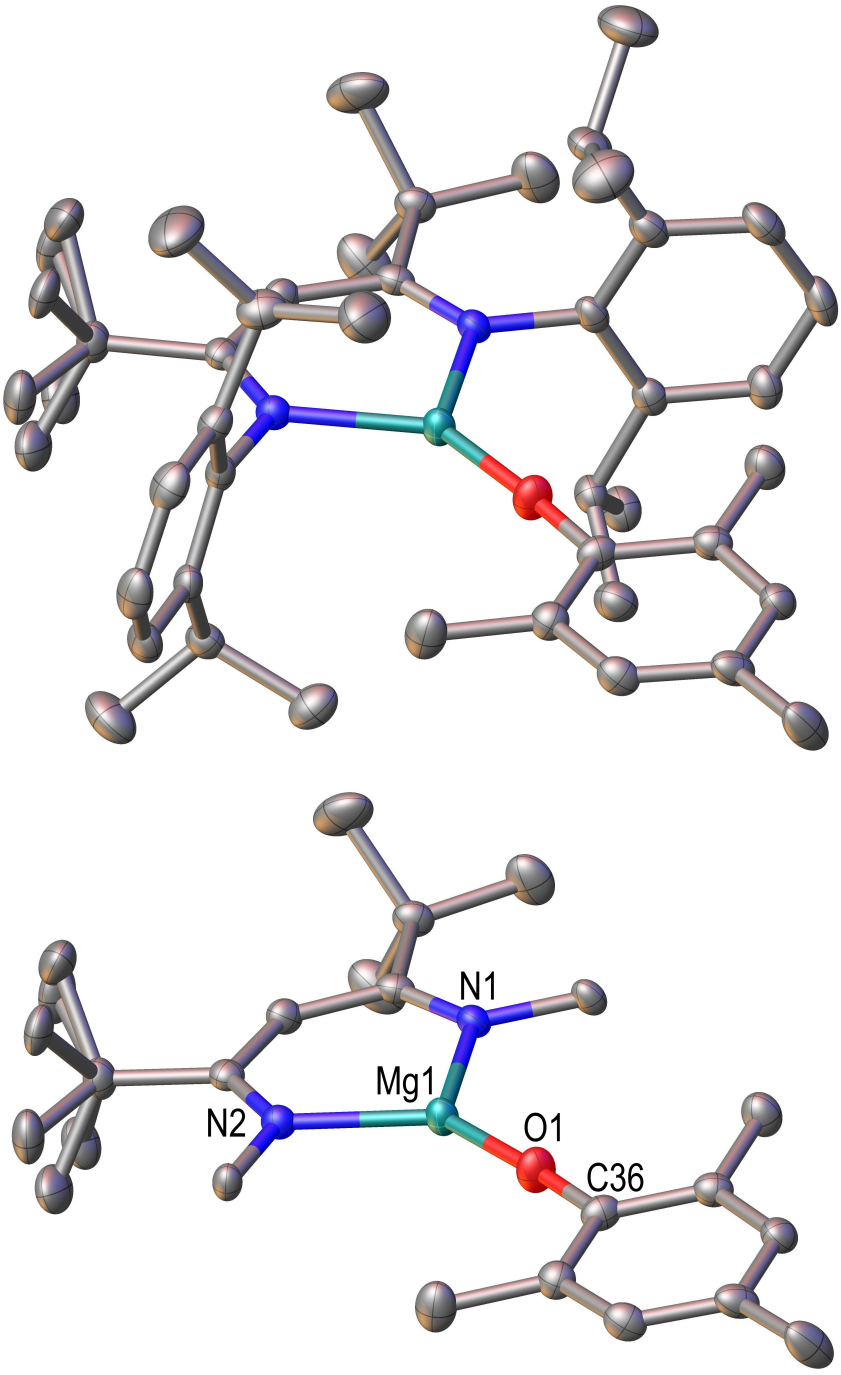

Figure 4.3: Molecular structure of **4.6** as determined by single crystal X-ray diffraction. The full structure is shown on top, the diisopropylphenyl groups have been removed from the structure on the bottom for clarity. One of the backbone *tert*-butyl groups is disordered. Thermal ellipsoids are drawn at the 50% probability level. Hydrogen atoms are omitted for clarity. Selected bond lengths (Å) and angles (deg): Mg1–O1 1.7998(13), Mg1–N1 2.0013(15), Mg1–N2 2.0065(14), O1–C36 1.346(2), Mg1–O1–C36 176.45(11).

reaction, showing that the issue is not a lack of reactivity between **4.2** and the substituted phenols, but the formation of an unidentified side-product which was insoluble in both polar (H_2O, THF, EtOH, MeCN, and DCM) and non-polar (hexane, toluene, and Et_2O) solvents in each case. It may also be the case that 2,4,6-trimethylphenoxide helps to stabilise **4.6** and prevent formation of the unidentified product, whereas the lack of steric bulk around the phenols shown in Scheme 4.9 means that they do not provide this stability.

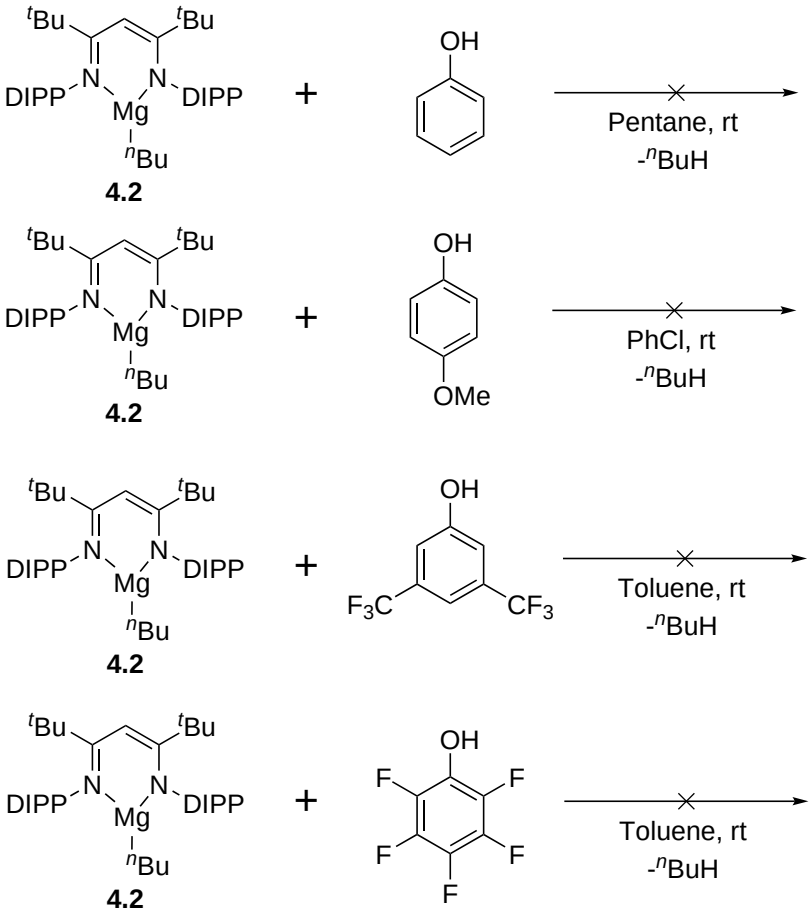

Scheme 4.9: Attempted syntheses of alternative Mg β-diketiminate phenoxide species.

The Gutmann-Beckett method was applied to both **4.2** and **4.6** in order to determine their respective Lewis acid strengths. This method involves comparing the ^{31}P NMR shift

of $Et_3P{=}O$ (when combined with the complexes in solution) to those of $Et_3P{=}O$ in hexane (δ 41.0 ppm) and in $SbCl_5$ (δ 86.1 ppm). An acceptor number (AN) is then calculated for each complex using equation (4.1) below, allowing them to be compared more clearly with other Lewis acids.[155–159]

$$AN = \frac{\delta_{complex} - \delta_x}{\delta_y - \delta_x} \times 100 \tag{4.1}$$

where δ_x = ^{31}P *shift of* $Et_3P{=}O$ *in hexane, and* δ_y = ^{31}P *NMR shift of* $Et_3P{=}O$ *in* $SbCl_5$

The ^{31}P NMR shift for the reaction of $Et_3P{=}O$ with **4.2** was found to be δ 59.6 ppm, with a shift of δ 64.2 ppm for **4.6**. This converts to AN values of 41.2 and 51.4 for **4.2** and **4.6** respectively, showing that the change in ligand from -^{n}Bu to -OMes has indeed increased the Lewis acidity of the complex. For comparison, the AN value of $B(C_6F_5)_3$ in C_6D_6 has been reported as between 76 and 81,[108] showing that **4.6** is still a relatively weak Lewis acid compared to other common electron-pair acceptors. However, despite this, it was decided to test the reactivity of this species to see if it was still capable of performing small molecule activations and transformations.

4.3.2 Interaction of magnesium Lewis acid with Lewis bases

4.6 was combined with the Lewis bases shown in Figure 4.4 to see if any interaction occurred. The Lewis bases were chosen on account of their varying basicity and steric bulk, in addition to their availability. In order to examine any interactions between the Lewis pairs, the sample mixtures were analysed by NMR. Upon combination of the phosphines or triethylamine with **4.6**, no change in the ^{1}H or ^{31}P NMR spectra was seen, indicating no interaction between the separate moieties.

The reaction between **4.6** and pyridine (**c**) resulted in the formation of an adduct,

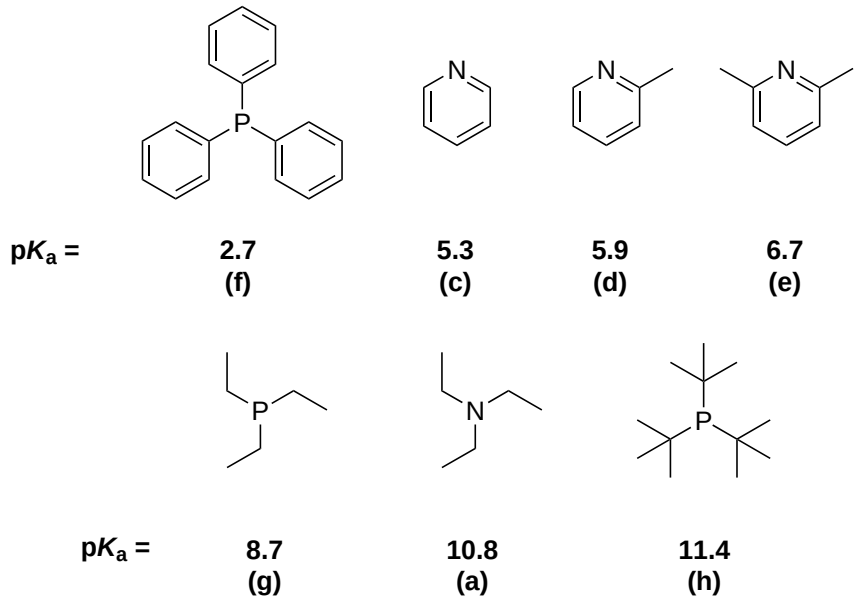

Figure 4.4: The Lewis bases used in this chapter in order of ascending pK_a. Each Lewis base has been assigned a letter in brackets.

the single crystal X-ray structure of which is shown in Figure 4.5. Interestingly the two molecules of **4.6c** in a single unit cell have slightly different structures. The most notable difference is the Mg–O–C angle for each, which is 153.24(14)° for the structure on the left, and 175.09(18)° for the structure on the right. The more acute angle implies greater electron donation towards the Mg centre from elsewhere, however, each of the three Mg1–N bonds very similar to their Mg2 counterparts. The cause of this difference in angle is therefore unclear, however, it could well be the result of the formation of the solid crystal structure. In both cases the Mg atom is shifted out of the plane of the heterocycle (the heterocycle is flat in the structure of **4.6**), which perhaps alleviates any steric strain created by the diisopropylphenyl groups.

A crystal structure was also obtained for the reaction between **4.6** and 2-methylpyridine (**d**) and is shown in Figure 4.6. Here, there is a slightly longer bond between the Mg centre and pyridine ring of 2.1779(16) Å, and a smaller Mg–O–C angle of 148.59(12)°. The Mg–

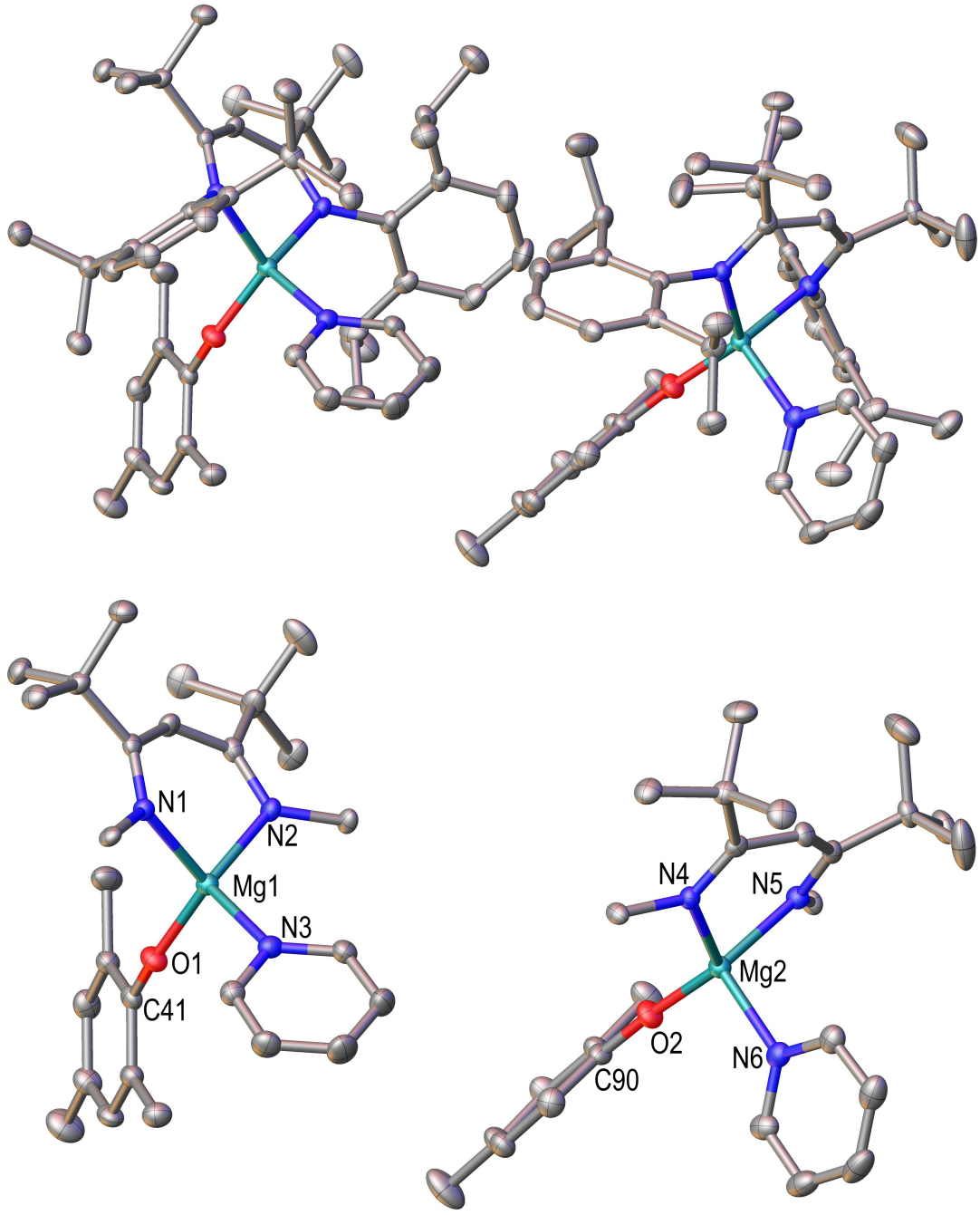

Figure 4.5: Molecular structure of **4.6c** as determined by single crystal X-ray diffraction. The full structure (top), and the structure with the diisopropylphenyl groups removed for clarity (bottom) are shown. Disorder on one of the *tert*-butyl groups has also been removed. Thermal ellipsoids are drawn at the 50% probability level. Hydrogen atoms are omitted for clarity. Selected bond lengths (Å) and angles (deg): (left) Mg1–O1 1.8521(15), Mg1–N1 2.064(2), Mg1–N2 2.0332(18), Mg1–N3 2.113(2), Mg1–O1–C41 153.24(14); (right) Mg2–O2 1.8325(15), Mg2–N4 2.0642(18), Mg2–N5 2.0510(18), Mg2–N6 2.152(3), Mg2–O2–C90 175.09(18).

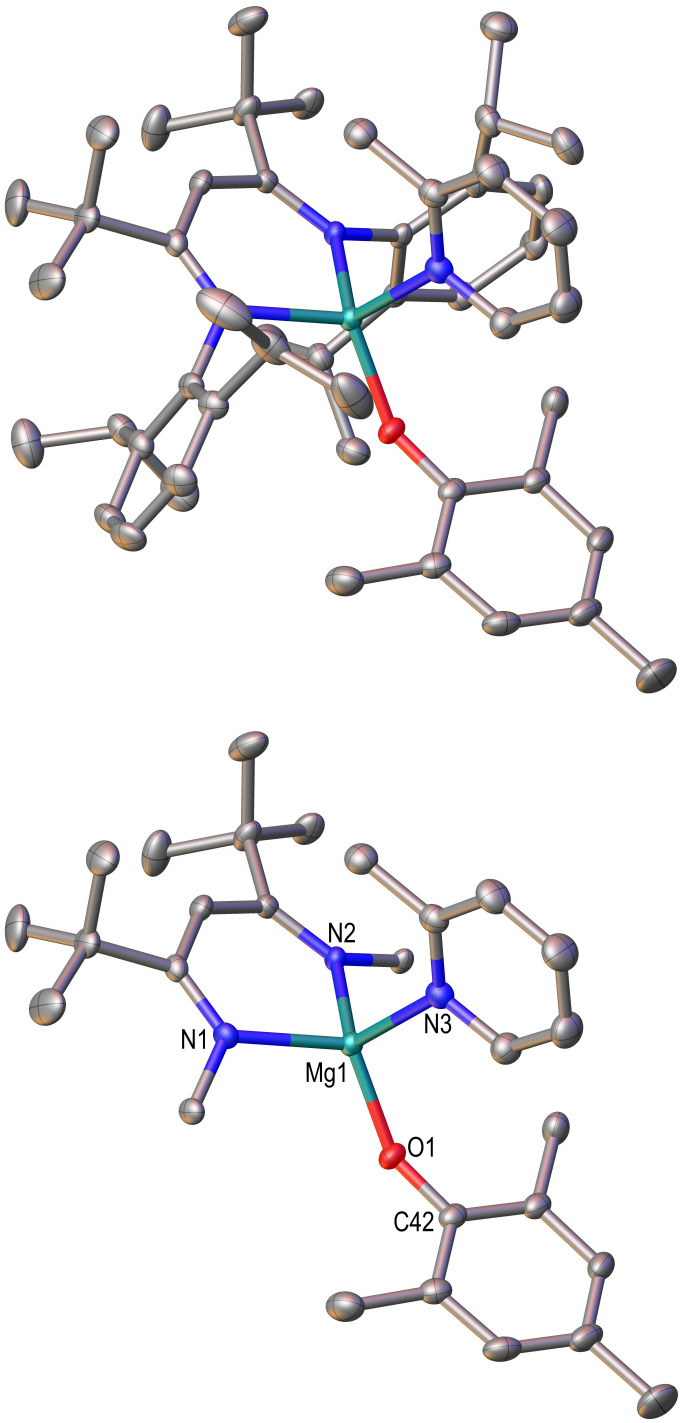

Figure 4.6: Molecular structure of **4.6d** as determined by single crystal X-ray diffraction. The full structure is shown on the left, with the diisopropylphenyl groups removed from the structure on the right for clarity. Thermal ellipsoids are drawn at the 50% probability level. Hydrogen atoms are omitted for clarity. Selected bond lengths (Å) and angles (deg): Mg1–O1 1.8703(12), Mg1–N1 2.0577(14), Mg1–N2 2.0836(13), Mg1–N3 2.1779(16), Mg1–O1–C42 148.59(12).

O bond is also marginally longer in **4.6d** than **4.6c**, with a length of 1.8703(12) Å. This could be due to less contribution from the O lone pair than in **4.6c**, despite the slightly greater steric bulk of **d** appearing to reduce the amount of donation from the Lewis base. However, the very small diifference in bond length means this may not be the case. The Mg centre is also shifted out of the heterocycle plane to a lesser degree, perhaps showing this crystal structure to be less sterically strained. This adds to the suggestion that the solid-state structure of **4.6c** influences the orientation of the ligands.

The reaction between **4.6** and the final Lewis base (**e**) also appeared to result in the formation of an adduct, with significant changes seen in the ^{1}H NMR spectra. The most notable of which is the change of one set of diisopropyl groups from δ 1.22 ppm to δ 1.11 ppm (which is very similar to the equivalent signals for **4.6c** at δ 1.11 and 1.09 ppm).

4.3.3 Small molecule reactions

4.3.3.1 Reactions with hydrogen gas

The next step was to see if any of these Lewis pairs were capable of small molecule activation. As the activation of dihydrogen is one of the most commonly tested reactions with FLPs, it was the first reaction for which these Lewis pairs were tested. Each of the Lewis pairs **4.6a**, and **4.6c**–**h** were exposed to 1 bar H_2 gas in C_6D_6 solutions of the NMR samples (Scheme 4.10). Unfortunately, the reaction was unsuccessful in all cases, with no visible change in the reaction, or observable change in ^{1}H or ^{31}P NMR spectra from the starting materials. This suggests that the Lewis acid is not acidic enough to facilitate the heterolytic cleavage of dihydrogen. However, one possibility could be that there is an insufficient HOMO-LUMO gap within the Lewis pair, meaning there is not enough potential energy for the cleavage of the substrate. It could also be the case that the small

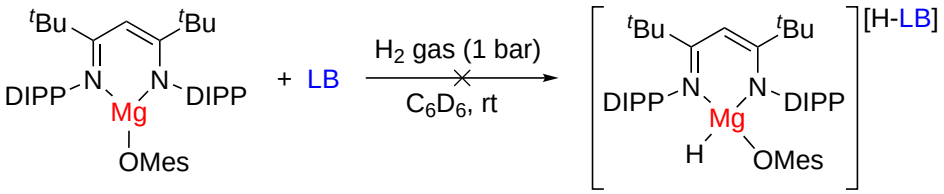

4.6a LB = NEt_3
4.6c LB = Py
4.6d LB = 2-MePy
4.6e LB = 2,6-MePy
4.6f LB = PPh_3
4.6g LB = PEt_3
4.6h LB = P^tBu_3

Scheme 4.10: Reaction of **4.6a**, and **4.6c**–**h** with H_2 (1 bar).

size of the hydrogen molecule, combined with the high steric bulk around the Mg centre, makes it difficult for Lewis base to be of close enough proximity for the reaction to occur.

4.3.3.2 Reactions with phenylacetylene-*d*

The activation of phenylacetylene is another reaction for which FLPs have been shown to be effective and—as discussed in Chapters 1 and 2—can result in deprotonation of the reactant to form a salt of the Lewis base with an acetylide species, or the formation of a 1,2-addition product. Each of the Lewis pairs **4.6a** and **4.6c**–**h** were reacted with phenylacetylene-*d* by adding the reactant to C_6D_6 solutions of each Lewis pair in an NMR tube (Scheme 4.11). Unfortunately, no reactivity was seen with any of the species, with no visible changes in the reaction solution or changes in the ^1H, ^2H, or ^{31}P NMR spectra observed. The reaction of phenylacetylene-*d* with **4.6** in the absence of a Lewis base also resulted in no interaction. It may be the case that this reaction is inhibited by the size of phenylacetylene, however, reactions with smaller terminal alkynes would be needed to confirm this, as even if no transformation takes place, an interaction between the Mg centre and π-bonds on the alkyne may be expected.

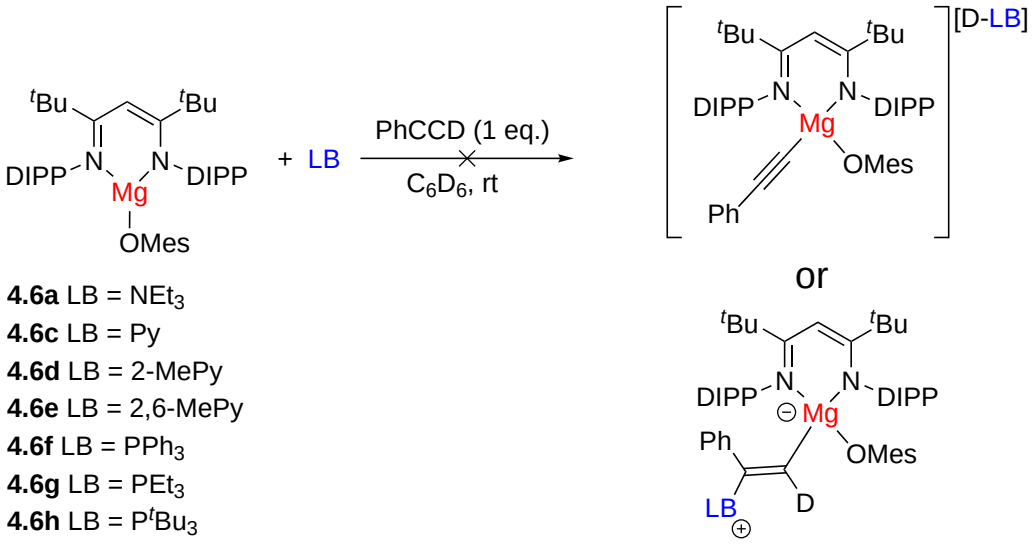

4.6a LB = NEt_3
4.6c LB = Py
4.6d LB = 2-MePy
4.6e LB = 2,6-MePy
4.6f LB = PPh_3
4.6g LB = PEt_3
4.6h LB = P^tBu_3

Scheme 4.11: Reaction of Lewis pairs **4.6a** and **4.6c–h** with phenylacetylene-*d*.

4.3.3.3 Reactions with benzaldehyde

In order to try and find a substrate which these Lewis pairs could activate, aldehydes were explored, as the activation of aldehydes with various FLPs has previously been demonstrated, including those that can perform subsequent hydrogenation with H_2 gas.[160–162] Benzaldehyde in particular has been widely used for these reactions, and so was chosen for initial experiments. Upon combination of **4.6** with benzaldehyde in solution (C_6D_6) an instant colour change from yellow to red is seen, with ^{1}H NMR data confirming the formation of a benzaldehyde adduct (Figure 4.7, **4.7**), with the substrate bonded to the Mg centre via an oxygen lone pair. The ^{1}H spectrum of **4.7** shows broadening of the diisopropylphenyl signals, corresponding to reduced rotation as a result of increased steric bulk, with the change in chemical shifts between **4.6** and **4.7** corresponding to the formation of other Mg β-diketiminate adducts.[75,76,104]

The Lewis pairs **4.6a** and **4.6c–h** were each reacted with an equimolar quantity of benzaldehyde in C_6D_6 (Scheme 4.12). The reactions of **4.6a**, **4.6e**, **4.6f**, and **4.6h** involved

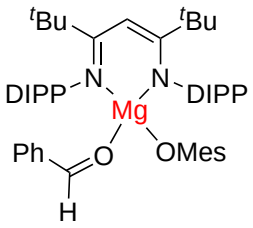

4.7

Figure 4.7: The adduct formed upon reaction of **4.6** with benzaldehyde (**4.7**).

the instant formation of **4.7** with no further reaction taking place. **4.6c** and **4.6d** showed no displacement of the bound Lewis base, with no interaction seen between the complex and benzaldehyde.

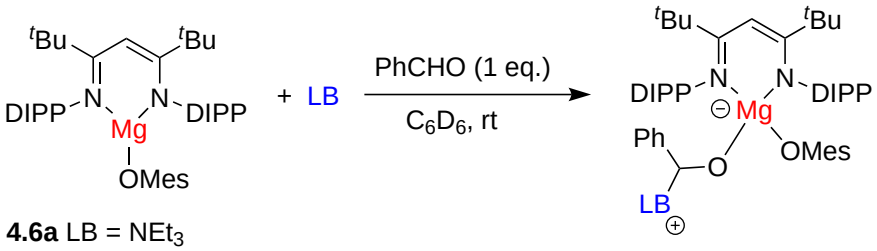

4.6a LB = NEt_3
4.6c LB = Py
4.6d LB = 2-MePy
4.6e LB = 2,6-MePy
4.6f LB = PPh_3
4.6g LB = PEt_3
4.6h LB = P^tBu_3

LB = PEt_3 (**g**)

Scheme 4.12: Reaction of Lewis pairs **4.6a** and **4.6c–h** with benzaldehyde.

The reaction with **4.6g** was the only one to demonstrate any bonding between the Lewis base and the benzaldehyde detectable by ^{1}H or ^{31}P NMR. In this case, the benzaldehyde still forms an adduct with **4.6** but there is also a significant bonding interaction with PEt_3—however, the exact nature of this is unclear. There is a shift in the ^{31}P NMR spectra from δ -19.7 ppm (free PEt_3) to a broad signal at δ 11.1 ppm, in addition to shifts in all proton environments from **4.7** (it should be noted that no reaction is seen when PEt_3 is combined with benzaldehyde alone). Examination of the DOSY spectrum of this

reaction (Figure 4.8) shows that the diffusion coefficient of **g** in this reaction is 12.8×10^{-6} cm^2 s^{-1}, whereas that of the Mg species is 5.82×10^{-6} cm^2 s^{-1} (D of free **g**: 23.8×10^{-6} cm^2 s^{-1}, D of **4.7**: 6.12×10^{-6} cm^2 s^{-1}). This shows that although there is significant interaction, there does not seem to be a persistent bond between the Lewis base and the Mg complex. This would suggest that the desired product has been formed but involves a transient interaction from the Lewis base.

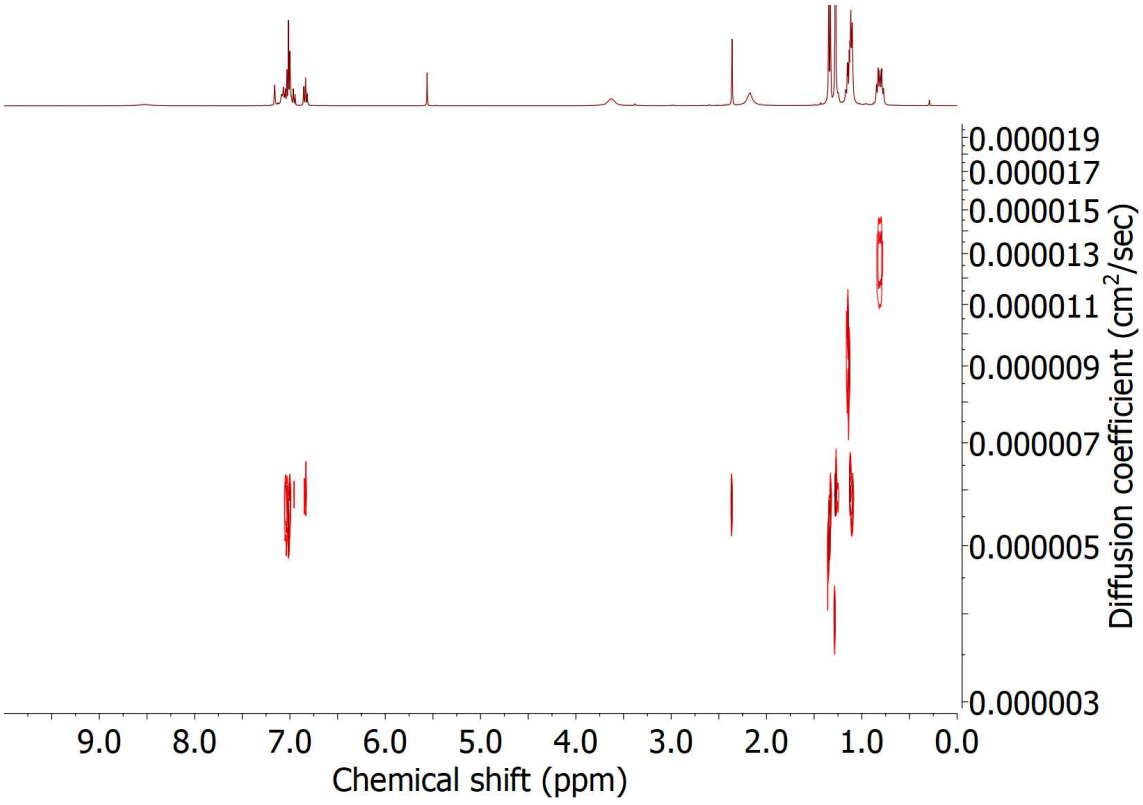

Figure 4.8: DOSY spectrum for the reaction between **4.6g** and benzaldehyde.

The hydrosilylation of benzaldehyde was attempted in order to ascertain whether or not these systems could functionalise the substrate. Both **4.6e** and **4.6g** were used in reactions combining benzaldehyde and triethylsilane in C_6D_6 solutions at 80 °C (Scheme 4.13). The reactions were followed by ^{29}Si-DEPT NMR (in addition to ^{1}H and ^{31}P NMR), however, the triethylsilane demonstrated no reactivity, with no visibile change in the reactions, or

any change in the NMR spectra when compared to the starting materials. This could be due to the selected silane itself (with other silanes such as the less sterically crowded $PhSiH_3$ perhaps having the potential to be more reactive), it could be due to steric bulk around the reaction centre, or it could be a result of the Lewis pair not activating the benzaldehyde to a sufficient degree to allow for reaction with Et_3SiH.

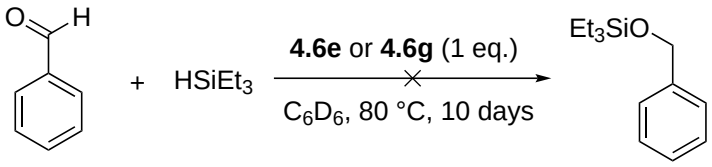

Scheme 4.13: Attempted hydrosilylation of benzaldehyde with triethylsilane using **4.6e** and **4.6g**.

4.3.3.4 Reactions with mesitaldehyde

The ability of **4.6a**, and **4.6c**–**h** to activate aldehydes was also tested with the more sterically hindered mesitaldehyde, with equimolar quantities of the substrate added to C_6D_6 solutions of the Lewis pairs at room temperature (Scheme 4.14). Unfortunately, no activation was seen in any of the reactions. For **4.6c** and **4.6d**, the Lewis base remained bound to the Mg centre and was not displaced. In all other cases, mesitaldehyde formed an adduct with no further reaction taking place. The formation of the adduct is evidenced by the similarity of the ^{1}H NMR spectrum with **4.7**, for which signal broadening is also seen, in addition to the shift of the aldehydic proton signal indicating binding at the aldehydic position. Greater signal broadening is seen in this case, indicating that the greater steric bulk of mesitaldehyde limits rotation of the functional groups even further than is observed with **4.7**.

An X-ray crystal structure of this mesitaldehyde adduct was obtained (**4.8**, Figure 4.9), and it is clear that there is significant bulk around the aldehydic carbon atom, which

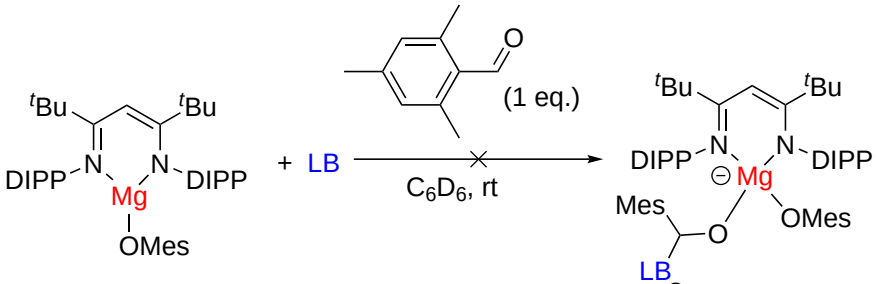

4.6a LB = NEt_3
4.6c LB = Py
4.6d LB = 2-MePy
4.6e LB = 2,6-MePy
4.6f LB = PPh_3
4.6g LB = PEt_3
4.6h LB = P^tBu_3

Scheme 4.14: Reaction of **4.6a**, and **4.6c**–**h** with mesitaldehyde.

likely explains why we do not see any nucleophilic attack from the Lewis bases used here. This bulk may also explain why the Mg centres lie further outside the plane of the β-diketiminate ligand than seen with **4.6c** or **4.6d**. The planarity of mesitaldehyde, when considered alongside the planarity of benzaldehyde, **c**, and **d**, may be the reason that it is able to overcome any steric hindrance and bind to the Mg centre of **4.6**.

4.3.3.5 Reactions with 3-pentanone

Ketones are another class of substrate that have been activated and functionalised using FLPs, with 3-pentanone one of many that has been efficiently hydrogenated in this way.[163] Upon addition of 3-pentanone to **4.6** alone in solution, an adduct was formed (**4.9**, Figure 4.10) for which—as seen with other Mg β-diketiminate adducts—we see ^{1}H NMR signal broadening, and loss of symmetry of the diisopropylphenyl groups (with broad chemical shifts at δ 3.79, and 3.35 ppm corresponding to the -CH(CH_3)$_2$ proton environments).[75,76,104] Chemical shifts of the β-diketiminate ligand are also similar to **4.7** and **4.8**. No additional reactivity was seen when the Lewis bases **4.6e**–**g** were added to sep-

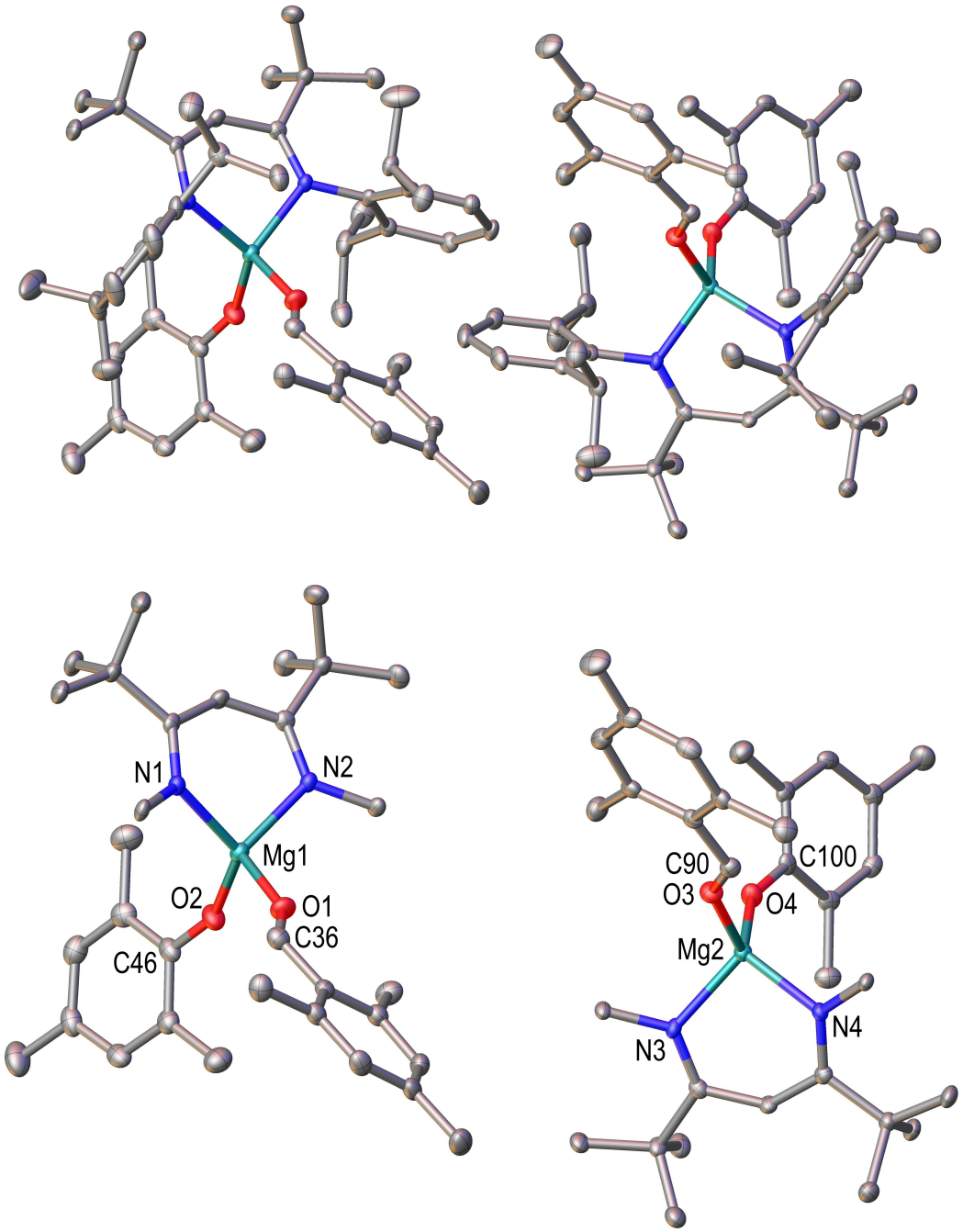

Figure 4.9: Molecular structure of **4.8** as determined by single crystal X-ray diffraction. Both the full structure (top), and the structure with the diisopropylphenyl groups removed (bottom) are shown. Thermal ellipsoids are drawn at the 50% probability level. Hydrogen atoms are omitted for clarity. Selected bond lengths (Å) and angles (deg): (left) Mg1–O1 1.9819(17), Mg1–O2 1.8486(17), Mg1–N1 2.0414(17), Mg1–N2 2.0387(17), O1–C36 1.232(3), O2–C46 1.327(3), Mg1–O2–C46 155.10(14), Mg1–O1–C36 148.91(15); (right) Mg2–O3 2.0021(15), Mg2–O4 1.8528(16), Mg2–N3 2.0404(18), Mg2–N4 2.0452(17), O3–C90 1.231(3), O4–C100 1.327(2), Mg2–O3–C90 141.87(15), Mg2–O4–C100 153.08(14).

arate solutions of **4.9** (Scheme 4.15), with no visible change in reaction or by ^{1}H or ^{31}P NMR. The small size of 3-pentanone may mean that little space is available for nucleophilic attack from a Lewis base due to the steric bulk of the diisopropylphenyl groups. However, it may also be the case that the polarity of 3-pentanone does not change significantly enough, upon binding to **4.6**, to enable attack by **e**, **f**, or **g**.

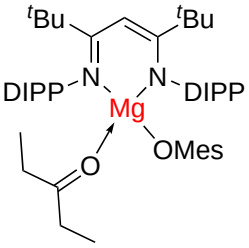

4.9

Figure 4.10: The adduct formed upon addition of 3-pentanone to **4.6**.

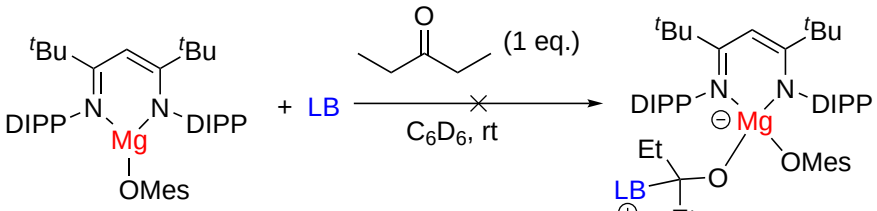

4.6e LB = 2,6-MePy
4.6f LB = PPh_3
4.6g LB = PEt_3

Scheme 4.15: Reaction of **4.6e**–**g** with 3-pentanone.

The hydrosilylation of 3-pentanone was also attempted, to see if functionalisation of the bound substrate was still possible despite no detectable interaction from the Lewis bases. To this end, benzaldehyde and triethylsilane were combined in solution (C_6D_6) with either **4.6e** or **4.6g**, and heated at 80 °C for 7 days (Scheme 4.16). The reactions were monitored by ^{29}Si-DEPT NMR (in addition to ^{1}H and ^{31}P NMR), however, the triethylsilane displayed no reactivity. As with the benzaldehyde reactions, this could be a result of the steric bulk of **4.6**, the unsuitability of Et_3SiH as a hydrosilylation agent,

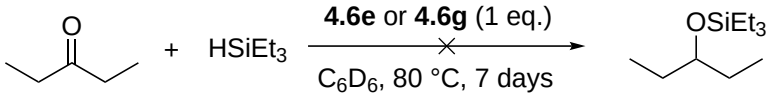

Scheme 4.16: Attempted hydrosilylation of 3-pentanone with triethylsilane using **4.6e** or **4.6g**.

or a sign that the bound 3-pentanone species is not sufficiently activated for reactivity to take place.

4.3.3.6 Dehydrocoupling of $Me_2NH{\cdot}BH_3$

The Lewis pairs **4.6a**–**h** were tested for their ability to catalyse the dehydrocoupling of $Me_2NH{\cdot}BH_3$, a reaction that has previously been performed by Mg β-diketiminate species (see Chapter 1). N,N-diisopropylethylamine (**b**) was also used for this reaction. $Me_2NH{\cdot}BH_3$ was added to 10 mol% of the catalyst in solution (C_6D_6) on an NMR scale, with the results shown in Table 4.1. Firstly, it is clear that all of these reactions are far slower than those seen using the Zr/N Lewis pairs in Chapter 3, with catalysts **4.6a**–**f** and **4.6h** only producing <1% of $[Me_2N–BH_2]_2$ after 14 h (>99% yield was achieved in the same time period with certain Zr/N catalysts). Only **4.6g** achieved a measurable yield, with 3% of product present after 14 h. Accurate conversion data is unavailable due to significant overlap between the $Me_2NH{\cdot}BH_3$ resonance and other compound resonances in the ^{11}B NMR spectra.

4.6c and **4.6d** were the least effective catalysts, with **4.6c** producing no yield even after 5 days, and **4.6d** only achieving a yield of 5% after 6 days. This is unsurprising as the bond formed between **4.6** and **c** or **d** has already been shown to inhibit the binding of other substrates, although this does show that the slightly greater steric bulk of **d** weakens the Mg–N bond and allows for a limited amount of catalysis to occur.

Table 4.1: Catalytic dehydrocoupling of $Me_2NH{\cdot}BH_3$ with **4.6a**–**h** in C_6D_6.

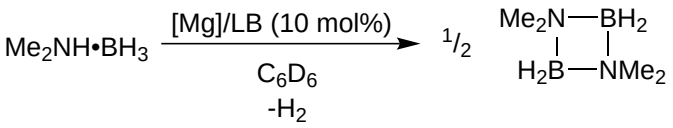

Catalyst	Temperature (°C)	Time (days)	Yield (%)
4.6a	25	0.5	<1
	25	5	55
	25	7	89
4.6b	25	0.5	<1
	25	6	40
	25	8	75
	25	9	90
4.6c	25	5	0
4.6d	25	0.5	0
	25	3	<1
	25	6	5
4.6e	25	0.5	<1
	25	4	11
	25	7	44
4.6f	25	0.5	<1
	25	5	35
	25	7	61
	25	10	94
4.6g	25	0.5	3
	25	2	24
	25	3	50
	25	4	75
4.6h	25	0.5	<1
	25	6	26
	25	8	45
	25	11	87

The most active catalyst is **4.6g**, which attained a yield of 50% after 3 days, and 75% after 4 days, with **4.6a** the second most active, with a yield of 55% after 5 days, rising to 89% after 7 days. Both of the Lewis bases **a** and **g** are relatively unhindered in relation to the rest (**c** and **d** aside), while also possessing higher pK_a values (**a** = 10.8, **g** = 8.7)

than **e** (pK_a = 6.7) and **f** (pK_a = 2.7), with **4.6e** and **4.6f** requiring 7 days to achieve yields of 44% and 61% respectively. The lower activity of **4.6h**, which required 8 days to achieve a 45% yield, is likely due to the high steric bulk of **h**, as the higher pK_a value of P^tBu_3 (11.4) would perhaps mean a slightly improved yield would be expected. However, the higher yield of **4.6f** seems to indicate that high basicity of the Lewis base is of less importance in this reaction. **4.6e** showed the poorest activity of the catalysts **4.6a**, **4.6b**, and **4.6e**–**g**, which is likely the result of a combination of steric and electronic factors—but may also indicate a stronger interaction between **e** and the Mg centre inhibiting binding of the substrate. Finally, **4.6b** proved to be less active than **4.6a**, requiring 9 days to obtain 90% yield whereas **4.6a** required 7 days to reach 89%, suggesting the slightly higher steric bulk hinders reactivity.

$Me_2NH{\cdot}BH_3$ was also reacted with just **4.6** in solution (1 eq. in C_6D_6), resulting in the formation of the desired product, with 25% yield after 20 h, and 90% yield after 3.5 days. Frustratingly, the reaction using 10 mol% **4.6** was not carried out, meaning direct comparisons with the Lewis pair catalysts is not possible. This information would be required to confirm whether any of the Lewis bases enhance or inhibit the reaction; however, it is likely that at least some of the Lewis bases are a hindrance, if not all. This reaction was also performed at 60 °C using **4.6** (10 mol%, in C_6D_6) with 93% yield obtained within 1 h (and 39% after 30 min). At this temperature, **4.6** is much closer in reactivity to the most effective Zr/N catalysts, which achieved comparable yields within 30 min at 60 °C (see Chapter 3).

The $^{11}B\{^1H\}$ NMR spectrum after 55 h for the reaction using **4.6g** (Figure 4.11) shows that the same reaction intermediates are present in this reaction as for the Zr/N reactions (Chapter 3). The intermediates $Me_2N{=}BH_2$, $HB(NMe_2)_2$, $Me_2NH{-}BH_2{-}NMe_2{-}BH_3$, and

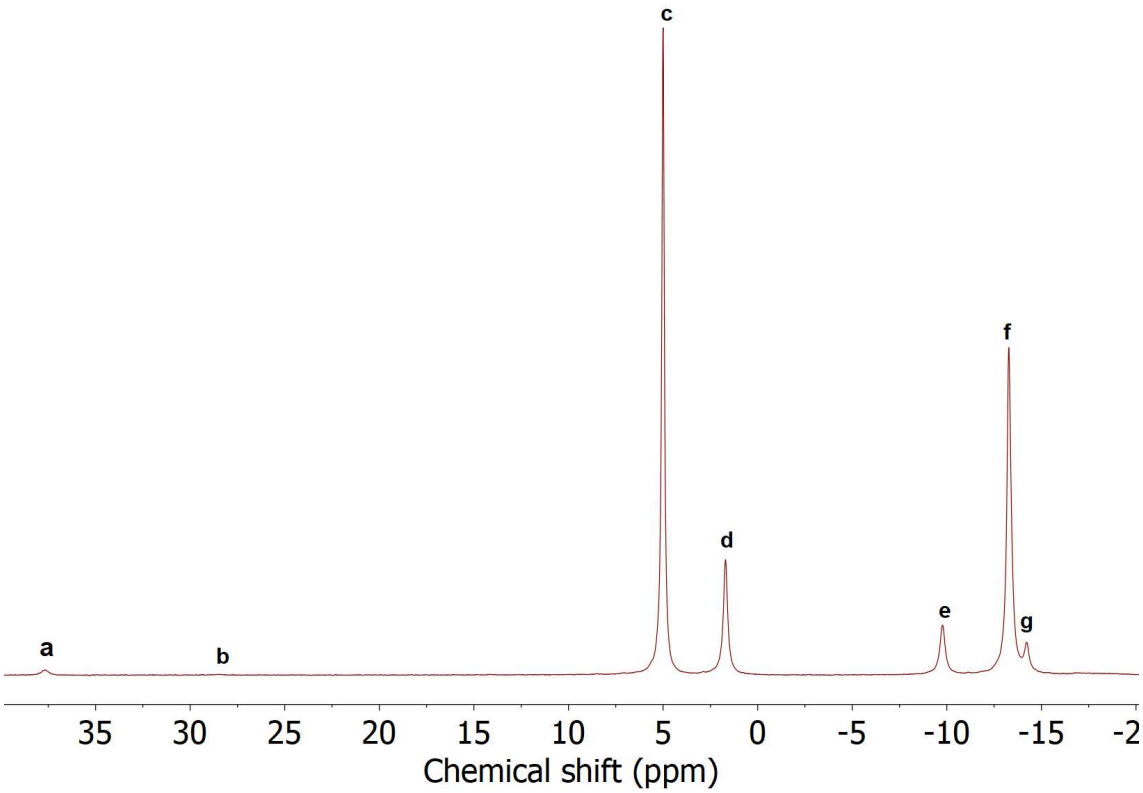

Figure 4.11: $^{11}B\{^{1}H\}$ NMR spectrum (96 MHz, 25 °C, C_6D_6, 55 h) of the reaction between $Me_2NH{\cdot}BH_3$ and **4.6g** (10 mol%). **a** = $Me_2N{=}BH_2$ (37.7 ppm), **b** = $HB(NMe_2)_2$ (28.6 ppm), **c** = $[Me_2N{-}BH_2]_2$ (5.00 ppm), **d** = $Me_2NH{-}BH_2{-}NMe_2{-}BH_3$ (1.70 ppm), **e** = $Mg{-}NMe_2{-}BH_3{-}PEt_3$ (-9.77 ppm), **f** = $Me_2NH{\cdot}BH_3$ (-13.3ppm), **g** = $Me_2N(B_2H_5)$ (-14.3 ppm).

$Me_2N(B_2H_5)$ are also seen in the reactions of **4.6**, **4.6a**, **4.6b**, **4.6e**, **4.6f**, and **4.6h**. However, the peak present at δ -9.77 ppm in Figure 4.11 is not seen in any of these other reactions. This may give a clue as to the improved reactivity of **4.6g** in relation to the other catalysts from **4.6a**–**h**. A similar peak is seen in a paper by Hill and co-workers which attributes the compound to a $LMgNMe_2BH_3$ species (the peak in Figure 4.11 is also a quartet in the proton coupled ^{11}B NMR spectrum).[88] It is possible that a similar intermediate is present here, with the proton loss facilitated by the PEt_3 Lewis base—an action that perhaps cannot be performed by the other Lewis bases or with no Lewis base at all. The only other peak in the ^{31}P NMR spectrum (aside from free PEt_3) is a broad

resonance at δ 4.12 ppm which might indicate interaction with a borane species. It is unclear what this species might be, however an interaction with the H atoms of a bound $Me_2NH{\cdot}BH_3$ is a possibility. $[H\text{-}PEt_3]^+$ cations are not seen in the ^{31}P NMR, meaning that if PEt_3 does assist with deprotonation of $Me_2NH{\cdot}BH_3$, the subsequent phosphonium salts must rapidly release dihydrogen gas upon reaction with the corresponding magnesium hydride.

With regards to the other intermediates, the fact they can form even in the absence of a Lewis base suggests a slightly different catalytic mechanism to that seen in Chapter 3. In the work published by Hill and co-workers, initial binding of $Me_2NH{\cdot}BH_3$ is achieved by loss of an R group from the Mg complex as RH, which allows β-hydride elimination to occur, resulting in the formation of $Me_2N{=}BH_2$ (Scheme 4.17).[88] However, in the reactions presented in this chapter the Mg complex remains intact throughout (as seen in ^1H NMR spectra), making a β-hydride elimination step similar to that shown in Scheme 4.17 highly unlikely. This is further confirmed by the absence of the intermediate LM–$NMe_2BH_2NMe_2BH_3$ in all reactions, along with LM–NMe_2BH_3 which is also absent from all ^{11}B NMR spectra apart from the reaction with **4.6g**.

Both ^1H and $^{11}B\{^1H\}$ NMR spectra show an initial binding of $Me_2NH{\cdot}BH_3$ through hydrogen bonding, but it is the mechanism by which the substrate becomes deprotonated that remains unclear, especially when no Lewis base is present. It is plausible that a Lewis base assists deprotonation in a similar manner to that seen in Chapter 3, however, when only **4.6** is present in solution, another process must be occurring, which could perhaps also be involved in the reactions of **4.6a**–**h**. Therein lies the possibility that the O atom of the -OMes ligand itself acts as a Lewis base and assists in deprotonation of $Me_2NH{\cdot}BH_3$ in a manner such as that shown in Scheme 4.18. However, further investigations would

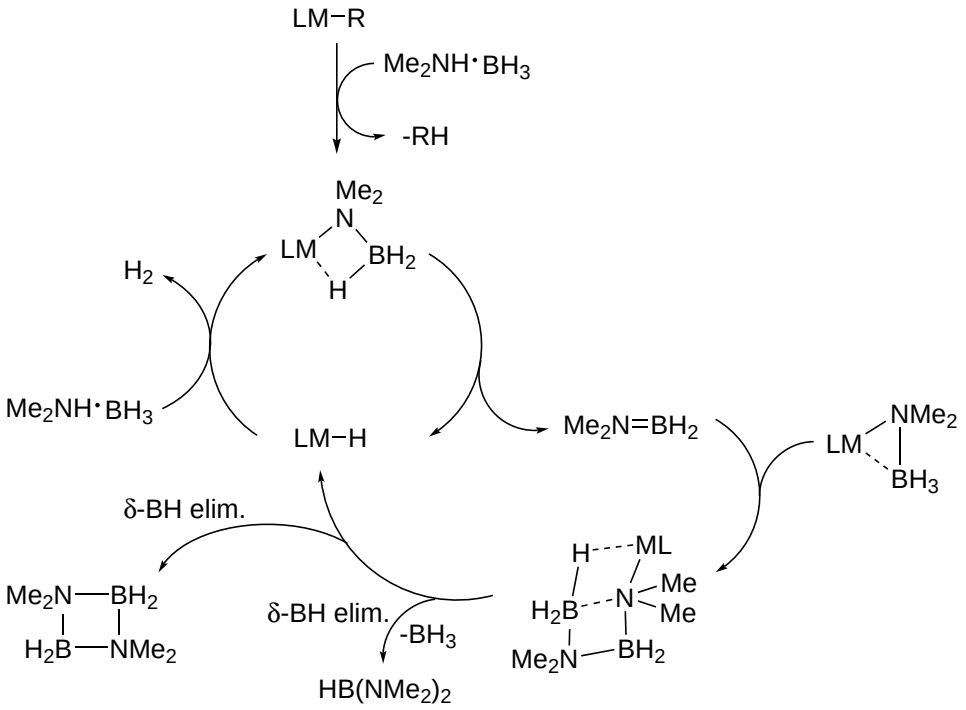

Scheme 4.17: Mechanism for the catalytic dehydrocoupling of $Me_2NH{\cdot}BH_3$, as published by Hill and co-workers.[88]

be required to confirm whether this process is taking place. Another possibility is that a second molecule of **4.6** assists in deprotonation, however, the large steric constraints of these complexes would make such interactions unlikely, as β-diketiminate ligands with -^{t}Bu groups along the backbone tend to inhibit dimerisation in Mg complexes.[154]

Once $Me_2N{=}BH_2$ has been produced, the final product and intermediates can be formed in a similar manner to that seen with the Zr/N species, with reaction occurring

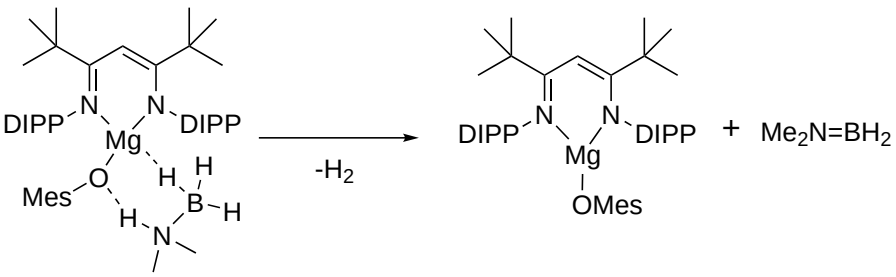

Scheme 4.18: Possible route to the formation of $Me_2N{=}BH_2$ by reaction of $Me_2NH{\cdot}BH_3$ with **4.6**. DIPP = diisopropylphenyl.

between $Me_2N{=}BH_2$ and $Me_2NH{\cdot}BH_3$ resulting in the formation of $Me_2NH{-}BH_2{-}NMe_2{-}BH_3$, and elimination of either Me_2NH or BH_3 preceding the formation of $HB(NMe_2)_2$ or $Me_2N(B_2H_5)$.

4.4 Conclusion

In this chapter, a novel Mg β-diketiminate complex has been synthesised and tested for its reactivity towards the activation of small molecules and the catalytic dehydrocoupling of $Me_2NH{\cdot}BH_3$ in combination with a series of phosphines and nitrogen-based Lewis bases. An initial examination of the relationship between **4.6** and the Lewis bases found limited interaction between them, apart from in the cases of pyridine (**c**), 2-methylpyridine (**d**), and 2,6-dimethylpyridine (**e**) which formed adducts upon combination in solution.

No reaction was seen upon addition of H_2 or PhCCD to **4.6a** and **4.6c**–**h**, which may be due to insufficient Lewis acidity of **4.6** or poor cooperativity between the Lewis pairs. Pentanone and mesitaldehyde both formed adducts with **4.6**, however, the Lewis bases appeared to show no change, which appears to be a result of the high steric bulk around the principle sites for nucleophilic attack. The issue of steric bulk with regards to mesitaldehyde was highlighted when the benzaldehyde was used in its place. This also resulted in the formation of adducts with **4.6**, however PEt_3 (**g**) was found to form what appears to be a dynamic bond with the aldehydic carbon of the bound benzaldehyde. It is likely that a similar bond would be formed with mesitaldehyde if not for the inhibitory *ortho*-methyl groups. Functionalisation of benzaldehyde may be possible as a result of this reaction, however, further study is required to discover what transformations are feasible.

The catalytic dehydrocoupling of $Me_2NH{\cdot}BH_3$ proved to be a successful, if sluggish,

reaction for **4.6a-b** and **4.6e–h**, whilst **4.6c** proved to be unreactive, and **4.6d** demonstrated very minor reactivity. Differences in reactivity between the Lewis bases are clear, with **4.6g** the most active, reaching a yield of 75% within 4 days. However, **4.6** is also capable of performing the transformation alone, and a catalytic reaction at 60 °C resulted in a yield of 93% within 1 h. However, without the catalytic data of **4.6** at room temperature, it is unclear to what degree the Lewis bases enhance or inhibit the reaction.

Overall, **4.6** has shown promise with regards to potential small molecule activation reactions, however appears to be limited by its lower acidity when compared to commonly used Lewis acids. Its reactivity for catalytic dehydrocoupling is more promising, with activity moving nearer to that of the Zr/N species discussed in previous chapters when reactions are performed at higher temperatures.

Chapter 5

Intramolecular magnesium-phosphine Lewis pairs

5.1 Introduction

The exploitation of the potential energy present as a result of the HOMO-LUMO gap within a frustrated Lewis pair (FLP) has been highly successful, and has led to the exploration of a new method for the transformation and functionalisation of small molecules.[2–4,6] Additionally, the need to forever seek cheaper and more abundant materials has led to significant research into the capability of elements such as magnesium. Magnesium chemistry has significantly expanded in recent years—and is no longer limited to stoichiometric Grignard reactions as it once was—with Mg β-diketiminate species in particular the subject of much study.[56,64]

Previous work within the Wass group has shown that intramolecular Zr(IV)/P species are highly adept at the activation of small molecules (Scheme 5.1), but the high strength bond formed between the Zr centre and the substrate/product prevents catalytic turnover in certain cases,[8,10] and so perhaps the use of a similar, less highly Lewis acidic, Mg(II)

complex has the potential to not only perform the same activations, but to also enable release of the product, and therefore allow catalytic turnover. The work within this chapter sought to synthesise Mg complexes such as these, and to test the validity of this idea by reacting them with a variety of small molecules.

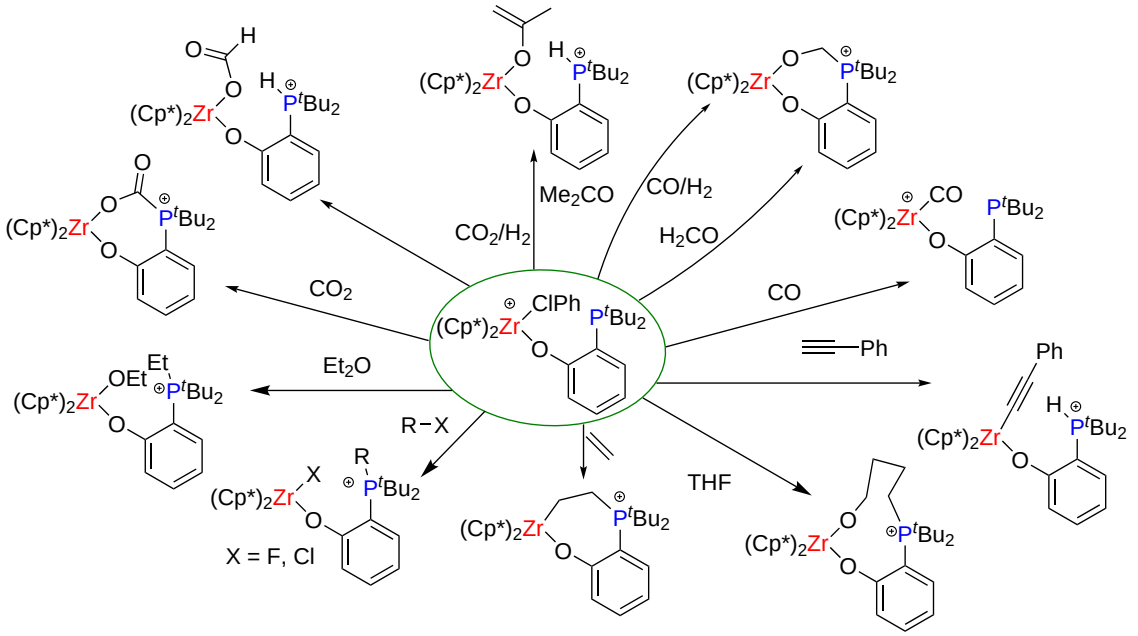

Scheme 5.1: Small molecule activation using a zirconocene-phosphinoaryloxide FLP.

5.2 Aims & Objectives

The work in this chapter seeks to build upon the work done in Chapter 4 with cooperative Mg/P Lewis pairs, but in an intramolecular rather than an intermolecular system. Bringing both the Lewis acidic and Lewis basic components to within the same molecule can have significant effects on reactivity, not least because it is entropically advantageous compared to intermolecular systems. With the aim of investigating the effectiveness of such compounds, the research within this chapter was carried out with the following goals in mind:

- Synthesise novel Mg/P Lewis pair complexes using Mg β-diketiminate compounds in combination with a phosphine moiety
- Test the reactivity of these complexes for the activation of various small molecules
- Test these complexes for the catalytic dehydrocoupling of amine-boranes

It should be noted that all X-ray crystallography experiments were performed by Dr Natalie Pridmore and Dr Hazel Sparkes (University of Bristol).

5.3 Results & Discussion

5.3.1 Synthesis of magnesium-phosphine Lewis pairs

The target in this chapter was to synthesise magnesium complexes containing a pendent phosphine that could then be tested for reactivity with various small molecules. The first stage in the synthetic process was the formation of a magnesium precursor which could be reacted with a number of different phosphines. Magnesium β-diketiminates were chosen as the basis of these complexes for the same reasons as outlined in the previous chapter, namely that they are highly modifiable ligands that have already been widely applied in magnesium chemistry. The β-diketiminate ligand **5.1** was used for this work, in addition to the more sterically bulky **4.1** (Figure 5.1). The fact that the target complexes in this chapter are intramolecular rather than intermolecular means there is not the same risk of ligand deprotonation—as was the case in the previous chapter—and so the *tert*-butyl groups are not necessarily a requirement in the final complexes. However, attempts were still made to synthesise complexes with **4.1** in order to see whether there are any differences in reactivity of the final Mg/P Lewis pairs. The synthetic route to **5.1** is much

simpler than that of **4.1**, and is a one-step literature procedure that involves the reaction of 2,4-pentanedione with the desired amine (in this case diisopropylaniline) in an acidic environment (Scheme 5.2).[164]

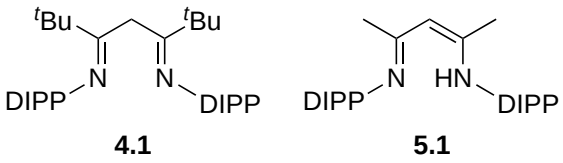

Figure 5.1: Compounds **4.1** and **5.1**—see Chapter 4 for the synthesis of **4.1**. DIPP = diisopropylphenyl.

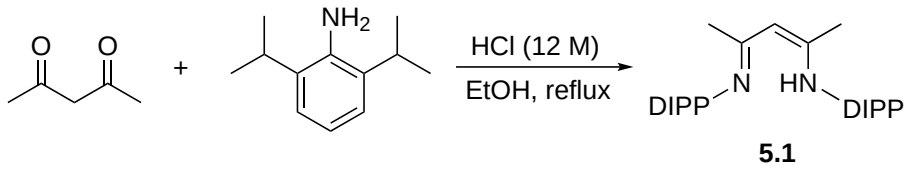

Scheme 5.2: Synthetic route to the β-diketiminate **5.1**. DIPP = diisopropylphenyl.

The compounds **4.2** and **4.3** were both synthesised again for the work in this chapter (Figure 5.2, see Chapter 4 for synthesis details), while **5.1** was reacted with dibutylmagnesium to make a congener of **4.2** following a literature procedure (**5.2**, Scheme 5.3).[165] Unlike with the synthesis of compound **4.2** and **4.3**, it is not necessary to use THF as the solvent for the synthesis, and the more weakly coordinating solvent toluene can be used in its place. This means that an additional step to remove any unwanted THF adduct is not required (see Chapter 4).

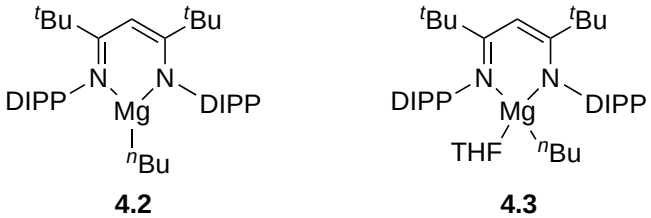

Figure 5.2: Compounds **4.2** and **4.3**—see Chapter 4 for synthesis. DIPP = diisopropylphenyl.

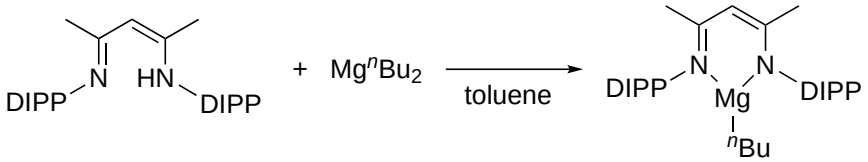

5.1 **5.2**

Scheme 5.3: Synthetic route to **5.2** through the reaction of **5.1** with dibutylmagnesium.[165] DIPP = diisopropylphenyl.

The aim at this stage was to form a complex of the type shown in Figure 5.3. In order to decide upon the final form of the phosphine moieties within the target complexes, inspiration was taken from previous work by both the Wass group and Erker and co-workers with Zr/P FLPs.[8,10,16,20] Both groups have synthesised cationic zirconocene species containing a phosphine bound by either an aryloxide or alkoxide linker, allowing the pendent phosphine to interact with the Zr centre whilst also permitting the insertion of a wide variety of substrates. With the aim of replicating these capabilities in conjunction with the Lewis acidic, Mg component of the Lewis pairs, the phosphines shown in Figure 5.4 were synthesised following literature procedures.[166,167] Compounds **5.5** and **5.6** were kindly provided by Dr Andy Chapman.

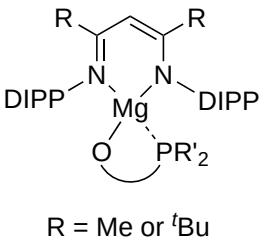

Figure 5.3: Target complexes to be used in small molecule activation reactions. DIPP = diisopropylphenyl.

There are some similarities and differences between the phosphines **5.3**–**6**, the first similarity being that they all possess significant bulk about the Lewis basic phosphine centre, which has proved useful for FLP-type reactivity. Phosphines **5.3** and **5.4** possess

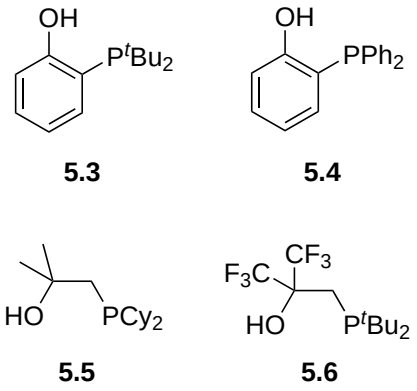

Figure 5.4: The phosphines **5.3-6**.

a more rigid linker than **5.5** and **5.6**, which not only could have the potential to affect any future reactivity of the target complexes but, as shown in this section, appears to significantly affect whether or not these complexes can be synthesised in the first place. An important addition to **5.6** is the inclusion of electron-withdrawing -CF_3 groups in place of the methyl groups of **5.5**. This has the potential to not only affect the synthesis of the desired Mg complexes, but also any future reactivity with small molecules by affecting the strength of the Lewis acidic Mg centre.

The next stage in the synthesis was to react the phosphines with the Mg β-diketiminate species. The aim was to combine the species in solution, with the alcohol group then reacting with the magnesium centre preceding elimination of butane to give the desired product. The Mg compound **4.3** was reacted separately with **5.3** and **5.4** in toluene and heated to reflux for several days (Scheme 5.4). However, no reactivity was displayed, with no visible change in the reactions or the ^{1}H and ^{31}P NMR spectra observed. This could both be due to the steric bulk and presence of THF in **4.3**, and due to the potential unsuitability of these phosphines for this reaction.

The Mg complex **4.2** was reacted with **5.5** and **5.6** in toluene (Scheme 5.5), and a mixture of products was obtained in both cases, as evidenced by the multiple ^{31}P signals

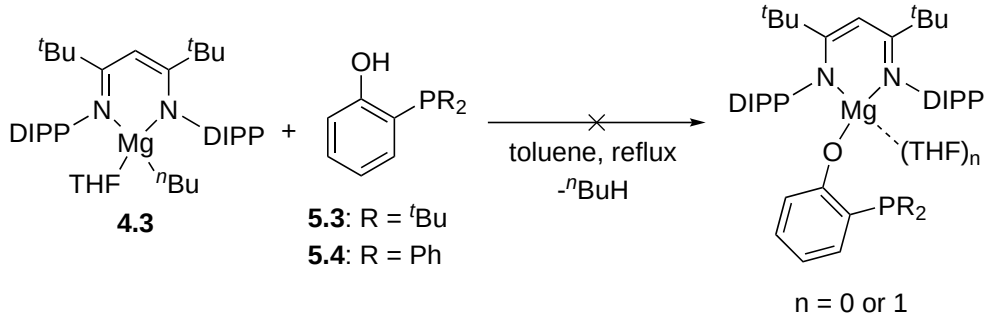

Scheme 5.4: Attempted synthesis of Mg/P Lewis pair through reaction of **4.3** with **5.3** and **5.4**. DIPP = diisopropylphenyl.

and number of β-diketiminate signals. Although a small quantity of the desired species may be present, it could not be isolated from the larger mixture, which also appeared to include some Mg compounds of the nature shown in Figure 5.5 (which itself could not be isolated), with new ^{31}P NMR peaks at δ -14.6 ppm (from δ -12.1 ppm for **5.5**), and at δ 9.12 ppm (from δ 4.85 ppm for **5.6**) for each reaction respectively, in addition to the disappearance of the alcoholic protons in each reaction. The butyl ligand is eliminated as butane through protonation. The steric hindrance imparted by the β-diketiminate ligand appears to prevent the formation of the desired species, and so the slightly less sterically-hindering ligand **5.2** was used in its place.

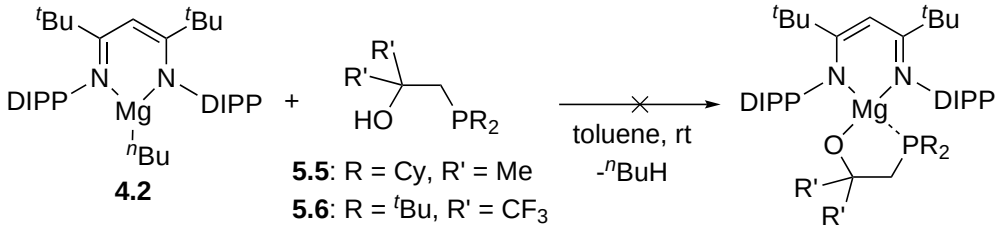

Scheme 5.5: Attempted synthesis of Mg/P Lewis pair through the reaction of **4.2** with either **5.5** or **5.6**. DIPP = diisopropylphenyl.

The Mg complex **5.2** and **5.6** were reacted together in toluene and heated at 50 °C for 2 h (Scheme 5.6). Unlike with the compounds **4.2** and **4.3**, this resulted in the formation of the desired product (**5.7**), which was isolated as white crystals in a modest yield of

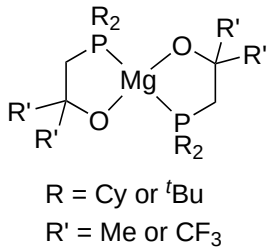

Figure 5.5: Possible side-product in attempted synthesis of Mg/P Lewis pair.

52%. It appears that the difference in steric hindrance between **4.2** and **5.2** is significant enough that **4.2** prevents the formation of the desired product, whereas **5.2** favours the formation of **5.7** over other possible products—such as those shown in Figure 5.5.

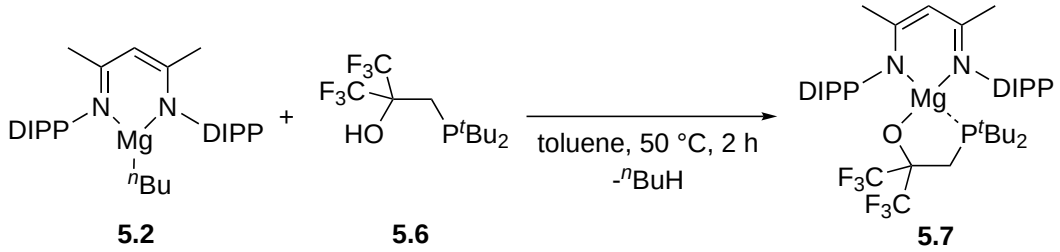

Scheme 5.6: Synthesis of Mg/P Lewis pair **5.7** through the reaction of **5.2** with **5.6**. DIPP = diisopropylphenyl.

Crystals of **5.7** suitable for X-ray crystallography were also obtained, with the determined structure shown in Figure 5.6. As expected, the two ligands are roughly perpendicular to one another, with the phosphine angled towards the Mg atom. The O atom is much more closely bonded to the Mg centre than the P atom, with a Mg–P distance of 2.8431(7) Å compared to a Mg1–O1 bond of 1.9028(9) Å. It is not clear to what degree the steric bulk of the diisopropylphenyl and *tert*-butyl groups affect the Mg–P distance, however, it is likely to have some influence due to their proximity. Indeed, the Mg–P bond is slightly longer than in other Mg phosphine complexes,[113,168,169] suggesting that steric bulk is increasing the bond length. However, this may actually favour any subsequent reactivity by making insertion of a small molecule into the Mg–P bond more favourable.

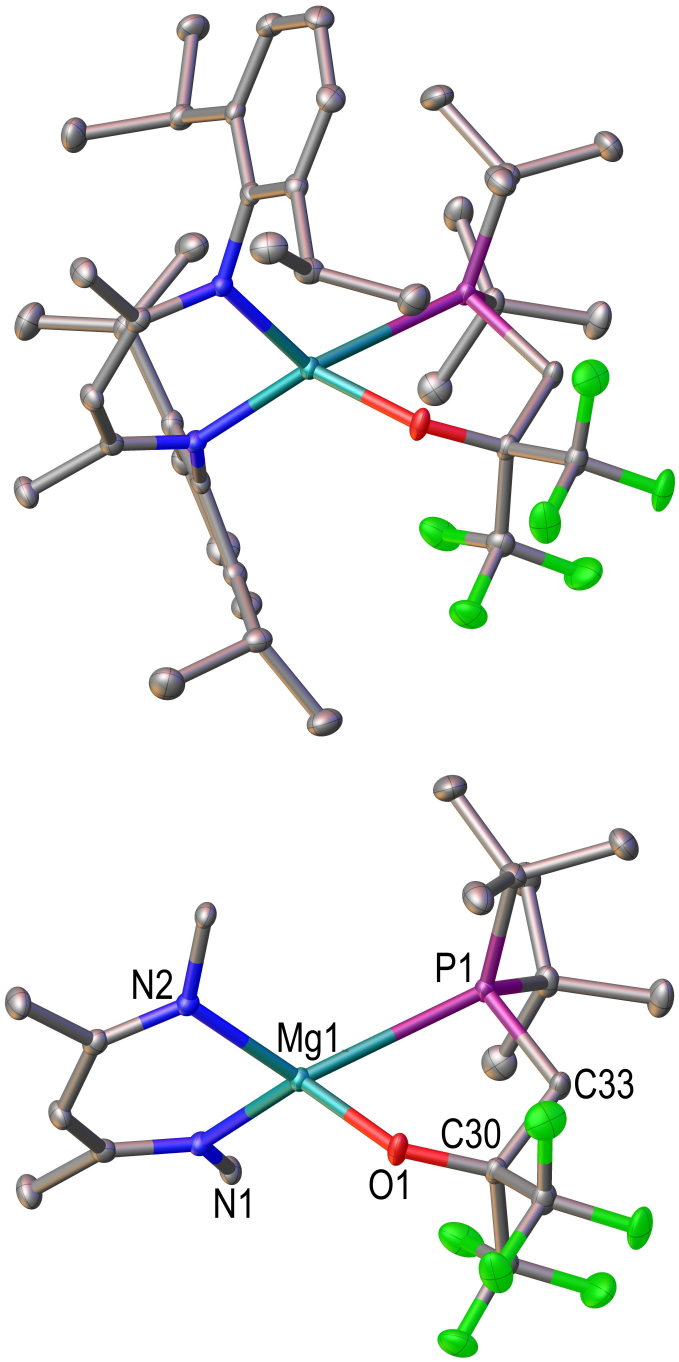

Figure 5.6: Structure of **5.7** as determined by single crystal X-ray diffraction. Thermal ellipsoids are drawn at the 50% probability level. The diisopropylphenyl groups have been removed from the image on the bottom for clarity, along with hydrogen atoms. Selected bond lengths (Å) and angles (deg): Mg1–N1 2.0824(12), Mg1–N2 2.0732(12), Mg1–O1 1.9028(9), Mg1–P1 2.8431(7), O1–C30 1.3584(17), P1–C33 1.8546(12), N1–Mg1–N2 92.80(5), P1–Mg1–O1 75.04(4), Mg1–O1–C30 133.67(9), Mg1–P1–C33 93.44(5).

The synthesis of the **5.5** congener to **5.7** was also attempted, with an NMR-scale reaction producing a mixture of compounds (Scheme 5.7). ^{1}H and ^{31}P NMR data suggests the desired species was not formed, although new signals in the ^{1}H NMR spectrum, and a new signal at δ -14.5 ppm in the ^{31}P NMR spectrum were observed. However, free β-diketiminate ligand was the major product, suggesting the protonation of this compound and the formation of a bisphosphine oxide Mg species (Figure 5.5). No product could be isolated from this reaction.

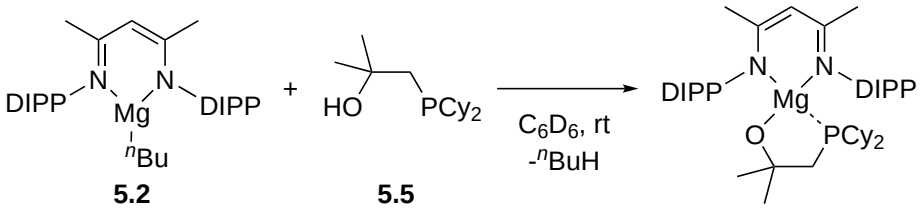

Scheme 5.7: Attempted synthesis of Mg/P Lewis pair through the reaction of **5.2** with **5.5**. DIPP = diisopropylphenyl.

In order to see whether an alternative synthetic route could assist in the formation of Mg/P Lewis pairs of **5.2** and **5.3**, the reaction shown in Scheme 5.8 was attempted. Complex **5.8** was synthesised using a literature procedure,[71] and the phosphine **5.9** is synthesised through the reaction of **5.3** with KH and was provided by Dr Owen Metters. Unfortunately, this reaction route also proved unsuccessful, with the β-diketiminate ligand once again being eliminated via protonation, alongside the formation of a new phosphine species which could not be isolated (^{31}P NMR (162 MHz, 25 °C, C_6D_6): δ 6.5 ppm). A similar signal is seen when Mg^nBu_2 is combined alone in solution with **5.3** (^{31}P NMR (122 MHz, 25 °C, C_6D_6): δ 6.4 ppm), suggesting a Mg phosphine species has been formed in the reaction between **5.8** and **5.9**.

Compound **5.7** was then taken forward and reacted with a series of small molecules containing various functional groups—of different polarities and sizes – in order to identify

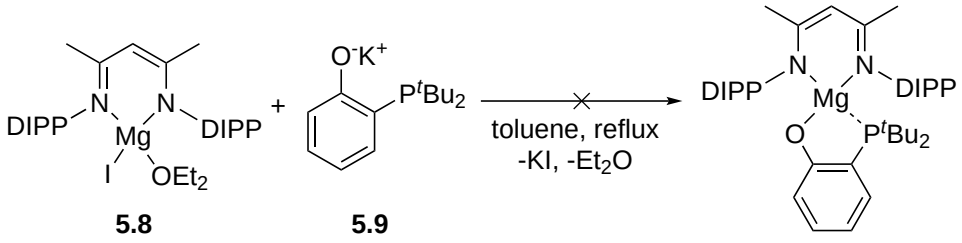

5.8 **5.9**

Scheme 5.8: Attempted synthesis of a Mg/P Lewis pair via salt metathesis.

what substrates are activated by **5.7**.

5.3.2 The reaction of 5.7 with hydrogen gas

The first small molecule that was reacted with **5.7** was hydrogen gas, with an NMR solution of **5.7** charged with 1 bar H_2 and left to react at room temperature for 5 days (Scheme 5.9). No reaction was seen, even upon raising the temperature to 80 °C. The exact reason for this is not known but it may suggest insufficient Lewis acidity at the Mg centre or an unsuitable HOMO-LUMO gap within the Lewis pair.

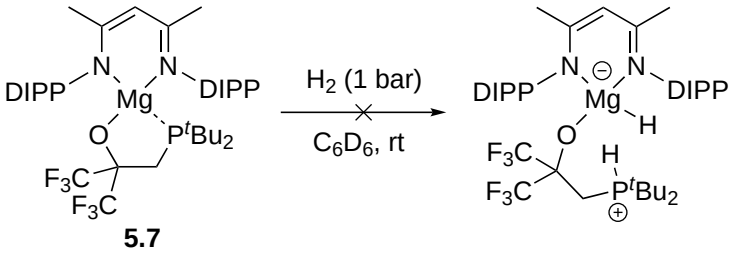

5.7

Scheme 5.9: Attempted activation of H_2 on an NMR scale using **5.7**. DIPP = diisopropylphenyl.

5.3.3 The reaction of 5.7 with carbon dioxide

No colour change was seen upon addition of 1 bar CO_2 to a C_6D_6 solution of **5.7**; however, NMR spectra taken within 30 min showed complete conversion to a mixture of products. Two new broad peaks in the ^{31}P NMR spectrum were present at δ 9.18 and 8.49 ppm,

along with new peaks at δ -76.1 and -76.2 ppm in the ^{19}F NMR spectrum—along with a significant number of undefined peaks between δ -73.5 and -79.0 ppm. After 3 days, degradation of some of the species occurred, with the signal at δ 8.49 ppm disappearing from the ^{31}P NMR spectrum. Attempts to isolate any species were unsuccessful, along with the use of analytical techniques such as mass spectrometry—the compounds proving too air sensitive to obtain any useful data. The formation of a cationic phosphorus centre would result in a more significant shift downfield,[8,25] therefore it is likely that one or more new Mg complexes have been formed instead.

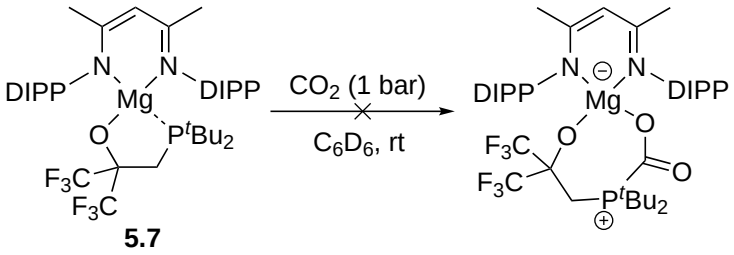

Scheme 5.10: Reaction of **5.7** with 1 bar CO_2. DIPP = diisopropylphenyl.

According to the NMR data, the species is different to the carbonate bridged magnesium(II) compound reported by Jones and co-workers (Figure 5.7),[170] which was formed upon reaction of CO_2 with a Mg(I) β-diketiminate compound. However, a dimer species with bridges formed between the phosphinoxide ligand and CO_2 could be one possible product. Another possibility is that the CO_2 molecule is coordinating to the Mg centre with no bonding occurring from the phosphine. ^{13}C NMR data of the reaction proved inconclusive (due to weak carbonyl signals), and therefore a reaction using $^{13}CO_2$ (to obtain a stronger NMR signal) would perhaps be required to more accurately deduce the product.

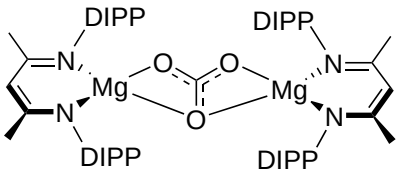

Figure 5.7: The carbonate bridged magnesium(II) complex reported by Jones and co-workers.[170] DIPP = diisopropylphenyl.

5.3.4 The reaction of 5.7 with phenylacetylene-*d*

The addition of phenylacetylene-*d* (PhCCD) to a C_6D_6 solution of **5.7** resulted in the slow conversion to an unknown product over 4 days (Scheme 5.11). From the ^{31}P NMR it is clear that the desired small molecule activation (the result of cooperation between the Mg and P Lewis centres) has not occurred, with a new signal at δ 9.14 ppm suggesting a very similar phosphine species to that seen for the reaction with CO_2. This signal also shows that a possible 1,2-addition product has not been formed either.

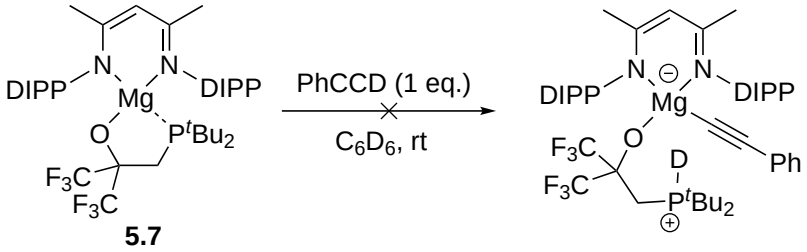

Scheme 5.11: The reaction between **5.7** and phenylacetylene-*d*. DIPP = diisopropylphenyl.

The ^{1}H NMR spectra show small shifts in all signals related to both the **5.7** complex and PhCCD, however, no significant changes are otherwise seen. It is possible that the PhCCD molecule is coordinating to the Mg centre, but no reaction occurs with regards to the Lewis base, resulting in a minor change in all ^{1}H and ^{31}P environments but without significant alteration of the structure (Figure 5.8). Coordination of an alkyne to a Mg β-diketiminate complex via π-bonding has previously been reported by Harder and co-

workers.[107] Once again, the product proved to be too air sensitive to obtain useful mass spectrometry data.

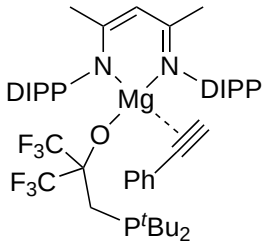

Figure 5.8: A possible product from the reaction of **5.7** with phenylacetylene-*d*. DIPP = diisopropylphenyl.

5.3.5 The reaction of 5.7 with phenylisocyanate

Compound **5.7** was also reacted with phenylisocyanate (1 eq., PhNCO) in C_6D_6 solution (Scheme 5.12). The ^{1}H and ^{31}P NMR spectra showed the immediate formation of several different products, however, none of them appear to be the cooperative Lewis pair product shown in Scheme 5.12, with no peaks corresponding to a cationic phosphine. Unfortunately, the products proved to be intractable, with mass spectrometry experiments also ineffective due to the air sensitivity of the compounds.

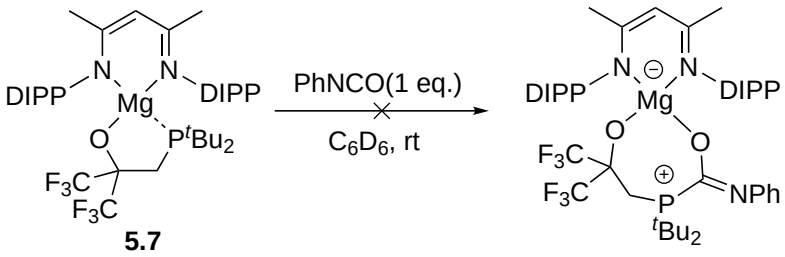

Scheme 5.12: Attempted synthesis of a cooperative Lewis pair product through reaction of **5.7** with phenylisocyanate. DIPP = diisopropylphenyl.

As the complexes reported by Jones and co-workers in Figure 5.9 show,[71,171] there is more than one possible product when isocyanates are reacted with Mg β-diketiminate complexes, and considering the multitude of products present in the reaction mixture it

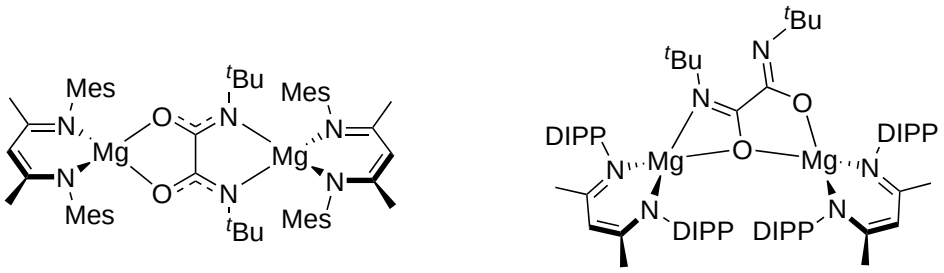

Figure 5.9: Products formed through the reaction of Mg β-diketiminate complexes with *tert*-butylisocyanate.[71,171] DIPP = diisopropylphenyl, Mes = mesityl.

is possible that one or more phenylisocyanate bridging complexes may be present.

Another possible product is the coordination complex shown in Figure 5.10, whereby the O atom from the PhNCO forms an adduct with the Mg centre; however it would be surprising if this did not result in any reactivity from the phosphine due to the proximity with a possible site for nucleophilic attack. This could suggest that either there is too great a degree of steric bulk about the phosphine, or that any bond formed with the Mg centre is not strong enough to induce a significant change in PhNCO polarity and enable an attack from the Lewis base.

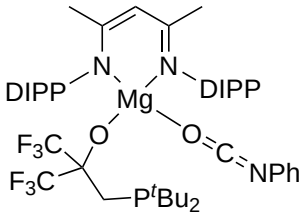

Figure 5.10: Possible coordination product for the reaction of **5.7** with phenylisocyanate. DIPP = diisopropylphenyl.

5.3.6 The reaction of 5.7 with dichloromethane-d_2

Complex **5.7** was reacted with an excess of dichloromethane-d_2 (CD_2Cl_2) in a C_6D_6 solution at room temperature (Scheme 5.13), and although there was no change in colour a reaction was observed within a minute (via NMR). A new signal appeared in the ^{31}P

NMR spectra at δ 43.9 ppm which correlates with a dichloromethane splitting product using a phosphine (**5.10**, Scheme 5.13),[8,25] along with new peaks in the ^{1}H and ^{19}F spectra. The ^{2}H NMR spectrum contains a broad signal at δ 4.88 ppm, which is in the expected region for a CD_2Cl_2 splitting product where a phosphine is used as the Lewis base.[8] It is promising that this product has been formed, and shows that even though **5.7** is unable to facilitate the activation of other small molecules—such as the heterolytic cleavage of H_2—it is still capable of performing certain activation reactions.

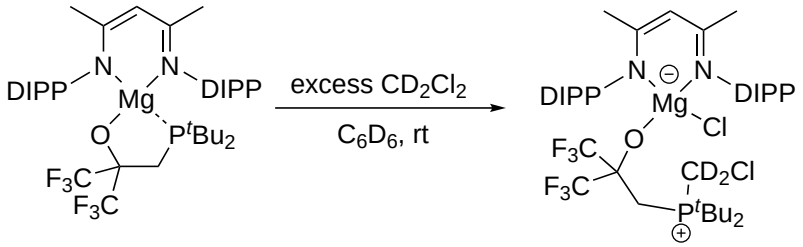

5.7 **5.10**

Scheme 5.13: Reaction between **5.7** and dichloromethane-d_2. DIPP = diisopropylphenyl.

The product slowly converted to a new compound over several days, with no trace of **5.10** left after 4 days. The new species possesses a ^{31}P NMR signal at δ 72.8 ppm which often indicates an oxidised phosphorus compound. However, the use of J. Youngs tap NMR tubes makes this unlikely to be the result of the reaction solution coming into contact with air or moisture. Especially considering that a singular compound appears to be present according the spectroscopic data, whereas several products might be expected if air or water did enter the reaction mixture. It is not entirely clear what this compound might be; however, the product of a rearrangement of **5.10**, or the formation of a dimeric species, could be a possibility.

5.3.7 The reaction of 5.7 with ethene

Another compound that has often been used in FLP-type chemistry is ethene, as it can be a good indicator of reactivity with other olefins. Ethene gas (1 bar) was added to a solution of **5.7** (C_6D_6) and left to react at room temperature (Scheme 5.14). No colour change was seen upon addition, and indeed, no reaction took place over 3 days. Increasing the reaction temperature to 50 °C for 16 h, and then to 80 °C for 14 days only resulted in slight degradation of **5.7**. This reaction may be hindered by the Lewis acidity of the magnesium centre, or by the non-polarity of ethene making it less suitable to attack by this Lewis pair.

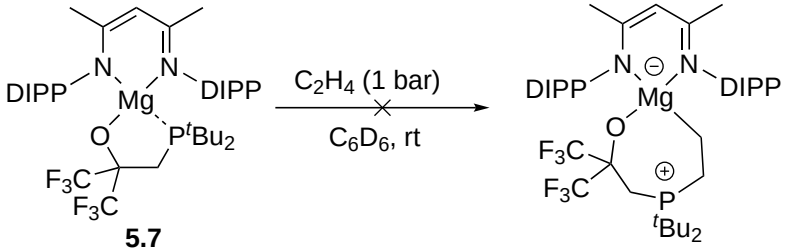

Scheme 5.14: Reaction of **5.7** with ethene gas (1 bar). DIPP = diisopropylphenyl.

5.3.8 The reaction of 5.7 with 3-pentanone

The reaction of **5.7** with 3-pentanone (1 eq. at rt in C_6D_6) simply resulted in the formation of an adduct through bonding of the ketonic O atom to the Mg centre—changing the solution from colourless to very pale yellow (Scheme 5.15). No further reaction took place, suggesting that the phosphine does not favour attack of the electrophilic carbon—perhaps the interaction between the Mg and the O atoms does not sufficiently increase the electrophilicity at this position. The reactions using the intermolecular Mg/P systems resulted in the same outcome, with the adduct forming and the Lewis base affecting no

additional reactivity. It appears that including the phosphine moiety within the system does not change the outcome for this particular reaction.

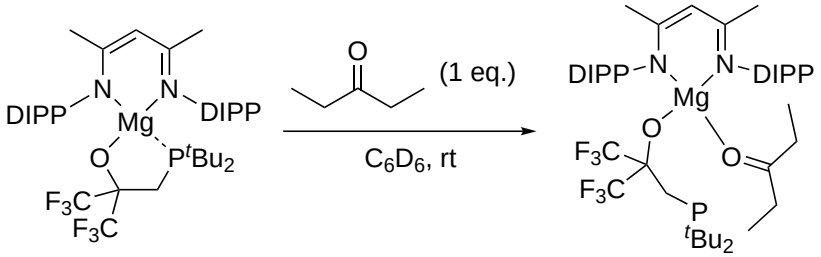

5.7 **5.11**

Scheme 5.15: Reaction of **5.7** with 3-pentanone. DIPP = diisopropylphenyl.

5.3.9 The reaction of 5.7 with benzaldehyde

One equivalent of benzaldehyde was added to a solution (C_6D_6) of **5.7** at room temperature (Scheme 5.16). The solution instantly changed colour from colourless to orange, with NMR data confirming the formation of a benzaldehyde adduct. This is evidenced through comparison with the equivalent reaction of **4.6**. The same signal broadening, along with a slight change in β-diketiminate signals, in the ^{1}H NMR spectra is seen, in addition to a slight upfield shift of the ^{31}P NMR signal (indicating decoordination of the phosphine). Within an hour, a small portion (<10% by ^{1}H NMR) of the sample converted to compound **5.12** (Scheme 5.16), with complete conversion occurring after several days—along with a change in solution colour from orange to yellow. The mechanism by which this occurs would appear to involve nucleophilic attack of the aldehydic carbon by the phosphine oxide O atom, in combination with the aldehydic proton being transferred to the phosphine moiety, eliminating it from the complex. Dimerisation would then follow, with the two carboxylate moieties acting as bridges between the Mg centres. However, it is possible that **5.12** was instead formed through reaction with a benzoic acid impurity

in the starting materials, as **5.12** has previously been synthesised through the reaction of benzoic acid with **5.2**.[165] However, no evidence of such an impurity was seen when the benzaldehyde was examined by ^{1}H NMR beforehand.

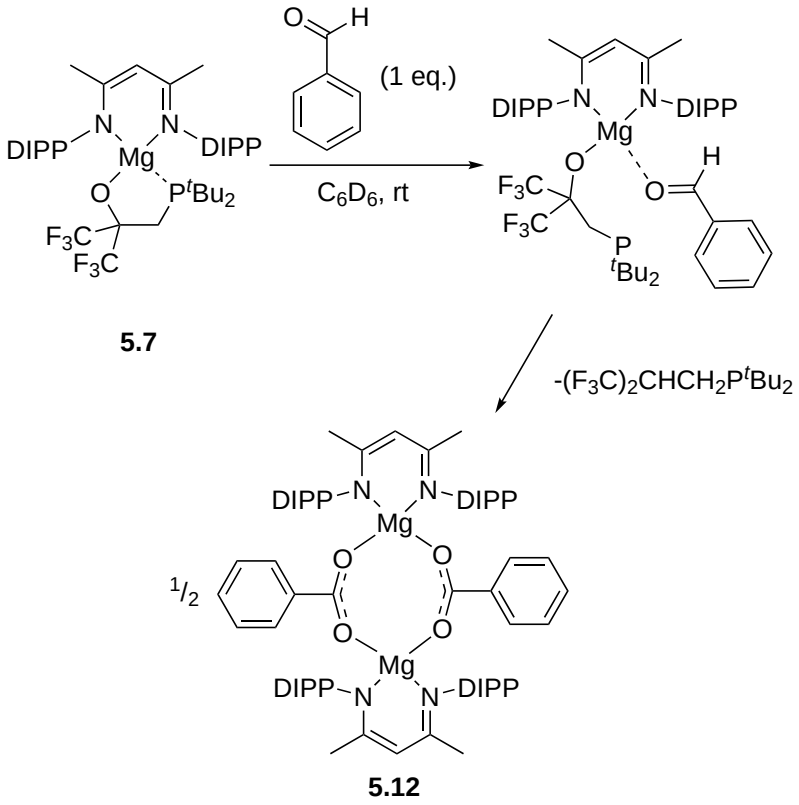

Scheme 5.16: The reaction of **5.7** with benzaldehyde. DIPP = diisopropylphenyl.

The structure of **5.12** was unambiguously determined when colourless crystals of **5.12** were isolated and characterised by single crystal X-ray diffraction, with the structure shown in Figure 5.11. The structure possesses C_{2h} symmetry, with the bond lengths and angles for each half identical in size, and each Mg β-diketiminate moiety lying along the same plane. The two carboxylate bridging species are not evenly spaced between each Mg centre, with the Mg1–O1 bonds of 1.9057(14) Å in length and the Mg1–O2 bonds at 1.9492(12) Å, suggesting the electron dispersion is not equal across the carboxylate groups. This is further confirmed by the slight differences in bond length between the carboxylate

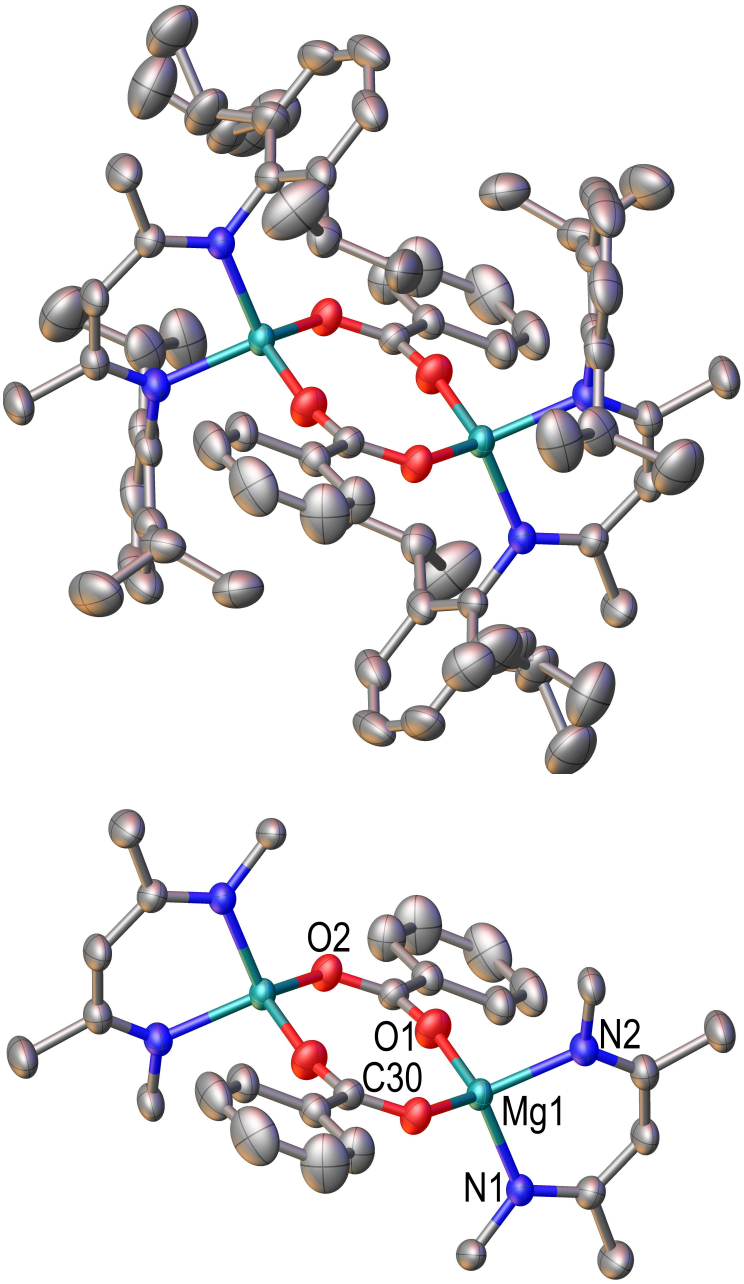

Figure 5.11: The structure of **5.12** as determined by single crystal X-ray diffraction. Thermal ellipsoids are drawn at the 50% probability level. The diisopropylphenyl groups have been removed from the image on the bottom for clarity, along with hydrogen atoms. The structure on top contains disorder in one of the diisopropylphenyl groups. The symmetry of the compound means the same atom numbers have been assigned to both halves of the molecule. Selected bond lengths (Å) and angles (deg): Mg1–N1 2.0302(15), Mg1–N2 2.0375(14), Mg1–O1 1.9057(14), Mg1–O2 1.9492(12), C30–O1 1.249(2), C30–O2 1.2618(19), O1–Mg1–O2 113.36(6), O1–C30–O2 123.21(15).

carbon and each oxygen (C30–O1 1.249(2) Å, C30–O2 1.262(2) Å).

5.3.10 The reaction of 5.7 with mesitaldehyde

Mesitaldehyde (1 eq.) was added to a solution of **5.7** (C_6D_6) in order to ascertain whether the slight increase in steric bulk on the substrate results in the same reactivity as seen with benzaldehyde (Scheme 5.17). An instant colour change to orange was seen upon addition, and NMR spectroscopic data confirmed the formation of an adduct with new, broad signals in the ^{1}H NMR spectrum for both the Mg complex and mesitaldehyde. This matches the changes in NMR spectra observed upon formation of other adducts with both **4.6** and **5.7**. A change in the ^{31}P NMR spectrum (δ 13.8 ppm) also indicates the phosphine is no longer bonding to the Mg centre, and has not formed a permanent bond with the mesitaldehyde. This is not surprising as the reactivity seen between **5.7** and benzaldehyde is unlikely to change when the relative polarities of both benzaldehyde and mesitaldehyde are very similar. The reaction did not result in the formation of an analogous compound to **5.12**, however, meaning the slight extra bulk imparted by the methyl groups on the aryl ring is enough to prevent this reaction route proceeding.

Compound **5.13** was isolated by slow evaporation from hexane, and an X-ray structure

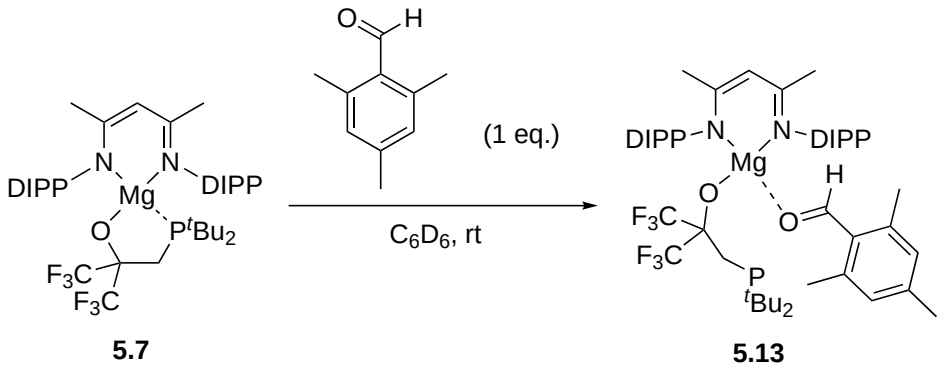

Scheme 5.17: Reaction between **5.7** and mesitaldehyde. DIPP = diisopropylphenyl.

was obtained (Figure 5.12). This structure shows more clearly that there is virtually no interaction between the phosphine and the aldehyde, with a distance of over 4 Å between the phosphorus atom and the aldehydic carbon. It is hard to tell whether this is purely the result of the steric bulk of the phosphine moiety, however, the fact that no interaction was seen even when benzaldehyde was employed makes this unlikely, with a lack of electronic driving force a more convincing reason. Although it should still be noted that the large diisopropylphenyl groups could be a hindrance in both reactions as well.

The mesitaldehyde lies almost exactly perpendicular to the β-diketiminate ligand, with the Mg atom lying slightly out of the ligand plane. The Mg1–O2–C11 angle of 154.96(13)$^\circ$ is slightly over 20° larger than in **5.7** (133.67(9)$^\circ$), and perhaps demonstrates the flexibility of **5.7** that allows for the insertion of molecules such as mesitaldehyde.

5.3.11 Catalytic dehydrocoupling of $Me_2NH{\cdot}BH_3$ using 5.7

Compound **5.7** was used as a catalyst for the same reaction that has been used in previous chapters, namely the dehydrocoupling of $Me_2NH{\cdot}BH_3$. The reaction was performed using the same conditions as with previous catalysts, using 10 mol% of **5.7** at 25 $^\circ$C and then also at 60 $^\circ$C, with the results shown in Table 5.1. Examining the reaction at 25 $^\circ$C first, it is clear that the catalyst has very poor activity, not even attaining a 1% yield after 14 h and only managing a yield of 7% after nearly 5 days. **5.7** is shown to be less effective than **4.6**, and each of **4.6a**, **4.6b**, and **4.6e-h** at this temperature. It would appear that the phosphine oxide moiety is highly disruptive of this catalytic process, and severely limits the capacity of **5.7** to carry out this reaction. It is likely to be the case that the presence of the phosphine hinders the binding of $Me_2NH{\cdot}BH_3$ to the Mg centre. It is not clear whether the Lewis base plays any role in the catalytic cycle, with the only signal visible in

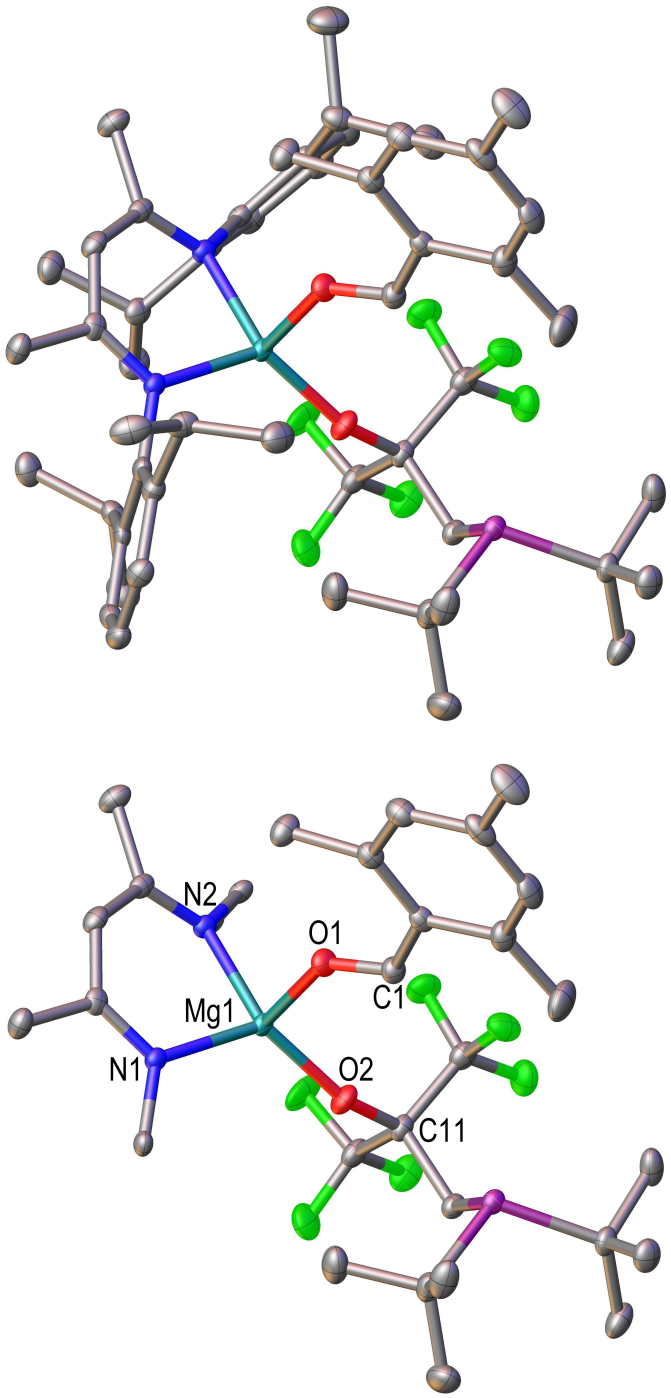

Figure 5.12: The structure of **5.13** as determined by single crystal X-ray diffraction. Thermal ellipsoids are drawn at the 50% probability level. The diisopropylphenyl groups have been removed from the image on the right for clarity, along with all hydrogen atoms from both structures. Selected bond lengths (Å) and angles (deg): Mg1–N1 2.0562(15), Mg1–N2 2.0473(17), Mg1–O1 2.0175(13), Mg1–O2 1.8644(14), O1–C1 1.233(2), O2–C11 1.356(2), Mg1–O1–C1 134.93(13), Mg1–O2–C11 154.96(13), O1–Mg1–O2 103.67(6).

Table 5.1: Catalytic dehydrocoupling of $Me_2NH{\cdot}BH_3$ using **5.7**. No conversion data is available for the reactions at 25 °C due to the overlapping of signals in the NMR spectra.

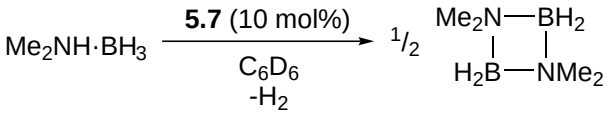

Temperature (°C)	Time (h)	Yield (%)	Conversion (%)
25	14	<1	-
25	38	3	-
25	114	7	-
60	1	41	55
60	3	93	>99

the ^{31}P NMR spectra at δ 9.27 ppm, consistent with the presence of a bound $Me_2NH{\cdot}BH_3$ molecule but suggesting no interaction between the substrate and the phosphine itself.

The reaction at 60 °C was far more successful, achieving a 93% yield with nearly complete conversion of $Me_2NH{\cdot}BH_3$ after 3 h. This result still demonstrates the poorer activity of **5.7** compared to **4.6**, which achieved the same yield within 1 h—**5.7** only managed a 41% yield within the same timeframe—however **5.7** still possesses reasonable activity at this temperature. The significant leap in reactivity between the two temperatures is consistent with the hypothesis that the phosphine hinders the reaction at 25 °C by preventing binding of the substrate to the Mg centre. At 60 °C, it is probable that the Mg–P interaction becomes more labile, making insertion of $Me_2NH{\cdot}BH_3$ far more favourable.

The reaction profile (60 °C) is shown in Figure 5.13, and is not too dissimilar from those seen in previous chapters. The significant intermediate is Me_2NH–BH_2–Me_2N–BH_3, which reaches a peak at around 50 min, while there is also a fairly consistent level of $Me_2N{=}BH_2$ throughout the reaction. $Me_2N(B_2H_5)$ and $HB(NMe_2)_2$ are also present in very small quantities, with $Me_2N(B_2H_5)$ no longer detectable after 170 min, suggesting it converts into the product. $HB(NMe_2)_2$ remains even after reaction completion however,

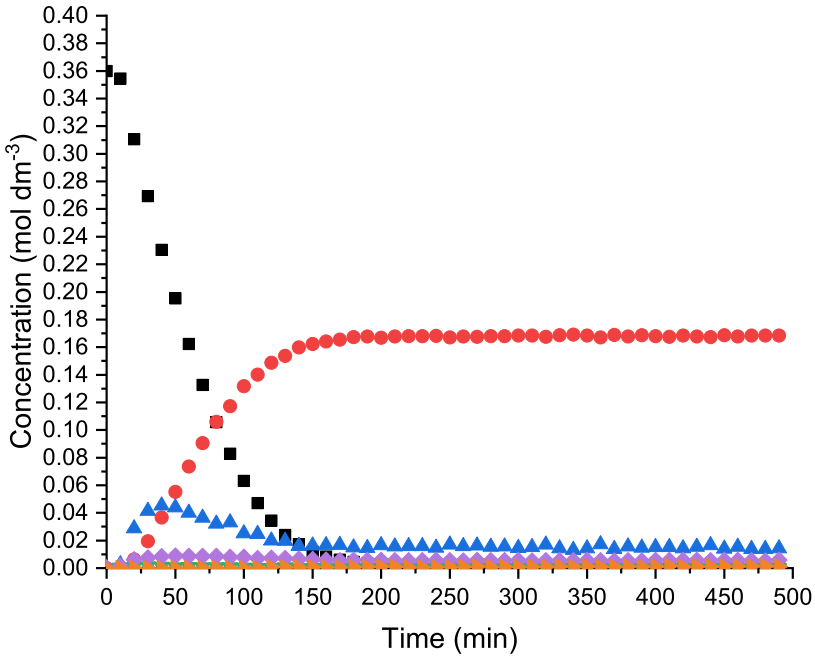

Figure 5.13: Reaction of **5.7** with $Me_2NH{\cdot}BH_3$ (60 °C, PhBr-d_5, 8 h): (■) $Me_2NH{\cdot}BH_3$; (●) $[Me_2N–BH_2]_2$; (▲) $Me_2NH–BH_2–Me_2N–BH_3$; (◆) $Me_2N{=}BH_2$; (▼) $Me_2N(B_2H_5)$; (▶) $HB(NMe_2)_2$.

and only becomes detectable after 110 min.

5.4 Conclusion

The purpose of this chapter was to explore whether an intramolecular magnesium-phosphine Lewis pair was capable of performing FLP-type activation of small molecules, and although the reactivity of the synthesised compound was not as broad as hoped, a degree of success has still been achieved with regards to this goal. The novel Mg/P complex **5.7** was synthesised, with several other phosphines found to be ineffective in forming similar complexes. **5.7** was then tested for its reactivity with a number of small molecules, but was only found to activate CD_2Cl_2 in an FLP-type manner. Interesting reactivity was seen with CO_2 and benzaldehyde, the latter of which formed a carboxylate bridged dimer, involving elimination of the pendent phosphine. Reactions with PhCCD, PhNCO, 3-pentanone, and

mesitaldehyde only resulted in the formation of an adduct, whereas no reactivity was seen with H_2 or C_2H_4 gases.

The catalytic dehydrocoupling of $Me_2NH{\cdot}BH_3$ was also performed using **5.7**, with a vast improvement in activity seen upon increasing the reaction temperature from 25 °C (7% yield after 114 h) to 60 °C (93% yield after 3 h). These results have led to the hypothesis that the phosphine moiety inhibits binding of the substrate at lower temperatures—therefore vastly decreasing the rate of reaction—and that by increasing the temperature the Mg–P bond becomes far more labile, consequently making the binding of $Me_2NH{\cdot}BH_3$ to the Mg centre far more favourable.

Insight into the reactivity of **5.7** (or lack thereof) could perhaps be obtained through computational studies, as it could be possible to ascertain the size of the HOMO-LUMO gap between the Lewis acid and Lewis base, and therefore whether the inability of **5.7** to activate certain molecules is simply the result of an insufficient energy potential, or due to something quite different.

Chapter 6

Future work

6.1 Development of Zr frustrated Lewis pairs

Chapters 2 and 3 of this thesis demonstrated that a range of nitrogen Lewis bases can match the reactivity of phosphines in a Zr frustrated Lewis pair (FLP) system, however the scope of Zr/N FLPs is still relatively unknown compared to their Zr/P counterparts. It would therefore be useful for any future investigations to make an attempt to correct this, with potential substrates for study including ketones, alkenes, and ethers, in addition to R–X (X = halogen) containing compounds (Scheme 6.1). All of these activations have been achieved by Zr/P FLPs,[8] so establishing whether the reactivity of Zr/N FLPs also stretches to these species would further help to define their limitations.

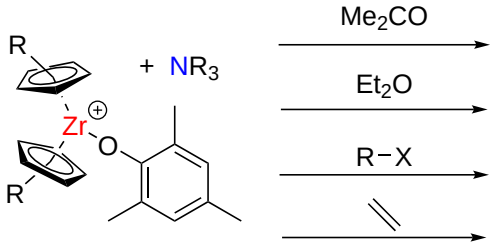

Scheme 6.1: Other possible small molecule activation reactions using intermolecular Zr/N FLPs.

These investigations should include both intra- and inter- molecular Zr/N FLPs, as although compound **1.50** (Figure 6.1) has been used for the activation of H_2, alkynes, and CH_2Cl_2, in addition to the hydrogenation of benzaldehyde and styrene,[51] it remains the only intramolecular Zr/N FLP to be studied so extensively, and the effects of varying every aspect of the FLP (including Zr ligands, -NR_2 groups, and alkoxide linker) remain very much unexplored. It would certainly be of interest to examine intramolecular Zr/N FLPs for amine-borane dehydrocoupling; their Zr/P counterparts were revealed to be highly effective for this reaction and so a comparison could prove very informative.[10] Moreover, the effectiveness of **1.50** for the hydrogenation of alkenes and alkynes means that the repetition of these experiments with intermolecular Zr/N FLPs would certainly be worth performing.

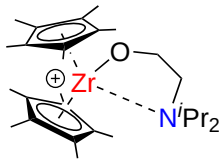

1.50

Figure 6.1: The intramolecular Zr/N FLP developed by Erker and co-workers.

6.2 Intermolecular magnesium FLPs

Despite the activation of benzaldehyde and the dehydrocoupling of $Me_2NH{\cdot}BH_3$ using the intermolecular Mg Lewis pairs in Chapter 4, the low Lewis acidity of the Mg complex **4.6** appears to be an issue for reactions with other substrates, with bound molecules not necessarily activated enough to allow for nucleophilic attack by a Lewis base. This issue could be alleviated through the use of cationic Mg diketiminate compounds, which have been reported by a few groups within the last few years with a view to performing

cooperative Lewis chemistry.[103,107,109,110] The right combination of ancillary ligand groups and Lewis base appearing to be needed for the desired reactivity to be achieved, with greater steric bulk around both Lewis pair moieties perhaps required. It remains to be seen whether the greater Lewis acidity afforded by a cationic Mg centre will result prove inhibitory for the release of products—as is seen with certain Zr FLP reactions—however, exploration of this topic is definitely worthwhile in order to establish overall reactivity, with it unlikely to be the case that no useful reactivity is discovered with these species (Figure 6.2).

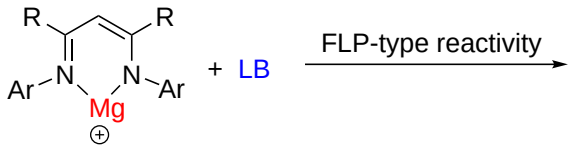

Figure 6.2: Possible future intermolecular Mg Lewis pair chemistry.

In terms of adding more directly to the chemistry reported in this thesis, extension of the reactions with amine-boranes could be useful for allowing greater comparison with other dehydrocoupling catalysts, both in terms of levels of activity, in addition to whether or not the same reaction products are seen. It would also be interesting to see whether the activation of benzaldehyde could be taken to the next stage, with hydrogenation (or different functionalisation) a possible route to a useful catalytic reaction.

It could perhaps also be worthwhile to attempt the same reactions using an analogous calcium species, as it is likely that at least some of the reactions with the herein reported substrates would result in different reactivity. Although the more ionic nature of calcium species may result in undesired reactivity, any differences are certainly worth investigation.

6.3 Intramolecular magnesium FLPs

Despite the intramolecular Mg/P Lewis pair **5.7** proving unable to perform the desired FLP type reactivity, the fact that the Mg–P bond was shown to be labile enough to allow for substrate insertion means that small molecule activation chemistry with similar species could be possible. The nature of the diketiminate ligand—in addition to the phosphine moiety—means that there are a number of potential modifications that could improve reactivity. Management of the steric and electronic environments at the Lewis acidic and basic centres is essential, with maximising the acidity of the Mg centre with electron-withdrawing groups one possibility, while reduction of the steric bulk at the phosphine perhaps required to more readily allow nucleophilic attack of any substrates (**6.1**, Figure 6.3). Replacing the phosphine with a different Lewis base, with carbenes (**6.2**) and amines (**6.3**) both potential alternatives.

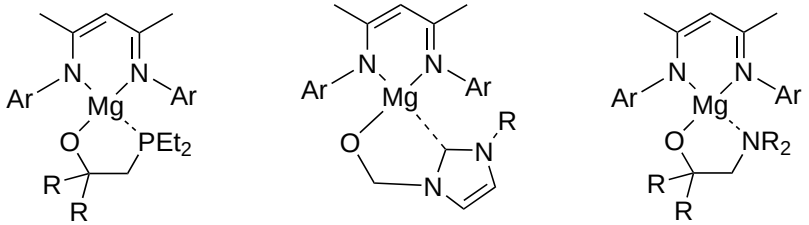

6.1 **6.2** **6.3**

Figure 6.3: Possible alternative Mg Lewis pairs for small molecule activation.

Incorporation of the Lewis basic moiety into the primary ligand is another possibility for exploration, with the general structure of compound **6.4** one way of achieving this (Figure 6.4). This ligand was used in a Sc/P Lewis pair system for the activation of methyl methacrylate and two of its cyclic analogues (Scheme 6.2),[172] and perhaps similar reactivity could be seen with a magnesium congener. By moving the phosphine onto the β-diketiminate ligand, an extra binding site for a different ligand is available. This could

pave the way for additional steric or electronic control of the reaction centre through bulky or electron-withdrawing groups, or it could be removed entirely to give a cationic species.

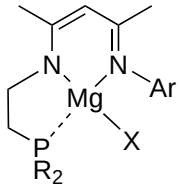

6.4

Figure 6.4: General structure of potential Mg complex for small molecule activation.

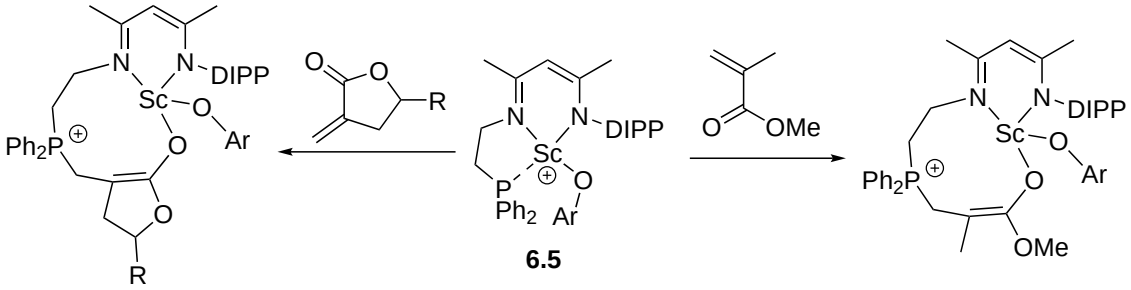

6.5

Scheme 6.2: Sc/P Lewis pair used for small molecule activation reactions.

Chapter 7

Experimental

7.1 General considerations

7.1.1 Experimental considerations

Unless otherwise stated, all manipulations were undertaken under an atmosphere of argon or nitrogen using standard glovebox (M. Braun O_2 <0.1 ppm, H_2O <0.1 ppm) and Schlenk line techniques. All glassware was dried in an oven at 200 °C overnight and cooled under vacuum prior to use. The compounds $[Cp_2ZrOMes][B(C_6F_5)_4]$, $[Cp^*_2ZrOMes][B(C_6F_5)_4]$,[25] **4.1**,[152] **4.3**,[173] **4.4**,[164] **4.5**,[152] **5.1**,[164] **5.2**,[165] **5.3**,[166] **5.4**,[166] and **5.8**[71] were synthesized following literature procedures. **5.5** and **5.6** were provided by Dr Andy Chapman, and **5.9** was provided by Dr Owen Metters. Triethylamine, *N*,*N*-diisopropylethylamine, pyridine, 2-methylpyridine, benzaldehyde, mesitaldehyde, 3-pentanone, and 2,6-dimethylpyridine were purchased from Sigma-Aldrich and distilled from CaH_2 prior to use. Triphenylphosphine, triethylphosphine, triethylsilane, triethylphosphine oxide, and tri-*tert*-butylphosphine were purchased from Sigma-Aldrich and used as received. 2,4,6-Trimethyphenol (MesOH) was purchased from Sigma-Aldrich and dried prior to use by stirring a hexane solution over CaH_2 before removal of the solvent in vacuo and sublimation (25 °C, 2 x 10^{-2} Torr). $Me_2NH{\cdot}BH_3$ was purchased from Sigma-Aldrich and purified by sublimation prior to use (25 °C, 2 10^{-2} Torr). Phenylacetylene-*d* was purchased from Sigma-Aldrich and purified by distillation before use. Reagent gases (D_2 and CO_2) were dried prior to using by passing through a -78 °C trap. Toluene, hexane, dichloromethane, and tetrahydrofuran were purified using a Grubbs type purification system. Chlorobenzene and pentane were purchased from Sigma-Aldrich and dried over 4 Å molecular sieves prior to use.

NMR spectra were recorded using Jeol ECS 300 (300 MHz), Bruker Nano 400 (400 MHz), Jeol ECS 400 (400 MHz), Varian VNMRS500 (500 MHz), and Bruker Avance III HD 500 Cryo (500 MHz) spectrometers. ^{15}N-HMBC NMR spectra are referenced to NH_3. Deuterated solvents were obtained from Sigma-Aldrich (benzene-d_6, dichloromethane-d_2, chlorobenzene-d_5, bromobenzene-d_5, and acetonitrile-d_3) and distilled from CaH_2 or dried

over 4 Å molecular sieves prior to use. Spectra of air-sensitive compounds were recorded using NMR tubes fitted with J. Young's valves. Spectra of boron-containing compounds were obtained using quartz NMR tubes fitted with J. Young's valves.

Mass spectrometry experiments were carried out by the University of Bristol Mass Spectrometry Service on a Bruker Daltronics MicrOTOF II with a TOF analyser or a Waters Synapt G2S with an IMS-Q-TOF analyser. All samples were run in pre-dried PhCl or CH_3CN.

7.1.2 Details of X-ray diffraction studies

All X-ray diffraction experiments were carried out by Dr. H. A. Sparkes and Dr. N. E. Pridmore, who are acknowledged for their input. X-ray diffraction experiments on **2.2c**, **2.2d**, **4.6**, **4.6c**, **4.6d**, **4.8**, **5.7**, **5.12**, and **5.13** were carried out at 100(2) K on a Bruker APEX II diffractometer using Mo-K_α radiation (λ = 0.71073 Å). Intensities were integrated in SAINT[174] and absorption corrections based on equivalent reflections were applied using SADABS.[175] Structure **2.2c** was solved using Superflip,[176,177] while **2.2d** was solved using ShelXT[178] all of the structures were refined by full matrix least squares against F^2 in ShelXL[179,180] using Olex2.[181] All of the non-hydrogen atoms were refined anisotropically. While all of the hydrogen atoms were located geometrically and refined using a riding model. In the case of **2.2c** the chlorobenzene was disordered over a symmetry element; the occupancies were fixed at 50%. In addition, Squeeze within Platon[182,183] was used to remove disordered solvent from the lattice of **2.2c** that could not be sensibly modelled. The largest residual peaks are in the vicinity of the modelled chlorobenzene and suggest that further disorder was present. Crystallographic data for compounds **2.2c** and **2.2d** have been deposited with the Cambridge Crystallographic Data Centre as supplementary publication CCDC 1898435-1898436. Copies of the data can be obtained free of charge on application to CCDC, 12 Union Road, Cambridge CB2 1EZ, UK [fax(+44) 1223 336033, e-mail: deposit@ccdc.cam.ac.uk].

7.2 Chapter 2 experimental

The majority of this experimental is taken from a first author publication of this work.[118]

7.2.1 Generation of FLPs

*$[Cp_2ZrOMes][B(C_6F_5)_4]$ // LB (**2.1a–e**)*

In a glovebox, **2.1** (30 mg, 0.029 mmol) was dissolved in bromobenzene-d_5 (0.5 mL) before the Lewis base (**a** = NEt_3 (4.1 μL, 0.029 mmol), **b** = $^iPr_2NEt$ (5.1 μL, 0.029 mmol), **c** = pyridine (2.4 μL, 0.029 mmol), **d** = 2-methylpyridine (2.9 μL, 0.029 mmol), **e** = 2,6-dimethylpyridine (3.4 μL, 0.029 mmol)) was added. A colour change (orange to yellow) was observed in each case. The FLP was then used *in situ* for reactions with substrates, without isolation.

2.1a. ^{1}H NMR (500 MHz, PhBr-d_5) δ 6.75 (2H, s, *m*-ArH), 6.10 (10H, s, Cp), 2.36 (6H, q, $^{3}J_{HH}$ = 7.2 Hz, N(CH_2CH$_3$)$_3$), 2.20 (3H, s, *p*-Ar-CH_3), 1.86 (6H, s, *o*-Ar-CH_3), 0.80 (9H, t, $^{3}J_{HH}$ = 7.2 Hz, N(CH$_2$CH_3)$_3$) ppm. ^{15}N-HMBC NMR (500 MHz, 51 MHz, PhBr-d_5) δ 163.5 (Zr-NEt$_3$) ppm. NB: NEt$_3$ δ = 47.6 ppm.

2.1b. ^{1}H NMR (500 MHz, PhBr-d_5) δ 6.75 (2H, s, *m*-ArH), 6.10 (10H, s, Cp), 2.90 (2H, *sept.*, $^{3}J_{HH}$ = 6.5 Hz, N(CH(CH$_3$)$_2$)$_2$), 2.37 (2H, q, $^{3}J_{HH}$ = 7.2 Hz, NCH_2CH$_3$), 2.19 (3H, s, *p*-Ar-CH_3), 1.86 (6H, s, *o*-Ar-CH_3), 1.04-0.58 (15H, br, CH_3CH$_2$N(CH(CH_3)$_2$)$_2$) ppm. ^{15}N-HMBC NMR (500 MHz, 51 MHz, PhBr-d_5) δ 185.5 (Zr-N(^{i}Pr)$_2$Et) ppm. NB: ^{i}Pr$_2$NEt δ = 57.5 ppm.

2.1c. ^{1}H NMR (500 MHz, PhBr-d_5) δ 8.19 (2H, m, *o*-PyH), 7.46 (1H, m, *m*-PyH), 7.10 (2H, m, *p*-PyH), 6.73 (2H, s, *m*-ArH), 5.97 (10H, s, Cp), 2.18 (3H, s, *p*-Ar-CH_3), 1.79 (6H, s, *o*-Ar-CH_3) ppm. ^{15}N-HMBC NMR (500 MHz, 51 MHz, PhBr-d_5) signal not seen for FLP (see Results and Discussion). NB: Pyridine δ = 318.9 ppm.

2.1d. ^{1}H NMR (500 MHz, PhBr-$\mathbf{d}_5$) δ 8.62 (1H, br, *o*-PyH), 7.96 (1H, m, *p*-PyH), 7.40 (2H, m, *m*-PyH), 6.74 (2H, s, *m*-ArH), 5.99 (10H, s, Cp), 2.18 (3H, s, *p*-Ar-CH_3), 2.11 (3H, br, *o*-Py-CH_3), 1.83 (6H, s, *o*-Ar-CH_3) ppm. ^{15}N-HMBC NMR (500 MHz, 51 MHz, PhBr-d_5) δ 302.1 (Zr-NC$_5$H$_4$CH$_3$) ppm. NB: 2-methylpyridine δ = 317.7 ppm.

2.1e. ^{1}H NMR (500 MHz, PhBr-d_5) δ 7.25 (1H, t, $^{3}J_{HH}$ = 7.7 Hz, *p*-PyH), 6.81 (2H, m, *m*-PyH), 6.71 (2H, s, *m*-ArH), 6.02 (10H, s, Cp), 2.27 (6H, s, *o*-Py-CH_3), 2.16 (3H, s, *p*-Ar-CH_3), 1.72 (6H, s, *o*-Ar-CH_3) ppm. ^{15}N-HMBC NMR (500 MHz, 51 MHz, PhBr-d_5) δ 249.8 (Zr-NC$_5$H$_3$(CH$_3$)$_2$) ppm. NB: 2,6-dimethylpyridine δ = 317.2 ppm.

[Cp$_2$ZrOMes][B(C$_6$F$_5$)$_4$] // LB (**2.2a–e**)*

In a glovebox, **2.2** (34.1 mg, 0.029 mmol) was dissolved in bromobenzene-d_5 (0.5 mL) before the Lewis base (**a** = NEt$_3$ (4.1 μL, 0.029 mmol), **b** = ^{i}Pr$_2$NEt (5.1 μL, 0.029 mmol), **c** = pyridine (2.4 μL, 0.029 mmol), **d** = 2-methylpyridine (2.9 μL, 0.029 mmol), **e** = 2,6-dimethylpyridine (3.4 μL, 0.029 mmol)) was added. A colour change (dark orange to red) was observed for **a**, **b** and **e**. The solution turned green upon addition of **c**, and slightly lightened in colour upon addition of **d**. The FLP was then used ztextitin situ for reactions with substrates, without isolation. However, crystals of **2.2c**, and **2.2d** suitable for X-ray crystallography were obtained by layering a PhCl solution of **2.2c**, and a PhBr-d_5 solution of **2.2d** with pentane.

2.2a. ^{1}H NMR (500 MHz, PhCl-d_5) δ 6.79 (2H, s, *m*-ArH), 2.37 (6H, q, $^{3}J_{HH}$ = 7.2 Hz, N(CH_2CH$_3$)$_3$), 2.20 (3H, s, *p*-Ar-CH_3), 1.73 (6H, s, *o*-Ar-CH_3), 1.64 (30H, s, Cp*), 0.82 (9H, t, $^{3}J_{HH}$ = 7.2 Hz, N(CH$_2$CH_3)$_3$) ppm. ^{15}N-HMBC NMR (500 MHz, 51 MHz, PhBr-d_5) δ 54.2 (Zr-NEt$_3$) ppm. NB: NEt$_3$ δ = 47.6 ppm.

2.2b. ^{1}H NMR (500 MHz, PhBr-d_5) δ 6.78 (2H, s, *m*-ArH), 2.91 (2H, *sept.*, $^{3}J_{HH}$ = 6.5 Hz, N(CH(CH$_3$)$_2$)$_2$), 2.37 (2H, q, $^{3}J_{HH}$ = 7.2 Hz, NCH_2CH$_3$), 2.20 (3H, s, *p*-Ar-CH_3), 1.73 (6H, s, *o*-Ar-CH_3), 1.64 (30H, s, Cp*), 1.05-0.63 (15H, br, CH_3CH$_2$N(CH(CH_3)$_2$)$_2$) ppm. ^{15}N-HMBC NMR (500 MHz, 51 MHz, PhBr-d_5) signal not seen for FLP (see Chapter 2).

2.2c. ^{1}H NMR (500 MHz, PhBr-d_5) δ 8.55 (1H, br, *o*-ArH), 8.38 (1H, br, *o*-ArH), 7.32 (1H, br, *p*-ArH), 7.07-6.97 (2H, m, *m*-ArH(Py)), 6.78 (1H, s, *m*-ArH(Mes)), 6.67 (1H, s, *m*-ArH(Mes)), 2.17 (3H, s, *p*-Ar-CH_3), 1.94 (3H, s, *o*-Ar-CH_3), 1.89 (3H, s, *o*-Ar-CH_3), 1.47 (30H, s, Cp*) ppm. ^{13}C NMR (125 MHz, PhBr-d_5) δ 156.4 (s, *i*-*C*), 151.7 (s, *o*-*C*H(Py)), 138.2 (s, *p*-*C*H(Py)), 130.7 and 130.2 (s, *m*-*C*H(Mes)), 126.5 (s,

o-*C*CH$_3$(Mes)), 125.8 (s, Cp*), 123.6 (s, *p*-*C*CH$_3$(Mes)), 21.7 and 20.4 (s, *o*-*C*H$_3$), 19.42 (s, *p*-*C*H$_3$), 11.5 (s, Cp*-Me) ppm. Remaining peaks obscured by PhBr-d_5 solvent. ^{15}N-HMBC NMR (500 MHz, 51 MHz, PhBr-d_5) δ 260.5 (Zr-Py) ppm. NB: Pyridine δ = 318.9 ppm. ESI-MS (+ve detection) 574.2645 *m/z*.

2.2d. ^{1}H NMR (500 MHz, PhBr-d_5) δ 7.94 (1H, br, *o*-Ar*H*), 7.41 (1H, m, *p*-Ar*H*), 7.16-7.12 (2H, m, *m*-Ar*H*(Py)), 6.73 and 6.71 (2H, s, *m*-Ar*H*(Mes)), 2.20 (3H, s, *o*-Ar-C*H*$_3$(Py)), 2.16 (3H, s, *p*-Ar-C*H*$_3$), 1.99 (3H, s, *o*-Ar-C*H*$_3$(Mes)), 1.78 (3H, s, *o*-Ar-C*H*$_3$(Mes)), 1.51 (30H, s, Cp*) ppm. ^{13}C NMR (125 MHz, PhBr-d_5) δ 155.8 (s, *o*-*C*CH$_3$(Py)), 148.4 (s, *o*-*C*H(Py)), 134.2 (s, *p*-*C*H(Py)), 128.6 (s, Cp*), 26.1 (s, *o*-*C*H$_3$(Py)), 20.8 and 20.4 (s, *o*-*C*H$_3$(Mes)), 19.3 (s, *p*-*C*H$_3$), 12.0 (s, Cp*-Me) ppm. Remaining peaks obscured by PhBr-d_5 solvent. ^{15}N-HMBC NMR (500 MHz, 51 MHz, PhBr-d_5) δ 261.1 (Zr-*N*C$_5$H$_4$(CH$_3$)) ppm. NB: 2-methylpyridine δ = 317.7 ppm.

2.2e. ^{1}H NMR (500 MHz, PhBr-d_5) δ 7.23 (1H, t, $^3J_{HH}$ = 7.8 Hz, *p*-Py*H*), 6.79 (2H, s, *m*-Ar*H*), 6.72 (2H, m, *m*-Py*H*), 2.30 (6H, s, *o*-Py-C*H*$_3$), 2.20 (3H, s, *p*-Ar-C*H*$_3$), 1.73 (6H, s, *o*-Ar-C*H*$_3$), 1.63 (30H, s, Cp*) ppm. ^{15}N-HMBC NMR (500 MHz, 51 MHz, PhBr-d_5) δ 286.0 (Zr-*N*C$_5$H$_3$(CH$_3$)$_2$) ppm. NB: 2,6-dimethylpyridine δ = 317.2 ppm.

7.2.2 DOSY studies of 2.1a–e and 2.2a–e

Samples of **2.1a–e** and **2.2a–e** and separate control samples of **a–e** were made as detailed above. ^{1}H DOSY NMR spectroscopy were carried out using 15 increments and a diffusion delay of 100 ms. All data were analysed using MestReNova.

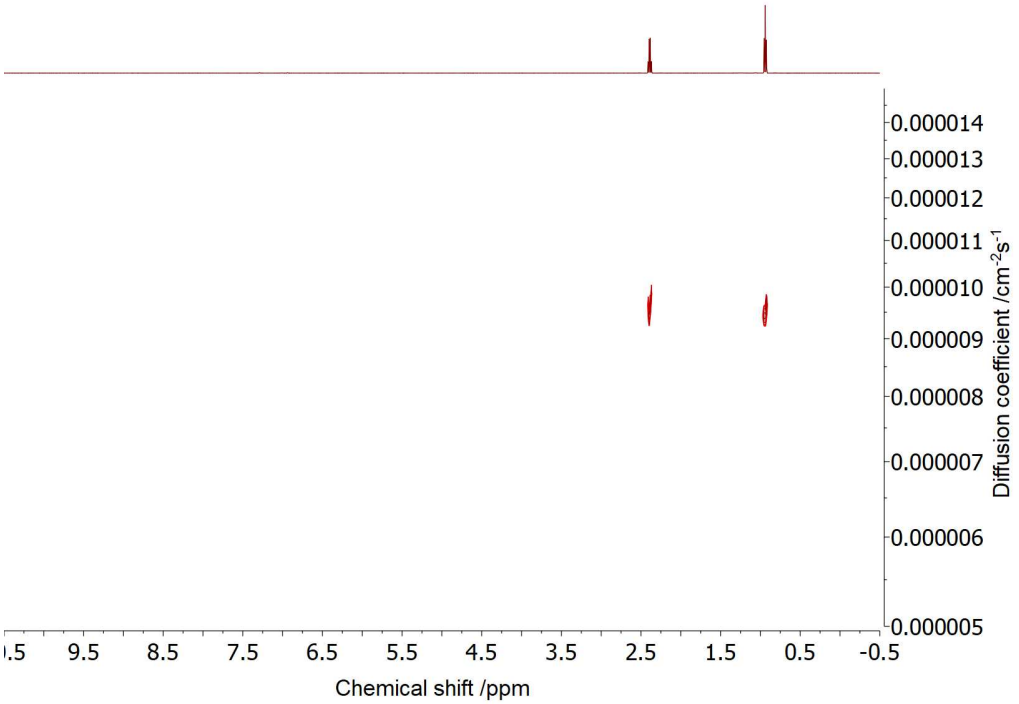

Figure 7.1: ^{1}H (500 MHz, 25 °C, PhBr-d_5) DOSY NMR spectrum of triethylamine.

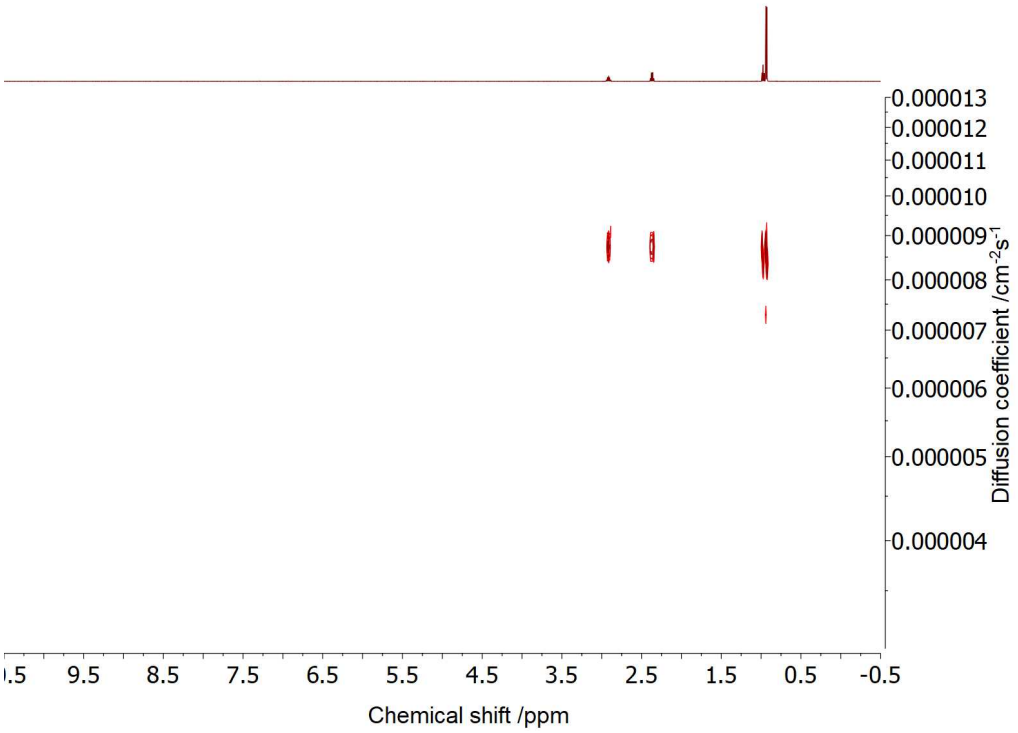

Figure 7.2: ^{1}H (500 MHz, 25 °C, PhBr-d_5) DOSY NMR spectrum of *N*,*N*-diisopropylethylamine.

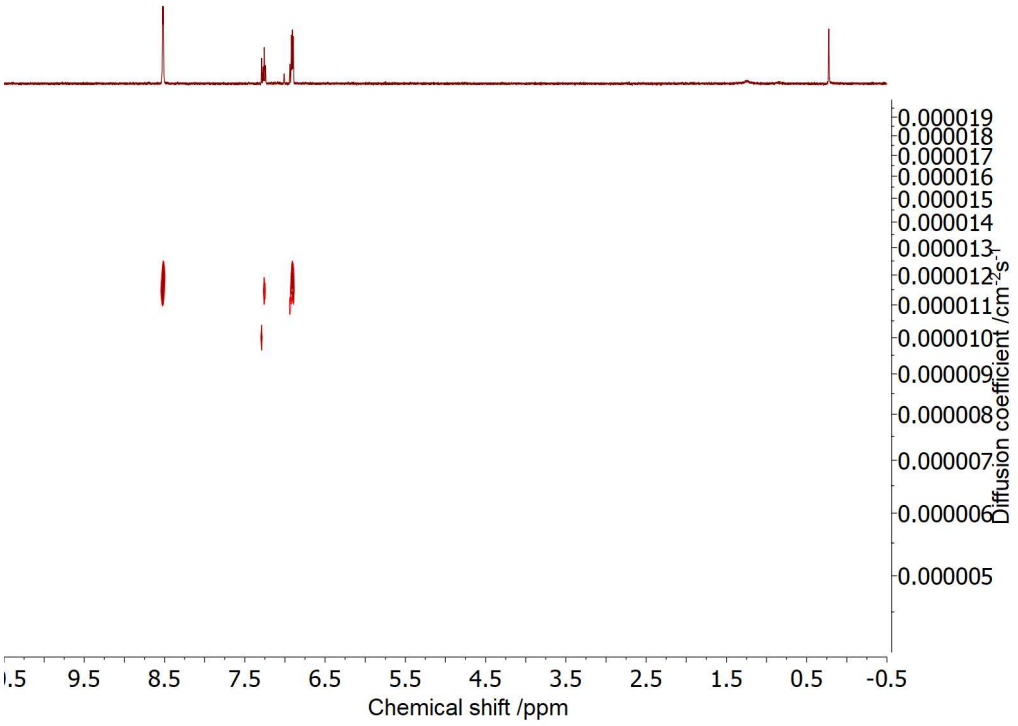

Figure 7.3: ^{1}H (500 MHz, 25 °C, PhBr-d_5) DOSY NMR spectrum of pyridine.

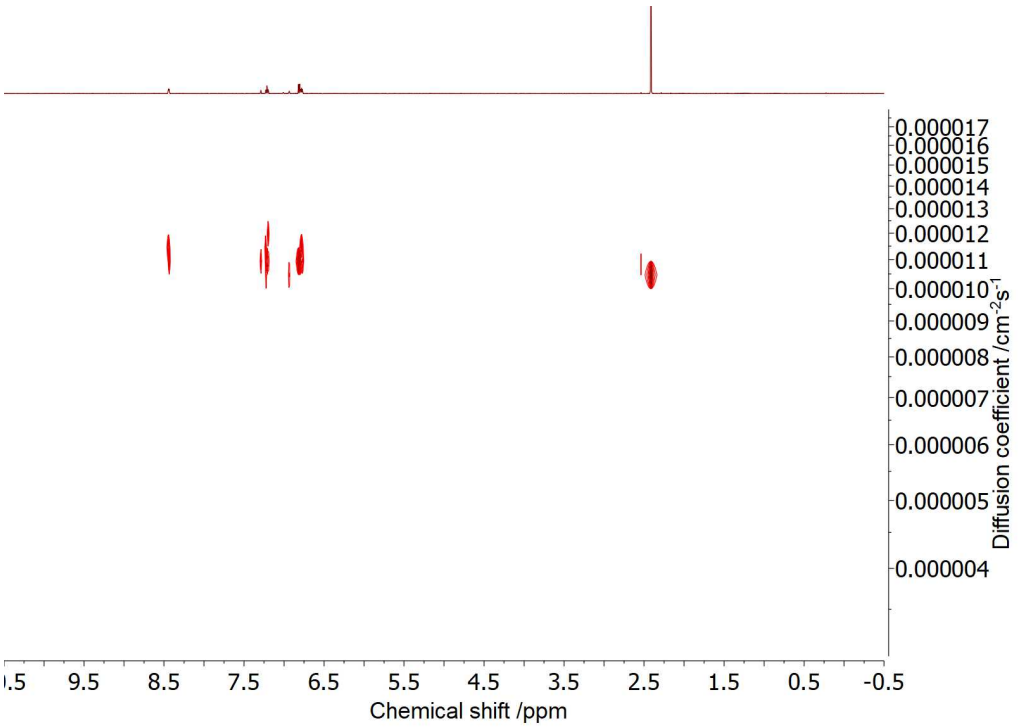

Figure 7.4: ^{1}H (500 MHz, 25 °C, PhBr-d_5) DOSY NMR spectrum of 2-methylpyridine.

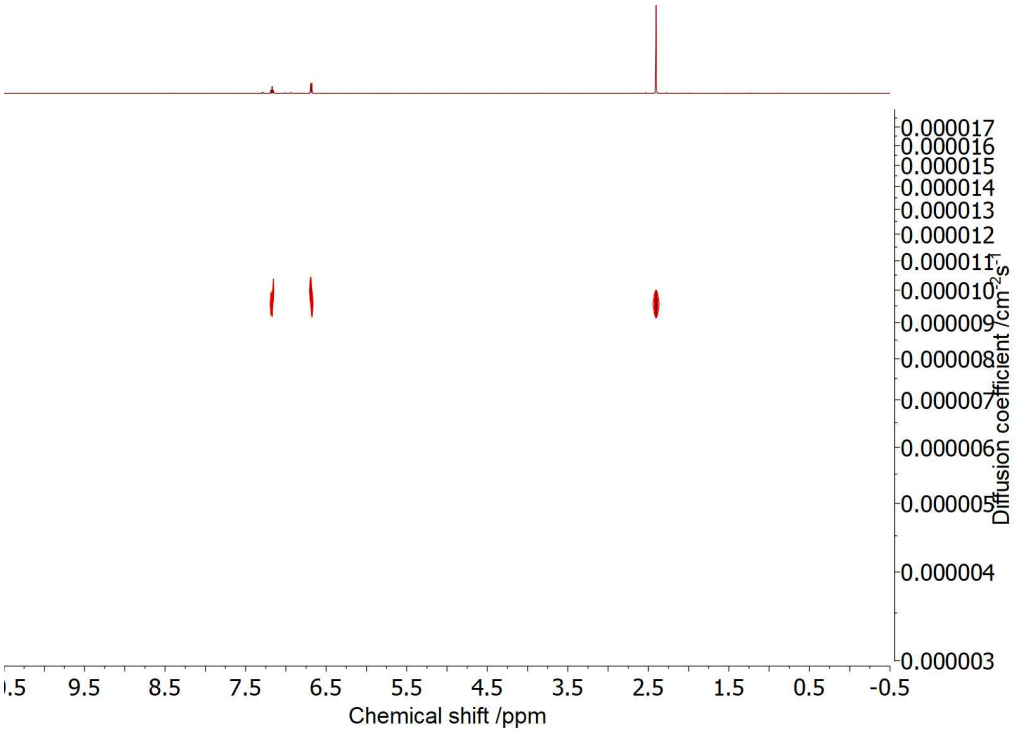

Figure 7.5: ^{1}H (500 MHz, 25 °C, PhBr-d_5) DOSY NMR spectrum of 2,6-dimethylpyridine.

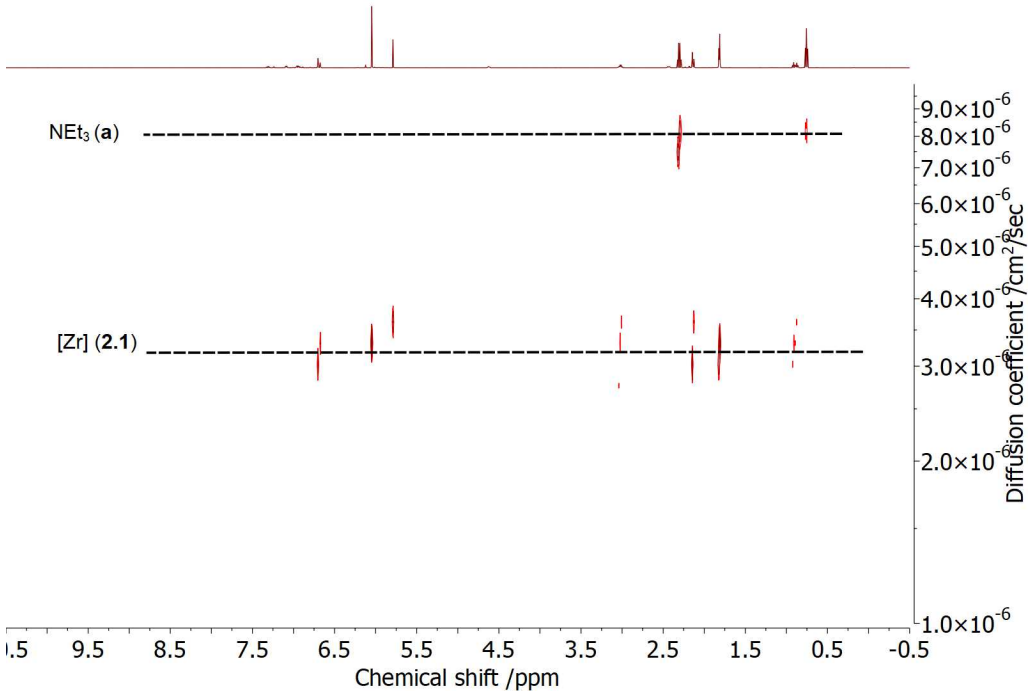

Figure 7.6: ^{1}H (500 MHz, 25 °C, PhBr-d_5) DOSY NMR spectrum of **2.1a**.

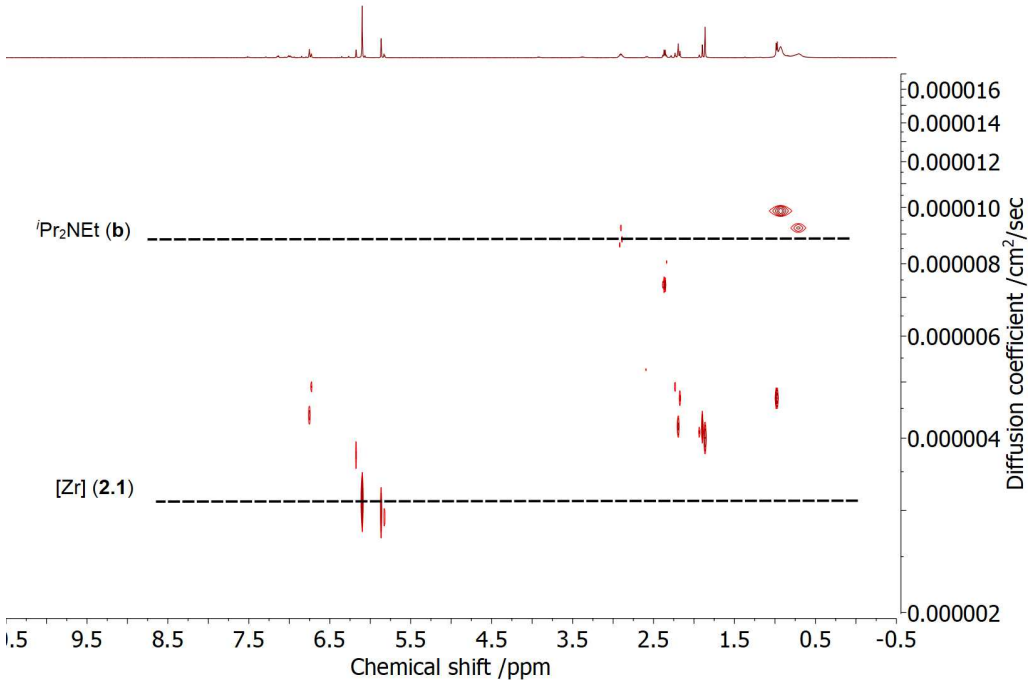

Figure 7.7: ^{1}H (500 MHz, 25 °C, PhBr-d_5) DOSY NMR spectrum of **2.1b**.

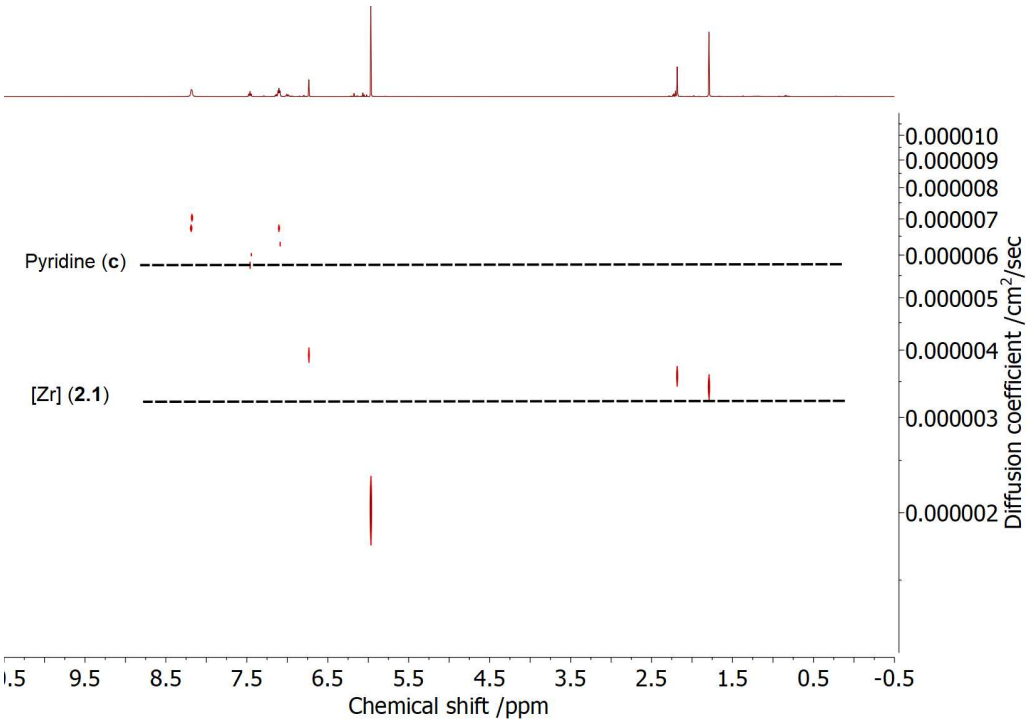

Figure 7.8: ^{1}H (500 MHz, 25 °C, PhBr-d_5) DOSY NMR spectrum of **2.1c**.

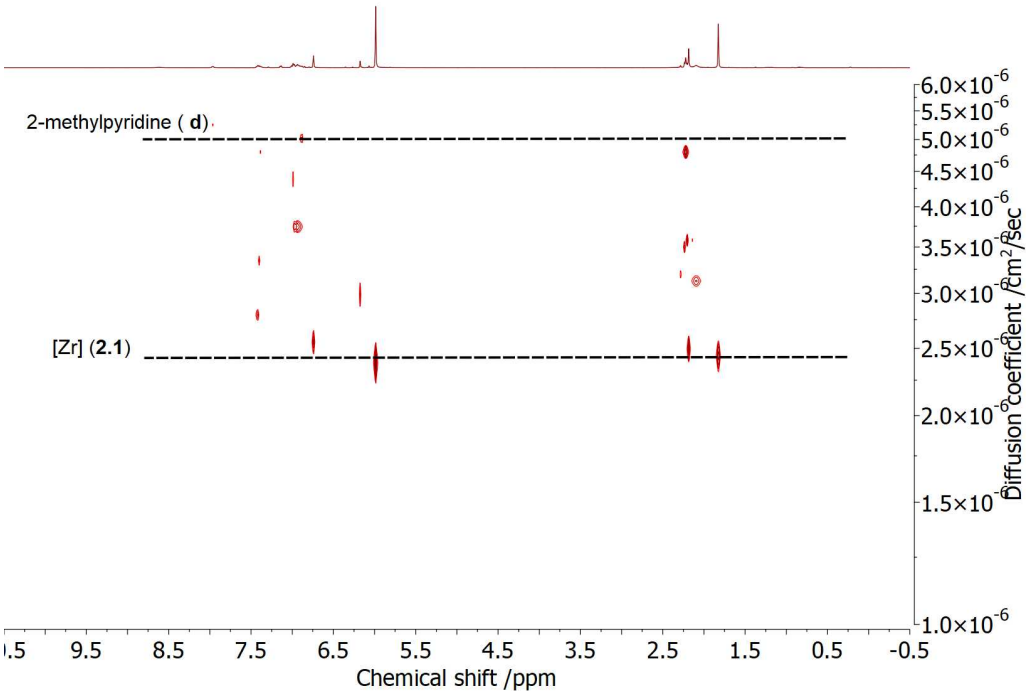

Figure 7.9: ^{1}H (500 MHz, 25 °C, PhBr-d_5) DOSY NMR spectrum of **2.1d**.

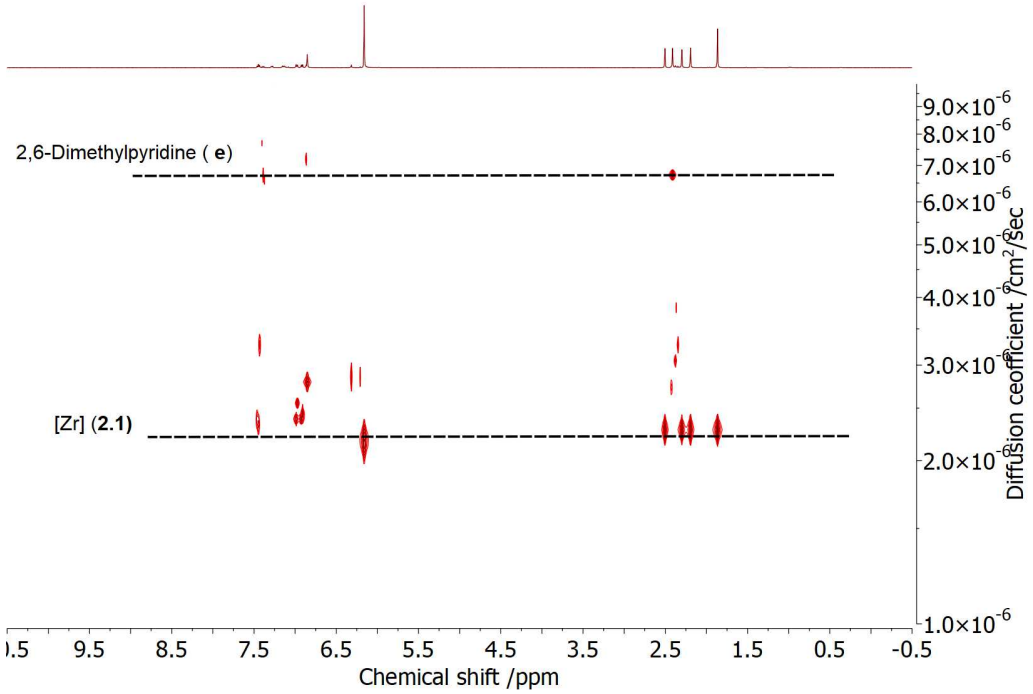

Figure 7.10: ^{1}H (500 MHz, 25 °C, PhBr-d_5) DOSY NMR spectrum of **2.1e**.

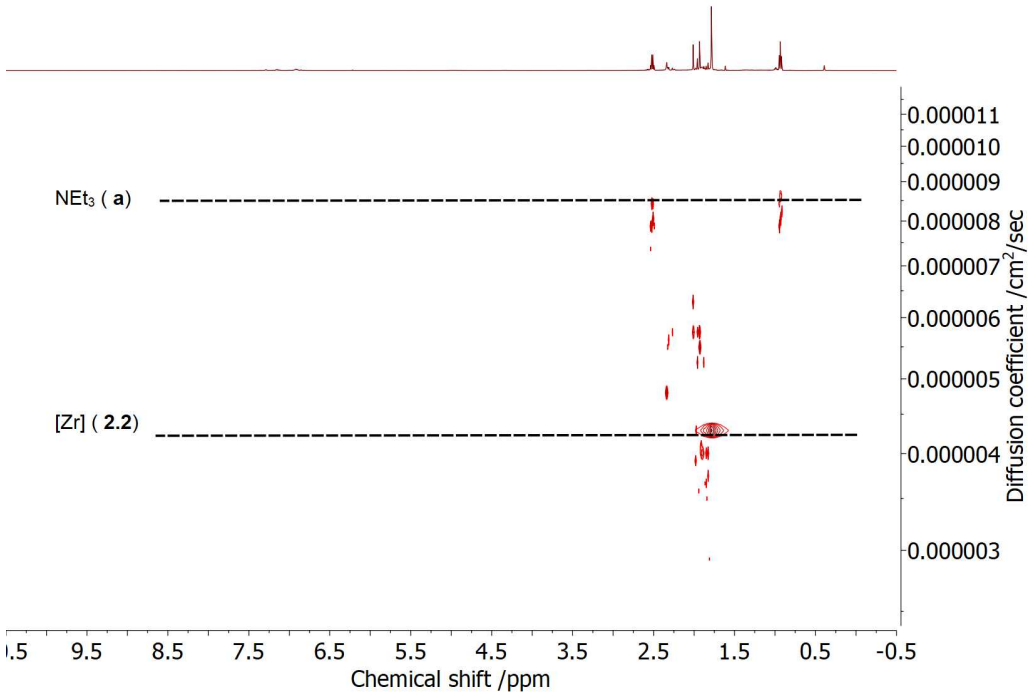

Figure 7.11: ^{1}H (500 MHz, 25 °C, PhBr-d_5) DOSY NMR spectrum of **2.2a**.

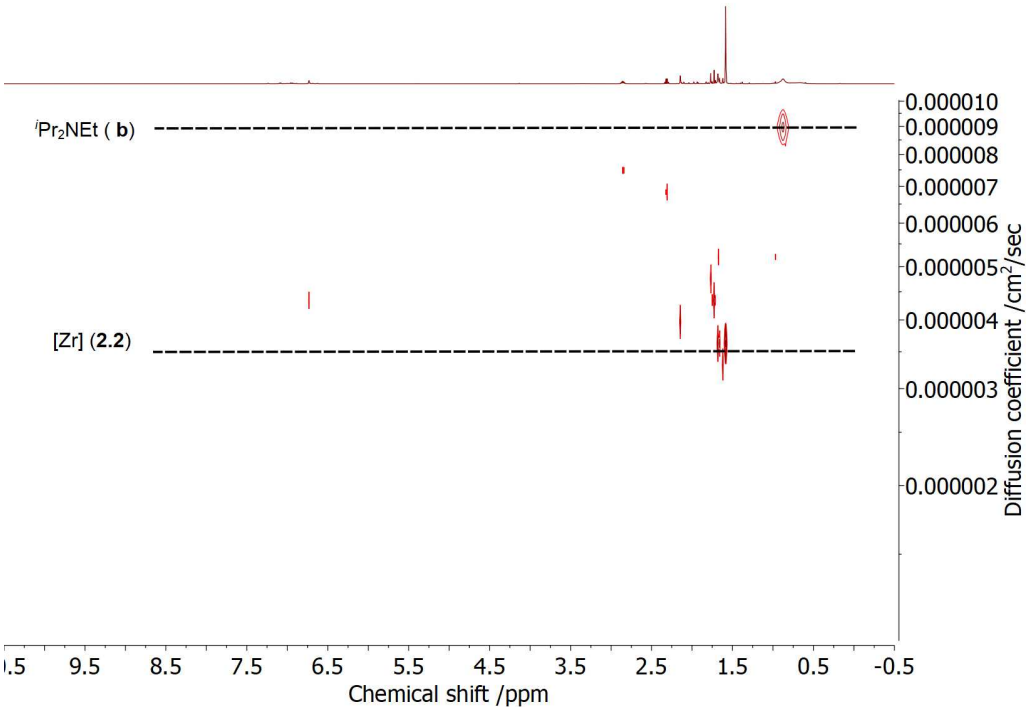

Figure 7.12: ^{1}H (500 MHz, 25 °C, PhBr-d_5) DOSY NMR spectrum of **2.2b**.

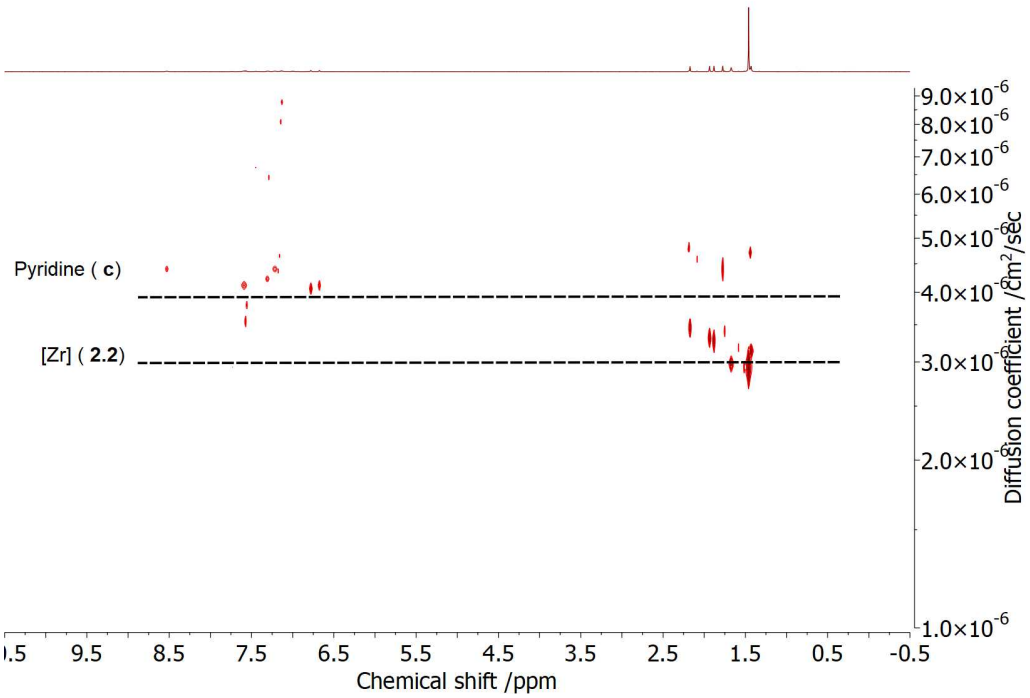

Figure 7.13: ^{1}H (500 MHz, 25 °C, PhBr-d_5) DOSY NMR spectrum of **2.2c**.

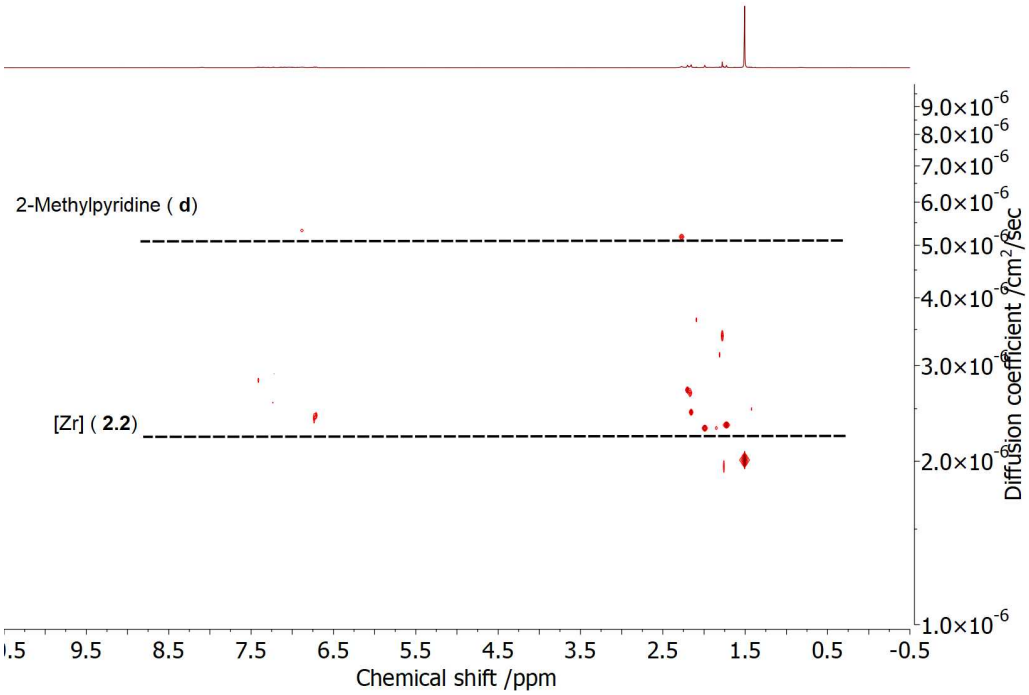

Figure 7.14: ^{1}H (500 MHz, 25 °C, PhBr-d_5) DOSY NMR spectrum of **2.2d**.

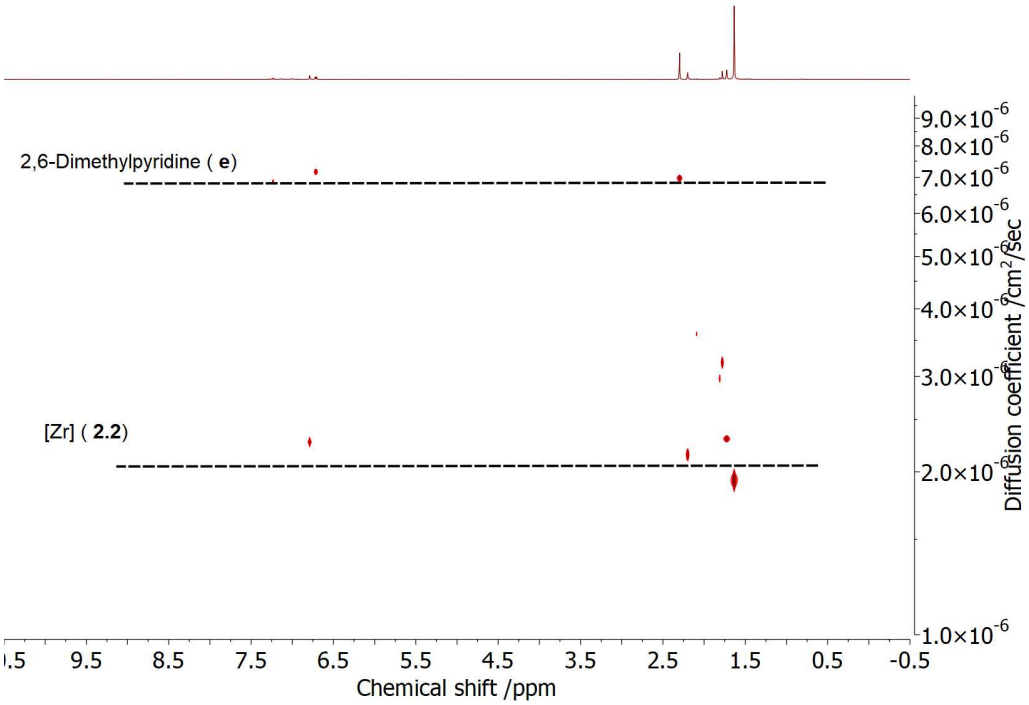

Figure 7.15: ^{1}H (500 MHz, 25 °C, PhBr-d_5) DOSY NMR spectrum of **2.2e**.

7.2.3 Reactions of Pairs with D_2

*Reactivity of [$Cp_2ZrOMes$][$B(C_6F_5)_4$] // LB (**2.1a–e**)*

In a glovebox, **2.1** (30 mg, 0.029 mmol) was dissolved in PhCl (0.5 mL) in an NMR tube fitted with a J. Young's valve, before C_6D_6 (one drop) was added to act as a reference in ^{2}H NMR spectra. An equimolar amount of the Lewis base (**a** = NEt_3 (4.1 μL, 0.029 mmol), **b** = $^iPr_2NEt$ (5.1 μL, 0.029 mmol), **c** = pyridine (2.4 μL, 0.029 mmol), **d** = 2-methylpyridine (2.9 μL, 0.029 mmol), **e** = 2,6-dimethylpyridine (3.4 μL, 0.029 mmol)) was then added. Outside of the glovebox, the sample was degassed twice via freeze-pump-thaw, before being refilled with D_2 gas (1 bar). In all cases, no change in the NMR spectra was seen.

*Reactivity of [$Cp^*_2ZrOMes$][$B(C_6F_5)_4$] // LB (**2.2a–e**)*

In a glovebox, **2.2** (34.1 mg, 0.029 mmol) was dissolved in PhCl (0.5 mL) in an NMR tube fitted with a J. Young's valve, before C_6D_6 (one drop) was added to act as a reference in ^{2}H NMR spectra. An equimolar amount of the Lewis base (**a** = NEt_3 (4.1 μL, 0.029 mmol), **b** = $^iPr_2NEt$ (5.1 μL, 0.029 mmol), **c** = pyridine (2.4 μL, 0.029 mmol), **d** = 2-methylpyridine (2.9 μL, 0.029 mmol), **e** = 2,6-dimethylpyridine (3.4 μL, 0.029 mmol)) was then added. Outside of the glovebox, the sample was degassed twice via freeze-pump-thaw, before being refilled with D_2 gas (1 bar). A colour change from red to yellow was seen for **2.2a**, **2.2b**, and **2.2e**. Collected spectral data are detailed below:

2.2a + D_2. ^{2}H NMR (77 MHz, PhCl/C_6D_6) δ 6.06 (s, Zr-D) ppm.

2.2b + D_2. ^{2}H NMR (77 MHz, PhCl/C_6D_6) δ 6.06 (s, Zr-D) ppm.

2.2e + D_2. ^{2}H NMR (77 MHz, PhCl/C_6D_6) δ 12.4 (br, N-D), 6.06 (s, Zr-D) ppm.

7.2.4 Reactions of pairs with CO_2

*Reactivity of [$Cp_2ZrOMes$][$B(C_6F_5)_4$] // LB (**2.1a–e**)*

In a glovebox, **2.1** (30 mg, 0.029 mmol) was dissolved in PhBr-d_5 (0.5 mL) in an NMR tube fitted with a J. Young's valve. An equimolar amount of the Lewis base (**a** = NEt_3 (4.1 μL, 0.029 mmol), **b** = $^iPr_2NEt$ (5.1 μL, 0.029 mmol), **c** = pyridine (2.4 μL, 0.029 mmol), **d** = 2-methylpyridine (2.9 μL, 0.029 mmol), **e** = 2,6-dimethylpyridine (3.4 μL, 0.029 mmol)) was then added. Outside of the glovebox, the sample was degassed twice via freeze-pump-thaw, before being refilled with CO_2 gas (1 bar) via a -78 °C trap. **2.1a**, **2.1b**, and **2.1d** showed a lightening in colour, whereas **2.1e** showed no clear colour change. Isolation of any products was attempted but not possible, and so all spectral data were obtained *in situ*. **2.1c** did not react.

2.1a + CO_2. ^{1}H NMR (500 MHz, PhBr-d_5) δ 6.85 (2H, s, m-ArH), 6.17 (10H, s, Cp), 2.37 (6H, q, N(CH_2CH_3)$_3$), 2.28 (3H, s, p-Ar-CH_3), 2.23 (6H, s, o-Ar-CH_3), 0.80 (9H, t,

$N(CH_2CH_3)_3$) ppm. ^{13}C NMR (125 MHz, PhBr-d_5) δ 165.3 (s, *C*(O)=O), 161.8 (s, *i-C*), 128.6 (s, *o-C*), 126.5 (s, *m-C*), 124.6 (s, *p-C*), 112.9 (s, Cp), 47.0 (s, $N(CH_2CH_3)_3$), 20.9 (s, *p*-CH_3), 18.6 (s, *o*-CH_3), 10.5 (s, $N(CH_2CH_3)_3$) ppm. ^{15}N-HMBC NMR (500 MHz, 51 MHz, PhBr-d_5) δ 446.0 (Zr-CO_2-*N*Et_3) ppm.

2.1b + CO_2. ^{1}H NMR (500 MHz, PhBr-d_5) δ 6.85 (2H, s, *m*-Ar*H*), 6.17 (10H, s, Cp), 2.92 (2H, *sept.*, $N(CH(CH_3)_2)_2$), 2.38 (2H, q, NCH_2CH_3), 2.28 (3H, s, *p*-Ar-CH_3), 2.23 (6H, s, *o*-Ar-CH_3), 1.00-0.65 (15H, br, $CH_3CH_2N(CH(CH_3)_2)_2$) ppm. ^{13}C NMR (125 MHz, PhBr-d_5) δ 168.2 (s, *C*(O)=O), 161.8 (s, *i-C*), 128.6 (s, *o-C*), 126.5 (s, *m-C*), 124.7 (s, *p-C*), 112.9 (s, Cp), 56.0 (s, $N(CH(CH_3)_2)_2$), 43.4 (s, NCH_2CH_3), 21.0 (s, $N(CH(CH_3)_2)_2$), 20.7 (s, *p*-CH_3), 18.7 (s, *o*-CH_3), 16.6 (s, NCH_2CH_3) ppm. ^{15}N-HMBC NMR (500 MHz, 51 MHz, PhBr-d_5) δ 446.5 (Zr-CO_2-*N*(^{i}Pr)$_2$Et) ppm.

2.1d + CO_2. ^{1}H NMR (500 MHz, PhBr-d_5) δ 8.62 (1H, br, *o*-Py*H*), 7.82 (1H, m, *p*-Py*H*), 7.44 (2H, m, *m*-Py*H*), 6.85 (2H, s, *m*-Ar*H*), 6.17 (10H, s, Cp), 2.28 (3H, s, *p*-Ar-CH_3), 2.17 (6H, s, *o*-Ar-CH_3), 2.10 (3H, br, *o*-Py-CH_3) ppm. ^{13}C NMR (125 MHz, PhBr-d_5) δ 161.6 (s, *C*(O)=O), 160.9 (s, *i-C*), 155.0 (s, *o-C*CH_3(Py)), 142.5 (s, *o-C*H(Py)), 134.0 (s, *p-C*(Py)), 128.4 (s, *o-C*(Mes)), 126.3 (s, *m-C*(Mes)), 124.7 (s, *p-C*(Mes)), 124.4 (s, *m-C*(Py)), 123.0 (s, *m-C*(Py)), 112.7 (s, Cp), 25.4 (s, *o-C*H_3(Py)), 20.6 (s, *p-C*H_3), 18.4 (s, *o-C*H_3(Mes)) ppm. ^{15}N-HMBC NMR (500 MHz, 51 MHz, PhBr-d_5) δ 450.1 (Zr-CO_2-*N*$C_5H_4CH_3$) ppm.

2.1e + CO_2. ^{1}H NMR (500 MHz, PhBr-d_5) δ 7.33 (1H, t, $^3J_{HH}$ = 7.7 Hz, *p*-Py*H*), 6.79 (2H, m, *m*-Py*H*), 6.74 (2H, s, *m*-Ar*H*), 6.14 (10H, s, Cp), 2.37 (3H, s, *p*-Ar-CH_3), 2.15 (6H, s, *o*-Ar-CH_3) 2.12 (6H, s, *o*-Py-CH_3), ppm. ^{13}C NMR (125 MHz, PhBr-d_5) δ 160.9 (s, *C*(O)=O), 160.5 (s, *i-C*), 155.4 (s, *o-C*(Py)), 140.0 (s, *p-C*(Py)), 128.6 (s, *o-C*(Mes)), 126.5 (s, *m-C*(Mes)), 124.7 (s, *p-C*(Mes)), 115.6 (s, Cp), 34.2 (s, *o-C*H_3(Py)), 21.6 (s, *p-C*H_3), 17.7 (s, *o-C*H_3(Mes)) ppm. Remaining peaks obscured by PhBr-d_5 solvent. ^{15}N-HMBC NMR (500 MHz, 51 MHz, PhBr-d_5) δ 464.0 (Zr-CO_2-*N*$C_5H_3(CH_3)_2$) ppm.

Reactivity of [Cp$_2$ZrOMes][B(C$_6$F$_5$)$_4$] // LB (**2.2a–e**)*

In a glovebox, **2.2** (34.1 mg, 0.029 mmol) was dissolved in PhBr-d_5 (0.5 mL) in an NMR tube fitted with a J. Young's valve. An equimolar amount of the Lewis base (**a** = NEt_3 (4.1 μL, 0.029 mmol), **b** = ^{i}Pr$_2$NEt (5.1 μL, 0.029 mmol), **c** = pyridine (2.4 μL, 0.029 mmol), **d** = 2-methylpyridine (2.9 μL, 0.029 mmol), **e** = 2,6-dimethylpyridine (3.4 μL, 0.029 mmol)) was then added. Outside of the glovebox, the sample was degassed twice via freeze-pump-thaw, before being refilled with CO_2 gas (1 bar) via a -78 °C. A colour change from to yellow was seen for **2.2a**, **2.2b**, **2.2d**, and **2.2e**. Isolation of any products was attempted but not possible, and so all spectral data were obtained in situ. **2.2c** did not react.

2.2a + CO_2. ^{1}H NMR (500 MHz, PhBr-d_5) δ 6.71 (2H, s, *m*-Ar*H*), 2.33 (6H, q, $N(CH_2CH_3)_3$), 2.15 (3H, s, *p*-Ar-CH_3), 1.94 (6H, s, *o*-Ar-CH_3), 1.83 (30H, s, Cp*), 0.75 (9H, t, $N(CH_2CH_3)_3$) ppm. ^{13}C NMR (125 MHz, PhCl) δ 162.7 (s, *C*(O)=O), 156.7 (s, *i-C*), 124.6 (s, *o-C*), 123.2 (s, *p-C*), 121.7 (s, Cp*), 46.9 (s, $N(CH_2CH_3)_3$), 20.3 (s, *p-C*H_3), 16.9 (s, *o-C*H_3), 10.9 (s, $N(CH_2CH_3)_3$), 9.4 (s, Cp*) ppm. ^{15}N-HMBC NMR (500 MHz, 51 MHz, PhBr-d_5) δ 343.3 (Zr-CO_2-*N*Et_3) ppm.

2.2b + CO_2. ^{1}H NMR (500 MHz, PhBr-d_5) δ 6.80 (2H, s, *m*-Ar*H*), 2.91 (2H, br, $N(CH(CH_3)_2)_2$), 2.38 (2H, q, $^3J_{HH}$ = 7.2 Hz, NCH_2CH_3), 2.16 (3H, s, *p*-Ar-CH_3), 1.90 (6H, s, *o*-Ar-CH_3), 1.83 (30H, s, Cp*), 1.00-0.74 (15H, br, $CH_3CH_2N(CH(CH_3)_2)_2$) ppm.

^{13}C NMR (125 MHz, PhBr-d_5) δ 161.4 (s, C(O)=O), 155.9 (s, *i*-C), 124.7 (s, *o*-C), 123.1 (s, *p*-C), 56.1 (s, N(CH(CH$_3$)$_2$)$_2$), 43.5 (s, NCH$_2$CH$_3$), 21.1 (s, N(CH(CH_3)$_2$)$_2$), 22.6 (s, *p*-CH$_3$), 18.4 (s, *o*-CH$_3$), 16.7 (s, NCH$_2$$CH_3$), 11.3 (s, Cp*) ppm. Remaining NMR peaks obscured by solvent. ^{15}N-HMBC NMR (500 MHz, 51 MHz, PhBr-d_5) signal not seen (see Chapter 2).

2.2d + CO_2. ^{1}H NMR (500 MHz, PhBr-d_5) δ 7.65 (1H, m, *p*-PyH), 7.47 (1H, m, *m*-PyH), 6.97-6.90 (2H, m, Py), 6.52 (2H, s, *m*-ArH), 6.17 (10H, s, Cp), 2.22 (3H, s, *p*-Ar-CH_3), 2.16 (3H, br, *o*-Py-CH_3), 1.88 (30H, s, Cp*), 1.75 (6H, s, *o*-Ar-CH_3), ppm. ^{15}N-HMBC NMR (500 MHz, 51 MHz, PhBr-d_5) δ 438.1 (Zr-CO$_2$-NC$_5$H$_4$CH$_3$) ppm.

2.2e + CO_2. ^{1}H NMR (500 MHz, PhBr-d_5) δ 7.30 (1H, t, $^3J_{HH}$ = 7.8 Hz, *p*-PyH), 6.80 (2H, s, *m*-ArH), 6.74 (2H, m, *m*-PyH), 2.18 (6H, s, *o*-Py-CH$_3$), 1.89 (3H, s, *p*-Ar-CH_3), 1.81 (30H, s, Cp*), 1.76 (6H, s, *o*-Ar-CH_3) ppm. ^{15}N-HMBC NMR (500 MHz, 51 MHz, PhBr-d_5) δ 466.1 (Zr-CO$_2$-NC$_5$H$_3$(CH$_3$)$_2$) ppm.

7.2.5 Reactions of pairs with tetrahydrofuran (THF)

*Reactivity of [Cp$_2$ZrOMes][B(C$_6$F$_5$)$_4$] // LB (**2.1a–e**)*

In a glovebox, **2.1** (30 mg, 0.029 mmol) was dissolved in PhBr-d_5 (0.5 mL) in an NMR tube fitted with a J. Young's valve. An equimolar amount of the Lewis base (**a** = NEt$_3$ (4.1 μL, 0.029 mmol), **b** = ^{i}Pr$_2$NEt (5.1 μL, 0.029 mmol), **c** = pyridine (2.4 μL, 0.029 mmol), **d** = 2-methylpyridine (2.9 μL, 0.029 mmol), **e** = 2,6-dimethylpyridine (3.4 μL, 0.029 mmol)) was then added. Tetrahydrofuran (THF, 2.4 μL, 0.029 mmol) was then added, with **2.1a**, **2.1b**, **2.1d**, and **2.1e** all forming yellow solutions (already yellow solutions darkened slightly). **2.1a** was left to react at room temperature for 24 h, all other reactions were heated to 80 °C for 3 days. Where sufficient quantities of product were present, the sample was precipitated out into stirring hexane, before being washed twice with hexane (2 × 1 mL) and once with pentane (1 mL) before being dried *in vacuo*.

2.1a + *THF*. Yield = 28.9 mg, 82%. ^{1}H NMR (400 MHz, PhBr-d_5): δ 6.80 (2H, s, ArH), 6.07 (10H, s, Cp), 3.90 (2H, m, α-CH_2), 2.50 (2H, m, δ-CH_2), 2.43 (6H, q, $^3J_{HH}$ = 7 Hz, N(CH_2CH$_3$)$_3$), 2.22 (3H, s, *p*-CH_3), 2.12 (6H, s, *o*-CH_3), 1.31 (4H, m, β-CH_2 and γ-CH_2), 0.68 (9H, m, N(CH$_2$CH_3)$_3$) ppm. ^{13}C NMR (125 MHz, PhBr-d_5): δ 161.0 (s, *i*-C), 127.4 (s, *o*-C), 124.6 (s, *p*-C), 112.8 (s, Cp), 71.9 (s, α-CH$_2$), 48.1 (s, β-CH_2), 30.5 (s, γ-CH_2), 20.8 (s, *p*-CH$_3$), 18.5 (s, δ-CH$_2$), 17.9 (s, *o*-CH$_3$), 11.8 (s, N(CH$_2$CH$_3$)), 6.73 (s, N(CH$_2$$CH_3$)) ppm. Remaining peaks obscured by PhBr-d_5 solvent. ^{15}N-HMBC NMR (500 MHz, 51 MHz, PhBr-d_5): δ 337.5 (-CH$_2$$NEt_3$) ppm. ESI-MS (+ve detection) 528.2422 *m/z* [M]$^+$, 174.1930 *m/z* [HO(C$_4$H$_8$)NEt$_3$]$^+$.

2.1b + *THF*. Yield = 17% (by ^{1}H NMR). Not enough product to isolate. ^{15}N-HMBC (500 MHz, 51 MHz, PhBr-d_5): δ 315.8 ppm. ESI-MS (+ve detection) 556.2742 *m/z* [M]$^+$, 202.2217 *m/z* [HO(C$_4$H$_8$)N(^{i}Pr)$_2$Et]$^+$.

2.1d + *THF*. Yield = 15.8 mg, 45%. ^{1}H NMR (400 MHz, PhBr-d_5): δ 7.65 (1H, m, *o*-ArH), 7.50-7.39 (1H, m, *p*-ArH), 6.99-6.86 (2H, m, *m*-ArH(Py)), 6.80 (2H, s, ArH(Mes)), 6.05 (10H, s, Cp), 3.93-3.85 (4H, m, α-CH_2 and δ-CH_2), 2.23 (3H, s, *p*-CH_3), 2.17 (3H, s, *o*-CH_3(Py)), 2.09 (6H, s, *o*-CH_3), 1.65 (2H, m, β-CH_2), 1.35 (2H, m, γ-CH_2) ppm. ^{13}C NMR (125 MHz, PhBr-d_5): δ 160.1 (s, *i*-C(Mes)), 154.6 (s, *o*-CCH$_3$(Py)), 141.5

(s, *p*-*C*H(Py)), 127.4 (s, *o*-*C*CH$_3$(Mes)), 125.6 (s, *m*-*C*H(Py)), 124.6 (s, *p*-*C*CH$_3$(Mes)), 123.6 (s, *m*-*C*H(Py)), 112.8 (s, Cp), 72.0 (s, α-*C*H$_2$), 34.3 (s, β-*C*H$_2$), 30.3 (s, γ-*C*H$_2$), 27.3 (s, *o*-*C*H$_3$(Py)), 20.8 (s, *p*-*C*H$_3$(Mes)), 19.4 (s, δ-*C*H$_2$), 17.9 (s, *o*-*C*H$_3$(Mes)) ppm. Remaining aromatic peaks obscured by PhBr-d_5 solvent. ^{15}N-HMBC NMR (500 MHz, 51 MHz, PhBr-d_5): δ 411.6 ppm. ESI-MS (+ve detection) 520.1796 *m/z* $[M]^+$, 166.1275 *m/z* $[HO(C_4H_8)N(CH_3)C_6H_4]^+$.

2.1e + *THF*. Yield = 23 mg, 65%. ^{1}H NMR (400 MHz, PhBr-d_5): δ 7.37 (1H, t, $^3J_{HH}$ = 8 Hz, *p*-Ar*H*), 6.82-6.72 (2H, m, *m*-Ar*H*(Py)), 6.80 (2H, s, Ar*H*(Mes)), 6.05 (10H, s, Cp), 3.93 (2H, t, $^3J_{HH}$ = 6 Hz, α-C*H*$_2$), 3.85 (2H, m, δ-C*H*$_2$), 2.26 (6H, s, *o*-C*H*$_3$(Py)), 2.23 (3H, s, *p*-C*H*$_3$), 2.10 (6H, s, *o*-C*H*$_3$), 1.58 (2H, m, β-C*H*$_2$), 1.45 (2H, m, γ-C*H*$_2$) ppm. ^{13}C NMR (125 MHz, PhBr-d_5): δ 161.0 (s, *i*-*C*(Mes)), 154.3 (s, *o*-*C*CH$_3$(Py)), 143.8 (s, *p*-*C*H(Py)), 127.4 (s, *o*-*C*CH$_3$(Mes)), 124.6 (s, *p*-*C*CH$_3$(Mes)), 124.0 (s, *m*-*C*H(Py)), 112.8 (s, Cp), 71.8 (s, α-*C*H$_2$), 34.3 (s, β-*C*H$_2$), 30.7 (s, γ-*C*H$_2$), 25.6 (s, *o*-*C*H$_3$(Py)), 20.8 (s, *p*-*C*H$_3$(Mes)), 19.8 (s, δ-*C*H$_2$), 17.9 (s, *o*-*C*H$_3$(Mes)) ppm. Remaining aromatic peaks obscured by PhBr-d_5 solvent. ^{15}N-HMBC (500 MHz, 51 MHz, PhBr-d_5): δ 411.8 ppm. ESI-MS (+ve detection) 534.1938 *m/z* $[M]^+$, 180.1436 *m/z* $[HO(C_4H_8)N(CH_3)_2C_6H_3]^+$.

Reactivity of [Cp$_2$ZrOMes][B(C$_6$F$_5$)$_4$] // LB (**2.2a–e**)*

In a glovebox, **2.2** (34 mg, 0.029 mmol) was dissolved in PhBr-d_5 (0.5 mL) in an NMR tube fitted with a J. Young's valve. An equimolar amount of the Lewis base (**a** = NEt_3 (4.1 μL, 0.029 mmol), **b** = ^{i}Pr$_2$NEt (5.1 μL, 0.029 mmol), **c** = pyridine (2.4 μL, 0.029 mmol), **d** = 2-methylpyridine (2.9 μL, 0.029 mmol), **e** = 2,6-dimethylpyridine (3.4 μL, 0.029 mmol)) was then added. Tetrahydrofuran (THF, 2.4 μL, 0.029 mmol) was then added, with **2.2a**, **2.2d**, and **2.2e** all forming yellow solutions. The reactions were heated at 80 °C for 5 days. Isolation of the products was not possible.

2.2a + *THF*. Yield = 17% (by ^{1}H NMR). ^{15}N-HMBC (500 MHz, 51 MHz, PhBr-d_5): δ 341.4 ppm. ESI-MS (+ve detection) 668.3975 *m/z* $[M+H]^+$, 174.1888 *m/z* $[HO(C_4H_8)NEt_3]^+$.

2.2d + *THF*. Yield = 40% (by ^{1}H NMR). ^{15}N-HMBC (500 MHz, 51 MHz, PhBr-d_5): δ 411.3 ppm. ESI-MS (+ve detection) 660.3350 *m/z* $[M+H]^+$, 166.1277 *m/z* $[HO(C_4H_8)N(CH_3)C_6H_4]^+$.

2.2e + *THF*. Yield = 7% (by ^{1}H NMR). Too little product for ^{15}N-HMBC NMR. ESI-MS (+ve detection) 674.3501 *m/z* $[M+H]^+$, 180.1418 *m/z* $[HO(C_4H_8)N(CH_3)_2C_6H_3]^+$.

7.2.6 Reaction of pairs with phenylacetylene-*d* (PhCCD)

*Reactivity of [Cp$_2$ZrOMes][B(C$_6$F$_5$)$_4$] // LB (**2.1a–e**)*

In a glovebox, **2.1** (30 mg, 0.029 mmol) was dissolved in PhBr-d_5 (0.5 mL) in an NMR tube fitted with a J. Young's valve. An equimolar amount of the Lewis base (**a** = NEt_3 (4.1 μL, 0.029 mmol), **b** = ^{i}Pr$_2$NEt (5.1 μL, 0.029 mmol), **c** = pyridine (2.4 μL, 0.029 mmol), **d** = 2-methylpyridine (2.9 μL, 0.029 mmol), **e** = 2,6-dimethylpyridine (3.4 μL, 0.029 mmol)) was then added. Excess phenylacetylene-*d* (3 drops) was then added, resulting in a lightening of the yellow colour for **2.1a** and **2.1b**, with no colour change seen for the reactions of **2.1c-e**. Neither **2.1c** nor **2.1d** demonstrated any reactivity. The Zr-acetylide complex could not be isolated in any reaction, so the spectral data was obtained

in situ.

$Cp_2Zr(OMes)CCPh$. ^{1}H NMR (500 MHz, PhBr-d_5) δ 7.53 (2H, m, *o*-Ar*H*), 7.18 (3H, m, *p*-Ar*H* & *m*-Ar*H*(Ph)), 6.76 (2H, s, *m*-Ar*H*(Mes)), 6.09 (10H, s, Cp), 2.21 (6H, s, *o*-Ar-CH_3), 2.19 (3H, s, *p*-Ar-CH_3) ppm.

2.1a + *PhCCD*. Mixture of products meant the Zr-acetylide complex could not be isolated. However colourless crystals of [D-NEt_3][$B(C_6F_5)_4$] formed in solution, which were filtered, washed with PhCl (3 × 0.5 mL) and dried *in vacuo*. ^{15}N-HMBC NMR (500 MHz, 51 MHz, PhBr-d_5) δ 452.2 (D-*N*Et_3) ppm. ^{1}H (400 MHz, CD_3CN) δ 3.22 (6H, q, D-N(C$H_2$$CH_3$)$_3$), 1.22 (9H, t, D-N($CH_2CH_3$)$_3$) ppm. Deuteride signal not visible in ^{2}H NMR spectrum due to solvent interactions. Nanospray (+ve detection) 103.1 *m/z* [D-NEt_3]$^+$.

2.1b + *PhCCD*. Mixture of products meant the Zr-acetylide complex could not be isolated. However colourless crystals of [D-N(^{i}Pr)$_2$Et][$B(C_6F_5)_4$] formed in solution, which were filtered, washed with PhCl (3 × 0.5 mL) and dried *in vacuo*. ^{15}N-HMBC NMR (500 MHz, 51 MHz, PhBr-d_5) δ 424.8 (D-*N*(^{i}Pr)$_2$Et) ppm. ^{1}H (400 MHz, CD_3CN) δ 3.67 (2H, *sept.*, N(C*H*(CH_3)$_2$)$_2$), 3.15 (2H, q, NC$H_2$$CH_3$), 1.38-1.25 (15H, m, N(CH(CH_3)$_2$)$_2$ and NCH_2CH_3) ppm. Deuteride signal not visible in ^{2}H NMR spectrum due to solvent interactions. Nanospray (+ve detection) 131.2 *m/z* [D-N(^{i}Pr)$_2$Et]$^+$.

2.1e + *PhCCD*. Mixture of products meant the Zr-acetylide complex could not be isolated. Spectral data shown for [D-$NC_5H_3(CH_3)_2$]$^+$. ^{15}N-HMBC NMR (500 MHz, 51 MHz, PhBr-d_5) δ 420.8 (D-*N*$C_5H_3(CH_3)_2$) ppm. ^{1}H NMR (400 MHz, CD_3CN) δ 7.85 (1H, t, *p*-Ar*H*), 7.27 (2H, dd, *m*-Ar*H*), 2.55 (6H, s, -CH_3) ppm. ^{2}H NMR (77 MHz, PhBr-d_5) δ 12.45 (br, *D*-$NC_5H_3(CH_3)_2$) ppm. Nanospray (+ve detection) 109.1 *m/z* [D-$NC_5H_3(CH_3)_2$]$^+$.

*Reactivity of [$Cp^*_2ZrOMes$][$B(C_6F_5)_4$] // LB (**2.2a–e**)*

In a glovebox, **2.2** (34.1 mg, 0.029 mmol) was dissolved in PhCl (0.5 mL) in an NMR tube fitted with a J. Young's valve and C_6D_6 (one drop) was added as a reference in ^{2}H spectra. An equimolar amount of the Lewis base (**a** = NEt_3 (4.1 μL, 0.029 mmol), **b** = ^{i}Pr_2NEt (5.1 μL, 0.029 mmol), **c** = pyridine (2.4 μL, 0.029 mmol), **d** = 2-methylpyridine (2.9 μL, 0.029 mmol), **e** = 2,6-dimethylpyridine (3.4 μL, 0.029 mmol)) was then added. Excess phenylacetylene-*d* (3 drops) was then added. Samples **2.2a** and **2.2b** turned yellow within 5 min. **2.2c** did not demonstrate any reactivity. The Zr-acetylide complex could not be isolated in any reaction, so the spectral data was obtained *in situ*.

$Cp^*_2Zr(OMes)CCPh$. ^{1}H NMR (500 MHz, PhCl) δ 7.56 (2H, m, *o*-Ar*H*), 6.69 (2H, s, *m*-Ar*H*(Mes)), 2.16 (3H, s, *p*-Ar-CH_3), 1.88 (30H, s, Cp*), 1.79 (6H, s, *o*-Ar-CH_3) ppm. Remaining peaks were obscured by the PhCl solvent.

2.2a + *PhCCD*. Mixture of products meant the Zr-acetylide complex could not be isolated. However colourless crystals of [D-NEt_3][$B(C_6F_5)_4$] formed in solution, which were filtered, washed with PhCl (3 × 0.5 mL) and dried *in vacuo*. ^{15}N-HMBC NMR (500 MHz, 51 MHz, PhCl/C_6D_6) δ 439.7 (D-*N*Et_3) ppm. ^{1}H (400 MHz, CH_3CN/C_6D_6) δ 3.06 (6H, q, D-N(C$H_2$$CH_3$)$_3$), 1.22 (9H, t, D-N($CH_2CH_3$)$_3$) ppm. Deuteride signal not visible in ^{2}H NMR spectrum due to solvent interactions. Nanospray (+ve detection) 103.1 *m/z* [D-NEt_3]$^+$.

2.2b + *PhCCD*. Mixture of products meant the Zr-acetylide complex could not be isolated. However colourless crystals of [D-N(^{i}Pr)$_2$Et][$B(C_6F_5)_4$] formed in solution, which

were filtered, washed with PhCl (3 × 0.5 mL) and dried *in vacuo*. ^{15}N-HMBC NMR (500 MHz, 51 MHz, PhCl/C_6D_6) signal not seen (see Chapter 2). ^{1}H (400 MHz, CH_3CN/C_6D_6) δ 3.59 (2H, *sept.*, $N(CH(CH_3)_2)_2$), 3.07 (2H, q, NCH_2CH_3), 1.33-1.25 (15H, m, $N(CH(CH_3)_2)_2$ and NCH_2CH_3) ppm. Deuteride signal not visible in ^{2}H NMR spectrum due to solvent interactions. Nanospray (+ve detection) 131.2 *m/z* $[D\text{-}N(^{i}Pr)_2Et]^+$.

2.2d + *PhCCD*. Mixture of products meant the Zr-acetylide complex could not be isolated. Spectral data shown for $[D\text{-}NC_5H_4(CH_3)]^+$. ^{15}N-HMBC NMR (500 MHz, 51 MHz, PhCl/C_6D_6) δ 426.5 (D-$N$$C_5H_4(CH_3)$) ppm. ^{1}H NMR (400 MHz, PhCl/C_6D_6) δ 2.05 (3H, s, -CH_3) ppm, aromatic peaks obscured. ^{2}H NMR (77 MHz, PhCl/C_6D_6) δ 12.38 (br, D-$NC_5H_4(CH_3)$) ppm. Nanospray (+ve detection) 95.1 *m/z* $[D\text{-}NC_5H_4(CH_3)]^+$.

2.2e + *PhCCD*. Mixture of products meant the Zr-acetylide complex could not be isolated. Spectral data shown for $[D\text{-}NC_5H_3(CH_3)_2]^+$. ^{15}N-HMBC NMR (500 MHz, 51 MHz, PhCl/C_6D_6) δ 421.6 (D-$N$$C_5H_3(CH_3)_2$) ppm. ^{1}H NMR (400 MHz, CD_3CN) δ 7.85 (1H, t, *p*-ArH), 7.27 (2H, dd, *m*-ArH), 2.55 (6H, s, -CH_3) ppm. ^{2}H NMR (77 MHz, CD_3CN) δ 12.47 (br, D-$NC_5H_3(CH_3)_2$) ppm. Nanospray (+ve detection) 109.1 *m/z* $[D\text{-}NC_5H_3(CH_3)_2]^+$.

7.2.7 X-ray diffraction data

Table 7.1: Crystal data and structure refinement for **2.2c** and **2.2d**.

Identification code	**2.2c**	**2.2d**
Empirical formula	$C_{62.5}H_{50}BCl_{0.5}F_{20}NOZr$	$C_{59}H_{48}BF_{20}NOZr$
Formula weight	1330.79	1269.01
Temperature /K	99.77	100(2)
Crystal system	triclinic	monoclinic
Space group	P-1	$P2_1/n$
a/Å	10.8833(3)	13.0017(5)
b/Å	12.6740(3)	22.5644(8)
c/Å	21.3290(6)	18.0327(6)
$\alpha/^\circ$	83.4993(15)	90
$\beta/^\circ$	84.1792(16)	94.020(2)
$\gamma/^\circ$	85.5595(17)	90
Volume /Å^3	2901.55(13)	5277.3(3)
Z	2	4
ρ_{calc}g/cm^3	1.5233	1.597
μ/mm^{-1}	0.320	0.323
F(000)	1347.0	2568.0
Crystal size /mm^3	0.529 × 0.33 × 0.268	0.217 × 0.143 × 0.124
Radiation	MoK$_\alpha$ (λ = 0.71073)	MoK$_\alpha$ (λ = 0.71073)
2Θ range for data collection /°	3.242 to 60.216	3.74 to 50.7
Index ranges	-15 ≤ h ≤ 14, -16 ≤ h ≤ 17, -30 ≤ h ≤ 30	-15 ≤ h ≤ 15, -27 ≤ h ≤ 26, -20 ≤ h ≤ 21
Reflections collected	65149	39357
R_{int} / R_{sigma}	0.0480 / 0.0482	0.1385 / 0.1257
Data/restraints/ parameters	17039/42/815	9669/0/762
Goodness-of-fit on F^2	1.085	1.004
Final R indexes [I<=2σ (I)]	R_1 = 0.0673, wR_2 = 0.1728	R_1 = 0.0583, wR_2 = 0.1069
Final R indexes [all data]	R_1 = 0.0880, wR_2 = 0.1851	R_1 = 0.1204, wR_2 = 0.1272
Largest diff. peak/hole / e Å^{-3}	1.93/-2.12	0.47/-0.52

7.3 Chapter 3 experimental

The majority of this experimental is taken from a first author publication.[118]

7.3.1 Catalytic dehydrocoupling of $Me_2NH{\cdot}BH_3$

*Reactivity of [$Cp_2ZrOMes$][$B(C_6F_5)_4$] // LB (**2.1a–e**)*

In a glovebox, **2.1** (18.7 mg, 0.018 mmol) and $Me_2NH{\cdot}BH_3$ (10.6 mg, 0.18 mmol) were weighed into separate vials and dissolved in PhBr-d_5 (0.5 mL). The relevant Lewis base (**a** = NEt_3 (2.5 μL, 0.018 mmol), **b** = $^{i}Pr_2NEt$ (3.2 μL, 0.018 mmol), **c** = pyridine (1.5 μL, 0.018 mmol), **d** = 2-methylpyridine (1.8 μL, 0.018 mmol), **e** = 2,6-dimethylpyridine (2.1 μL, 0.018 mmol)) was then added to **2.1**. The two solutions were then combined, and the fully mixed solution was transferred to a quartz J. Young's NMR tube before the relevant spectra were then collected. No reaction was seen for **2.1c**.

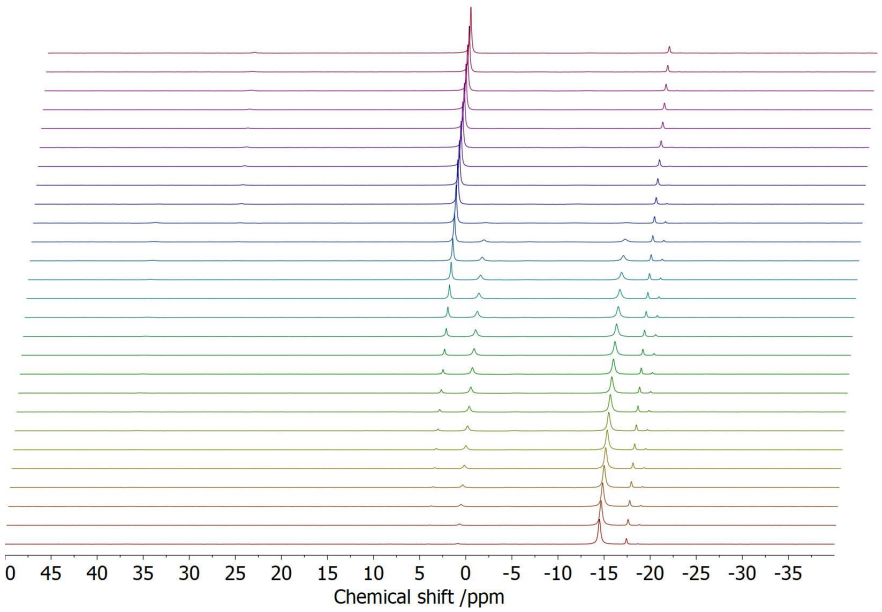

Figure 7.16: $^{11}B\{^{1}H\}$ NMR spectra (25 °C, PhBr-d_5) for the reaction between $Me_2NH{\cdot}BH_3$ and 10 mol% **2.1a**. Each spectrum was obtained at an interval of 30 min. $Me_2N(B_2H_5)$ (-18.7 ppm), $[B(C_6F_5)_4]^-$ (-17.5 ppm), $Me_2NH{\cdot}BH_3$ (-14.5 ppm), Me_2NH–BH_2–Me_2N–BH_3 (-14.5 and 0.8 ppm), $[Me_2N–BH_2]_2$ (4.0 ppm), $HB(NMe_2)_2$ (27.5 ppm), $Me_2N{=}BH_2$ (36.6 ppm).

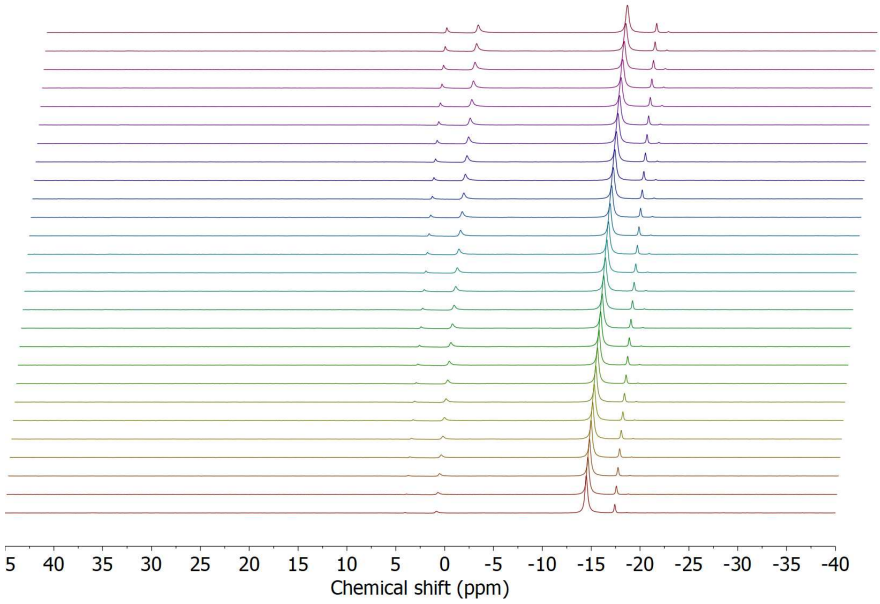

Figure 7.17: $^{11}B\{^{1}H\}$ NMR spectra (25 °C, PhBr-d_5) for the reaction between $Me_2NH{\cdot}BH_3$ and 10 mol% **2.1b**. Each spectrum was obtained at an interval of 30 min. $Me_2N(B_2H_5)$ (-18.7 ppm), $[B(C_6F_5)_4]^-$ (-17.5 ppm), $Me_2NH{\cdot}BH_3$ (-14.5 ppm), Me_2NH–BH_2–Me_2N–BH_3 (-14.5 and 0.8 ppm), $[Me_2N–BH_2]_2$ (4.0 ppm), $HB(NMe_2)_2$ (27.5 ppm), $Me_2N{=}BH_2$ (36.6 ppm).

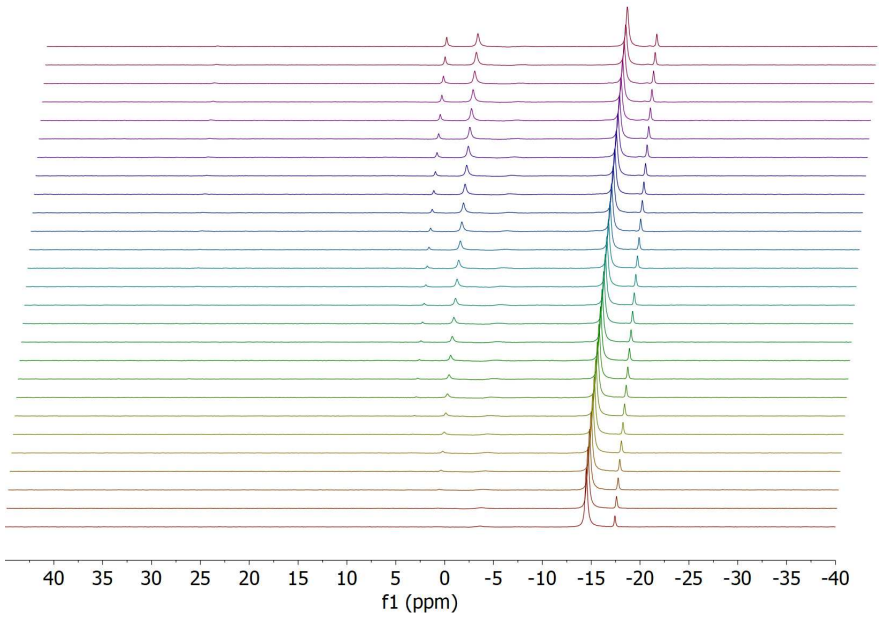

Figure 7.18: $^{11}B\{^{1}H\}$ NMR spectra (25 °C, PhBr-d_5) for the reaction between $Me_2NH{\cdot}BH_3$ and 10 mol% **2.1d**. Each spectrum was obtained at an interval of 30 min. $Me_2N(B_2H_5)$ (-18.7 ppm), $[B(C_6F_5)_4]^-$ (-17.5 ppm), $Me_2NH{\cdot}BH_3$ (-14.5 ppm), Me_2NH–BH_2–Me_2N–BH_3 (-14.5 and 0.8 ppm), $[Me_2N–BH_2]_2$ (4.0 ppm), $HB(NMe_2)_2$ (27.5 ppm), $Me_2N{=}BH_2$ (36.6 ppm).

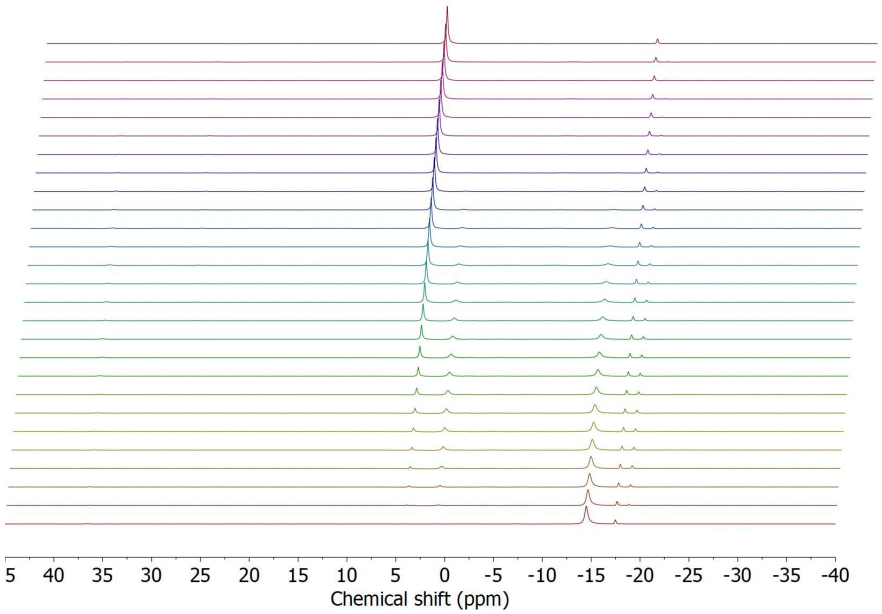

Figure 7.19: $^{11}B\{^{1}H\}$ NMR spectra (25 °C, PhBr-d_5) for the reaction between $Me_2NH{\cdot}BH_3$ and 10 mol% **2.1e**. Each spectrum was obtained at an interval of 30 min. $Me_2N(B_2H_5)$ (-18.7 ppm), $[B(C_6F_5)_4]^-$ (-17.5 ppm), $Me_2NH{\cdot}BH_3$ (-14.5 ppm), Me_2NH–BH_2–Me_2N–BH_3 (-14.5 and 0.8 ppm), $[Me_2N–BH_2]_2$ (4.0 ppm), $HB(NMe_2)_2$ (27.5 ppm), $Me_2N{=}BH_2$ (36.6 ppm).

Reactivity of [Cp$_2$ZrOMes][B(C$_6$F$_5$)$_4$] // LB (**2.2a–e**)*

In a glovebox, **2.2** (21.2 mg, 0.018 mmol) and $Me_2NH{\cdot}BH_3$ (10.6 mg, 0.18 mmol) were weighed into separate vials and dissolved in PhBr-d_5 (0.5 mL). The relevant Lewis base (**a** = NEt_3 (2.5 μL, 0.018 mmol), **b** = $^{i}Pr_2NEt$ (3.2 μL, 0.018 mmol), **c** = pyridine (1.5 μL, 0.018 mmol), **d** = 2-methylpyridine (1.8 μL, 0.018 mmol), **e** = 2,6-dimethylpyridine (2.1 μL, 0.018 mmol)) was then added to **2.2**. The two solutions were then combined, and the fully mixed solution was transferred to a quartz J. Youngs NMR tube before the relevant spectra were then collected.

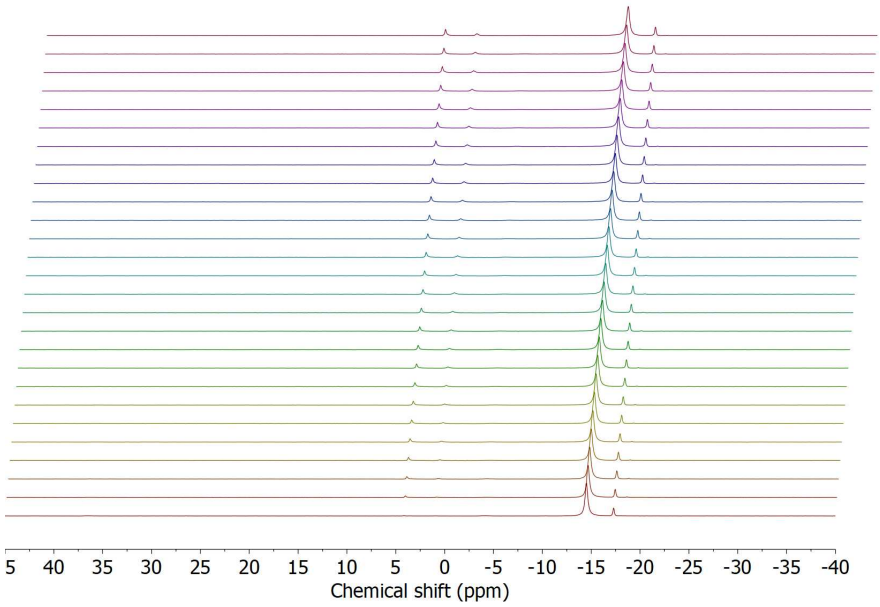

Figure 7.20: $^{11}B\{^1H\}$ NMR spectra (25 °C, PhBr-d_5) for the reaction between $Me_2NH{\cdot}BH_3$ and 10 mol% **2.2a**. Each spectrum was obtained at an interval of 30 min. $Me_2N(B_2H_5)$ (-18.7 ppm), $[B(C_6F_5)_4]^-$ (-17.5 ppm), $Me_2NH{\cdot}BH_3$ (-14.5 ppm), Me_2NH–BH_2–Me_2N–BH_3 (-14.5 and 0.8 ppm), $[Me_2N–BH_2]_2$ (4.0 ppm), $HB(NMe_2)_2$ (27.5 ppm), $Me_2N{=}BH_2$ (36.6 ppm).

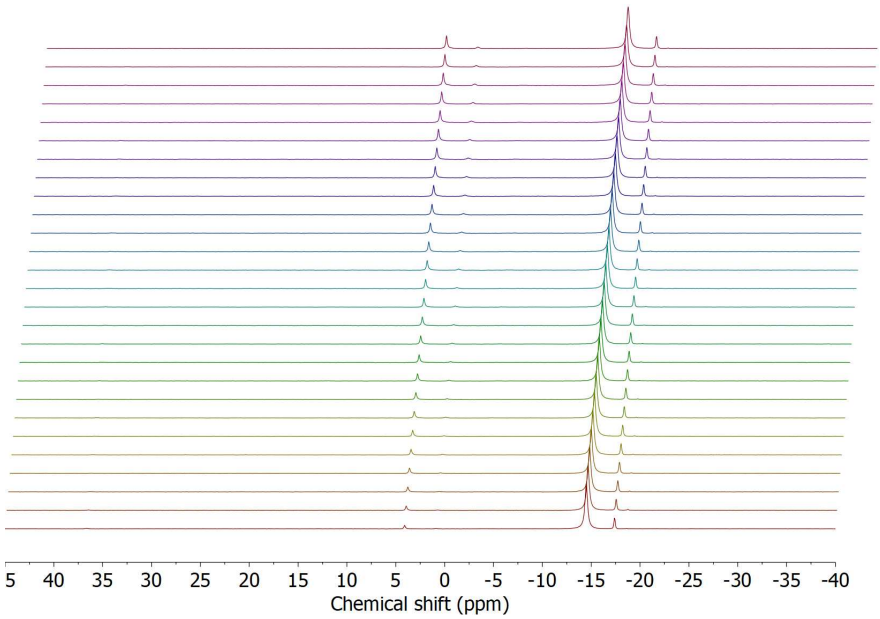

Figure 7.21: $^{11}B\{^1H\}$ NMR spectra (25 °C, PhBr-d_5) for the reaction between $Me_2NH{\cdot}BH_3$ and 10 mol% **2.2b**. Each spectrum was obtained at an interval of 30 min. $Me_2N(B_2H_5)$ (-18.7 ppm), $[B(C_6F_5)_4]^-$ (-17.5 ppm), $Me_2NH{\cdot}BH_3$ (-14.5 ppm), Me_2NH–BH_2–Me_2N–BH_3 (-14.5 and 0.8 ppm), $[Me_2N–BH_2]_2$ (4.0 ppm), $HB(NMe_2)_2$ (27.5 ppm), $Me_2N{=}BH_2$ (36.6 ppm).

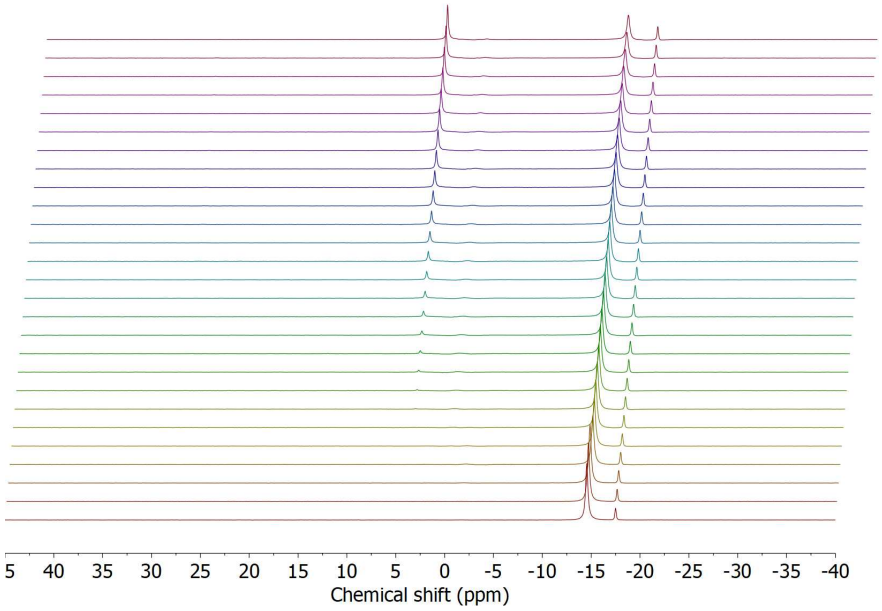

Figure 7.22: $^{11}B\{^{1}H\}$ NMR spectra (25 °C, PhBr-d_5) for the reaction between $Me_2NH{\cdot}BH_3$ and 10 mol% **2.2c**. Each spectrum was obtained at an interval of 30 min. $Me_2N(B_2H_5)$ (-18.7 ppm), $[B(C_6F_5)_4]^-$ (-17.5 ppm), $Me_2NH{\cdot}BH_3$ (-14.5 ppm), Me_2NH–BH_2–Me_2N–BH_3 (-14.5 and 0.8 ppm), $[Me_2N–BH_2]_2$ (4.0 ppm), $HB(NMe_2)_2$ (27.5 ppm), $Me_2N{=}BH_2$ (36.6 ppm).

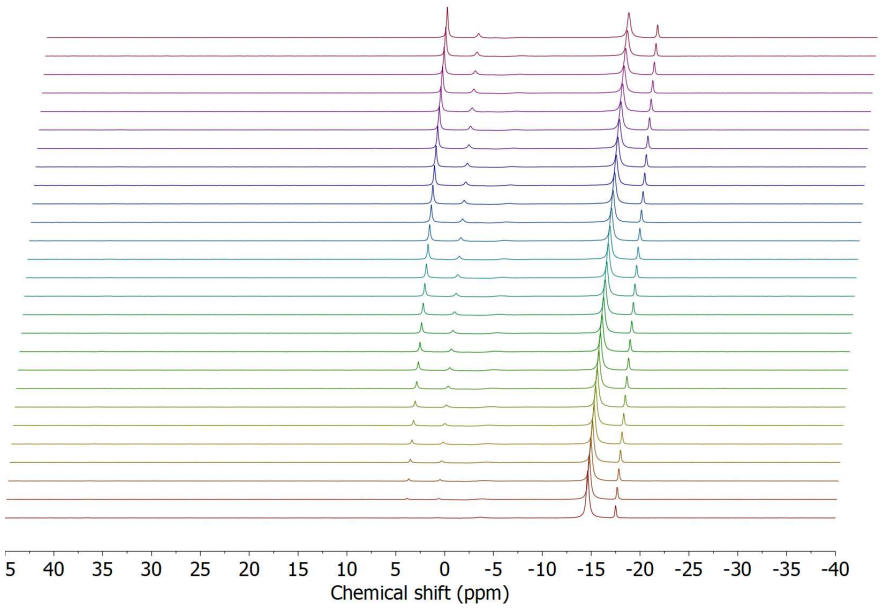

Figure 7.23: $^{11}B\{^{1}H\}$ NMR spectra (25 °C, PhBr-d_5) for the reaction between $Me_2NH{\cdot}BH_3$ and 10 mol% **2.2d**. Each spectrum was obtained at an interval of 30 min. $Me_2N(B_2H_5)$ (-18.7 ppm), $[B(C_6F_5)_4]^-$ (-17.5 ppm), $Me_2NH{\cdot}BH_3$ (-14.5 ppm), Me_2NH–BH_2–Me_2N–BH_3 (-14.5 and 0.8 ppm), $[Me_2N–BH_2]_2$ (4.0 ppm), $HB(NMe_2)_2$ (27.5 ppm), $Me_2N{=}BH_2$ (36.6 ppm).

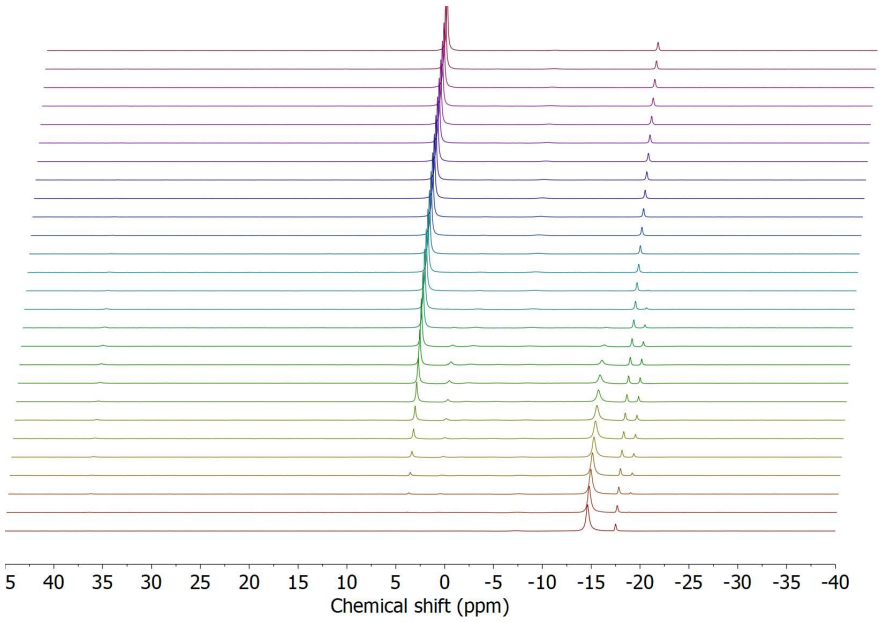

Figure 7.24: $^{11}B\{^{1}H\}$ NMR spectra (25 °C, PhBr-d_5) for the reaction between $Me_2NH{\cdot}BH_3$ and 10 mol% **2.2e**. Each spectrum was obtained at an interval of 30 min. $Me_2N(B_2H_5)$ (-18.7 ppm), $[B(C_6F_5)_4]^-$ (-17.5 ppm), $Me_2NH{\cdot}BH_3$ (-14.5 ppm), Me_2NH–BH_2–Me_2N–BH_3 (-14.5 and 0.8 ppm), $[Me_2N–BH_2]_2$ (4.0 ppm), $HB(NMe_2)_2$ (27.5 ppm), $Me_2N{=}BH_2$ (36.6 ppm).

7.3.2 Catalytic dehydrocoupling of $Me_2NH{\cdot}BH_3$ at 60 °C

Reactions were prepared for **2.1a**, **2.1e**, and **2.2e** using the same method for the previous reactions, with the spectra then collected in an NMR spectrometer set to 60 °C.

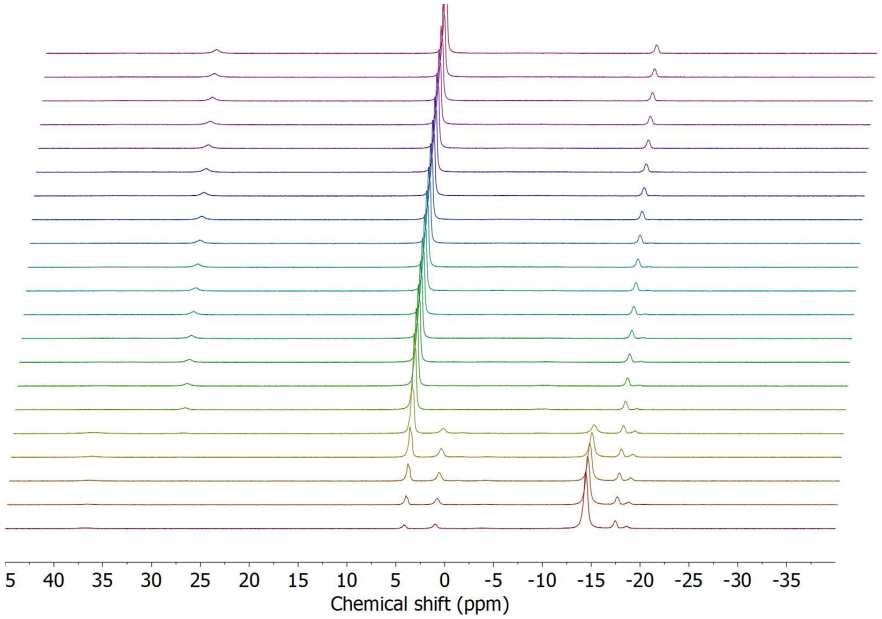

Figure 7.25: $^{11}B\{^1H\}$ NMR spectra (60 °C, PhBr-d_5) for the reaction between $Me_2NH{\cdot}BH_3$ and 10 mol% **2.1a**. Each spectrum was obtained at an interval of 3 min. $Me_2N(B_2H_5)$ (-18.7 ppm), $[B(C_6F_5)_4]^-$ (-17.5 ppm), $Me_2NH{\cdot}BH_3$ (-14.5 ppm), Me_2NH–BH_2–Me_2N–BH_3 (-14.5 and 0.8 ppm), $[Me_2N–BH_2]_2$ (4.0 ppm), $HB(NMe_2)_2$ (27.5 ppm), $Me_2N{=}BH_2$ (36.6 ppm).

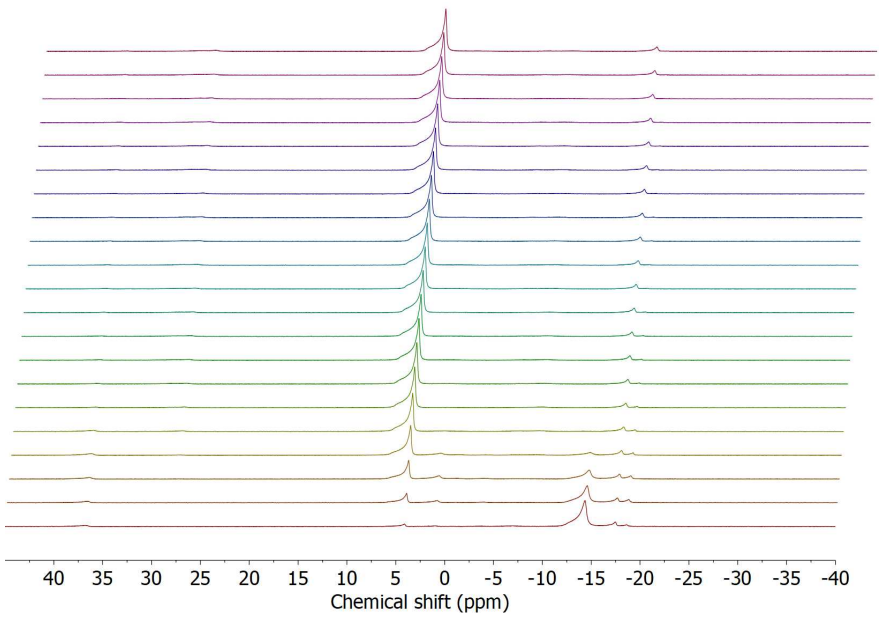

Figure 7.26: $^{11}B\{^1H\}$ NMR spectra (60 °C, PhBr-d_5) for the reaction between $Me_2NH{\cdot}BH_3$ and 10 mol% **2.1e**. Each spectrum was obtained at an interval of 3 min. $Me_2N(B_2H_5)$ (-18.7 ppm), $[B(C_6F_5)_4]^-$ (-17.5 ppm), $Me_2NH{\cdot}BH_3$ (-14.5 ppm), Me_2NH–BH_2–Me_2N–BH_3 (-14.5 and 0.8 ppm), $[Me_2N–BH_2]_2$ (4.0 ppm), $HB(NMe_2)_2$ (27.5 ppm), $Me_2N{=}BH_2$ (36.6 ppm).

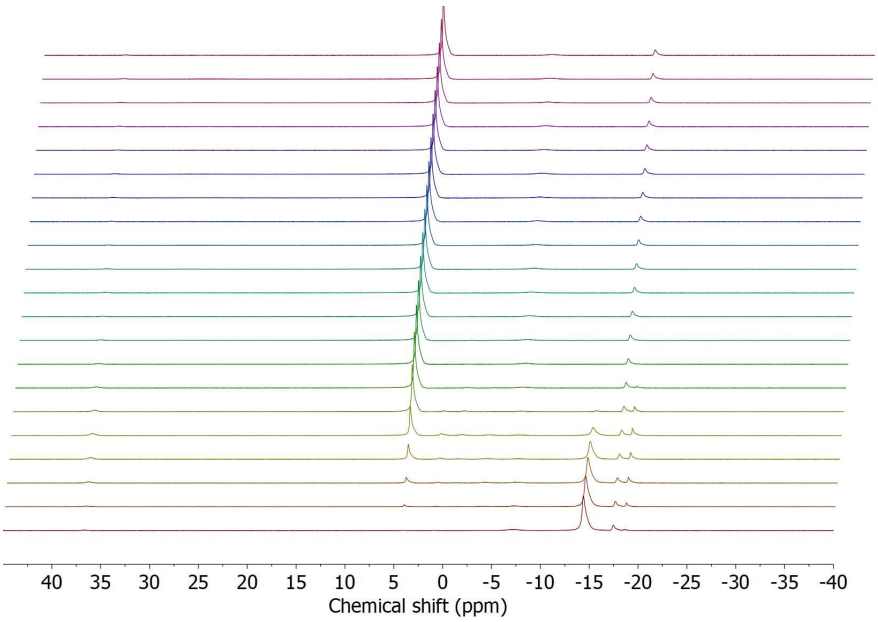

Figure 7.27: $^{11}B\{^{1}H\}$ NMR spectra (60 °C, PhBr-d_5) for the reaction between $Me_2NH{\cdot}BH_3$ and 10 mol% **2.2e**. Each spectrum was obtained at an interval of 3 min. $Me_2N(B_2H_5)$ (-18.7 ppm), $[B(C_6F_5)_4]^-$ (-17.5 ppm), $Me_2NH{\cdot}BH_3$ (-14.5 ppm), Me_2NH–BH_2–Me_2N–BH_3 (-14.5 and 0.8 ppm), $[Me_2N–BH_2]_2$ (4.0 ppm), $HB(NMe_2)_2$ (27.5 ppm), $Me_2N{=}BH_2$ (36.6 ppm).

7.4 Chapter 4 experimental

7.4.1 Synthesis of 4.2

4.3 (1 g, 1.53 mmol) was heated at 115 °C under a high vacuum (1×10^{-7} mbar) for 3 days, resulting in in a slight lightening of the yellow colour. Yield = 100%. The NMR spectra matched the literature data.[184]

7.4.2 Synthesis of 4.6

4.2 (100 mg, 0.171 mmol) and 2,4,6-trimethylphenol (23.4 mg, 0.171 mmol) were dissolved in pentane (4 mL) and stirred for 5 min. The reaction was then filtered, and the yellow solution was left to evaporate slowly, resulting in the formation of yellow crystals suitable for X-ray diffraction, which were washed with hexane (2 × 2 mL). Yield = 99.7 mg (88%).

^{1}H NMR (400 MHz, C_6D_6): δ 7.10-6.97 (6H, m, *m*-Ar*H* and *p*-Ar*H*), 6.77 (2H, s, *m*-Ar*H*(Mes)), 5.51 (1H, s, β-C*H*), 3.30 (4H, *sept.*, $^{3}J_{HH}$ = 6.9 Hz, -C*H*$(CH_3)_2$), 2.20 (3H, s, *p*-CH_3), 1.33 (6H, s, *o*-CH_3), 1.26-1.21 (24H, m, -CH(CH_3)$_2$), 1.13 (18H, s, -(CH_3)$_3$) ppm. ^{13}C NMR (125 MHz, C_6D_6): δ 178.0 (s, β-*C*-N), 148.0 (s, *i*-*C*(Ar)), 144.7 (s, *i*-*C*(Mes)), 141.7 (s, *o*-*C*(Ar)), 128.9 (s, *m*-*C*H(Mes)), 126.0 (s, *p*-*C*(Mes)), 125.7 (s, *o*-*C*(Mes)), 124.1 (s, *m*-*C*H(Ar)), 123.1 (s, *p*-*C*H(Ar)), 95.2 (s, γ-*C*H), 44.3 (s, -*C*$(CH_3)_3$),

32.9 (s, -C(CH$_3$)$_3$), 28.8 (s, -CH(CH$_3$)$_2$), 25.2 and 25.2 (s, -CH(CH$_3$)$_2$), 20.8 (s, p-CH$_3$), 16.9 (s, o-CH$_3$) ppm.

7.4.3 Gutmann-Beckett Lewis acidity tests of 4.2 and 4.6

Compounds **4.2** (23.3 mg, 0.04 mmol) and **4.6** (26.5 mg, 0.04 mmol) were separately dissolved in C_6D_6 (0.5 mL) before PEt_3=O (5.4 mg, 0.04 mmol) was added and NMR spectra were collected.

4.2 + *PEt$_3$=O*: ^{1}H (400 MHz, C_6D_6): δ 7.13-6.99 (6H, m, ArH), 5.38 (1H, s, γ-CH), 4.13 (2H, *sept.*, $^3J_{HH}$ = 6.8 Hz, -CH(CH$_3$)$_2$), 3.49 (2H, *sept.*, $^3J_{HH}$ = 6.8 Hz, -CH(CH$_3$)$_2$), 1.56 (6H, d, $^3J_{HH}$ = 6.8 Hz, -CH(CH_3)$_2$), 1.45 (6H, d, $^3J_{HH}$ = 6.8 Hz, -CH(CH_3)$_2$), 1.43 (6H, d, $^3J_{HH}$ = 6.8 Hz, -CH(CH_3)$_2$), 1.34 (3H, t, $^3J_{HH}$ = 7.3 Hz, MgCH$_2$(CH$_2$)$_2$CH_3), 1.30 (18H, s, -C(CH_3)$_3$), 1.24 (6H, d, $^3J_{HH}$ = 6.8 Hz, -CH(CH_3)$_2$), 1.19-1.11 (6H, m, P(CH_2CH$_3$)$_3$), 0.76 (4H, m, MgCH$_2$(CH_2)$_2$CH$_3$), 0.22 (9H, m, P(CH$_2$CH_3)$_3$), -0.08 (2H, m, MgCH_2(CH$_2$)$_2$CH$_3$) ppm. ^{31}P NMR (162 MHz, C_6D_6): δ 59.6 ppm.

4.6 + *PEt$_3$=O*: ^{1}H (400 MHz, C_6D_6): δ 7.14-6.96 (8H, m, ArH), 5.45 (1H, s, γ-CH), 3.87 (2H, *sept.*, $^3J_{HH}$ = 6.8 Hz, -CH(CH$_3$)$_2$), 3.43 (2H, *sept.*, $^3J_{HH}$ = 6.8 Hz, -CH(CH$_3$)$_2$), 2.69 (3H, s, p-CH_3), 2.44 (3H, s, o-CH_3), 2.29 (3H, s, o-CH_3), 1.42 (6H, d, $^3J_{HH}$ = 6.8 Hz, -CH(CH_3)$_2$), 1.29 (6H, d, $^3J_{HH}$ = 6.8 Hz, -CH(CH_3)$_2$), 1.27 (18H, s, -C(CH_3)$_3$), 1.24 (6H, d, $^3J_{HH}$ = 6.8 Hz, -CH(CH_3)$_2$), 1.19-1.08 (6H, m, P(CH_2CH$_3$)$_3$), 1.13 (6H, d, $^3J_{HH}$ = 6.8 Hz, -CH(CH_3)$_2$), 0.10 (9H, m, P(CH$_2$CH_3)$_3$) ppm. ^{31}P NMR (162 MHz, C_6D_6): δ 64.2 ppm.

7.4.4 Reactions of 4.6 with Lewis bases

4.6 (26.5 mg, 0.04 mmol) and one of the following Lewis bases: NEt_3 (**a**, 5.6 μL, 0.04 mmol), pyridine (**c**, 3.2 μL, 0.04 mmol), 2-methylpyridine (**d**, 4.0 μL, 0.04 mmol), 2,6-dimethylpyridine (**e**, 4.7 μL, 0.04 mmol), PPh_3 (**f**, 10.5 mg, 0.04 mmol), PEt_3 (**g**, 5.9 μL, 0.04 mmol), or P^{t}Bu$_3$ (**h**, 8.1 mg, 0.04 mmol), were combined in C_6D_6 (0.5 mL) in a J. Youngs NMR tube before NMR spectra were collected. No change in NMR data was seen for **4.6a**, or **4.6e**–**h**; however **4.6c** and **4.6d** resulted in the formation of adducts. Crystals suitable for X-ray diffraction were obtained by slow evaporation of a hexane (**4.6c**) or PhCl (**4.6d**) solution of the sample.

4.6c ^{1}H NMR (400 MHz, C_6D_6): δ 8.75 (2H, br, o-CH(Py)), 7.17-6.95 (6H, m, m-ArH and p-ArH), 6.86 (2H, s, m-ArH(Mes)), 6.83 (1H, m, p-ArH(Py)), 6.66 (2H, m, m-ArH(Py)), 5.62 (1H, s, γ-CH), 3.56 (2H, *sept.*, $^3J_{HH}$ = 6.9 Hz, -CH(CH$_3$)$_2$), 2.81 (2H, *sept.*, $^3J_{HH}$ = 6.9 Hz, -CH(CH$_3$)$_2$), 2.24 (3H, s, p-CH_3), 1.53 (6H, s, o-CH_3), 1.38 (6H, d, $^3J_{HH}$ = 6.9 Hz, -CH(CH_3)$_2$), 1.31 (6H, d, $^3J_{HH}$ = 6.9 Hz, -CH(CH_3)$_2$), 1.24 (18H, s, -C(CH_3)$_3$), 1.11 (6H, d, $^3J_{HH}$ = 6.9 Hz, -CH(CH_3)$_2$), 1.09 (6H, d, $^3J_{HH}$ = 6.9 Hz, -CH(CH_3)$_2$) ppm.

4.6d ^{1}H NMR (400 MHz, C_6D_6): δ 8.61 (1H, br, o-CH(Py)), 7.15-6.89 (6H, m, m-ArH and p-ArH), 6.87 (2H, s, m-ArH(Mes)), 6.69 (1H, m, p-ArH(Py)), 6.60 (1H, m, m-ArH(Py)), 6.49 (1H, m, m-ArH(Py)), 5.56 (1H, s, γ-CH), 3.56 (2H, br, -CH(CH$_3$)$_2$), 3.01 (2H, br, -CH(CH$_3$)$_2$), 2.62 (3H, s, o-CH_3(Py)), 2.24 (3H, s, p-CH_3), 1.42 (6H, s, o-CH_3(Mes)), 1.37-1.25 (12H, m, -CH(CH_3)$_2$), 1.21 (18H, s, -C(CH_3)$_3$), 1.18 (6H, br,

-CH(CH_3)$_2$), 0.31 (6H, br, -CH(CH_3)$_2$) ppm. ^{13}C NMR (125 MHz, C_6D_6): δ 177.1 (s, β-*C*-N), 158.8 (s, *o*-*C*H(Py)), 152.4 (s, *i*-*C*(Ar)), 150.0 (s, *o*-*C*CH$_3$(Py)), 141.9 (s, *o*-*C*(Ar)), 139.0 (s, *p*-*C*H(Py)), 129.3 (s, *m*-*C*H(Mes)), 125.8 (s, *p*-*C*(Mes)), 125.3 (s, *o*-*C*(Mes)), 125.0 (s, *m*-*C*H(Py)), 124.5 (s, *m*-*C*H(Ar)), 123.7 (s, *p*-*C*H(Ar)), 122.0 (s, *m*-*C*H(Py)), 97.1 (s, γ-*C*H), 44.3 (s, -*C*(CH$_3$)$_3$), 33.3 (s, -C(*C*H$_3$)$_3$), 28.6 (s, -*C*H(CH$_3$)$_2$), 24.3 (s, -CH(*C*H$_3$)$_2$), 20.9 (s, *p*-*C*H$_3$), 16.5 (s, *o*-*C*H$_3$) ppm.

7.4.5 Reactions of 4.6a–h with hydrogen gas

Compound **4.6** (26.5 mg, 0.04 mmol) was dissolved in C_6D_6 (0.5 mL) in a J. Youngs NMR tube before the respective Lewis base (NEt$_3$ (**a**, 5.6 μL, 0.04 mmol), pyridine (**c**, 3.2 μL, 0.04 mmol), 2-methylpyridine (**d**, 4.0 μL, 0.04 mmol), 2,6-dimethylpyridine (**e**, 4.7 μL, 0.04 mmol), PPh$_3$ (**f**, 10.5 mg, 0.04 mmol), PEt$_3$ (**g**, 5.9 μL, 0.04 mmol), or P^{t}Bu$_3$ (**h**, 8.1 mg, 0.04 mmol)) was added. The sample was degassed twice via freeze-pump-thaw before being refilled H_2 gas (1 bar); NMR spectra were then collected. No change was seen in any reaction.

7.4.6 Reactions of 4.6a–h with phenylacetylene-*d*

Compound **4.6** (26.5 mg, 0.04 mmol) was dissolved in C_6D_6 (0.5 mL) in a J. Youngs NMR tube before the respective Lewis base (NEt$_3$ (**a**, 5.6 μL, 0.04 mmol), pyridine (**c**, 3.2 μL, 0.04 mmol), 2-methylpyridine (**d**, 4.0 μL, 0.04 mmol), 2,6-dimethylpyridine (**e**, 4.7 μL, 0.04 mmol), PPh$_3$ (**f**, 10.5 mg, 0.04 mmol), PEt$_3$ (**g**, 5.9 μL, 0.04 mmol), or P^{t}Bu$_3$ (**h**, 8.1 mg, 0.04 mmol)) was added. Phenylacetylene-*d* (4.4 μL, 0.04 mmol) was then added, before NMR spectra were collected. No change was seen in any reaction.

7.4.7 Reactions of 4.6 and 4.6a–h with benzaldehyde

Synthesis of ***4.7***

Compound **4.6** (26.5 mg, 0.04 mmol) was dissolved in C_6D_6 (0.5 mL) before benzaldehyde (4.1 μL, 0.04 mmol) was added, forming a red solution of **4.7**. ^{1}H, ^{13}C, and DOSY NMR spectra were then collected.

^{1}H NMR (400 MHz, C_6D_6): δ 9.02 (1H, br, -C*H*(O)), 7.12 (2H, m, *o*-C*H*), 7.08-6.99 (6H, m, Ar*H*(DIPP)), 6.98 (2H, s, *m*-Ar*H*(Mes)), 6.92 (1H, m, *p*-C*H*(Ph)), 6.76 (2H, m, *m*-C*H*(Ph)), 5.59 (1H, s, γ-C*H*), 3.57 (4H, br, -C*H*(CH$_3$)$_2$), 2.34 (3H, s, *p*-C*H*$_3$), 2.07 (6H, br, *o*-C*H*$_3$), 1.32 (12H, d, $^3J_{HH}$ = 6.8 Hz, -CH(C*H*$_3$)$_2$), 1.27 (18H, s, -C(C*H*$_3$)$_3$), 1.10 (12H, br, -CH(C*H*$_3$)$_2$) ppm. ^{13}C NMR (125 MHz, C_6D_6): δ 199.6 (s, *C*H(O)), 177.7 (s, β-*C*-N), 159.2 (s, *i*-*C*(DIPP)), 146.6 (s, *i*-*C*(Mes)), 142.8 (br, *o*-*C*(DIPP)), 137.1 (s, *i*-*C*(Ph)), 134.8 (s, *p*-*C*(Ph)), 131.9 (s, *m*-*C*H(Mes)), 129.3 (s, *o*-*C*H(Ph)), 129.1 (s, *m*-*C*H(Ph)), 125.1 (s, *p*-*C*CH$_3$), 124.8 (s, *o*-*C*CH$_3$), 123.9 (br, *m*-*C*H(DIPP)), 121.5 (s, *p*-*C*H(DIPP)), 95.8 (s, γ-*C*H), 44.4 (s, -*C*(CH$_3$)$_3$), 33.2 (s, -C(*C*H$_3$)$_3$), 28.1 (s, -*C*(CH$_3$)$_2$), 24.3 (s, -C(*C*H$_3$)$_2$), 21.1 (s, *p*-*C*H$_3$), 18.2 (s, *o*-*C*H$_3$) ppm.

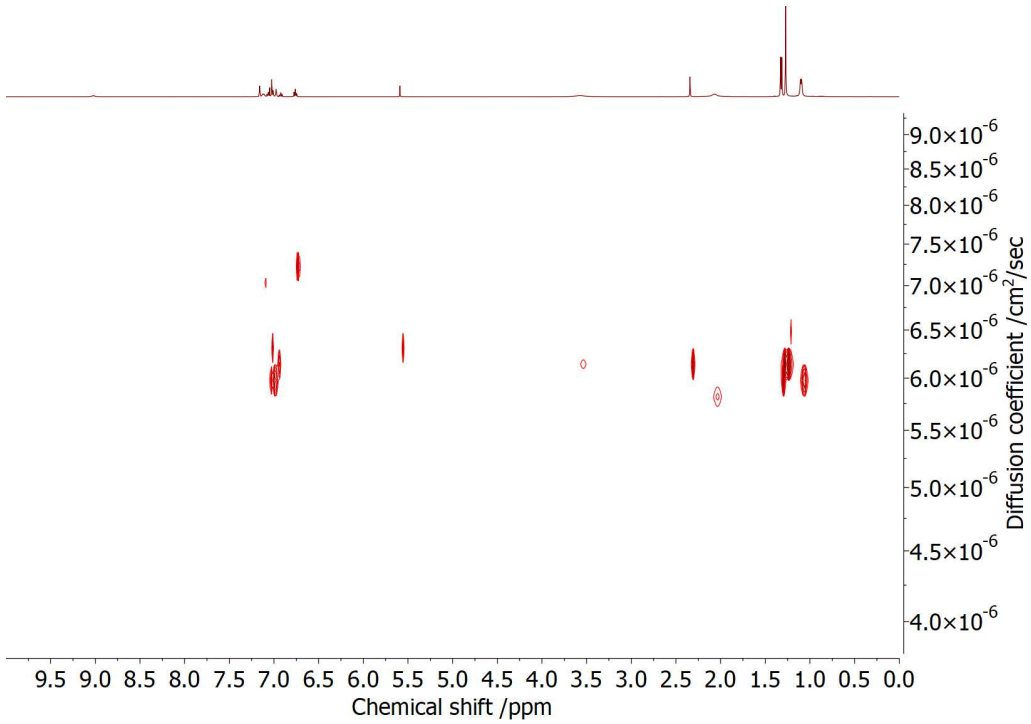

Figure 7.28: DOSY NMR spectrum of **4.7**.

*Reactions of **4.6a–h** with benzaldehyde*

Compound **4.6** (26.5 mg, 0.04 mmol) was dissolved in C_6D_6 (0.5 mL) in a J. Youngs NMR tube before the respective Lewis base (NEt_3 (**a**, 5.6 μL, 0.04 mmol), pyridine (**c**, 3.2 μL, 0.04 mmol), 2-methylpyridine (**d**, 4.0 μL, 0.04 mmol), 2,6-dimethylpyridine (**e**, 4.7 μL, 0.04 mmol), PPh_3 (**f**, 10.5 mg, 0.04 mmol), PEt_3 (**g**, 5.9 μL, 0.04 mmol), or P^tBu_3 (**h**, 8.1 mg, 0.04 mmol)) was added. Benzaldehyde (4.1 μL, 0.04 mmol) was then added, before NMR spectra were collected. The reactions of **4.6a**, **4.6e**, **4.6f**, and **4.6h** resulted in the formation of **4.7** with no further reaction taking place. No reaction was seen with **4.6c** and **4.6d**. The reaction with **4.6g** resulted in new NMR signal data.

4.6g + *PhCHO*: ^{1}H NMR (400 MHz, C_6D_6): δ 8.53 (1H, br, -C*H*(O)), 7.13-6.99 (10H, m, *o*-C*H*(Ph), *m*-C*H*(Mes), *m*-C*H*(DIPP), *p*-C*H*(DIPP)), 6.96 (1H, m, *p*-C*H*(Ph)), 6.84 (2H, m, *m*-C*H*(Ph)), 5.56 (1H, s, γ-C*H*), 3.63 (4H, br, -C*H*$(CH_3)_2$), 2.36 (3H, s, *p*-CH_3), 2.17 (6H, br, *o*-CH_3), 1.34 (12H, d, $^3J_{HH}$ = 6.8 Hz, -CH(CH_3)$_2$), 1.28 (18H, s, -C(CH_3)$_3$), 1.13 (6H, m, P(CH_2CH$_3$)$_3$), 1.11 (12H, br, -CH(CH_3)$_2$), 0.81 (9H, m, P(CH$_2$CH_3)$_3$) ppm. ^{31}P{1H} NMR (162 MHz, C_6D_6): δ 11.2 (br, PEt_3) ppm.

7.4.8 Reactions of 4.6 and 4.6a–h with mesitaldehyde

*Synthesis of **4.8***

Compound **4.6** (26.5 mg, 0.04 mmol) was dissolved in C_6D_6 (0.5 mL) before mesitaldehyde (5.9 μL, 0.04 mmol) was added, forming an orange solution of **4.8**. ^{1}H and

DOSY NMR spectra were then collected. Orange crystals suitable for X-ray diffraction were grown by slow evaporation of a PhCl solution. Yield = 19.1 mg (59%).

^{1}H NMR (400 MHz, C_6D_6): δ 9.84 (1H, br, -CH(O)), 7.13-6.91 (8H, br, ArH(DIPP), m-CH(Mes)), 6.33 (2H, br, m-ArH(mesitaldehyde)), 5.57 (1H, s, γ-CH), 3.84 (2H, br, -CH(CH_3)$_2$), 3.40 (2H, br, -CH(CH_3)$_2$), 2.35 (3H, s, p-CH_3(Mes)), 2.04 (6H, br, o-CH_3(Mes)), 1.77 (3H, br, p-CH_3(mesitaldehyde)), 1.33 (12H, d, $^3J_{HH}$ = 6.8 Hz, -CH(CH_3)$_2$), 1.29 (18H, s, -C(CH_3)$_3$), 1.17 (12H, br, -CH(CH_3)$_2$), 1.02 (6H, br, o-CH_3(mesitaldehyde)) ppm.

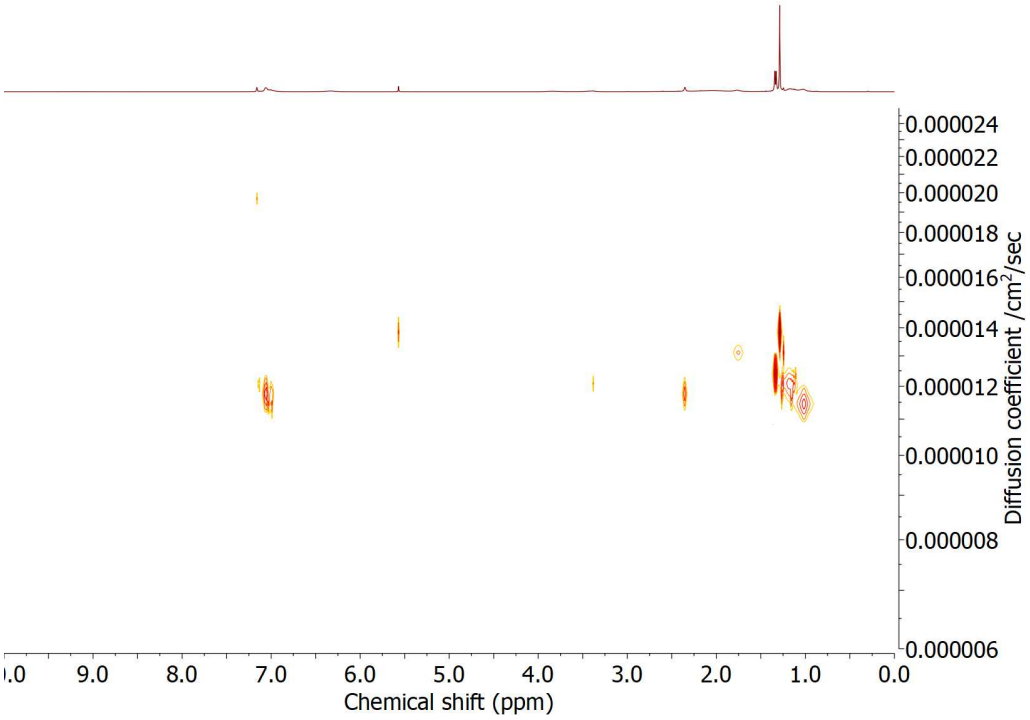

Figure 7.29: DOSY NMR spectrum of **4.8**.

*Reactions of **4.6a–h** with mesitaldehyde*

Compound **4.6** (26.5 mg, 0.04 mmol) was dissolved in C_6D_6 (0.5 mL) in a J. Youngs NMR tube before the respective Lewis base (NEt_3 (**a**, 5.6 μL, 0.04 mmol), pyridine (**c**, 3.2 μL, 0.04 mmol), 2-methylpyridine (**d**, 4.0 μL, 0.04 mmol), 2,6-dimethylpyridine (**e**, 4.7 μL, 0.04 mmol), PPh_3 (**f**, 10.5 mg, 0.04 mmol), PEt_3 (**g**, 5.9 μL, 0.04 mmol), or P^tBu_3 (**h**, 8.1 mg, 0.04 mmol)) was added. Mesitaldehyde (5.9 μL, 0.04 mmol) was then added, before NMR spectra were collected. The reactions of **4.6a** and **4.6e-h** resulted in the formation of **4.8** with no further reaction taking place. No reaction was seen with **4.6c** and **4.6d**.

7.4.9 Reactions of 4.6 and 4.6a–h with 3-pentanone

*Synthesis of **4.9***

Compound **4.6** (26.5 mg, 0.04 mmol) was dissolved in C_6D_6 (0.5 mL) before 3-

pentanone (4.2 μL, 0.04 mmol) was added, with no visible colour change occurring upon formation of **4.9**.

^{1}H NMR (400 MHz, C_6D_6): δ 7.15-6.95 (8H, m, Ar*H*), 5.51 (1H, s, γ-C*H*), 3.79 (2H, br, -C*H*$(CH_3)_2$), 3.35 (2H, br, -C*H*$(CH_3)_2$), 2.62 (4H, br, C(CH_2CH$_3)_2$), 2.41 (3H, s, *p*-CH_3(Mes)), 1.99 (6H, br, *o*-CH_3(Mes)), 1.54-0.91 (30H, br, C(CH_2C$H_3)_2$, -CH(C$H_3)_2$), 1.27 (18H, s, -C(C$H_3)_3$), 1.17 (12H, br, -CH(C$H_3)_2$) ppm.

*Reactions of **4.6e–g** with 3-pentanone*

Compound **4.6** (26.5 mg, 0.04 mmol) was dissolved in C_6D_6 (0.5 mL) in a J. Youngs NMR tube before the respective Lewis base (2,6-dimethylpyridine (**e**, 4.7 μL, 0.04 mmol), PPh_3 (**f**, 10.5 mg, 0.04 mmol), PEt_3 (**g**, 5.9 μL, 0.04 mmol)) was added. 3-Pentanone (4.2 μL, 0.04 mmol) was then added, before NMR spectra were collected. All reactions resulted in the formation of **4.9** with no further reaction taking place.

7.4.10 Hydrosilylation reactions

Attempted hydrosilylation of benzaldehyde

Compounds **4.6** (26.5 mg, 0.04 mmol), benzaldehyde (4.1 μL, 0.04 mmol), triethylsilane (6.4 μL, 0.04 mmol), and the Lewis base (2,6-dimethylpyridine (**e**, 4.7 μL, 0.04 mmol) or PEt_3 (**g**, 5.9 μL, 0.04 mmol)) were combined in C_6D_6 (0.5 mL) in and J. Youngs NMR tube. The reactions were heated to 80 °C and monitored by ^{1}H, ^{31}P, and ^{29}Si-DEPT NMR spectroscopy for 14 days. No reaction was seen in either case.

Attempted hydrosilylation of 3-pentanone

Compounds **4.6** (26.5 mg, 0.04 mmol), 3-pentanone (4.2 μL, 0.04 mmol), triethylsilane (6.4 μL, 0.04 mmol), and the Lewis base (2,6-dimethylpyridine (**e**, 4.7 μL, 0.04 mmol) or PEt_3 (**g**, 5.9 μL, 0.04 mmol)) were combined in C_6D_6 (0.5 mL) in a J. Youngs NMR tube. The reactions were heated to 80 °C and monitored by ^{1}H, ^{31}P, and ^{29}Si-DEPT NMR spectroscopy for 7 days. No reaction was seen in either case.

7.4.11 Catalytic dehydrocoupling of $Me_2NH{\cdot}BH_3$

*Reaction of **4.6** with $Me_2NH{\cdot}BH_3$*

In a glovebox, **4.6** (30 mg, 0.045 mmol) and $Me_2NH{\cdot}BH_3$ (2.7 mg, 0.045 mmol) were weighed into separate vials and dissolved in C_6D_6 (0.5 mL). The two solutions were then combined, and the fully mixed solution was transferred to a quartz J. Youngs NMR tube before the relevant spectra were then collected.

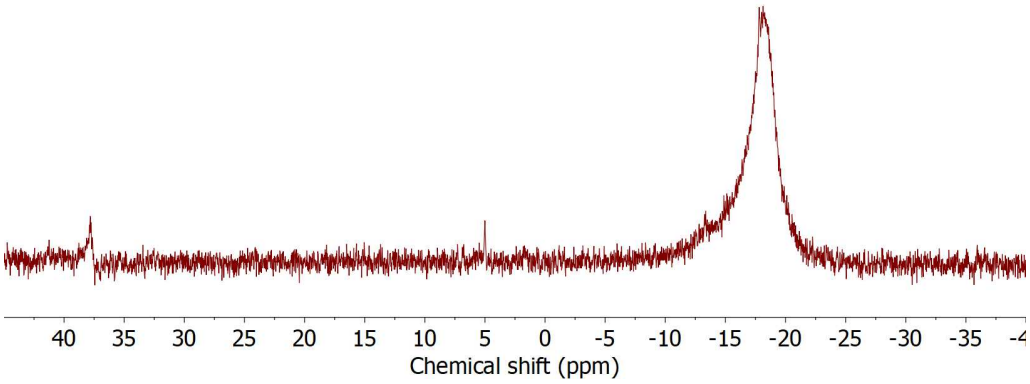

Figure 7.30: $^{11}B\{^{1}H\}$ NMR spectrum (25 °C, C_6D_6, 5 min) for the reaction between $Me_2NH{\cdot}BH_3$ and **4.6**. $Me_2NH{\cdot}BH_3$ and $Me_2NH–BH_2–Me_2N–BH_3$ (-18.6 ppm), $[Me_2N–BH_2]_2$ (5 ppm), $Me_2N{=}BH_2$ (37.8 ppm).

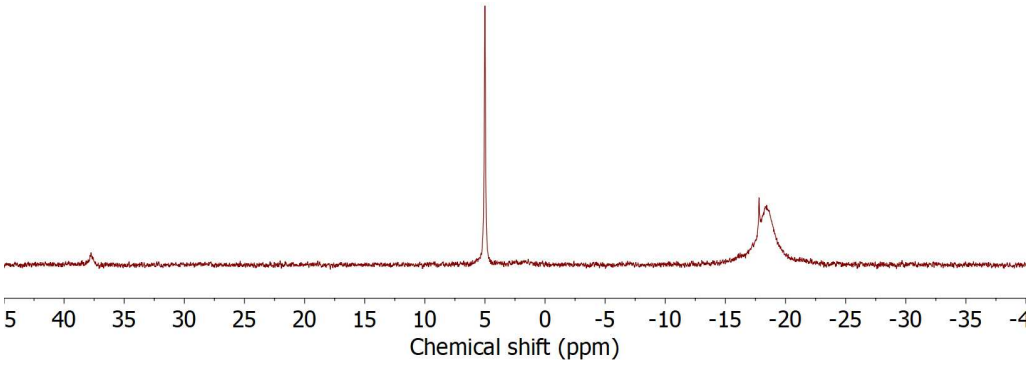

Figure 7.31: $^{11}B\{^{1}H\}$ NMR spectrum (25 °C, C_6D_6, 20 h) for the reaction between $Me_2NH{\cdot}BH_3$ and **4.6**. $Me_2NH{\cdot}BH_3$ and $Me_2NH–BH_2–Me_2N–BH_3$ (-18.6 ppm), $[Me_2N–BH_2]_2$ (5 ppm), $Me_2N{=}BH_2$ (37.8 ppm).

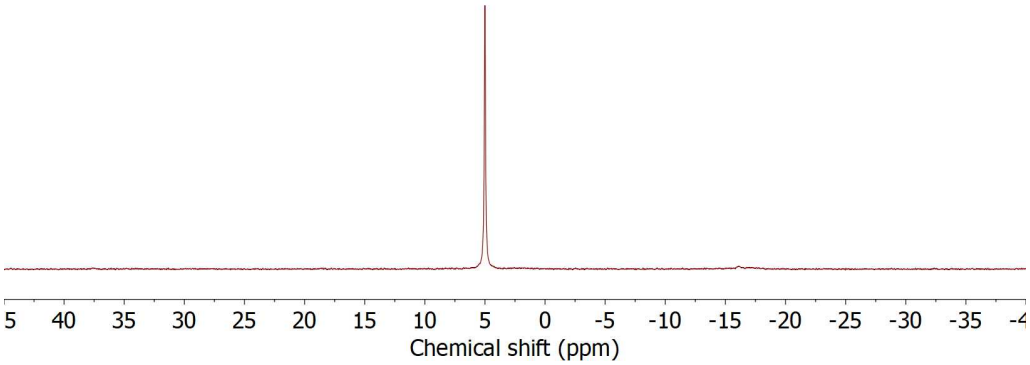

Figure 7.32: $^{11}B\{^{1}H\}$ NMR spectrum (25 °C, C_6D_6, 4 days) for the reaction between $Me_2NH{\cdot}BH_3$ and **4.6**. $Me_2NH{\cdot}BH_3$ and $Me_2NH–BH_2–Me_2N–BH_3$ (-18.6 ppm), $[Me_2N–BH_2]_2$ (5 ppm).

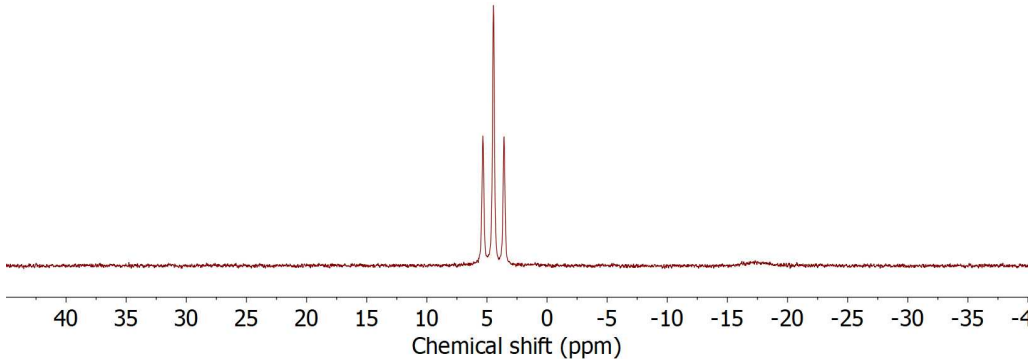

Figure 7.33: ^{11}B NMR spectrum (25 °C, C_6D_6, 4 days) for the reaction between $Me_2NH{\cdot}BH_3$ and **4.6**. $Me_2NH{\cdot}BH_3$ and Me_2NH–BH_2–Me_2N–BH_3 (-18.6 ppm), [Me_2N–BH_2]$_2$ (5 ppm).

*Reaction of **4.6a–h** with $Me_2NH{\cdot}BH_3$*

In a glovebox, **4.6** (11.9 mg, 0.018 mmol) and $Me_2NH{\cdot}BH_3$ (10.6 mg, 0.18 mmol) were weighed into separate vials and dissolved in C_6D_6 (0.5 mL). The relevant Lewis base (**a** = NEt_3 (2.5 μL, 0.018 mmol), **b** = $^{i}Pr_2NEt$ (3.2 μL, 0.018 mmol), **c** = pyridine (1.5 μL, 0.018 mmol), **d** = 2-methylpyridine (1.8 μL, 0.018 mmol), **e** = 2,6-dimethylpyridine (2.1 μL, 0.018 mmol), **f** = PPh_3 (4.7 mg, 0.018 mmol), **g** = PEt_3 (2.7 μL, 0.018 mmol), **h** = P^tBu_3 (3.7 mg, 0.018 mmol)) was then added to **4.6**. The two solutions were then combined, and the fully mixed solution was transferred to a quartz J. Youngs NMR tube before the relevant spectra were then collected. No reaction was seen for **4.6c**.

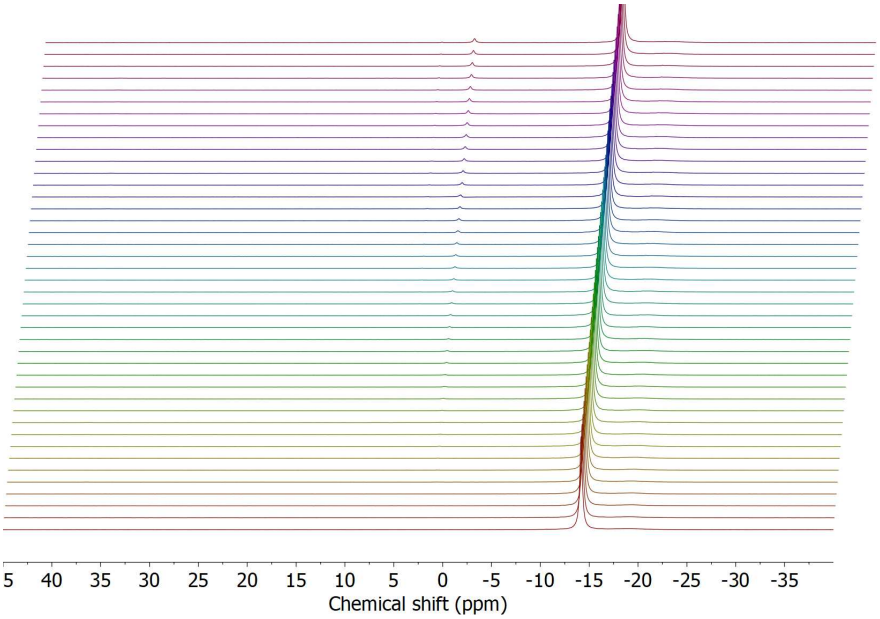

Figure 7.34: ^{11}B{^{1}H} NMR spectra (25 °C, C_6D_6) for the reaction between $Me_2NH{\cdot}BH_3$ and 10 mol% **4.6a**. Each spectrum was obtained at an interval of 20 min. $Me_2NH{\cdot}BH_3$ and Me_2NH–BH_2–Me_2N–BH_3 (-18.6 ppm), [Me_2N–BH_2]$_2$ (5 ppm).

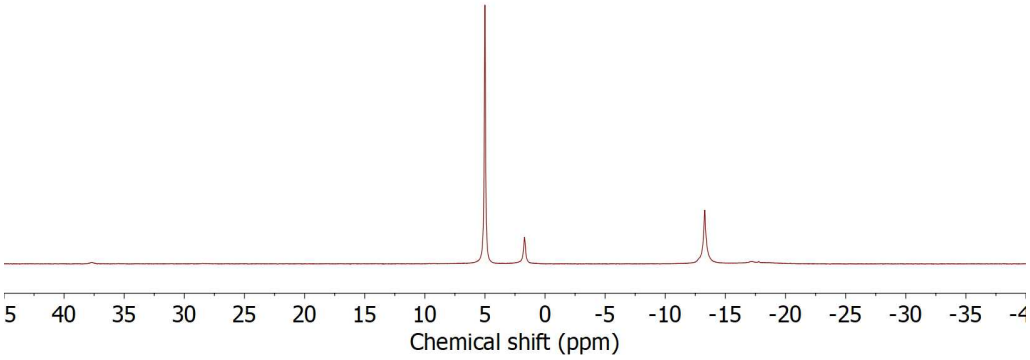

Figure 7.35: $^{11}B\{^{1}H\}$ NMR spectrum (25 °C, C_6D_6, 5 days) for the reaction between $Me_2NH{\cdot}BH_3$ and 10 mol% **4.6a**. $Me_2N(B_2H_5)$ (-17.3 ppm), $Me_2NH{\cdot}BH_3$ (-13.3), Me_2NH–BH_2–Me_2N–BH_3 (-1.7 ppm), $[Me_2N–BH_2]_2$ (5 ppm), $Me_2N{=}BH_2$ (37.7 ppm).

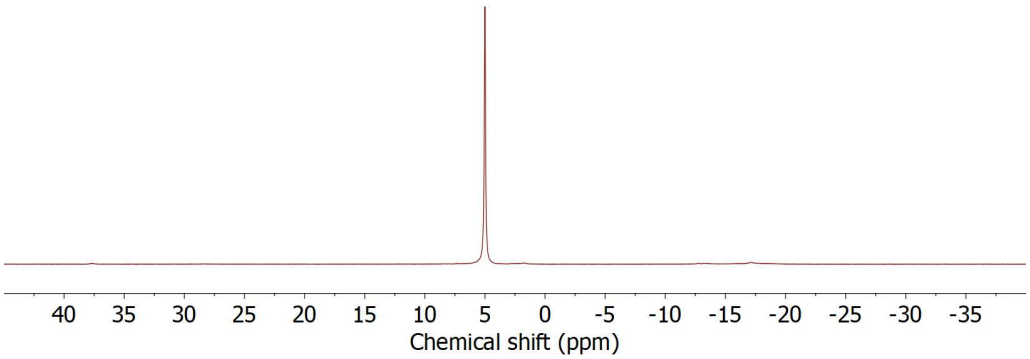

Figure 7.36: $^{11}B\{^{1}H\}$ NMR spectrum (25 °C, C_6D_6, 7 days) for the reaction between $Me_2NH{\cdot}BH_3$ and 10 mol% **4.6a**. $Me_2N(B_2H_5)$ (-17.3 ppm), $Me_2NH{\cdot}BH_3$ (-13.3), Me_2NH–BH_2–Me_2N–BH_3 (-1.7 ppm), $[Me_2N–BH_2]_2$ (5 ppm), $Me_2N{=}BH_2$ (37.7 ppm).

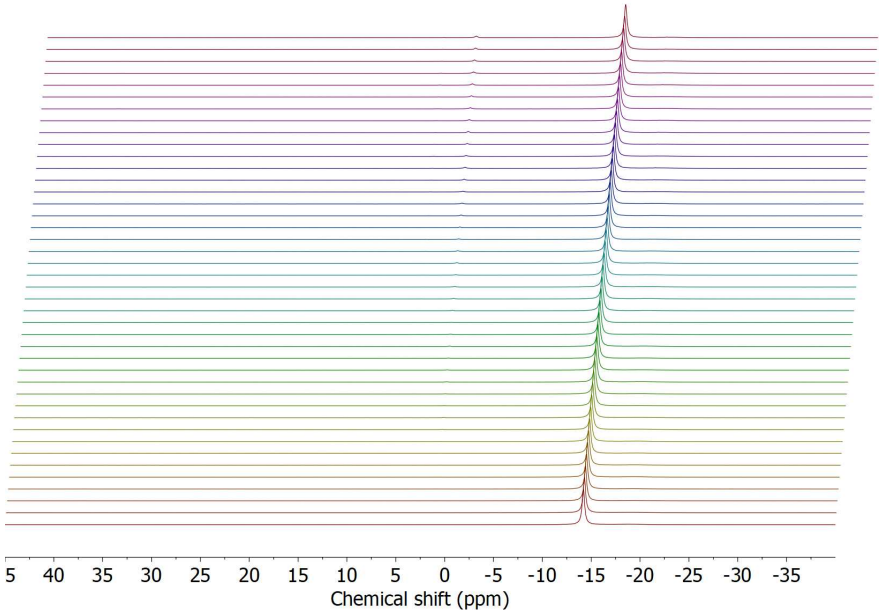

Figure 7.37: $^{11}B\{^{1}H\}$ NMR spectra (25 °C, C_6D_6) for the reaction between $Me_2NH{\cdot}BH_3$ and 10 mol% **4.6b**. Each spectrum was obtained at an interval of 20 min. $Me_2NH{\cdot}BH_3$ and $Me_2NH–BH_2–Me_2N–BH_3$ (-18.6 ppm), $[Me_2N–BH_2]_2$ (5 ppm).

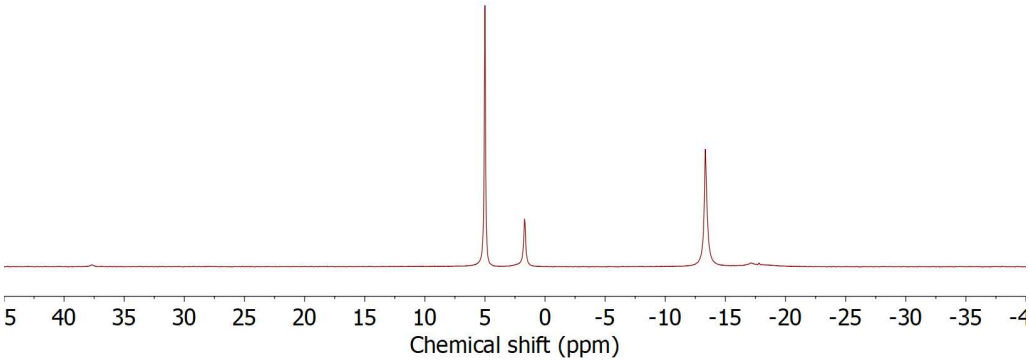

Figure 7.38: $^{11}B\{^{1}H\}$ NMR spectrum (25 °C, C_6D_6, 6 days) for the reaction between $Me_2NH{\cdot}BH_3$ and 10 mol% **4.6b**. $Me_2N(B_2H_5)$ (-17.2 ppm), $Me_2NH{\cdot}BH_3$ (-13.4), $Me_2NH–BH_2–Me_2N–BH_3$ (-1.7 ppm), $[Me_2N–BH_2]_2$ (5 ppm), $Me_2N{=}BH_2$ (37.7 ppm).

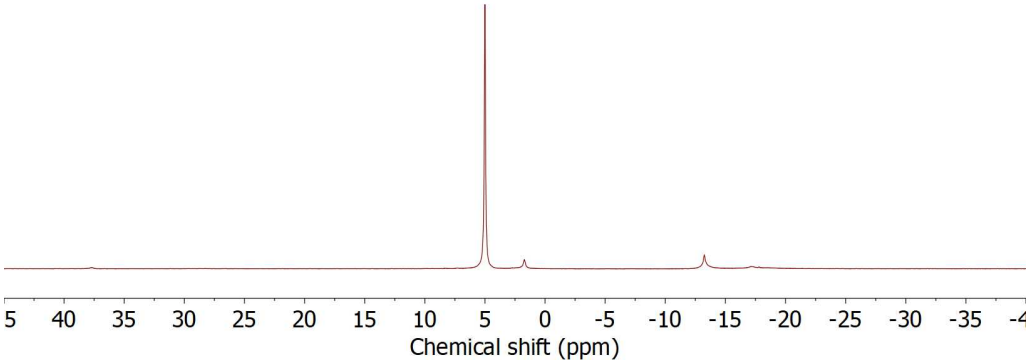

Figure 7.39: $^{11}B\{^{1}H\}$ NMR spectrum (25 °C, C_6D_6, 8 days) for the reaction between $Me_2NH{\cdot}BH_3$ and 10 mol% **4.6b**. $Me_2N(B_2H_5)$ (-17.2 ppm), $Me_2NH{\cdot}BH_3$ (-13.4), Me_2NH–BH_2–Me_2N–BH_3 (-1.7 ppm), $[Me_2N–BH_2]_2$ (5 ppm), $Me_2N{=}BH_2$ (37.7 ppm).

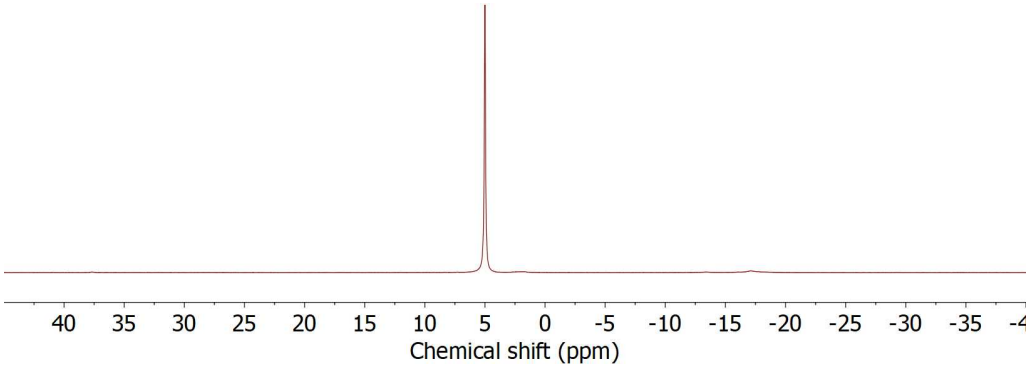

Figure 7.40: $^{11}B\{^{1}H\}$ NMR spectrum (25 °C, C_6D_6, 9 days) for the reaction between $Me_2NH{\cdot}BH_3$ and 10 mol% **4.6b**. $Me_2N(B_2H_5)$ (-17.2 ppm), $Me_2NH{\cdot}BH_3$ (-13.4), Me_2NH–BH_2–Me_2N–BH_3 (-1.7 ppm), $[Me_2N–BH_2]_2$ (5 ppm), $Me_2N{=}BH_2$ (37.7 ppm).

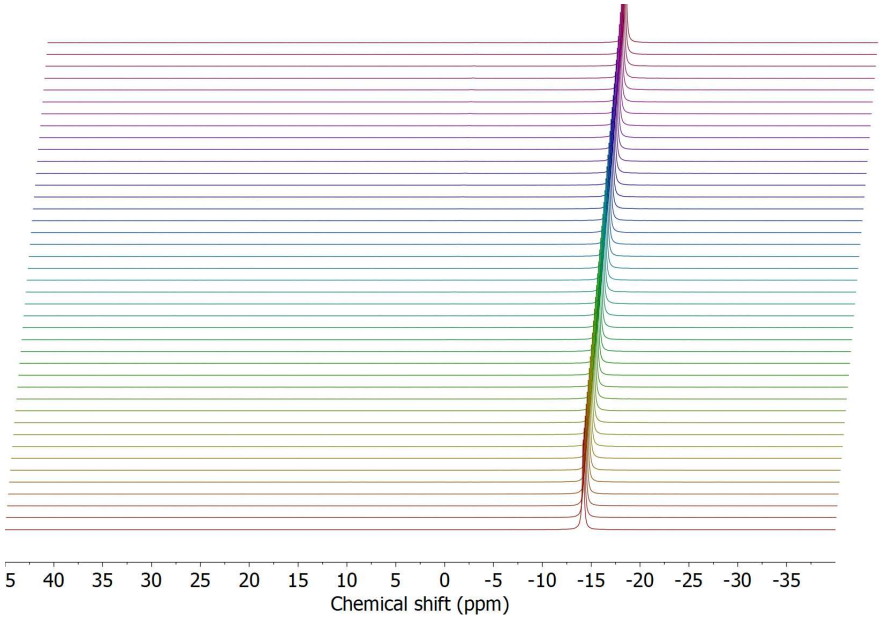

Figure 7.41: $^{11}B\{^{1}H\}$ NMR spectra (25 °C, C_6D_6) for the reaction between $Me_2NH{\cdot}BH_3$ and 10 mol% **4.6d**. Each spectrum was obtained at an interval of 20 min. $Me_2NH{\cdot}BH_3$ and $Me_2NH–BH_2–Me_2N–BH_3$ (-18.6 ppm), $[Me_2N–BH_2]_2$ (5 ppm).

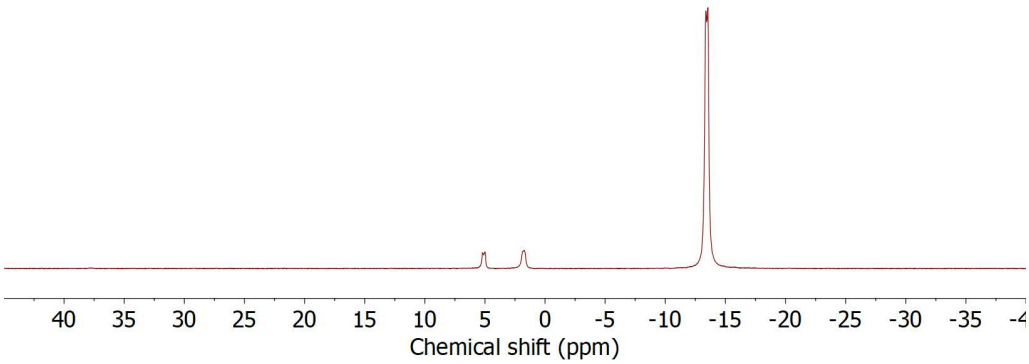

Figure 7.42: $^{11}B\{^{1}H\}$ NMR spectrum (25 °C, C_6D_6, 6 days) for the reaction between $Me_2NH{\cdot}BH_3$ and 10 mol% **4.6d**. $Me_2NH{\cdot}BH_3$ (-13.4), $Me_2NH–BH_2–Me_2N–BH_3$ (-1.7 ppm), $[Me_2N–BH_2]_2$ (5 ppm).

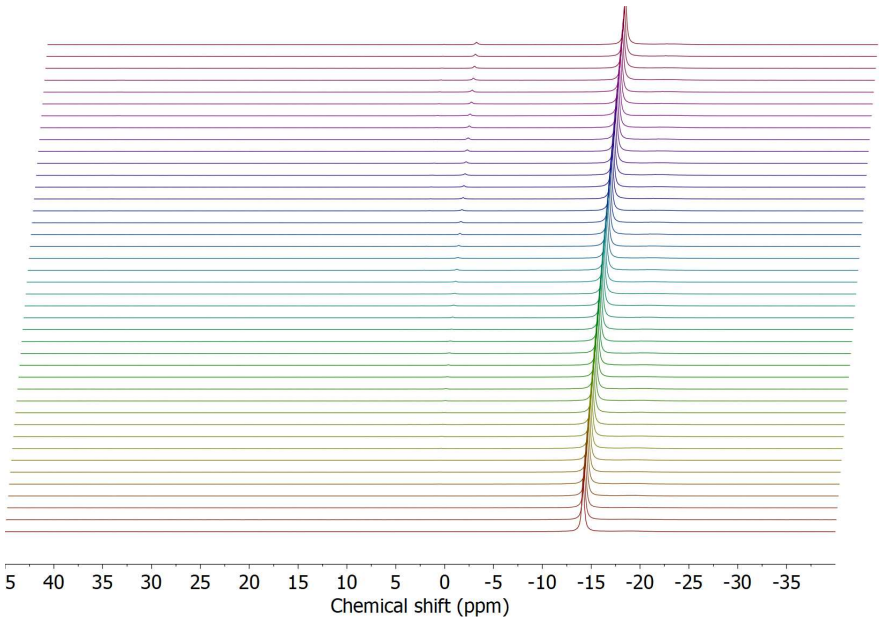

Figure 7.43: $^{11}B\{^{1}H\}$ NMR spectra (25 °C, C_6D_6) for the reaction between $Me_2NH{\cdot}BH_3$ and 10 mol% **4.6e**. Each spectrum was obtained at an interval of 20 min. $Me_2NH{\cdot}BH_3$ (-13.4 ppm), $Me_2NH–BH_2–Me_2N–BH_3$ (1.7 ppm), $[Me_2N–BH_2]_2$ (5 ppm).

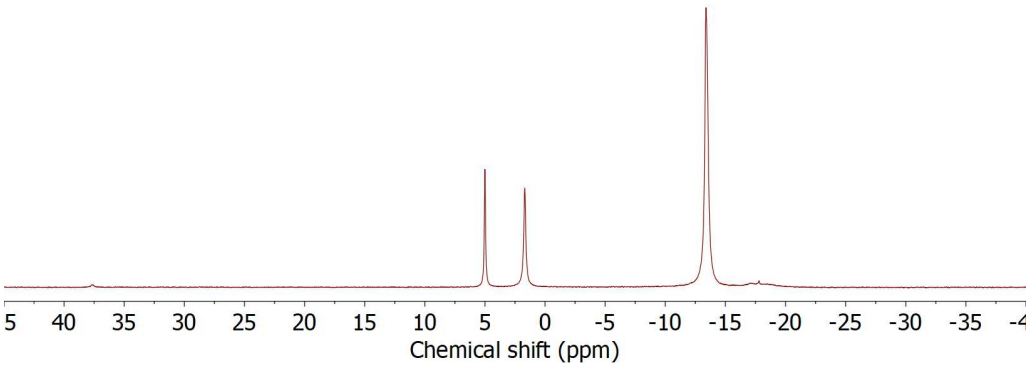

Figure 7.44: $^{11}B\{^{1}H\}$ NMR spectrum (25 °C, C_6D_6, 4 days) for the reaction between $Me_2NH{\cdot}BH_3$ and 10 mol% **4.6e**. $Me_2N(B_2H_5)$ (-17.2 ppm), $Me_2NH{\cdot}BH_3$ (-13.4), $Me_2NH–BH_2–Me_2N–BH_3$ (-1.7 ppm), $[Me_2N–BH_2]_2$ (5 ppm), $Me_2N{=}BH_2$ (37.7 ppm).

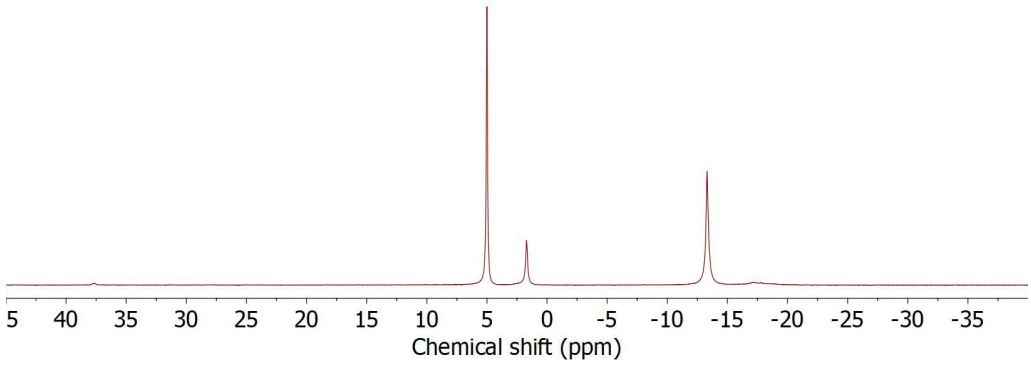

Figure 7.45: $^{11}B\{^{1}H\}$ NMR spectrum (25 °C, C_6D_6, 7 days) for the reaction between $Me_2NH{\cdot}BH_3$ and 10 mol% **4.6e**. $Me_2N(B_2H_5)$ (-17.2 ppm), $Me_2NH{\cdot}BH_3$ (-13.4), Me_2NH–BH_2–Me_2N–BH_3 (-1.7 ppm), $[Me_2N–BH_2]_2$ (5 ppm), $Me_2N{=}BH_2$ (37.7 ppm).

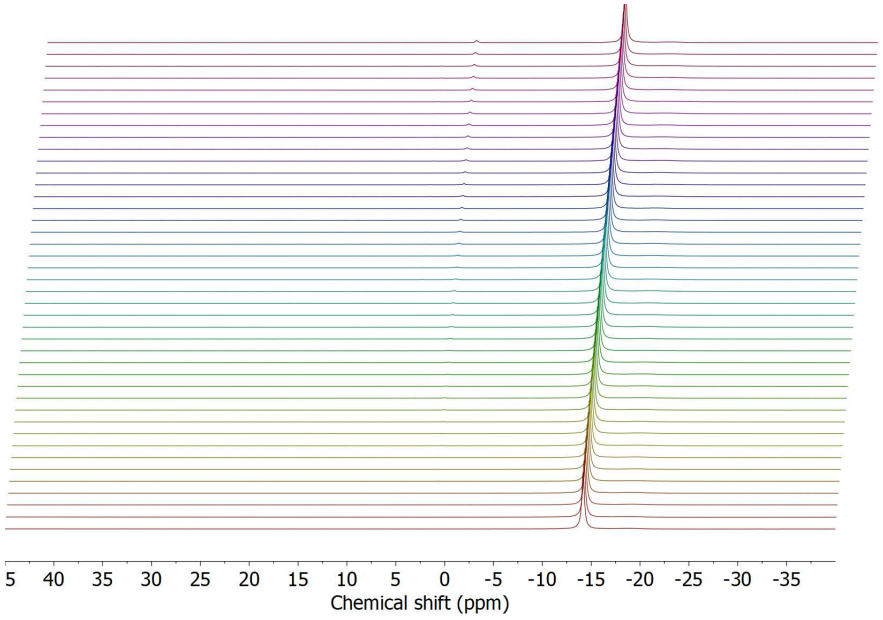

Figure 7.46: $^{11}B\{^{1}H\}$ NMR spectra (25 °C, C_6D_6) for the reaction between $Me_2NH{\cdot}BH_3$ and 10 mol% **4.6f**. Each spectrum was obtained at an interval of 20 min. $Me_2NH{\cdot}BH_3$ (-13.4 ppm), Me_2NH–BH_2–Me_2N–BH_3 (1.7 ppm), $[Me_2N–BH_2]_2$ (5 ppm).

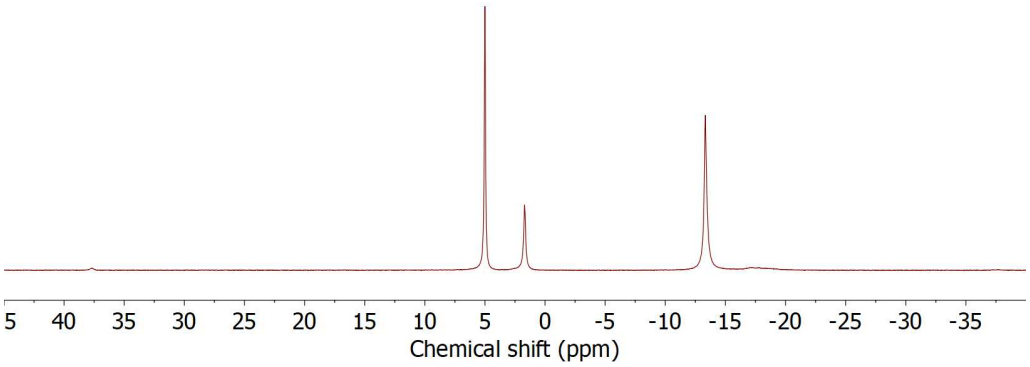

Figure 7.47: $^{11}B\{^{1}H\}$ NMR spectrum (25 °C, C_6D_6, 5 days) for the reaction between $Me_2NH{\cdot}BH_3$ and 10 mol% **4.6f**. $Me_2N(B_2H_5)$ (-17.2 ppm), $Me_2NH{\cdot}BH_3$ (-13.4), Me_2NH–BH_2–Me_2N–BH_3 (-1.7 ppm), $[Me_2N–BH_2]_2$ (5 ppm), $Me_2N{=}BH_2$ (37.7 ppm).

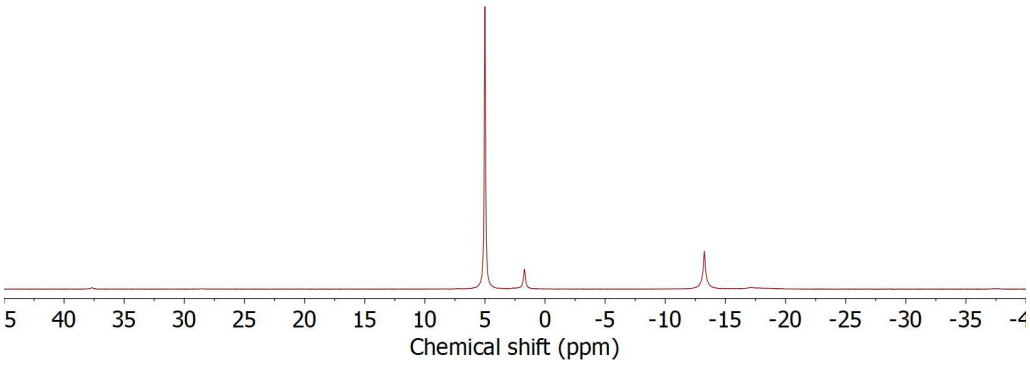

Figure 7.48: $^{11}B\{^{1}H\}$ NMR spectrum (25 °C, C_6D_6, 7 days) for the reaction between $Me_2NH{\cdot}BH_3$ and 10 mol% **4.6f**. $Me_2N(B_2H_5)$ (-17.2 ppm), $Me_2NH{\cdot}BH_3$ (-13.4), Me_2NH–BH_2–Me_2N–BH_3 (-1.7 ppm), $[Me_2N–BH_2]_2$ (5 ppm), $Me_2N{=}BH_2$ (37.7 ppm).

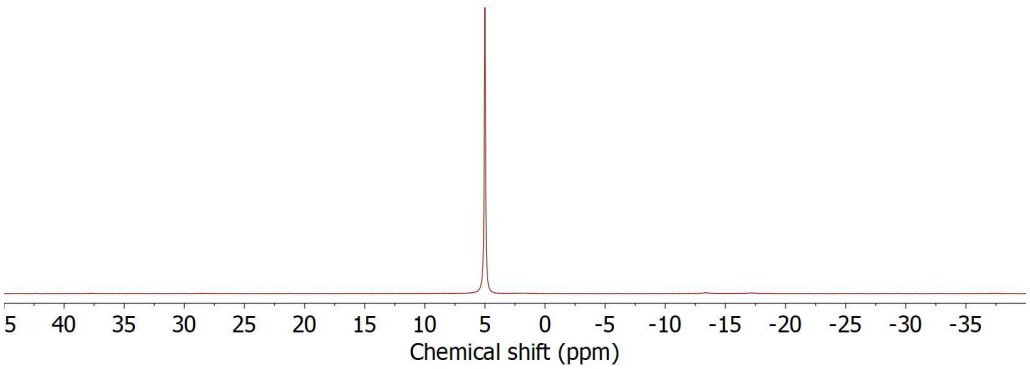

Figure 7.49: $^{11}B\{^{1}H\}$ NMR spectrum (25 °C, C_6D_6, 10 days) for the reaction between $Me_2NH{\cdot}BH_3$ and 10 mol% **4.6f**. $Me_2N(B_2H_5)$ (-17.2 ppm), $Me_2NH{\cdot}BH_3$ (-13.4), Me_2NH–BH_2–Me_2N–BH_3 (-1.7 ppm), $[Me_2N–BH_2]_2$ (5 ppm), $Me_2N{=}BH_2$ (37.7 ppm).

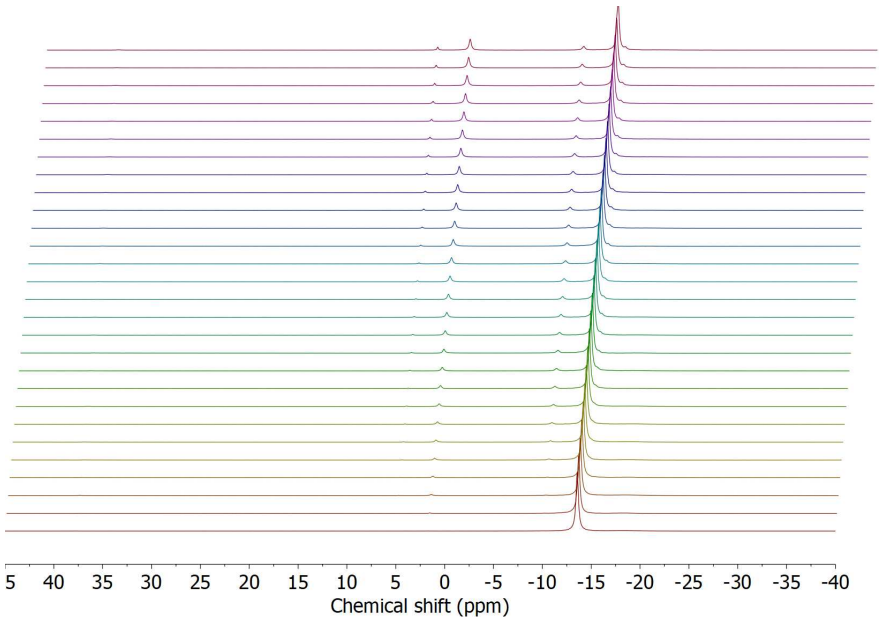

Figure 7.50: $^{11}B\{^{1}H\}$ NMR spectra (25 °C, C_6D_6) for the reaction between $Me_2NH{\cdot}BH_3$ and 10 mol% **4.6g**. Each spectrum was obtained at an interval of 30 min. $Me_2N(B_2H_5)$ (-17.2 ppm), $Me_2NH{\cdot}BH_3$ (-13.4 ppm), $Me_2NH–BH_2–Me_2N–BH_3$ (1.7 ppm), $[Me_2N–BH_2]_2$ (5 ppm), $Me_2N{=}BH_2$ (37.7 ppm).

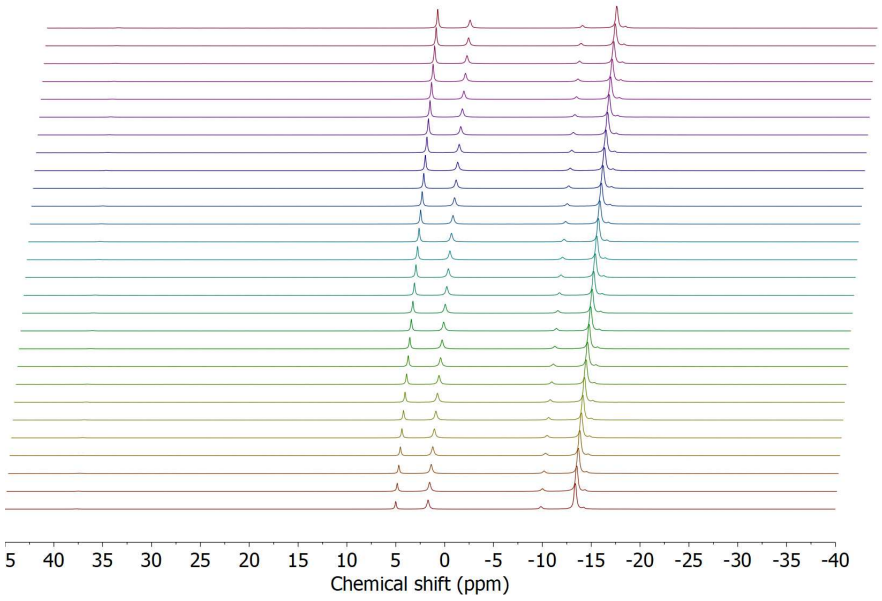

Figure 7.51: $^{11}B\{^{1}H\}$ NMR spectra (25 °C, C_6D_6) for the reaction between $Me_2NH{\cdot}BH_3$ and 10 mol% **4.6g**. Each spectrum was obtained at an interval of 30 min. First scan after 1 day. $Me_2N(B_2H_5)$ (-17.2 ppm), $Me_2NH{\cdot}BH_3$ (-13.4 ppm), $Me_2NH–BH_2–Me_2N–BH_3$ (1.7 ppm), $[Me_2N–BH_2]_2$ (5 ppm), $Me_2N{=}BH_2$ (37.7 ppm).

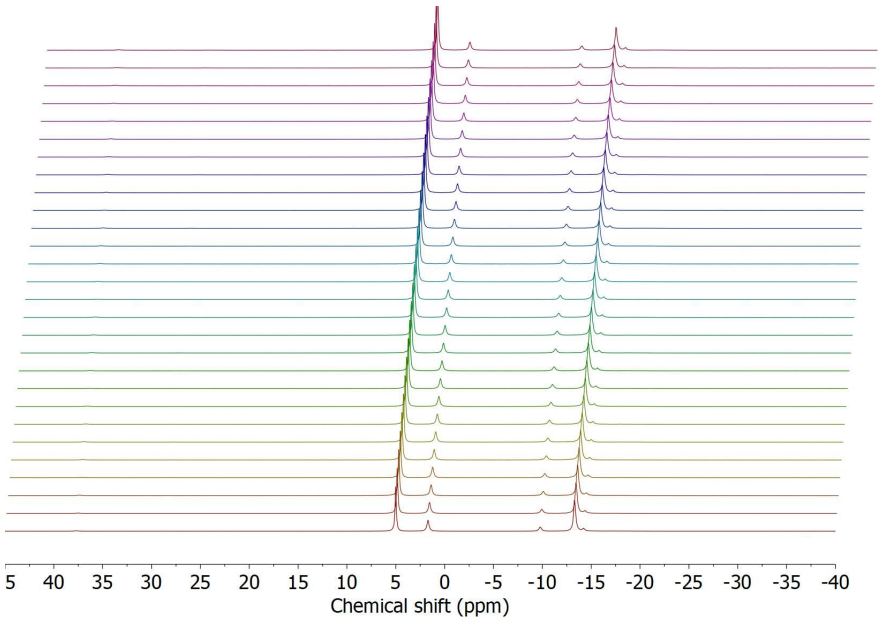

Figure 7.52: $^{11}B\{^{1}H\}$ NMR spectra (25 °C, C_6D_6) for the reaction between $Me_2NH{\cdot}BH_3$ and 10 mol% **4.6g**. Each spectrum was obtained at an interval of 30 min. First scan after 2 days. $Me_2N(B_2H_5)$ (-17.2 ppm), $Me_2NH{\cdot}BH_3$ (-13.4 ppm), $Me_2NH–BH_2–Me_2N–BH_3$ (1.7 ppm), $[Me_2N–BH_2]_2$ (5 ppm), $Me_2N{=}BH_2$ (37.7 ppm).

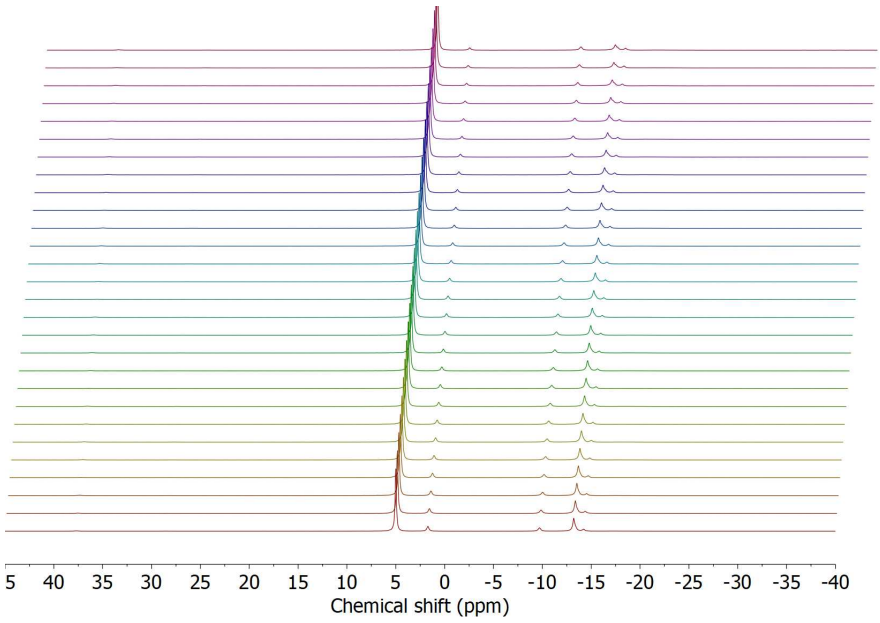

Figure 7.53: $^{11}B\{^{1}H\}$ NMR spectra (25 °C, C_6D_6) for the reaction between $Me_2NH{\cdot}BH_3$ and 10 mol% **4.6g**. Each spectrum was obtained at an interval of 30 min. First scan after 3 days. $Me_2N(B_2H_5)$ (-17.2 ppm), $Me_2NH{\cdot}BH_3$ (-13.4 ppm), $Me_2NH–BH_2–Me_2N–BH_3$ (1.7 ppm), $[Me_2N–BH_2]_2$ (5 ppm), $Me_2N{=}BH_2$ (37.7 ppm).

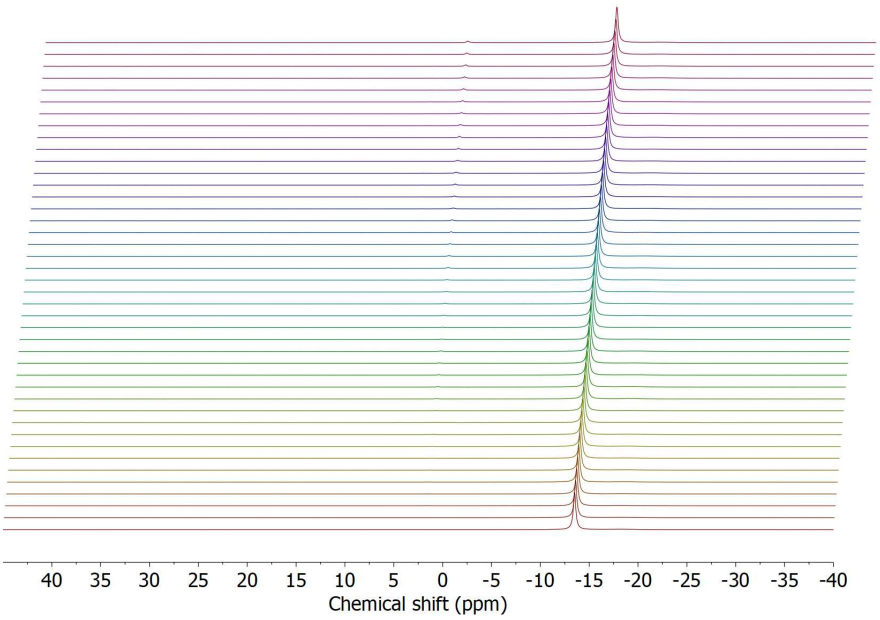

Figure 7.54: $^{11}B\{^{1}H\}$ NMR spectra (25 °C, C_6D_6) for the reaction between $Me_2NH{\cdot}BH_3$ and 10 mol% **4.6h**. Each spectrum was obtained at an interval of 20 min. $Me_2N(B_2H_5)$ (-17.2 ppm), $Me_2NH{\cdot}BH_3$ (-13.4 ppm), $Me_2NH–BH_2–Me_2N–BH_3$ (1.7 ppm), $[Me_2N–BH_2]_2$ (5 ppm), $Me_2N{=}BH_2$ (37.7 ppm).

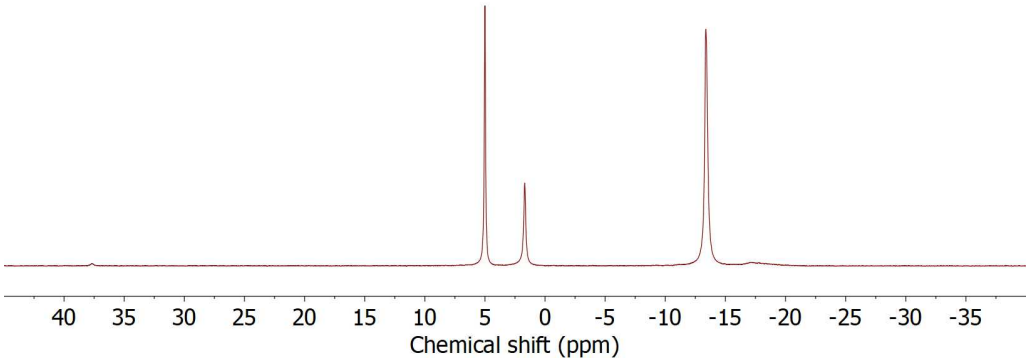

Figure 7.55: $^{11}B\{^{1}H\}$ NMR spectrum (25 °C, C_6D_6, 6 days) for the reaction between $Me_2NH{\cdot}BH_3$ and 10 mol% **4.6h**. $Me_2N(B_2H_5)$ (-17.2 ppm), $Me_2NH{\cdot}BH_3$ (-13.4 ppm), $Me_2NH–BH_2–Me_2N–BH_3$ (-1.7 ppm), $[Me_2N–BH_2]_2$ (5 ppm), $Me_2N{=}BH_2$ (37.7 ppm).

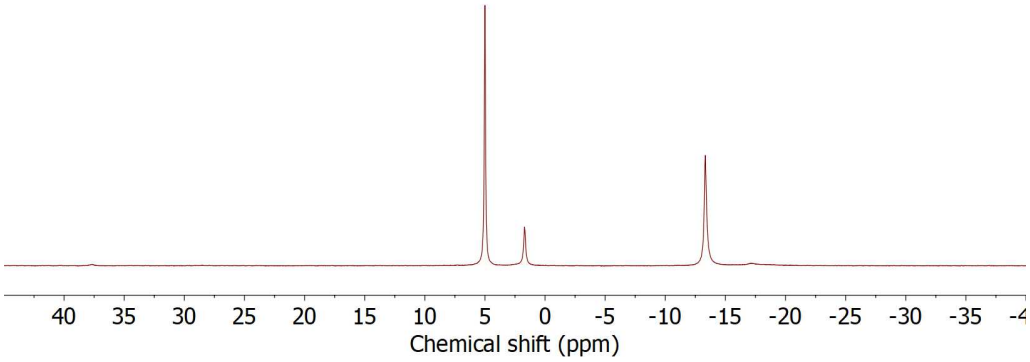

Figure 7.56: $^{11}B\{^{1}H\}$ NMR spectrum (25 °C, C_6D_6, 8 days) for the reaction between $Me_2NH{\cdot}BH_3$ and 10 mol% **4.6h**. $Me_2N(B_2H_5)$ (-17.2 ppm), $Me_2NH{\cdot}BH_3$ (-13.4 ppm), $Me_2NH–BH_2–Me_2N–BH_3$ (-1.7 ppm), $[Me_2N–BH_2]_2$ (5 ppm), $Me_2N{=}BH_2$ (37.7 ppm).

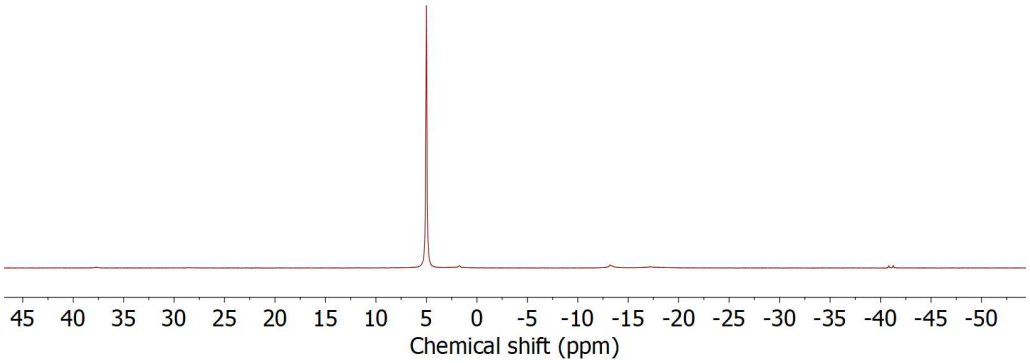

Figure 7.57: $^{11}B\{^{1}H\}$ NMR spectrum (25 °C, C_6D_6, 11 days) for the reaction between $Me_2NH{\cdot}BH_3$ and 10 mol% **4.6h**. $Me_2N(B_2H_5)$ (-17.2 ppm), $Me_2NH{\cdot}BH_3$ (-13.4 ppm), $Me_2NH–BH_2–Me_2N–BH_3$ (-1.7 ppm), $[Me_2N–BH_2]_2$ (5 ppm), $Me_2N{=}BH_2$ (37.7 ppm).

7.4.12 Catalytic dehydrocoupling of $Me_2NH{\cdot}BH_3$ at 60 °C

In a glovebox, **4.6** (11.9 mg, 0.018 mmol) and $Me_2NH{\cdot}BH_3$ (10.6 mg, 0.18 mmol) were weighed into separate vials and dissolved in C_6D_6 (0.5 mL). The two solutions were then combined, and the fully mixed solution was transferred to a quartz J. Youngs NMR tube before the relevant spectra were then collected in a NMR spectrometer set to 60 °C.

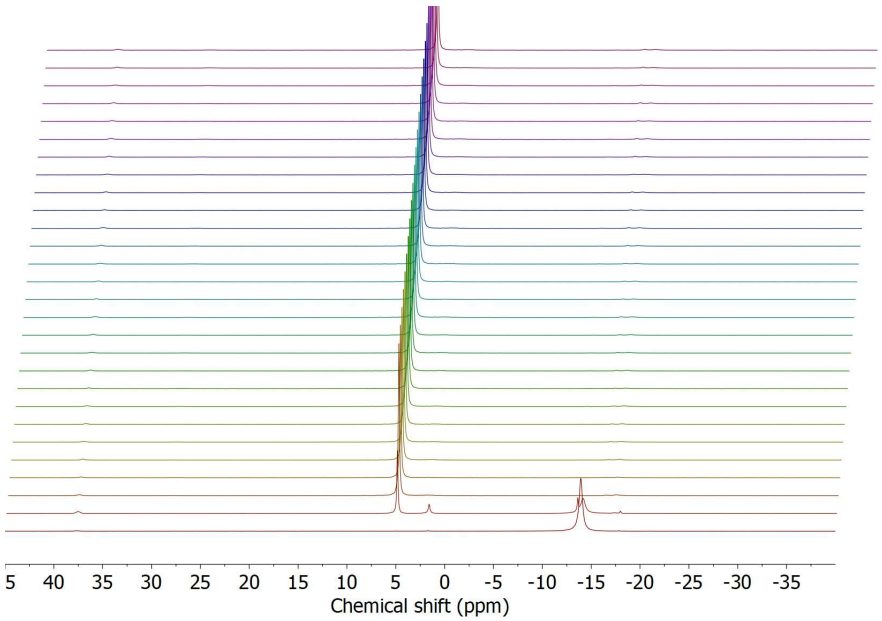

Figure 7.58: $^{11}B\{^1H\}$ NMR spectra (60 °C, C_6D_6) for the reaction between $Me_2NH{\cdot}BH_3$ and 10 mol% **4.6**. Each spectrum was obtained at an interval of 30 min. $Me_2N(B_2H_5)$ (-17.8 ppm), $Me_2NH{\cdot}BH_3$ (-13.5 ppm), $Me_2NH{-}BH_2{-}Me_2N{-}BH_3$ (1.7 and -14.0 ppm), $[Me_2N{-}BH_2]_2$ (5 ppm), $Me_2N{=}BH_2$ (37.6 ppm).

7.4.13 X-ray diffraction data

Table 7.2: Crystal data and structure refinement for **4.6** and **4.6c**.

Identification code	**4.6**	**4.6c**
Empirical formula	$C_{44}H_{64}MgN_2O$	$C_{50.5}H_{72.5}MgN_3O$
Formula weight	661.28	761.92
Temperature/K	100(2)	100(2)
Crystal system	monoclinic	triclinic
Space group	$P2_1/c$	P-1
a/Å	17.1914(5)	12.4395(3)
b/Å	10.5569(3)	19.9806(5)
c/Å	22.3355(6)	20.6648(5)
$\alpha/^\circ$	90	71.211(2)
$\beta/^\circ$	96.819(2)	81.654(2)
$\gamma/^\circ$	90	73.135(2)
Volume/Å^3	4024.9(2)	4645.8(2)
Z	4	4
ρ_{calc}g/cm^3	1.091	1.089
μ/mm^{-1}	0.078	0.076
F(000)	1448.0	1666.0
Crystal size/mm^3	0.447 × 0.243 × 0.225	0.496 × 0.217 × 0.191
Radiation	MoK$_\alpha$ (λ = 0.71073)	MoK$_\alpha$ (λ = 0.71073)
2Θ range for data collection /°	3.672 to 55.998	2.564 to 53.05
Index ranges	-22 ≤ h ≤ 21, -13 ≤ h ≤ 13, -29 ≤ h ≤ 27	-15 ≤ h ≤ 15, -25 ≤ h ≤ 24, -25 ≤ h ≤ 25
Reflections collected	34150	73938
R_{int} / R_{sigma}	0.0650 / 0.0675	0.0897 / 0.0890
Data/restraints/ parameters	9660/42/481	19179/45/1066
Goodness-of-fit on F^2	1.024	1.014
Final R indexes [I<=2σ (I)]	R_1 = 0.0510, wR_2 = 0.1162	R_1 = 0.0565, wR_2 = 0.1155
Final R indexes [all data]	R_1 = 0.0969, wR_2 = 0.1357	R_1 = 0.1100, wR_2 = 0.1370
Largest diff. peak/hole /e Å^{-3}	0.41/-0.24	0.39/-0.33

Table 7.3: Crystal data and structure refinement for **4.6d** and **4.8**.

Identification code	**4.6d**	**4.8**
Empirical formula	$C_{50}H_{71}MgN_3O$	$C_{54}H_{76}MgN_2O_2$
Formula weight	754.40	809.47
Temperature/K	100(2)	100(2)
Crystal system	monoclinic	monoclinic
Space group	$P2_1/c$	$P2_1/c$
a/Å	19.6608(5)	11.3144(9)
b/Å	12.4389(4)	21.3804(16)
c/Å	19.4252(6)	40.439(3)
$\alpha/^\circ$	90	90
$\beta/^\circ$	101.490(2)	91.098(2)
$\gamma/^\circ$	90	90
Volume/Å^3	4655.4(2)	9780.6(13)
Z	4	8
ρ_{calc}g/cm^3	1.076	1.099
μ/mm^{-1}	0.075	0.077
F(000)	1648.0	3536.0
Crystal size/mm^3	0.385 × 0.284 × 0.138	0.345 × 0.333 × 0.314
Radiation	MoK$_\alpha$ (λ = 0.71073)	MoK$_\alpha$ (λ = 0.71073)
2Θ range for data collection /°	3.898 to 55.878	2.771 to 52.744
Index ranges	-25 ≤ h ≤ 24, -16 ≤ h ≤ 16, -25 ≤ h ≤ 24	-14 ≤ h ≤ 14, -26 ≤ h ≤ 26, -50 ≤ h ≤ 50
Reflections collected	42121	79112
R_{int} / R_{sigma}	0.0615 / 0.0576	0.0752 / 0.0723
Data/restraints/ parameters	11148/0/514	20005/0/1102
Goodness-of-fit on F^2	1.021	1.014
Final R indexes [I<=2σ (I)]	R_1 = 0.0495, wR_2 = 0.1091	R_1 = 0.0554, wR_2 = 0.1039
Final R indexes [all data]	R_1 = 0.0878, wR_2 = 0.1240	R_1 = 0.0944, wR_2 = 0.1179
Largest diff. peak/hole /e Å^{-3}	0.32/-0.29	0.31/-0.27

7.5 Chapter 5 experimental

7.5.1 Synthesis of 5.7

Compound **5.2** (473 mg, 0.947 mmol) was dissolved in toluene (10 mL), before a toluene (10 mL) solution of **5.6** (309 mg, 0.947 mmol) was added dropwise at room temperature. The solution was heated to 50 °C and left to stir for 2 h, before it was cooled to rt, and all volatiles were removed in vacuo. The orange residue was then dissolved in hot hexane and filtered to give a pale yellow solution. The solvent volume was reduced, resulting in the formation of white crystals suitable for X-ray diffraction, which were washed with cold hexane (3 × 2 mL). Yield = 374 mg (52%).

^{1}H NMR (400 MHz, C_6D_6): δ 7.14 (6H, m, Ar*H*), 4.90 (1H, s, γ-C*H*), 3.24 (4H, *sept.*, -C*H*$(CH_3)_2$), 1.94 (2H, d, $^{2}J_{HP}$ = 5.6 Hz, -CH_2P^{t}Bu$_2$), 1.63 (6H, s, β-CH_3), 1.39 (12H, d, $^{3}J_{HH}$ = 6.8 Hz, -CH(CH_3)$_2$), 1.16 (12H, d, $^{3}J_{HH}$ = 6.8 Hz, -CH(CH_3)$_2$), 0.80 (18H, d, $^{3}J_{HP}$ = 11.7 Hz, -P(C(CH_3)$_3$)$_2$) ppm. ^{13}C NMR (125 MHz, C_6D_6): δ 171.0 (s, β-*C*-N), 145.5 (s, *i*-*C*), 142.5 (s, *o*-*C*), 126.0 (s, *p*-*C*), 124.3 (s, *m*-*C*), 95.5 (s, γ-*C*H), 31.6 (d, $^{1}J_{CP}$ = 14.7 Hz, *C*H$_2$), 30.0 (d, $^{2}J_{CP}$ = 12.6 Hz, P(*C*$(CH_3)_3)_2$), 28.9 (s, -*C*H$(CH_3)_2$), 25.2 (d, $^{1}J_{CP}$ = 15.0 Hz, P(*C*$(CH_3)_3)_2$), 25.1 (s, β-C*C*H$_3$), 24.6 and 24.6 (s, -CH(*C*H$_3$)$_2$) ppm. Remaining ^{13}C NMR signals too weak for detection. ^{31}P{^{1}H} NMR (162 MHz, C_6D_6): δ 12.5 (*sept.*, $^{4}J_{PF}$ = 11.7 Hz) ppm. ^{19}F NMR (376 MHz, C_6D_6): δ -77.0 (d, $^{4}J_{FP}$ = 11.7 Hz) ppm.

7.5.2 The reaction of 5.7 with hydrogen gas

Compound **5.7** (30 mg, 0.039 mmol) was dissolved in C_6D_6 (0.5 mL) in a J. Youngs NMR tube. The sample was degassed twice by freeze-pump-thaw, before being refilled with H_2 gas (1 bar). The sample was analysed by ^{1}H, ^{31}P, ^{31}P{^{1}H}, and ^{19}F NMR spectroscopy, with no change seen. The sample was heated at 80 °C for 16 h, with no further reaction occurring.

7.5.3 The reaction of 5.7 with carbon dioxide gas

Compound **5.7** (30 mg, 0.039 mmol) was dissolved in C_6D_6 (0.5 mL) in a J. Youngs NMR tube. The sample was degassed twice by freeze-pump-thaw, before being refilled with CO_2 gas (1 bar). The sample was analysed by ^{1}H, ^{31}P, ^{31}P{^{1}H}, and ^{19}F NMR spectroscopy. More than one new product was seen in the NMR; however, attempts to isolate them were unsuccessful, with other analytical techniques including mass spectrometry proving ineffectual due to the air sensitivity of the products.

7.5.4 The reaction of 5.7 with phenylacetylene-*d*

Compound **5.7** (30 mg, 0.039 mmol) was dissolved in C_6D_6 (0.5 mL) in a J. Youngs NMR tube. Phenylacetylene-*d* (4.3 μL, 0.039 mmol) was then added. The sample was analysed by ^{1}H, ^{2}H, and ^{31}P{^{1}H} NMR spectroscopy, with new NMR signals attributed to a Mg-(PhCCD) adduct which could not be isolated.

^{1}H NMR (400 MHz, C_6D_6): δ 7.67 (2H, m, *o*-C*H*), 7.19-7.07 (9H, m, *m*-Ar*H*, *p*-Ar*H*), 5.01 (1H, s, γ-C*H*), 3.56 (4H, *sept.*, $^{3}J_{HH}$ = 6.9 Hz, -C*H*(CH_3)$_2$),), 1.67 (2H, d, -CH_2P^{t}Bu$_2$), 1.64 (6H, s, β-CH_3), 1.28 (12H, d, $^{3}J_{HH}$ = 6.8 Hz, -CH(CH_3)$_2$), 1.09 (18H, d, $^{3}J_{HP}$ = 10.9 Hz, -P(C(CH_3)$_3$)$_2$), 0.40 (12H, d, $^{3}J_{HH}$ = 6.8 Hz, -CH(CH_3)$_2$) ppm. ^{2}H NMR (61 MHz, C$_6$D6): δ 2.68 (s) ppm. ^{31}P{^{1}H} NMR (162 MHz, C_6D_6): δ 9.14 (*sept.*, $^{4}J_{PF}$ = 4.7 Hz) ppm.

7.5.5 The reaction of 5.7 with phenylisocyanate

Compound **5.7** (30 mg, 0.039 mmol) was dissolved in C_6D_6 (0.5 mL) in a J. Youngs NMR tube. Phenylisocyanate (4.3 μL, 0.039 mmol) was then added. The sample was analysed by ^{1}H and ^{31}P{^{1}H} NMR spectroscopy. More than one new product was seen in the NMR; however, attempts to isolate them were unsuccessful, with other analytical techniques including mass spectrometry proving ineffectual due to the air sensitivity of the products.

7.5.6 The reaction of 5.7 with dichloromethane-d_2

Compound **5.7** (30 mg, 0.039 mmol) was dissolved in C_6D_6 (0.5 mL) in a J. Youngs NMR tube. An excess of dichloromethane-d_2 (3 drops) was then added, with no visible colour change upon addition. The sample was analysed by ^{1}H, ^{2}H, ^{19}F, and ^{31}P{^{1}H} NMR spectroscopy. The FLP reaction product **5.10** was formed, but could not be isolated.

^{1}H NMR (400 MHz, C_6D_6): δ 7.34-7.19 (6H, m, Ar*H*), 5.03 (1H, s, γ-C*H*), 4.10 (2H, *sept.*, $^{3}J_{HH}$ = 6.8 Hz, -C*H*(CH_3)$_2$), 3.63 (2H, *sept.*, $^{3}J_{HH}$ = 6.8 Hz, -C*H*(CH_3)$_2$), 2.08 (2H, d, $^{4}J_{FP}$ = 12.3 Hz, -CH_2P^{t}Bu$_2$), 1.83 (6H, s, β-CH_3), 1.62 (6H, d, $^{3}J_{HH}$ = 6.6 Hz, -CH(CH_3)$_2$), 1.55 (6H, d, $^{3}J_{HH}$ = 6.8 Hz, -CH(CH_3)$_2$), 1.40 (6H, d, $^{3}J_{HH}$ = 6.8 Hz, -CH(CH_3)$_2$), 1.31 (6H, d, $^{3}J_{HH}$ = 6.7 Hz, -CH(CH_3)$_2$), 0.70 (18H, d, $^{3}J_{HP}$ = 15.5 Hz, P(C(CH_3)$_3$)$_2$) ppm. ^{2}H NMR (61 MHz, C_6D_6): δ 4.87 (br) ppm. ^{31}P{^{1}H} NMR (162 MHz, C_6D_6): δ 43.9 (s) ppm. ^{19}F NMR (377 MHz, C_6D_6): δ -78.0 (s) ppm.

7.5.7 The reaction of 5.7 with ethene gas

Compound **5.7** (30 mg, 0.039 mmol) was dissolved in C_6D_6 (0.5 mL) in a J. Youngs NMR tube. The sample was degassed twice by freeze-pump-thaw, before being refilled with ethene gas (1 bar). The sample was analysed by ^{1}H, ^{31}P, ^{31}P{^{1}H}, and ^{19}F NMR spectroscopy. No reaction was seen after 3 days at room temperature, with a temperature increase to 50 °C for 16 h, and 80 °C for 14 days also resulting in no reaction.

7.5.8 The reaction of 5.7 with 3-pentanone

Compound **5.7** (30 mg, 0.039 mmol) was dissolved in C_6D_6 (0.5 mL) in a J. Youngs NMR tube. 3-Pentanone (4.2 μL, 0.039 mmol) was then added, forming a pale yellow solution of **5.11**. The sample was analysed by ^{1}H, ^{19}F, and ^{31}P{^{1}H} NMR spectroscopy, however all attempts to isolate **5.11** were unsuccessful.

^{1}H NMR (400 MHz, C_6D_6): δ 7.21-7.16 (6H, m, Ar*H*), 4.80 (1H, s, γ-C*H*), 3.14 (4H, br, -C*H*(CH_3)$_2$), 2.15 (4H, br, OC(CH_2CH_3)$_2$), 1.86 (2H, br, CH_2P), 1.60 (6H, s, β-CH_3), 1.34 (12H, br, -CH(CH_3)$_2$), 1.20 (12H, br, -CH(CH_3)$_2$), 1.02 (18H, d, $^{3}J_{HP}$ = 10.6 Hz, P(C(CH_3)$_3$)$_2$), 0.86 (6h, br, OC(CH_2CH_3)$_2$) ppm. ^{31}P NMR (162 MHz, C_6D_6): δ 15.4 (*sept.*, $^{4}J_{PF}$ = 9.7 Hz) ppm. ^{19}F NMR (377 MHz, C_6D_6): δ -75.6 (d, $^{4}J_{FP}$ = 21.9 Hz) ppm.

7.5.9 The reaction of 5.7 with benzaldehyde

Compound **5.7** (30 mg, 0.039 mmol) was dissolved in C_6D_6 (0.5 mL) in a J. Youngs NMR tube. Benzaldehyde (4.0 μL, 0.039 mmol) was then added, forming an orange solution. The sample was analysed by ^{1}H, ^{19}F, and ^{31}P{^{1}H} NMR spectroscopy, showing the formation of **5.12**. Crystals suitable for X-ray diffraction were obtained from dissolving the sample in hot hexane and allowing it to cool. The NMR data of **5.12** matched that in the literature.[165]

7.5.10 The reaction of 5.7 with mesitaldehyde

Compound **5.7** (30 mg, 0.039 mmol) was dissolved in C_6D_6 (0.5 mL) in a J. Youngs NMR tube. Mesitaldehyde (5.8 μL, 0.039 mmol) was then added, turning the colourless solution orange. ^{1}H, ^{19}F, ^{13}C, and ^{31}P{^{1}H} NMR spectra showed the formation of the adduct **5.13**. Crystals suitable for X-ray diffraction were grown by slow evaporation of a PhCl solution of **5.13**.

^{1}H NMR (400 MHz, C_6D_6): δ 10.6 (1H, br, C(*H*)O), 7.27-7.05 (6H, m, Ar*H*(DIPP)), 6.52 (2H, s, *m*-C*H*), 4.93 (1H, s, γ-C*H*), 3.52 (2H, br, -C*H*(CH_3)$_2$), 3.11 (2H, br, -C*H*(CH_3)$_2$), 2.61 (6H, s, *o*-CH_3), 1.93 (2H, br, CH_2P), 1.86 (3H, s, *p*-CH_3), 1.69 (6H, s, β-CH_3), 1.58 (6H, br, -CH(CH_3)$_2$), 1.28 (6H, br, -CH(CH_3)$_2$), 1.10 (12H, br, -CH(CH_3)$_2$), 1.00 (18H, d, $^{3}J_{HP}$ = 10.7 Hz, P(C(CH_3)$_3$)$_2$) ppm. ^{13}C NMR (126 MHz, C_6D_6): δ 201.1 (br, *C*H(O)), 169.3 (s, β-*C*-N), 146.9 (s, *i*-*C*(DIPP)), 142.8 (s, *o*-*C*(DIPP)), 142.4 (br, *p*-*C*CH_3), 141.9 (br, *o*-*C*CH_3), 136.4 (s, *i*-*C*(Mes)), 131.3 (br, *m*-*C*H(Mes)), 125.4 (s, *p*-*C*H), 124.0 (s, *C*F_3), 123.4 (s, *m*-*C*H(DIPP)), 94.2 (s, γ-*C*H), 53.0 (s, *C*(CF_3)$_2$), 31.6 (d, $^{1}J_{CP}$ = 23.1 Hz, *C*H_2), 30.2 (d, $^{2}J_{CP}$ = 15.0 Hz, P(C(*C*H_3)$_3$)$_2$), 30.0 (d, $^{1}J_{CP}$ = 10.0 Hz, P(*C*(CH_3)$_3$)$_2$), 28.4 (s, -*C*H(CH_3)$_2$), 24.6 (s, β-C*C*H_3), 23.8 and 23.1 (s, -CH(*C*H_3)$_2$), 20.8 (s, *p*-*C*H_3), 20.5 (s, *o*-*C*H_3) ppm. ^{31}P{^{1}H} NMR (162 MHz, C_6D_6): δ 13.8 (*sept.*, $^{4}J_{PF}$ = 18.8 Hz) ppm. ^{19}F NMR (377 MHz, C_6D_6): δ -76.2 (d, $^{4}J_{FP}$ = 18.8 Hz) ppm.

7.5.11 Catalytic dehydrocoupling of $Me_2NH{\cdot}BH_3$ using 5.7

Catalytic dehydrocoupling of $Me_2NH{\cdot}BH_3$ at room temperature

In a glovebox, **5.7** (13.8 mg, 0.018 mmol) and $Me_2NH{\cdot}BH_3$ (10.6 mg, 0.18 mmol) were weighed into separate vials and dissolved in C_6D_6 (0.5 mL). The two solutions were then combined, and the fully mixed solution was transferred to a quartz J. Youngs NMR tube before the relevant spectra were then collected.

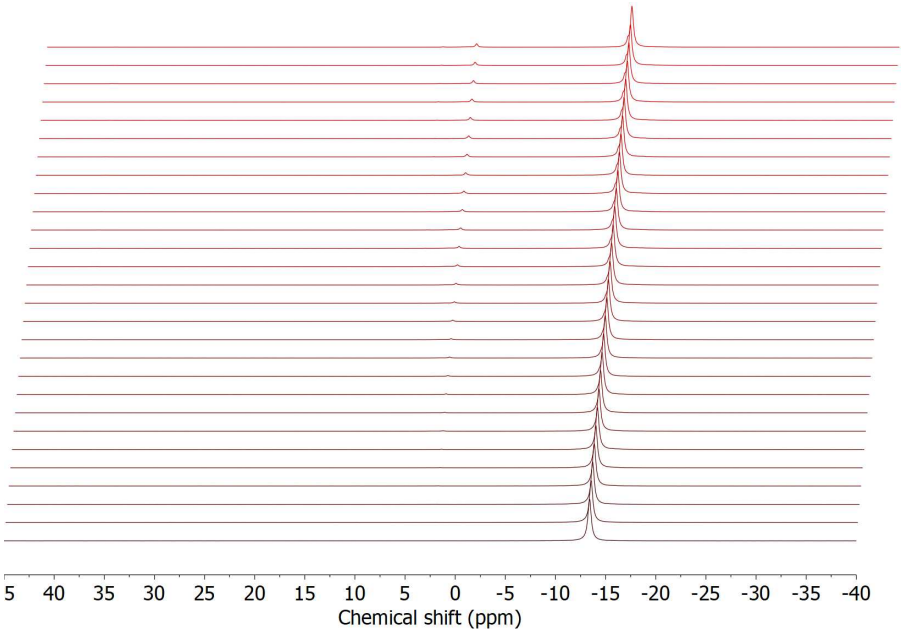

Figure 7.59: $^{11}B\{^{1}H\}$ NMR spectra (25 °C, C_6D_6) for the reaction between $Me_2NH{\cdot}BH_3$ and 10 mol% **5.7**. Each spectrum was obtained at an interval of 30 min. $Me_2N(B_2H_5)$ (-17.2 ppm), $Me_2NH{\cdot}BH_3$ (-13.4 ppm), $Me_2NH–BH_2–Me_2N–BH_3$ (1.7 ppm), $[Me_2N–BH_2]_2$ (5 ppm), $Me_2N{=}BH_2$ (37.7 ppm).

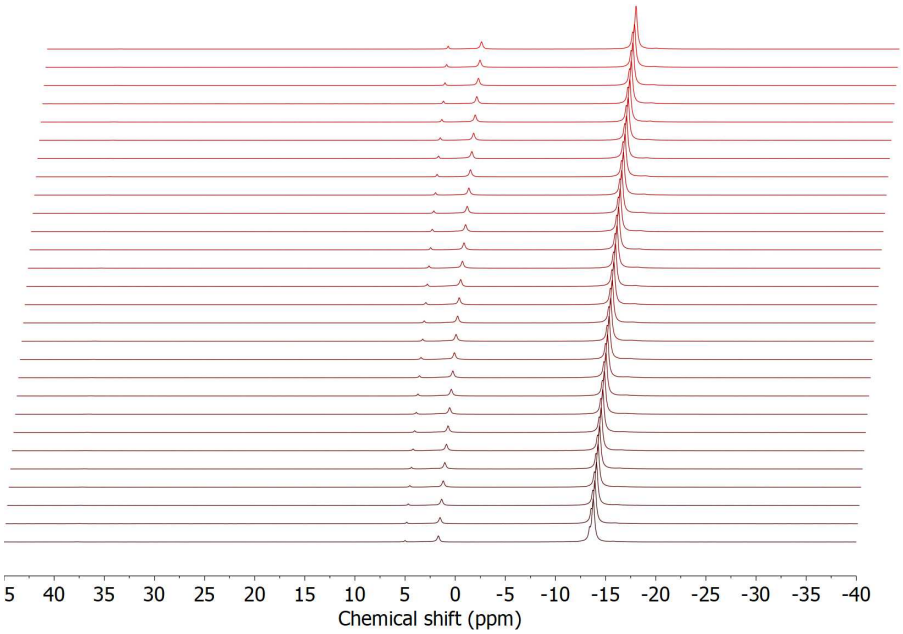

Figure 7.60: $^{11}B\{^{1}H\}$ NMR spectra (25 °C, C_6D_6) for the reaction between $Me_2NH{\cdot}BH_3$ and 10 mol% **5.7**. Each spectrum was obtained at an interval of 30 min. First scan after 1 day. $Me_2N(B_2H_5)$ (-17.2 ppm), $Me_2NH{\cdot}BH_3$ (-13.4 ppm), $Me_2NH–BH_2–Me_2N–BH_3$ (1.7 ppm), $[Me_2N–BH_2]_2$ (5 ppm), $Me_2N{=}BH_2$ (37.7 ppm).

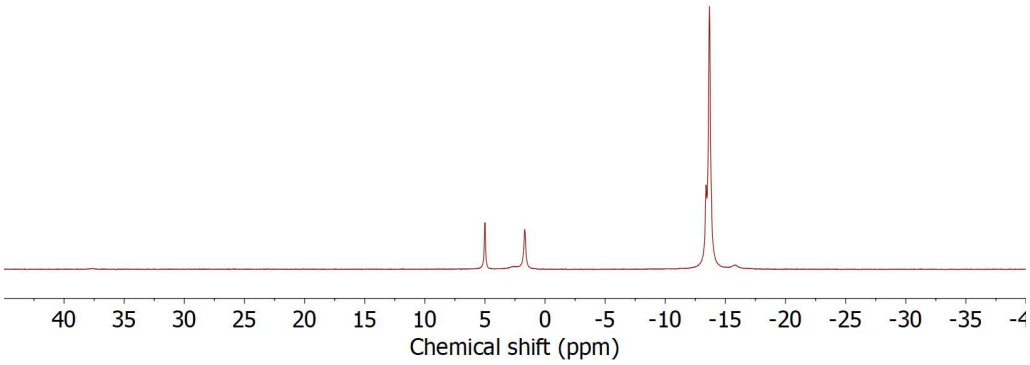

Figure 7.61: $^{11}B\{^{1}H\}$ NMR spectrum (25 °C, C_6D_6, 5 days) for the reaction between $Me_2NH{\cdot}BH_3$ and 10 mol% **5.7**. Each spectrum was obtained at an interval of 30 min. $Me_2N(B_2H_5)$ (-17.2 ppm), $Me_2NH{\cdot}BH_3$ (-13.4 ppm), $Me_2NH–BH_2–Me_2N–BH_3$ (1.7 ppm), $[Me_2N–BH_2]_2$ (5 ppm), $Me_2N{=}BH_2$ (37.7 ppm).

Catalytic dehydrocoupling of $Me_2NH{\cdot}BH_3$ at 60 °C

In a glovebox, **5.7** (13.8 mg, 0.018 mmol) and $Me_2NH{\cdot}BH_3$ (10.6 mg, 0.18 mmol) were weighed into separate vials and dissolved in C_6D_6 (0.5 mL). The two solutions were then combined, and the fully mixed solution was transferred to a quartz J. Youngs NMR tube before the relevant spectra were then collected in a NMR spectrometer set to 60 °C.

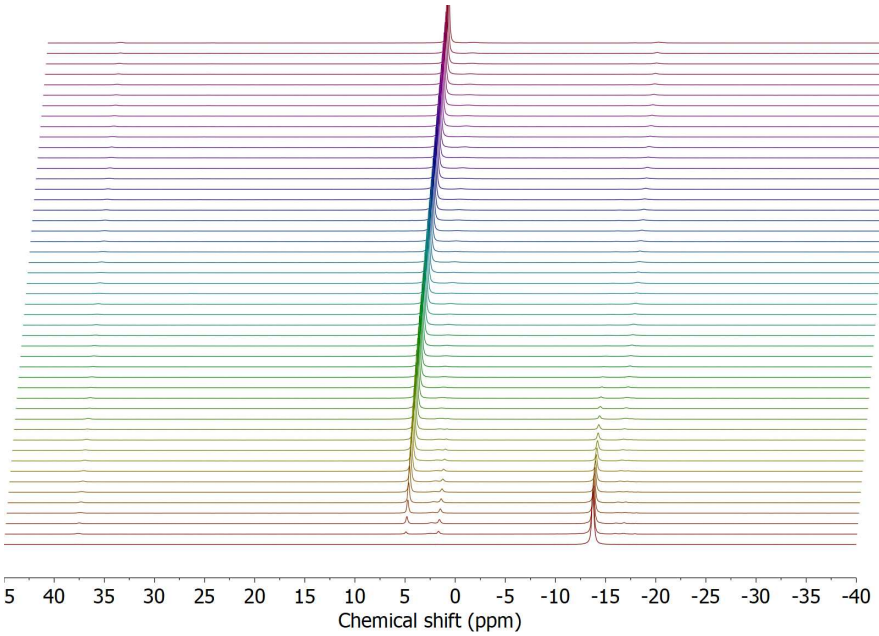

Figure 7.62: $^{11}B\{^{1}H\}$ NMR spectra (60 °C, C_6D_6) for the reaction between $Me_2NH{\cdot}BH_3$ and 10 mol% **5.7**. Each spectrum was obtained at an interval of 10 min. $Me_2N(B_2H_5)$ (-17.2 ppm), $Me_2NH{\cdot}BH_3$ (-13.4 ppm), $Me_2NH–BH_2–Me_2N–BH_3$ (1.7 ppm), $[Me_2N–BH_2]_2$ (5 ppm), $Me_2N{=}BH_2$ (37.7 ppm).

7.5.12 X-ray diffraction data

Table 7.4: Crystal data and structure refinement for **5.7** and **5.12**.

Identification code	**5.7**	**5.12**
Empirical formula	$C_{41}H_{61}F_6MgN_2OP$	$C_{78}H_{106}Mg_2N_4O_4$
Formula weight	767.19	1212.28
Temperature/K	99.98	100(2)
Crystal system	triclinic	monoclinic
Space group	P-1	$P2_1/n$
a/Å	9.3388(2)	13.5314(4)
b/Å	11.1656(3)	14.3832(4)
c/Å	20.6204(5)	19.2883(5)
$\alpha/^\circ$	89.0327(15)	90
$\beta/^\circ$	89.4546(16)	90.305(2)
$\gamma/^\circ$	71.9110(15)	90
Volume/Å^3	2043.58(9)	3753.93(18)
Z	2	2
ρ_{calc}g/cm^3	1.247	1.072
μ/mm^{-1}	0.143	0.080
F(000)	820.0	1316.0
Crystal size/mm^3	0.587 × 0.252 × 0.165	0.422 × 0.38 × 0.22
Radiation	MoK$_\alpha$ (λ = 0.71073)	MoK$_\alpha$ (λ = 0.71073)
2Θ range for data collection /°	3.838 to 55.878	3.532 to 51.364
Index ranges	-12 ≤ h ≤ 12, -14 ≤ h ≤ 14, -27 ≤ h ≤ 27	-13 ≤ h ≤ 16, -17 ≤ h ≤ 17, -23 ≤ h ≤ 22
Reflections collected	36812	28102
R_{int} / R_{sigma}	0.0342 / 0.0332	0.0353 / 0.0310
Data/restraints/ parameters	9778/0/485	7141/267/522
Goodness-of-fit on F^2	1.026	1.025
Final R indexes [I<=2σ (I)]	R_1 = 0.0380, wR_2 = 0.0854	R_1 = 0.0462, wR_2 = 0.1206
Final R indexes [all data]	R_1 = 0.0537, wR_2 = 0.0919	R_1 = 0.0693, wR_2 = 0.1372
Largest diff. peak/hole / e Å^{-3}	0.39/-0.27	0.24/-0.21

Table 7.5: Crystal data and structure refinement for **5.13**.

Identification code	**5.13**
Empirical formula	$C_{51}H_{73}F_6MgN_2O_2P$
Formula weight	915.39
Temperature/K	100(2)
Crystal system	monoclinic
Space group	$P2_1/n$
a/Å	13.4612(3)
b/Å	17.9060(4)
c/Å	21.0840(5)
$\alpha/^\circ$	90
$\beta/^\circ$	101.3362(15)
$\gamma/^\circ$	90
Volume/Å^3	4982.9(2)
Z	4
ρ_{calc}g/cm^3	1.220
μ/mm^{-1}	0.130
F(000)	1960.0
Crystal size/mm^3	0.321 × 0.291 × 0.108
Radiation	MoK$_\alpha$ (λ = 0.71073)
2Θ range for data collection /$^\circ$	3.01 to 50.698
Index ranges	-16 ≤ h ≤ 16, -21 ≤ h ≤ 21, -25 ≤ h ≤ 24
Reflections collected	55550
R_{int} / R_{sigma}	0.0680 / 0.0440
Data/restraints/ parameters	9119/0/587
Goodness-of-fit on F^2	1.007
Final R indexes [I<=2σ (I)]	R_1 = 0.0393, wR_2 = 0.0880
Final R indexes [all data]	R_1 = 0.0602, wR_2 = 0.0981
Largest diff. peak/hole /e Å^{-3}	0.32/-0.28

References

[1] G. N. Lewis, *Valence and the Structure of Atoms and Molecules*, The Chemical Catalog Company, Inc., New York, 1923, p. 172.
[2] G. C. Welch, R. R. San Juan, J. D. Masuda and D. W. Stephan, *Science*, 2006, **314**, 1124–1126.
[3] D. Stephan and G. Erker, *Angew. Chem. Int. Ed.*, 2010, **49**, 46–76.
[4] D. W. Stephan and G. Erker, *Angew. Chem. Int. Ed.*, 2015, **54**, 6400–6441.
[5] D. W. Stephan, *J. Am. Chem. Soc.*, 2015, **137**, 10018–10032.
[6] S. R. Flynn and D. F. Wass, *ACS Catal.*, 2013, **3**, 2574–2581.
[7] R. C. Neu, E. Otten, A. Lough and D. W. Stephan, *Chem. Sci.*, 2011, **2**, 170–176.
[8] A. M. Chapman, M. F. Haddow and D. F. Wass, *J. Am. Chem. Soc.*, 2011, **133**, 18463–18478.
[9] R. F. Jordan, C. S. Bajgur, W. E. Dasher and A. L. Rheingold, *Organometallics*, 1987, **6**, 1041–1051.
[10] A. M. Chapman, M. F. Haddow and D. F. Wass, *J. Am. Chem. Soc.*, 2011, **133**, 8826–8829.
[11] O. J. Metters, S. R. Flynn, C. K. Dowds, H. A. Sparkes, I. Manners and D. F. Wass, *ACS Catal.*, 2016, **6**, 6601–6611.
[12] X. Xu, G. Kehr, C. G. Daniliuc and G. Erker, *Angew. Chem. Int. Ed.*, 2013, **52**, 13629–13632.
[13] X. Xu, G. Kehr, C. G. Daniliuc and G. Erker, *J. Am. Chem. Soc.*, 2014, **136**, 12431–12443.
[14] X. Xu, R. Frohlich, C. G. Daniliuc, G. Kehr and G. Erker, *Chem. Commun.*, 2012, **48**, 6109–6111.
[15] X. Xu, G. Kehr, C. G. Daniliuc and G. Erker, *J. Am. Chem. Soc.*, 2013, **135**, 6465–6476.
[16] X. Xu, G. Kehr, C. G. Daniliuc and G. Erker, *Organometallics*, 2015, **34**, 2655–2661.
[17] A. T. Normand, C. G. Daniliuc, B. Wibbeling, G. Kehr, P. Le Gendre and G. Erker, *J. Am. Chem. Soc.*, 2015, **137**, 10796–10808.
[18] A. T. Normand, C. G. Daniliuc, B. Wibbeling, G. Kehr, P. LeGendre and G. Erker, *Chem. Eur. J.*, 2016, **22**, 4285–4293.
[19] Z. Jian, C. G. Daniliuc, G. Kehr and G. Erker, *Organometallics*, 2017, **36**, 424–434.
[20] A. M. Chapman, M. F. Haddow and D. F. Wass, *Eur. J. Inorg. Chem.*, 2012, **2012**, 1546–1554.
[21] T. L. Breen and D. W. Stephan, *Organometallics*, 1996, **15**, 5729–5737.
[22] T. L. Breen and D. W. Stephan, *J. Am. Chem. Soc.*, 1996, **118**, 4204–4205.

[23] A. M. Chapman and D. F. Wass, *Dalton Trans.*, 2012, **41**, 9067–9072.
[24] D. F. Wass and A. M. Chapman, *Top. Curr. Chem.*, 2013, **334**, 261–80.
[25] O. J. Metters, S. J. K. Forrest, H. A. Sparkes, I. Manners and D. F. Wass, *J. Am. Chem. Soc.*, 2016, **138**, 1994–2003.
[26] S. R. Flynn, O. J. Metters, I. Manners and D. F. Wass, *Organometallics*, 2016, **35**, 847–850.
[27] O. J. Metters, *PhD Thesis*, University of Bristol, 2016.
[28] S. Frömel, G. Kehr, R. Fröhlich, C. G. Daniliuc and G. Erker, *Dalton Trans.*, 2013, **42**, 14531–14536.
[29] C. Mömming, E. Otten, G. Kehr, R. Fröhlich, S. Grimme, D. Stephan and G. Erker, *Angew. Chem. Int. Ed.*, 2009, **48**, 6643–6646.
[30] X. Xu, G. Kehr, C. G. Daniliuc and G. Erker, *Organometallics*, 2013, **32**, 7306–7311.
[31] J. Paradies, *Angew. Chem. Int. Ed.*, 2014, **53**, 3552–3557.
[32] J. Paradies, *Synlett*, 2013, **24**, 777–780.
[33] D. W. Stephan, *Acc. Chem. Res.*, 2015, **48**, 306–316.
[34] K. Chernichenko, B. Kótai, I. PÁpai, V. Zhivonitko, M. Nieger, M. Leskel and T. Repo, *Angew. Chem. Int. Ed.*, 2015, **54**, 1749–1753.
[35] S. C. Binding, H. Zaher, F. Mark Chadwick and D. O'Hare, *Dalton Trans.*, 2012, **41**, 9061–9066.
[36] A. Berkefeld, W. E. Piers and M. Parvez, *J. Am. Chem. Soc.*, 2010, **132**, 10660–10661.
[37] K. Chernichenko, M. Nieger, M. Leskela and T. Repo, *Dalton Trans.*, 2012, **41**, 9029–9032.
[38] M.-A. Courtemanche, E. Rochette, M.-A. Legare, W. Bi and F.-G. Fontaine, *Dalton Trans.*, 2016, **45**, 6129–6135.
[39] K. Chernichenko, M. Lindqvist, B. Kótai, M. Nieger, K. Sorochkina, I. PÁpai and T. Repo, *J. Am. Chem. Soc.*, 2016, **138**, 4860–4868.
[40] M.-A. Legare, E. Rochette, J. Legare Lavergne, N. Bouchard and F.-G. Fontaine, *Chem. Commun.*, 2016, **52**, 5387–5390.
[41] N. von Wolff, G. Lefvre, J. C. Berthet, P. Thury and T. Cantat, *ACS Catal.*, 2016, **6**, 4526–4535.
[42] D. Winkelhaus, B. Neumann, H.-G. Stammler and N. W. Mitzel, *Dalton Trans.*, 2012, **41**, 9143–9150.
[43] L. A. Korte, S. Blomeyer, S. Heidemeyer, A. Mix, B. Neumann and N. W. Mitzel, *Chem. Commun.*, 2016, **52**, 9949–9952.
[44] V. Iashin, K. Chernichenko, I. Ppai and T. Repo, *Angew. Chem. Int. Ed.*, 2016, **55**, 14146–14150.
[45] Y. Zhang, G. M. Miyake, M. G. John, L. Falivene, L. Caporaso, L. Cavallo and E. Y. X. Chen, *Dalton Trans.*, 2012, **41**, 9119–9134.
[46] D. W. Stephan, S. Greenberg, T. W. Graham, P. Chase, J. J. Hastie, S. J. Geier, J. M. Farrell, C. C. Brown, Z. M. Heiden, G. C. Welch and M. Ullrich, *Inorg. Chem.*, 2011, **50**, 12338–12348.
[47] S. Li, G. Li, W. Meng and H. Du, *J. Am. Chem. Soc.*, 2016, **138**, 12956–12962.
[48] E. Dorkó, B. Kótai, T. Földes, A. Gyömöre, I. Pápai and T. Soós, *J. Organomet. Chem.*, 2017, **847**, 258–262.
[49] P. A. Chase, T. Jurca and D. W. Stephan, *Chem. Commun.*, 2008, 1701–1703.
[50] Y.-L. Liu, G. Kehr, C. G. Daniliuc and G. Erker, *Organometallics*, 2017, **36**, 3407–

3414.
[51] X. Xu, G. Kehr, C. G. Daniliuc and G. Erker, *J. Am. Chem. Soc.*, 2015, **137**, 4550–4557.
[52] V. Grignard, *Comptes Rendus Acad. Sci.*, 1900, 1322–1324.
[53] M. Westerhausen, *Angew. Chem. Int. Ed.*, 2008, **47**, 2185–2187.
[54] A. Stasch and C. Jones, *Dalton Trans.*, 2011, **40**, 5659–5672.
[55] T. E. Stennett and S. Harder, *Chem. Soc. Rev.*, 2016, **45**, 1112–1128.
[56] M. S. Hill, D. J. Liptrot and C. Weetman, *Chem. Soc. Rev.*, 2016, **45**, 972–988.
[57] L. Bourget-Merle, M. F. Lappert and J. R. Severn, *Chem. Rev.*, 2002, **102**, 3031–3066.
[58] A. Causero, G. Ballmann, J. Pahl, C. Farber, J. Intemann and S. Harder, *Dalton Trans.*, 2017, **46**, 1822–1831.
[59] H. M. El-Kaderi, M. J. Heeg and C. H. Winter, *Polyhedron*, 2006, **25**, 224–234.
[60] J. F. Dunne, S. R. Neal, J. Engelkemier, A. Ellern and A. D. Sadow, *J. Am. Chem. Soc.*, 2011, **133**, 16782–16785.
[61] J. S. Wixey and B. D. Ward, *Dalton Trans.*, 2011, **40**, 7693–7696.
[62] G. A. Molander and J. A. C. Romero, *Chem. Rev.*, 2002, **102**, 2161–2186.
[63] S. Hong and T. J. Marks, *Acc. Chem. Res.*, 2004, **37**, 673–686.
[64] M. Arrowsmith and M. S. Hill, in *Alkaline Earth Chemistry: Applications in Catalysis*, ed. K. Poeppelmeier, Elsevier, Amsterdam, 2nd edn., 2013, vol. 1, book section 1.38, pp. 1189–1216.
[65] R. Rochat, M. J. Lopez, H. Tsurugi and K. Mashima, *ChemCatChem*, 2016, **8**, 10–20.
[66] V. C. Gibson, J. A. Segal, A. J. P. White and D. J. Williams, *J. Am. Chem. Soc.*, 2000, **122**, 7120–7121.
[67] S. P. Green, C. Jones and A. Stasch, *Science*, 2007, **318**, 1754–1757.
[68] D. Mukherjee and J. Okuda, *Angew. Chem. Int. Ed.*, 2018, **57**, 1458–1473.
[69] S. Harder, J. Spielmann, J. Intemann and H. Bandmann, *Angew. Chem. Int. Ed.*, 2011, **50**, 4156–4160.
[70] S. P. Green, C. Jones and A. Stasch, *Angew. Chem. Int. Ed.*, 2008, **47**, 9079–9083.
[71] S. Bonyhady, C. Jones, S. Nembenna, A. Stasch, A. Edwards and G. McIntyre, *Chem. Eur. J.*, 2010, **16**, 938–955.
[72] A. Datta, *J. Phys. Chem. C*, 2008, **112**, 18727–18729.
[73] R. Lalrempuia, C. E. Kefalidis, S. J. Bonyhady, B. Schwarze, L. Maron, A. Stasch and C. Jones, *J. Am. Chem. Soc.*, 2015, **137**, 8944–8947.
[74] S. J. Bonyhady, D. Collis, G. Frenking, N. Holzmann, C. Jones and A. Stasch, *Nat. Chem.*, 2010, **2**, 865–869.
[75] M. Arrowsmith, B. Maitland, G. Kociok-Kohn, A. Stasch, C. Jones and M. S. Hill, *Inorg. Chem.*, 2014, **53**, 10543–10552.
[76] M. S. Hill, G. Kociok-Koehn, D. J. MacDougall, M. F. Mahon and C. Weetman, *Dalton Trans.*, 2011, **40**, 12500–12509.
[77] M. S. Hill, D. J. MacDougall and M. F. Mahon, *Dalton Trans.*, 2010, **39**, 11129–11131.
[78] C. Weetman, M. S. Hill and M. F. Mahon, *Polyhedron*, 2016, **103**, 115–120.
[79] M. Arrowsmith, M. S. Hill, T. Hadlington, G. Kociok-Kohn and C. Weetman, *Organometallics*, 2011, **30**, 5556–5559.
[80] M. Arrowsmith, T. J. Hadlington, M. S. Hill and G. Kociok-Kohn, *Chem. Commun.*,

2012, **48**, 4567–4569.
[81] M. Arrowsmith, M. S. Hill and G. Kociok-Köhn, *Chem. Eur. J.*, 2013, **19**, 2776–2783.
[82] C. Weetman, M. S. Hill and M. F. Mahon, *Chem. Commun.*, 2015, **51**, 14477–14480.
[83] C. Weetman, M. S. Hill and M. F. Mahon, *Chem. Eur. J.*, 2016, **22**, 7158–7162.
[84] C. Weetman, M. D. Anker, M. Arrowsmith, M. S. Hill, G. Kociok-Kohn, D. J. Liptrot and M. F. Mahon, *Chem. Sci.*, 2016, **7**, 628–641.
[85] Y. Yang, M. D. Anker, J. Fang, M. F. Mahon, L. Maron, C. Weetman and M. S. Hill, *Chem. Sci.*, 2017, **8**, 3529–3537.
[86] J. Intemann, M. Lutz and S. Harder, *Organometallics*, 2014, **33**, 5722–5729.
[87] J. Spielmann, M. Bolte and S. Harder, *Chem. Commun.*, 2009, 6934–6936.
[88] D. Liptrot, M. Hill, M. Mahon and D. MacDougall, *Chem. Eur. J.*, 2010, **16**, 8508–8515.
[89] M. S. Hill, M. Hodgson, D. J. Liptrot and M. F. Mahon, *Dalton Trans.*, 2011, **40**, 7783–7790.
[90] D. J. Liptrot, M. Arrowsmith, A. L. Colebatch, T. J. Hadlington, M. S. Hill, G. Kociok-Köhn and M. F. Mahon, *Angew. Chem. Int. Ed.*, 2015, **54**, 15280–15283.
[91] E. A. Romero, J. L. Peltier, R. Jazzar and G. Bertrand, *Chem. Commun.*, 2016, **52**, 10563–10565.
[92] M. R. Crimmin, I. J. Casely and M. S. Hill, *J. Am. Chem. Soc.*, 2005, **127**, 2042–2043.
[93] A. G. M. Barrett, M. R. Crimmin, M. S. Hill, P. B. Hitchcock, G. Kociok-Köhn and P. A. Procopiou, *Inorg. Chem.*, 2008, **47**, 7366–7376.
[94] M. R. Crimmin, M. Arrowsmith, A. G. M. Barrett, I. J. Casely, M. S. Hill and P. A. Procopiou, *J. Am. Chem. Soc.*, 2009, **131**, 9670–9685.
[95] A. G. M. Barrett, I. J. Casely, M. R. Crimmin, M. S. Hill, J. R. Lachs, M. F. Mahon and P. A. Procopiou, *Inorg. Chem.*, 2009, **48**, 4445–4453.
[96] L. Davin, R. McLellan, A. Hernan-Gomez, W. Clegg, A. R. Kennedy, M. Mertens, I. A. Stepek and E. Hevia, *Chem. Commun.*, 2017, **53**, 3653–3656.
[97] L. Davin, R. McLellan, A. R. Kennedy and E. Hevia, *Chem. Commun.*, 2017, **53**, 11650–11653.
[98] L. J. Bole, L. Davin, A. R. Kennedy, R. McLellan and E. Hevia, *Chem. Commun.*, 2019, **55**, 4339–4342.
[99] M. D. Anker, M. S. Hill, J. P. Lowe and M. F. Mahon, *Angew. Chem. Int. Ed.*, 2015, **54**, 10009–10011.
[100] M. D. Anker, C. E. Kefalidis, Y. Yang, J. Fang, M. S. Hill, M. F. Mahon and L. Maron, *J. Am. Chem. Soc.*, 2017, **139**, 10036–10054.
[101] W. Ren, S. Zhang, Z. Xu and X. Ma, *Dalton Trans.*, 2019, **48**, 3109–3115.
[102] C. Camp and J. Arnold, *Dalton Trans.*, 2016, **45**, 14462–14498.
[103] M. D. Anker, M. Arrowsmith, P. Bellham, M. S. Hill, G. Kociok-Kohn, D. J. Liptrot, M. F. Mahon and C. Weetman, *Chem. Sci.*, 2014, **5**, 2826–2830.
[104] M. S. Hill, D. J. MacDougall, G. Kociok-Kohn, M. F. Mahon and C. Weetman, *Organometallics*, 2015, **34**, 2590–2599.
[105] T. Pietrzak, I. Justyniak, J. V. Park, M. Terlecki, Ł. Kapuśniak and J. Lewiński, *Chem. - Eur. J.*, 2019, **25**, 2503–2510.
[106] T. Pietrzak, M. Kubisiak, I. Justyniak, K. Zelga, E. Bojarski, E. Tratkiewicz, Z. Ochal and J. Lewiński, *Chem. Eur. J.*, 2016, **22**, 17776–17783.

[107] J. Pahl, S. Brand, H. Elsen and S. Harder, *Chem. Commun.*, 2018, **54**, 8685–8688.
[108] I. B. Sivaev and V. I. Bregadze, *Coord. Chem. Rev.*, 2014, **270-271**, 75–88.
[109] A. Friedrich, J. Pahl, H. Elsen and S. Harder, *Dalton Trans.*, 2019, **48**, 5560–5568.
[110] L. Garcia, M. D. Anker, M. F. Mahon, L. Maron and M. S. Hill, *Dalton Trans.*, 2018, **47**, 12684–12693.
[111] N. L. Lampland, A. Pindwal, S. R. Neal, S. Schlauderaff, A. Ellern and A. D. Sadow, *Chem. Sci.*, 2015, **6**, 6901–6907.
[112] L. E. Lemmerz, D. Mukherjee, T. P. Spaniol, A. Wong, G. Ménard, L. Maron and J. Okuda, *Chem. Commun.*, 2019, **55**, 3199–3202.
[113] J. Langer, I. Kosygin, R. Puchta, J. Pahl and S. Harder, *Chem. Eur. J.*, 2016, **22**, 17425–17435.
[114] S. Brand, J. Pahl, H. Elsen and S. Harder, *Eur. J. Inorg. Chem.*, 2017, **2017**, 4187–4195.
[115] J. Campos, *J. Am. Chem. Soc.*, 2017, **139**, 2944–2947.
[116] N. S. Lambic, R. D. Sommer and E. A. Ison, *J. Am. Chem. Soc.*, 2016, **138**, 4832–4842.
[117] A. Simonneau, R. Turrel, L. Vendier and M. Etienne, *Angew. Chem. Int. Ed.*, 2017, **56**, 12268–12272.
[118] H. B. Hamilton, A. M. King, H. A. Sparkes, N. E. Pridmore and D. F. Wass, *Inorg. Chem.*, 2019, **58**, 6399–6409.
[119] R. Linnell, *J. Org. Chem.*, 1960, **25**, 290–290.
[120] T. Fujii, H. Nishida, Y. Abiru, M. Yamamoto and M. Kise, *Chem. Pharm. Bull.*, 1995, **43**, 1872–1877.
[121] J. M. E. Matos and B. S. Lima-Neto, *J. Mol. Catal. A: Chem.*, 2006, **259**, 286–291.
[122] K. Clarke and K. Rothwell, *J. Chem. Soc.*, 1960, 1885–1895.
[123] M. M. Rahman, H. Y. Liu, K. Eriks, A. Prock and W. P. Giering, *Organometallics*, 1989, **8**, 1–7.
[124] P. Sampson and Y. Y. Novikov, in *1-Bromo-1-lithioethene*, American Cancer Society, 2007.
[125] J. W. Lauher and R. Hoffmann, *J. Am. Chem. Soc.*, 1976, **98**, 1729–1742.
[126] R. A. Stapleton, B. R. Galan, S. Collins, R. S. Simons, J. C. Garrison and W. J. Youngs, *J. Am. Chem. Soc.*, 2003, **125**, 9246–9247.
[127] F. Wu and R. F. Jordan, *Organometallics*, 2005, **24**, 2688–2697.
[128] E. J. Stoebenau and R. F. Jordan, *J. Am. Chem. Soc.*, 2006, **128**, 8162–8175.
[129] J. Zhao, S. Zhang, W.-X. Zhang and Z. Xi, *Organometallics*, 2012, **31**, 8370–8374.
[130] T. A. Rokob, A. Hamza, A. Stirling, T. Soós and I. PÁpai, *Angew. Chem. Int. Ed.*, 2008, **47**, 2435–2438.
[131] S. Grimme, H. Kruse, L. Goerigk and G. Erker, *Angew. Chem. Int. Ed.*, 2010, **49**, 1402–1405.
[132] R. H. Crabtree, *Chem. Rev.*, 2016, **116**, 8750–8769.
[133] M. Hill and O. F. Wendt, *Organometallics*, 2005, **24**, 5772–5775.
[134] K. Lau, B. J. Petro, S. Bontemps, and R. F. Jordan, *Organometallics*, 2013, **32**, 6895–6898.
[135] B. Birkmann, T. Voss, S. J. Geier, M. Ullrich, G. Kehr, G. Erker and D. W. Stephan, *Organometallics*, 2010, **29**, 5310–5319.
[136] J. A. Bilbrey, A. H. Kazez, J. Locklin and W. D. Allen, *J. Comput. Chem.*, 2013, **34**, 1189–1197.

[137] C. Rosorius, C. G. Daniliuc, R. Fröhlich, G. Kehr and G. Erker, *J. Organomet. Chem.*, 2013, **744**, 149–155.
[138] C. Rosorius, G. Kehr, R. Fröhlich, S. Grimme and G. Erker, *Organometallics*, 2011, **30**, 4211–4219.
[139] R. Liedtke, R. Fröhlich, G. Kehr and G. Erker, *Organometallics*, 2011, **30**, 5222–5232.
[140] F. H. Stephens, V. Pons and R. T. Baker, *Dalton Trans.*, 2007, 2613–2626.
[141] A. Staubitz, A. P. M. Robertson, M. E. Sloan and I. Manners, *Chem. Rev.*, 2010, **110**, 4023–4078.
[142] N. C. Smythe and J. C. Gordon, *Eur. J. Inorg. Chem.*, 2010, **2010**, 509–521.
[143] C. W. Hamilton, R. T. Baker, A. Staubitz and I. Manners, *Chem. Soc. Rev.*, 2009, **38**, 279–293.
[144] A. Staubitz, A. P. M. Robertson and I. Manners, *Chem. Rev.*, 2010, **110**, 4079–4124.
[145] A. Staubitz, A. PresaSoto and I. Manners, *Angew. Chem. Int. Ed.*, 2008, **47**, 6212–6215.
[146] A. Ledoux, P. Larini, C. Boisson, V. Monteil, J. Raynaud and E. Lacte, *Angew. Chem. Int. Ed.*, 2015, **54**, 15744–15749.
[147] T. Lorenz, A. Lik, F. A. Plamper and H. Helten, *Angew. Chem. Int. Ed.*, 2016, **55**, 7236–7241.
[148] R. L. Melen, *Chem. Soc. Rev.*, 2016, **45**, 775–788.
[149] A. J. M. Miller and J. E. Bercaw, *Chem. Commun.*, 2010, **46**, 1709–1711.
[150] G. R. Whittell, E. I. Balmond, A. P. M. Robertson, S. K. Patra, M. F. Haddow and I. Manners, *Eur. J. Inorg. Chem.*, 2010, **2010**, 3967–3975.
[151] D. J. Liptrot, M. S. Hill, M. F. Mahon and A. S. S. Wilson, *Angew. Chem. Int. Ed.*, 2015, **54**, 13362–13365.
[152] P. H. M. Budzelaar, A. B. Van Oort and A. G. Orpen, *Eur. J. Inorg. Chem.*, 1998, 1485–1494.
[153] J. E. Steves, M. D. Kennedy, K. P. Chiang, W. S. Kassel, W. G. Dougherty, T. J. Dudley and D. L. Zubris, *Dalton Trans.*, 2009, 1214–1222.
[154] P. J. Bailey, R. A. Coxall, C. M. Dick, S. Fabre and S. Parsons, *Organometallics*, 2001, **20**, 798–801.
[155] M. A. Beckett, D. S. Brassington, S. J. Coles and M. B. Hursthouse, *Inorg. Chem. Commun.*, 2000, **3**, 530–533.
[156] M. A. Beckett, G. C. Strickland, J. R. Holland and K. Sukumar Varma, *Polymer*, 1996, **37**, 4629–4631.
[157] M. A. Beckett, D. S. Brassington, M. E. Light and M. B. Hursthouse, *J. Chem. Soc., Dalton Trans.*, 2001, 1768–1772.
[158] U. Mayer, V. Gutmann and W. Gerger, *Monatsh. Chem.*, 1975, **106**, 1235–1257.
[159] V. Gutmann, *Coord. Chem. Rev.*, 1976, **18**, 225–255.
[160] O. Ekkert, G. Kehr, C. G. Daniliuc, R. Fröhlich, B. Wibbeling, J. L. Petersen and G. Erker, *Z. Anorg. Allg. Chem.*, 2013, **639**, 2455–2462.
[161] W. Uhl and C. Appelt, *Organometallics*, 2013, **32**, 5008–5014.
[162] A. Gyömöre, M. Bakos, T. Földes, I. Pápai, A. Domján and T. Soós, *ACS Catal.*, 2015, **5**, 5366–5372.
[163] T. Mahdi and D. W. Stephan, *J. Am. Chem. Soc.*, 2014, **136**, 15809–15812.
[164] M. Stender, R. J. Wright, B. E. Eichler, J. Prust, M. M. Olmstead, H. W. Roesky and P. P. Power, *J. Chem. Soc., Dalton Trans.*, 2001, 3465–3469.

[165] A. P. Dove, V. C. Gibson, P. Hormnirun, E. L. Marshall, J. A. Segal, A. J. P. White and D. J. Williams, *Dalton Trans.*, 2003, 3088–3097.
[166] M. Bornand, S. Torker and P. Chen, *Organometallics*, 2007, **26**, 3585–3596.
[167] A. M. Chapman, M. F. Haddow, J. P. H. Orton and D. F. Wass, *Dalton Trans.*, 2010, **39**, 6184–6186.
[168] D. E. Gindelberger and J. Arnold, *Inorg. Chem.*, 1994, **33**, 6293–6299.
[169] H. H. Karsch and M. Reisky, *Eur. J. Inorg. Chem.*, 1998, **1998**, 905–911.
[170] R. Lalrempuia, A. Stasch and C. Jones, *Chem. Sci.*, 2013, **4**, 4383–4388.
[171] S. Bonyhady, S. Green, C. Jones, S. Nembenna and A. Stasch, *Angew. Chem. Int. Ed.*, 2009, **48**, 2973–2977.
[172] P. Xu, Y. Yao and X. Xu, *Chem. Eur. J.*, 2017, **23**, 1263–1267.
[173] C. N. Ayala, M. H. Chisholm, J. C. Gallucci and C. Krempner, *Dalton Trans.*, 2009, 9237–9245.
[174] Bruker, *SADABS 2014/5, Bruker AXS area detector scaling and absorption correction, Bruker Analytical X-ray Instruments Inc., Madison, Wisconsin, USA*, 2014/5.
[175] Bruker, *SAINT+ v8.38A Integration Engine, Data Reduction Software, Bruker Analytical X-ray Instruments Inc., Madison, WI, USA*, 2015.
[176] L. Palatinus and G. Chapuis, *J. Appl. Cryst.*, 2007, **40**, 786–790.
[177] L. Palatinus, S. J. Prathapa and S. van Smaalen, *J. Appl. Cryst.*, 2012, **45**, 575–580.
[178] G. M. Sheldrick, *Acta Cryst. A*, 2015, **71**, 3–8.
[179] G. M. Sheldrick, *Acta Cryst. A*, 2008, **64**, 112–122.
[180] G. M. Sheldrick, *Acta Cryst. C*, 2015, **71**, 3–8.
[181] O. V. Dolomanov, L. J. Bourhis, R. J. Gildea, J. A. K. Howard and H. Puschmann, *J. Appl. Cryst.*, 2009, **42**, 339–341.
[182] A. L. Spek, *J. Appl. Cryst.*, 2003, **36**, 7–13.
[183] A. L. Spek, *Acta Cryst. D*, 2009, **65**, 148–155.
[184] V. Balasanthiran, M. H. Chisholm, K. Choojun, C. B. Durr and P. M. Wambua, *Polyhedron*, 2016, **103, Part B**, 235–240.